

Report No. CCEER 10-03

**PROPOSED SEISMIC PROVISIONS  
AND COMMENTARY FOR STEEL PLATE  
GIRDER SUPERSTRUCTURES**

Ahmad M. Itani  
Michael A. Grubb  
Eric V. Monzon

---

**Center for Civil Engineering Earthquake Research**  
University of Nevada, Reno

June 2010

1. Report No. UNR/CCEER-10-03		2. Government Accession No.		3. Recipient's Catalog No.	
4. Title and Subtitle <b>Proposed Seismic Provisions and Commentary for Steel Plate Girder Superstructures</b>				5. Report Date 2010	
				6. Performing Organization Code	
7. Authors A. Itani, M. Grubb, E. Monzon, L. Carden, H. Bahrami, K. Friskel				8. Performing Organization Report No. UNR/CCEER-10-03	
9. Performing Organization Name and Address Department of Civil and Environmental Engineering University of Nevada, Reno, Nevada 89557-0208 Fax: A. Itani: (775) 784-1362, e-mail: <a href="mailto:itani@unr.edu">itani@unr.edu</a>				10. Work Unit No. (TRAIS)	
				11. Contract or Grant No.	
12. Sponsoring Agency Name and Address American Iron and Steel Institute, Washington, D.C.				13. Type of Report and Period Covered Final Report	
				14. Sponsoring Agency Code	
15. Supplementary Notes The development project herein was performed in the Center for Civil Engineering Earthquake Research at the University of Nevada, Reno. The project was sponsored by the American Iron and Steel Institute. The opinions expressed in this report are those of the authors and do not necessarily reflect the views of the University of Nevada, Reno, the Sponsor, or the individuals whose names appear in this report.					
16. Abstract  The seismic provisions of the current AASHTO LRFD Specifications (AASHTO, 2007) are based on the NCHRP Project 20-7/45. These provisions were updated in 2008 to include the 2006 USGS 1000-year maps and several revisions to keep the specifications current with the recent advances in the seismic analysis and design. However, none of these changes reflected the new information that was gained in the seismic analysis and design of steel plate girder superstructures. In an effort, to bridge this gap in the specifications, the American Iron and Steel Institute commissioned this report to propose updates for the seismic design of steel plate girder superstructures to AASHTO LRFD Specifications.  The objectives of this study are to: 1) Present the state-of-the art summary of research related to the seismic analysis and design of steel plate girder bridges; 2) Develop code language and commentary that can be adopted in the AASHTO LRFD Specifications; 3) Develop design examples that show how the proposed language can be used in the seismic analysis and design of steel plate girder bridges. To achieve these objectives, Chapter 1 of this report discusses related research to the seismic behavior and design of steel plate girder bridges. Chapter 2 presents the proposed language and commentary for the seismic design of steel plate girder bridges. Chapter 3 presents detailed seismic analysis and design examples for a single span and a two span continuous steel plate girder bridge with a single column bent and a dropped cap. Appendix 1 presents a summary of all existing seismic specifications that are related to steel plate girder bridges.					
17. Key Words Seismic Analysis and Design, Steel Plate Girders, Cross-Frames, Experiments, Specifications				18. Distribution Statement No restriction. This Document is available to the public through the Center for Civil Engineering Earthquake Research, University of Nevada, Reno, NV 89557-0208 and American and Iron Steel Institute	
19. Security Classif. (of this Report) Unclassified		20. Security Classif. (of this page) Unclassified		21. No. of Pages 272	
				22. Price \$XX.XX+ Applicable Sales Tax	

## **Abstract**

The seismic provisions of the current AASHTO LRFD Specifications (AASHTO, 2007) are based on the NCHRP Project 20-7/45. These provisions were updated in 2008 to include the 2006 USGS 1000-year maps and several revisions to keep the specifications current with the recent advances in the seismic analysis and design. However, none of these changes reflected the new information that was gained in the seismic analysis and design of steel plate girder superstructures. In an effort, to bridge this gap in the specifications, the American Iron and Steel Institute commissioned this report to propose updates for the seismic design of steel plate girder superstructures in AASHTO LRFD Specifications.

The objectives of this study are to: 1) Present the state-of-the art summary of research related to the seismic analysis and design of steel plate girder bridges; 2) Develop code language and commentary that can be adopted in the AASHTO LRFD Specifications; 3) Develop design examples that show how the proposed language can be used in the seismic analysis and design of steel plate girder bridges. To achieve these objectives, Chapter 1 of this report discusses related research to the seismic behavior and design of steel plate girder bridges. Chapter 2 presents the proposed language and commentary for the seismic design of steel plate girder bridges. Chapter 3 presents detailed seismic analysis and design examples for a single span and a two span continuous steel plate girder bridge with a single column bent and a dropped cap. Appendix 1 presents a summary of all existing seismic specifications that are related to steel plate girder bridges.

## **Acknowledgement**

The authors would like to acknowledge American Iron and Steel Institute for the support to conduct this study. Mr. Dan Snyder was contact manager for this project. The authors would like to sincerely acknowledge him along with Mr. Alexander Wilson and Mr. Edward Wasserman Chair of AASHTO T-14 technical committee. Mr. Wasserman and other members and friends of T-14 interest and feedback were very helpful during the preparation of the final report.

# Table of Contents

List of Tables .....	iii
List of Figures.....	iv
List of Symbols.....	x
List of Symbols.....	x
Chapter 1 Introduction and Background .....	1
1.1. Introduction.....	1
1.2. Seismic Design Specifications for Steel Bridges.....	2
1.3. Objectives and Scope.....	4
1.4. Performance of Steel Bridges during Recent Earthquakes.....	4
1.4.1. Behavior of Steel Bridges during the Petrolia Earthquakes .....	4
1.4.2. Behavior of Steel Bridges during the Northridge Earthquake.....	5
1.4.3. Behavior of Steel Superstructure during the Hyogoken-Nanbu ‘Kobe’ Earthquake .....	5
1.5. Behavior of Steel Plate Girder Bridges under Lateral Loading.....	6
1.5.1. Seismic Modeling of Steel Plate Girder Superstructures .....	6
1.5.2. Lateral Load Path and Effect of Composite Action .....	7
1.6. Behavior of End Cross Frame under Lateral Cyclic Loading .....	9
1.6.1. Types and Configurations of Bridge Cross Frames.....	9
1.6.1.1. Introduction .....	9
1.6.1.2. Attachment of R/C Deck to Steel Plate Girders and Cross Frames.....	10
1.6.2. Behavior of Shear Connectors under Shear and Axial Forces .....	11
1.6.2.1 Connectors under Shear Forces .....	11
1.6.2.2. Connectors under Axial loads and Combined Tension and Shear Forces .....	12
1.6.2.3. Behavior of R/C Deck and Plate Girder Studded Joint .....	13
1.6.3. Behavior of Cross Frame under Lateral Loading .....	15
1.6.3.1. Behavior of Special Diagonal Members.....	15
1.6.4. Ductile End Cross Frames Design and Detail Requirements .....	21
1.7. Experimental Investigations on the End Cross Frame Subassembly Models .....	23
1.7.1. Introduction .....	23
1.7.2. Description of Test Specimens .....	23
1.7.2.1. Specimen F1A .....	24
1.7.2.2. Specimen F1B.....	24
1.7.2.3. Specimen F1B_1.....	24
1.7.2.4. Specimen F1C.....	25
1.7.3. Material Properties of Test Specimens and Testing Protocol.....	25
1.7.4. Cyclic Response of Specimen F1A .....	26
1.7.4.1. Experimental Observations.....	26
1.7.4.2. Sequence of Yielding and Failure Modes.....	27

1.7.5. Cyclic Response of Specimen F1B .....	28
1.7.5.1. Experimental Observations.....	28
1.7.5.2. Sequence of Yielding and Failure Modes.....	29
1.7.6. Cyclic Response of Specimen F1B_1 .....	30
1.7.6.1. Experimental Observations.....	30
1.7.6.2. Sequence of Yielding and Failure Modes.....	30
1.7.7. Cyclic Response of Specimen F1C .....	31
1.7.7.1. Experimental Observations.....	32
1.7.7.2. Sequence of Yielding and Failure Modes.....	32
1.8. Seismic Performance of Plate Girder Bridges with Ductile End Cross Frames....	33
1.8.1. General.....	33
1.8.2. Description of Bridge Model.....	35
1.8.3. Reversed Static Load Experiments.....	37
1.8.4. Shake Table Experiments .....	40
1.8.5. Response Comparison between Elastic and Ductile Cross Frames.....	41
References .....	42
Appendix 1 .....	148
Chapter 2 Proposed Seismic Provisions and Commentary .....	155
Chapter 3 Seismic Design Examples.....	173
3.1 Introduction .....	173
3.2 Single-Span Bridge.....	173
3.2.1 Description.....	173
3.2.2 Analytical Model .....	174
3.2.3 Seismic Analysis.....	174
3.2.4 Seismic Design of a Single-Span Bridge with Elastic Superstructure .....	174
3.2.5 Seismic Design of a Single-Span Bridge with Ductile Superstructure .....	181
3.3 Two-Span Bridge.....	188
3.3.1 Description.....	188
3.3.2 Analytical Model .....	189
3.3.3 Seismic Analysis.....	189
3.3.4 Seismic Design of a Two-Span Bridge with Ductile Superstructure .....	190
Appendix 3-A .....	200
Appendix 3-B .....	211
Appendix 3-C .....	223

## List of Tables

Table 1-1. Comparison of bridge model response with ductile X-braces and elastic X-braces. ....	49
Table 1-2. List of Cyclic Axial Single Angle Experiments.....	50
Table 1-3. Failure Mode, Maximum Effective Axial Strains, and Cumulative Effective Plastic Axial Strains in the Angles.....	51
Table 1-4. Tensile and Compressive Strengths of Single Angle Specimens Compared with Expected Properties .....	52

## List of Figures

Figure 1-1. JRA Specifications, reinforcement at bearing support. ....	54
Figure 1-2. JRA Specifications, minimized space at lower ends of lateral support. ....	54
Figure 1-3. JRA Specifications, application of horizontal earthquake force.....	55
Figure 1-4. Damage to Bearing during the 1994 Northridge Earthquake. ....	55
Figure 1-5. Damage to End Cross Frames during the 1994 Northridge Earthquake.....	56
Figure 1-6. Damage to Web Stiffeners during the 1994 Northridge Earthquake.....	56
Figure 1-7. Damage to End Cross Frames and Girders during 1995 Kobe Earthquake..	57
Figure 1-8. Failure of Shear Connectors in Bridge Model during Transverse Cyclic Loading. ....	57
Figure 1-9. Bent cross frames with V-pattern diagonals.....	58
Figure 1-10. Bent cross frames with X-pattern diagonals.....	58
Figure 1-11. Abutment cross frames with V-pattern diagonals.....	59
Figure 1-12. Abutment cross frames with V-pattern diagonals.....	59
Figure 1-13. Built up I-section diaphragm with transverse stiffener.....	60
Figure 1-14. Rolled shape diaphragm.....	60
Figure 1-15. Details of cross frames with inverted V-pattern diagonals.....	61
Figure 1-16. Details of cross frames with inverted V-pattern diagonals.....	61
Figure 1-17. End details of cross frames with inverted V-pattern.....	62
Figure 1-18. Details of cross frames with X-pattern diagonals.....	62
Figure 1-19. End details of cross frames with X-pattern.....	63
Figure 1-20. End details of cross frames with X-pattern.....	63
Figure 1-21. Details of cross frames with X-pattern diagonals.....	64
Figure 1-22. End details of cross frames with bolted members.....	64
Figure 1-23. Middle details of bolted cross frames with X pattern.....	65
Figure 1-24. Preferred details for abutment cross frames.....	65
Figure 1-25. Preferred details for intermediate cross frames subjected to large forces ...	66
Figure 1-26. Preferred details for intermediate cross frame subjected to low forces.....	66
Figure 1-27. Preferred details of cross frames at bent locations.....	67
Figure 1-28. Cross frame detail used on alternative design of I5/SR14 interchange.....	67
Figure 1-29. Detail used in the State of Tennessee where cross frames are used during erection.....	68
Figure 1-30. Kinematics of a support cross frame with shear connectors on the top girder flanges.....	69
Figure 1-31. Kinematics of a support cross frame with shear connectors on the top chords.....	69
Figure 1-32. Test specimen used in two-slab push-out experiment.....	70
Figure 1-33. Deck-girder moment connection – concrete breakout failure in the stud in tension.....	70
Figure 1-34. Moment connection of deck-girder studded joint.....	71
Figure 1-35. Transverse shear distribution in shear connectors on one girder for.....	71

Figure 1-36. Longitudinal shear distribution in shear connectors on one girder for elastic superstructure without top chord attachment.....	72
Figure 1-37. Limitation of D/S ratio for 4% drift limit.....	72
Figure 1-38. Free body diagram of internal forces due to lateral loading with connectors on top flange.....	73
Figure 1-39. Free body diagram of internal forces due to lateral loading with connectors on top chord.....	74
Figure 1-40. Experimental setup of cyclic axial experiments on angles.....	75
Figure 1-41. Hysteresis loops from single angle axial experiments.....	75
Figure 1-42. Hysteresis loops from single angle axial experiments.....	76
Figure 1-43. Hysteresis loops from single angle axial experiments.....	77
Figure 1-44. Hysteresis loops from single angle axial experiments.....	78
Figure 1-45. Hysteresis loops from single angle axial experiments.....	79
Figure 1-46. Fracture of bolted single angle specimen.....	80
Figure 1-47. Fracture of single angle specimen with thickened bolted connection.....	80
Figure 1-48. Fracture of single angle specimen with welded connections.....	81
Figure 1-49. Different connection configurations for diagonal members of ductile end cross frames.....	82
Figure 1-50. Energy dissipated per cycle as a percentage of "ideal" for single angle specimens.....	83
Figure 1-51. Dimension of transverse cross section of the bridge model.....	83
Figure 1-52. Single span design chart for displacement ductility of 8.0.....	84
Figure 1-53. Dimensions and details of Specimen F1A.....	84
Figure 1-54. Plan view of top flange showing shear connector pattern for F1A.....	85
Figure 1-55. Support detail for Specimens F1A, F1B, and F1B_1.....	85
Figure 1-56. Close-up view of support detail for Specimens F1A, F1B, and F1B_1.....	86
Figure 1-57. View of Specimen F1A before testing.....	86
Figure 1-58. Dimensions and details of Specimen F1B.....	87
Figure 1-59. View of Specimen F1B before testing.....	87
Figure 1-60. Dimensions and details of Specimen F1B_1.....	88
Figure 1-61. View of Specimen F1B_1 before testing.....	88
Figure 1-62. Specimen F1C details.....	89
Figure 1-63. Three dimensional drawing of Specimen F1C.....	89
Figure 1-64. Shear connector detail for Specimen F1C.....	90
Figure 1-65. Specimen F1C deck reinforcement.....	90
Figure 1-66. Fabricated chevron bracing components before assembly in Specimen F1C.....	91
Figure 1-67. Rebar arrangement for Specimen F1C.....	91
Figure 1-68. Transverse cross section of deck slab between girders for Specimen F1C.....	92
Figure 1-69. Specimen F1C: rebar detail near shear connectors.....	92
Figure 1-70. Specimen F1C: completed rebar and formwork.....	93
Figure 1-71. Pouring concrete for Specimen F1C.....	93
Figure 1-72. Specimen F1C before test.....	94
Figure 1-73. Shear connector coupon tests (3/8 in.).....	94
Figure 1-74. L 1x1x1/8 diagonal coupon test (Specimen F1B_1).....	95

Figure 1-75. Displacement controlled testing protocol .....	96
Figure 1-76. Specimen F1A: Actuator force versus differential girder displacement .....	97
Figure 1-77. F1A at 1.5% drift showing flexural cracking in concrete deck .....	97
Figure 1-78. F1A Specimen, buckled brace at (a) 2% drift, (b) 3% drift, and (c) 4% drift .....	98
Figure 1-79. F1A Specimen, the studded connection over Girder 2 shows some uplift at 1.5% drift .....	98
Figure 1-80. F1A Specimen, studded deck to girder connection over Girder 2 at 3.5% drift.....	99
Figure 1-81. F1A Specimen, studded deck to girder connection over Girder 3 at 3.5% drift.....	99
Figure 1-82. F1A Specimen, rupture of one diagonal brace at 5% drift .....	100
Figure 1-83. View of Specimen F1A at 7.5% drift .....	100
Figure 1-84. F1A Specimen, studded deck to girder connection over Girder 2 at 7.5% drift.....	101
Figure 1-85. Studded deck to girder connection over Girder 3, Specimen F1A at 7.5% drift.....	101
Figure 1-86. Studded deck to girder connection over Girder 1, Specimen F1A at 7.5% drift.....	102
Figure 1-87. View of Specimen F1A at 7.5% drift .....	102
Figure 1-88. Specimen F1A: final damage state at zero displacement .....	103
Figure 1-89. Specimen F1A: close-up of cross frame at final damage state at zero displacement .....	103
Figure 1-90. Specimen F1A: base shear at peak displacement cycles .....	104
Figure 1-91. Specimen F1A: strain gauge measurement on top chord .....	104
Figure 1-92. Specimen F1A: strain gauge measurement on top chord .....	105
Figure 1-93. Specimen F1A: strain gauge measurement on bottom chord .....	105
Figure 1-94. Specimen F1A: strain gauge measurement on bottom chord .....	106
Figure 1-95. Specimen F1A: strain gauge measurement at top of bearing stiffeners ....	106
Figure 1-96. Specimen F1A: strain gauge measurement at mid-height of bearing stiffeners.....	107
Figure 1-97. Specimen F1A: rotation of girder support bearings .....	107
Figure 1-98. Specimen F1A: rotation of deck over girders.....	108
Figure 1-99. Specimen F1A: horizontal support reactions.....	108
Figure 1-100. Specimen F1A: vertical support reactions.....	109
Figure 1-101. Specimen F1B: Actuator force versus differential girder displacement..	109
Figure 1-102. View of Specimen F1B before testing.....	110
Figure 1-103. Specimen F1B: relative deformation between top chord and deck at 2% drift.....	110
Figure 1-104. Specimen F1B: relative deformation between top chord and deck at 2% drift.....	111
Figure 1-105. Specimen F1B: buckled brace at a) 1.5% drift, b) 2% drift, and c) 2.5% drift.....	111
Figure 1-106. Specimen F1B: separation of top chord and deck at 2.5% drift .....	112
Figure 1-107. F1B Specimen: final damage state at zero displacement.....	112

Figure 1-108. F1B Specimen: close-up of underside of deck showing premature failure of stud connections.....	113
Figure 1-109. Specimen F1B: base shear at peak displacement cycles .....	113
Figure 1-110. Specimen F1B: strain gauge measurement on top chord .....	114
Figure 1-111. Specimen F1B: strain gauge measurement on top chord .....	114
Figure 1-112. Specimen F1B: strain gauge measurement on bottom chord .....	115
Figure 1-113. Specimen F1B: strain gauge measurement on bottom chord .....	115
Figure 1-114. Specimen F1B: strain gauge measurement at top of bearing stiffeners...	116
Figure 1-115. Specimen F1B: strain gauge measurement at mid-height of bearing stiffeners.....	116
Figure 1-116. Specimen F1B: Rotation of girder support bearings .....	117
Figure 1-117. Specimen F1B: rotation of deck over girders.....	117
Figure 1-118. Specimen F1B: horizontal support reactions.....	118
Figure 1-119. Specimen F1B: vertical support reactions.....	118
Figure 1-120. Specimen F1B_1: Actuator force versus differential girder displacement .....	119
Figure 1-121. View of Specimen F1B_1 before testing.....	119
Figure 1-122. Specimen F1B_1: X-Frame buckling at 1% drift.....	120
Figure 1-123. Specimen F1B_1: X-Frame yielding at 2% drift, top chord shows signs of yielding .....	120
Figure 1-124. Specimen F1B_1: X-Frame deforming near gusset plate at 3% drift.....	121
Figure 1-125. Specimen F1B_1: deck and girder separation at 3% drift .....	121
Figure 1-126. Specimen F1B_1: top chord at 3% drift .....	122
Figure 1-127. Specimen F1B_1: deformations at 4% drift .....	122
Figure 1-128. Specimen F1B_1: Middle girder rotation at 5% drift.....	123
Figure 1-129. Specimen F1B_1: deformations at 6% drift .....	123
Figure 1-130. Specimen F1B_1: diagonal failure during 7% drift cycle .....	124
Figure 1-131. Specimen F1B_1: diagonal failure during 7% drift cycle .....	124
Figure 1-132. Specimen F1B_1: top chord failure during 7% drift cycle (typical) .....	125
Figure 1-133. Specimen F1B_1: deck cracks and permanent deck-girder separation – final state.....	125
Figure 1-134. Specimen F1B_1: final state - 0% drift .....	126
Figure 1-135. Specimen F1B_1: base shear at peak displacement cycles .....	126
Figure 1-136. Specimen F1B_1: strain gauge measurement on top chord .....	127
Figure 1-137. Specimen F1B_1: strain gauge measurement on top chord .....	127
Figure 1-138. Specimen F1B_1: strain gauge measurements on bottom chord.....	128
Figure 1-139. Specimen F1B_1: strain gauge measurement on bottom chord .....	128
Figure 1-140. Specimen F1B_1: strain gauge measurement at top of bearing stiffeners .....	129
Figure 1-141. Specimen F1B_1: strain gauge measurement at mid-height of bearing stiffeners.....	129
Figure 1-142. Specimen F1B_1: Rotation of girder support bearings .....	130
Figure 1-143. Specimen F1B_1: rotation of deck over girders.....	130
Figure 1-144. Specimen F1B_1: horizontal support reactions.....	131
Figure 1-145. Specimen F1B_1: vertical support reactions.....	131

Figure 1-146. Specimen F1C: Actuator force versus actuator displacement (deck displacement) .....	132
Figure 1-147. Specimens F1C: deformed shape at 2% drift .....	132
Figure 1-148. Specimen F1C: buckled brace at (a) 4% and (b) 5% drift.....	133
Figure 1-149. Specimen F1C: distortion of buckled angle bracing near the gusset at 2% drift.....	133
Figure 1-150. Specimen F1C: rotation of the deck over Girder 3 as a result of bending in the deck.....	134
Figure 1-151. Specimen F1C: abrasion of underside of deck shows sliding of the deck .....	134
Figure 1-152. Specimen F1C after the test.....	135
Figure 1-153. Specimen F1C: large permanent axial deformations was observed in braces .....	135
Figure 1-154. Specimen F1C: no damage in the concrete deck after the test .....	136
Figure 1-155. Specimen F1C: base shear at peak displacement cycles .....	136
Figure 1-156. Specimen F1C: strain measurements on the chevron braces between G1 and G2.....	137
Figure 1-157. Specimen F1C: strain measurements on the chevron braces between G2 and G3 .....	137
Figure 1-158. Specimen F1C: strain gauge measurement on bottom chord at Girder 2	138
Figure 1-159. . Specimen F1C: strain gauge measurement on bottom chord at Girder 2 .....	138
Figure 1-160. Rotation of the supports in Specimen F1C.....	139
Figure 1-161. Rotation of the deck at girder locations in Specimen F1C .....	139
Figure 1-162. Specimen F1C: strain measurements at the bottom of the girders .....	140
Figure 1-163. Specimen F1C: small strain measurements at the top of the girders.....	140
Figure 1-164. Specimen F1C: horizontal support reactions.....	141
Figure 1-165. Specimen F1C: vertical support reactions .....	141
Figure 1-166. Buckled end cross frame member in Capitol Arch Bridge during the 2001 Nisqually Earthquake in Washington. ....	142
Figure 1-167. Two-girder steel bridge model subjected to reversed static load transverse loading.....	143
Figure 1-168. Bridge model during shake table experiments with X-braces at the ends. ....	143
Figure 1-169. Cross section of bridge model at intermediate cross frame location.....	144
Figure 1-170. Single angle X-braces as end cross frames in bridge model. ....	144
Figure 1-171. "Rocking" mechanism at the ends of the girders to allow relatively large girder drifts.....	145
Figure 1-172. Hysteresis loops for each end of bridge model during the reversed static load experiment.....	145
Figure 1-173. South end of bridge model after reversed static load experiment with ductile X-braces. ....	146
Figure 1-174. Hysteresis loops for north end of bridge model during shake table experiments while subjected to increasing amplitudes of the 1940 El Centro earthquake. ....	146

Figure 1-175. Hysteresis loops for south end of bridge model during shake table experiments while subjected to increasing amplitudes of the 1940 El Centro earthquake. .... 147

Figure 1-176. Displacement time histories at the ends of the bridge model in response to increasing amplitudes of the 1940 El Centro earthquake (eg. 0.25 = 0.25 times the El Centro earthquake). .... 147

## List of Symbols

A	Acceleration coefficient
$A_{\text{bearing}}$	Bearing area of stud head, in <sup>2</sup>
$A_g$	Gross cross sectional area of member
$A_{\text{se}}$	Cross sectional area of shear stud connector
$A_{\text{NC}}$	Projected concrete failure area for a group of stud
$A_{\text{NC0}}$	Projected concrete failure area for a single stud
$b_{\text{ws}}$	Width of web stiffeners
B	Damping coefficient
$C_s$	Seismic coefficient
d	Diameter of shear connector, total displacement, distance between the centroid of rows of shear connectors in tension and shear connector row in compression
$d_y$	Transverse displacement at yield in ductile end cross frame
D	Total displacement
$D_{\text{sub}}$	Displacement of substructure
$D_{\text{decf}}$	Displacement of ductile end cross frame
E	Elastic modulus of steel
$E_c$	Elastic modulus of concrete
$f_c'$	Concrete compressive strength
$F_i$	Lateral seismic force applied at superstructure joint i
$F_y$	Nominal yield strength
$F_{ye}$	Expected yield strength
$F_u$	Ultimate strength
$F_{\text{uta}}$	Ultimate strength of stud
g	Acceleration due to gravity
G	Shear modulus
h	Thickness of haunch in bridge deck, girder height
$h_{\text{ef}}$	Effective embedment length of shear connectors
I	Moment of inertia
J	Torsion constant
K	Effective length factor
$K_{\text{beam}}$	Stiffness matrix for beam element
$K_{\text{bridge}}$	Coupled stiffness matrix of superstructure in multi-span bridges
$K_d$	Post-yield stiffness of superstructure response
$K_{\text{eff\_decf}}$	Effective stiffness of ductile end cross frame
$K_{\text{eff\_super}}$	Effective stiffness of ductile end cross frame and system effects
$K_f$	Bilinear stiffness of ductile end cross frame
$K_i$	Initial stiffness of system of ductile end cross frame and system effects
$K_s$	Stiffness contribution from system effects

$K_{sub}$	Transverse substructure stiffness
$K_1$	Elastic stiffness of ductile end cross frame
$K_2$	Post-yield stiffness of ductile end cross frame
$L$	Length of bridge span
$L_1$	Length of girder between end and first intermediate cross frame
$L_y$	Distance from end of bridge over which the shear connectors fail
$L_{stud}$	Length of shear connector
$M$	Bending moment
$M_{y\_joint}$	Yield bending moment in deck-girder studded joint
$n$	Number of studs, number of girders, number of cross frame bays
$N$	Shape function vector
$N_b$	Basic concrete breakout strength
$N_{cb}$	Concrete breakout strength in tension
$N_f$	Number of sets (transverse row) of shear connectors in the failure zone
$N_{sa}$	Tensile strength of shear connector
$N_u$	Tensile load on shear connector
$P_i$	Transverse seismic load ordinate
$P_{cr}$	Critical buckling load
$P_{nt}$	Nominal tension yield force in member
$P_{nc}$	Nominal compression strength in member
$P_s$	Axial tension force in shear stud
$P_u$	Ultimate axial force
$P_{ye}$	Expected yield force
$P_{y\_stud}$	Axial yield force in shear connector
$q(x)$	transverse load function per span
$Q_d$	Characteristic strength of ductile end cross frame with system effects
$Q_{dt}$	Characteristic strength of overall system with elastic substructure
$r$	Radius of gyration
$R_i$	Support reaction at substructure $i$
$S$	Site soil coefficient
$SF$	Scale factor
$t$	Deck thickness
$t_w$	Thickness of web
$t_{ws}$	Thickness of web stiffener
$T$	Period, axial force
$T_{eff}$	Effective period
$U_i$	Degree of freedom $i$ in multispan bridges
$v_i$	Translational displacements at degree of freedom $i$
$V_i$	Shear force corresponding to moment developed deck-girder joint in the failure zone
$V_{sa}$	Shear strength of shear connector
$V_y$	Yield strength of ductile end cross frame
$V_u$	Shear load on shear connector
$w$	Weight per unit length of superstructure
$W$	Tributary weight of the superstructure at support cross frames

$x$	Vector for location of support cross frames, distance from support
$\alpha$	Parameter in Single-Mode Spectral Method, ratio of superstructure to substructure stiffness
$\beta$	Parameter in Single-Mode Spectral Method
$\beta_i$	Equivalent viscous damping of end cross frame
$\Delta_{ecf}$	Transverse displacement at ductile end cross frame
$\Delta_{y\_stud}$	Axial yield displacement of steel shear connector
$\gamma$	Parameter in Single-Mode Spectral Method
$\theta_{ecf}$	Rotation of the girder at ductile end cross frames about longitudinal axis
$\theta_{y\_joint}$	Yield Rotation at the studded deck-girder joint
$\theta(\bar{x})$	Rotation of the studded deck-girder joint along the span
$\mu$	Displacement ductility
$\xi$	Viscous damping as a ratio of critical viscous damping
$\phi$	Strength reduction factor
$\Gamma$	Consistent load vector
$\Omega$	Overstrength factor

# Chapter 1 INTRODUCTION AND BACKGROUND

## 1.1. Introduction

Steel bridges are generally considered to perform well in earthquakes, and the implication is often made that they should be used more frequently in seismically active regions. It seems that this argument is based on the fact that few, if any, steel bridges have collapsed in earthquakes in the United States, in contrast to the performance of concrete bridges.

If a steel bridge is defined as one with a steel superstructure and a steel substructure, there are very few of these in the western North America, and even fewer have been subjected to strong ground motions in the last decade or so. However, if a steel bridge includes those with concrete substructures (piers) the population increases significantly, but is still far less than that of concrete bridges (in western North America). Even so, performance data for these bridges is hard to find, and especially for bridges subject to strong shaking (experience from recent North American earthquakes is generally for bridges in areas of low-to-moderate shaking).

Nevertheless, it can be inferred from this data, that steel bridge superstructures are susceptible to damage, even during low-to-moderate shaking, and appear to be more fragile than concrete superstructures in this regard. Typical damage includes unseated girders and failures in connections, bearings, cross-frames, and expansion joints. In a few cases (notably during the Kobe earthquake) major gravity load-carrying members have failed, triggered in some instances, by the failure of components elsewhere in the superstructure (a bearing for example).

It may therefore be argued that the reputation enjoyed by steel bridges is due to the fact that very few steel bridges have been subjected to strong ground motion, and the absence of collapse may be due to a lack of exposure rather than the inherent capacity of steel bridges. Supporting this view is the observation that, damage during low-to-moderate shaking shows a degree of fragility in steel bridges not seen in concrete superstructures.

It is important to note in this argument that seismic design specifications for bridges in the United States do not require the explicit design of bridge superstructures (concrete or steel) for earthquake loads. The assumption is made that a superstructure that is designed for gravity loads has sufficient strength, by default, to resist in-plane earthquake loads. This assumption appears to be justified for concrete box girder superstructures, which are heavier and stiffer than their steel counterparts, but may be unfounded for certain types of steel superstructures, such as a trusses or a slab-and-girder superstructures, both of which may be flexible in-plane.

Improvement in the seismic performance of steel bridges appears to be warranted, along with design guidelines for both steel sub- and super- structures. Better insight is required regarding the load path as well as the capacities of individual components and assembled systems. Applications of innovative technologies, such as ductile end cross frames (or diaphragms) and other embedded

energy dissipators deserve further study. This report describes the behavior of steel plate girder superstructure under lateral loading and presents the State-of-the-Art knowledge on the seismic behavior of steel plate girder bridges supported on seat type abutments and dropped caps.. Recent analytical and experimental investigations as discussed in this report show that several components of steel plate girder bridges should be explicitly designed to transmit lateral forces. Chapter 2 of this report presents proposed provisions and commentary for the seismic design of steel superstructures with seat type abutments and dropped caps.

## 1.2. Seismic Design Specifications for Steel Bridges

The AASHTO LRFD Specifications (2007) for the seismic design of steel bridges are relatively limited compared to those for concrete bridges. This is partly because the Specifications assume that all bridge superstructures have sufficient in-plane strength by default, and remain elastic during the design earthquake. Thus no special provisions are required for their seismic design, apart from those requiring a continuous load path be identified and designed (for strength). Whereas this may be a satisfactory approach for concrete superstructures (especially box girders), it is not necessarily true for steel plate girder bridges, as seen in the damage described later in this report.

Specifications for the seismic design of steel superstructures are therefore required, and a set of recommended provisions were developed as part of the effort from 1998 to 2001 to develop a new seismic design specification for highway bridges, based on the results of recent research and the performance of bridges in recent earthquakes. Under this AASHTO-sponsored, National Cooperative Highway Research Program project (NCHRP 12-49), a joint venture of the Applied Research Council (ATC) and the Multi-disciplinary Center for Earthquake Engineering Research (MCEER) was established to develop a comprehensive set of recommended provisions for consideration by AASHTO. One subtask of this effort was the development of draft provisions for steel superstructures and a comprehensive set of special detailing requirements was developed for steel components expected to yield and dissipate energy in a stable and ductile manner during earthquake loading.

These draft provisions were not approved by AASHTO at the time, but were subsequently included in a set of *Guide Specifications* for seismic design, that were adopted by AASHTO in 2008 (AASHTO 2008). These Guide Specifications are a legally acceptable alternate to the seismic provisions in the LRFD Specifications. However the LRFD requirements for steel bridges remain to be updated and before such an update is likely to take place, additional research is required regarding those superstructures with yielding components but expected to remain functional (carry permanent and unreduced live loads) immediately following an earthquake.

The Japan Specification for Highway Bridges (Japan 2002) does not specifically mention ductile superstructure as part of an acceptable earthquake resisting system. However, after the observations of steel bridge seismic response in the Kobe earthquake it allows limited secondary hinging in the superstructure, provided careful analysis and design is performed. Bridges are grouped into three Seismic Performance Categories. Seismic Performance 1 bridges shall keep their sound function during an earthquake and remain elastic. Seismic Performance 2 bridges shall sustain limited damage with easy functional recovery. Seismic Performance 3 bridges

sustain no critical damage. The specification follows a two-level design approach. The first level corresponds to an earthquake with high probability of occurrence during service life of the bridge (called Seismic Motion Level 1). The second level corresponds to a strong but less probable earthquake that can cause critical damage (called Seismic Motion Level 2).

Depending on their importance, bridges are classified into two groups. Class A bridges are of standard importance and important bridges are included in Class B group. Both Class A and B bridges shall be designed for Seismic Performance 1 during Seismic Motion Level 1. Class A bridges shall also be designed for Seismic Performance 3 under Seismic Motion Level 2, while Class B bridges shall be designed for Seismic Performance 2 under Seismic Motion Level 2.

This specification limits non-linearity in the superstructure to controlled secondary plastic hinges in Seismic Performance 2 and 3. It also states that due to insufficient research, plastic hinging in steel superstructures remains unclear and, as a result, careful investigation on allowable ranges of plastic behavior are necessary. Section 14.2.1 “Strength and Allowable Displacement” of the JRA Specifications states that, due to a lack of accumulated research results and experimental data, many issues still remain unclear concerning the ultimate strength and deformation of steel superstructures subjected to reciprocated loading during an earthquake. Analysis of steel superstructures under these loading conditions are to take into consideration the ultimate strength and deformation performance of steel in the plastic range and should be compared to applicable experimental and testing results.

Section 14.2.2 “Structural Details” of the JRA Specifications states that vertical reinforcing steel members shall be placed above support locations where local deformations are likely to occur due to concentrated loading, an example is shown in Figure 1-1. Also, in order to transfer inertia forces between girders and reduce in plane deformation, the lower ends of the cross frame or diaphragm shall be placed as close to the bottom flange of the girders as possible, as shown in Figure 1-2.

Section 15.2 (2) “Design Seismic Force for Verification of Bearing Support System” of the JRA Specifications states that, for a structure capable of resisting a seismic force without loss of function (Type A bearing support subjected to Seismic Motion Level 1), the design horizontal force,  $H_B$ , shall be equal to the inertia force calculated using the proper design horizontal seismic coefficient (defined in Sections 6.3.3 and 4.4 of the JRA Specifications) and applying the force as shown in Figure 1-3. In order to prevent large differential displacement between the substructure and superstructure, excessive displacement stoppers are also required.

Appendix I of this report presents a summary of seismic specifications and codes that are related to steel plate girder bridges. As can be seen from this summary, the information on the seismic analysis and design are scattered among many of these specifications in addition to many research reports and papers.

### **1.3. Objectives and Scope**

The objectives of this study are to:

- Present the *state-of-the art* summary of knowledge and research related to the seismic analysis and design of steel plate girder bridges.
- Develop code language and commentary that can be adopted in the AASHTO LRFD Specifications.
- Develop two design examples that show how the proposed language can be used in the seismic analysis and design of steel plate girder bridges.

To achieve these objectives, Chapter 1 of this report discusses related research to the seismic behavior and design of steel plate girder bridges. Chapter 2 presents the proposed language and commentary for the seismic design of steel plate girder bridges. Chapter 3 presents detailed seismic analysis and design examples for a single span and two span continuous steel plate girder bridge with a single column bent and a dropped cap. Appendix I presents summary of all existing seismic specifications that are related to steel plate girder bridges.

### **1.4. Performance of Steel Bridges during Recent Earthquakes**

Steel plate girder bridges have generally suffered minor/moderate damage in past earthquakes compared to the significant damage suffered by concrete structures. However these earthquakes have identified vulnerable components in the superstructure and substructure, which should be designed and detailed to resist seismic demand.

#### **1.4.1. Behavior of Steel Bridges during the Petrolia Earthquakes**

In 1992, three earthquakes of magnitudes 7.0, 6.0 and 6.5, respectively occurred in a 24-hour period near the town of Petrolia in Northern California (Caltrans 1992). These earthquakes caused notable damage to two steel plate girder bridges, the first being the Southbound Van Duzen River Bridge. In this straight steel plate girder bridge, buckling was observed at the end cross frames and the horizontal bracing. In addition, there was spalling of concrete at the connection of the reinforced concrete deck and top flange of the steel girders at the end of one span, indicating insufficient shear connectors in this region.

The second steel plate girder bridge damaged during the Petrolia earthquakes was the South Fork Eel River bridge, a curved steel girder bridge located 30 miles from the epicenters, 10 miles further than any other highway structure with reported damage. It suffered considerable damage including buckling and fracture of end cross frames and their connections and also damage at the hinge locations. The damage had a large impact on the service load capacity of the bridge causing large observed deformations during the passage of trucks.

This earthquake highlighted the significance of shear connectors in transferring the lateral inertia forces that are generated by the mass of the deck. These connectors should have sufficient strength to transfer the lateral force to the steel girders. In addition, it showed that the abutment and bent/pier cross frames play an important role in transferring the lateral forces to the bearings. It also showed the potential of allowing these cross frames to yield and buckle in a controlled manner and in doing so, dissipate energy from the earthquake

#### **1.4.2. Behavior of Steel Bridges during the Northridge Earthquake**

During the 1994 Northridge earthquake several steel plate girder bridges suffered structural damage (Astaneh-Asl, 1994). Most of these bridges were located along Interstate 5 near the center of Newhall in Southern California. This region is located where the rupture of the causative hidden thrust fault would have projected to the surface. The nearest observation of the ground motions was recorded at Newhall and showed peak ground accelerations of 0.63g and 0.62g in the horizontal and vertical directions respectively. Typical damage included anchorage failure of bearings on the abutments, pier caps, as shown in Figure 1-4, causing damage to the substructure at these locations. Observed bearing damage coupled with relatively small seat widths, based on modern standards, almost caused unseating of the superstructures in some of these bridges. Typical damage in the superstructures included buckling of end cross frames or fracture of the connections between the end cross frames, gusset plates and web stiffeners as shown in Figure 1-5. In the case of the Pico-Lyons over-crossing there was no positive connection between web/bearing stiffeners and the bottom flange of the girders at the end cross frame locations. As a result, the web was damaged at the termination of the weld between the web and the stiffener as illustrated in Figure 1-6. For these bridges there was minimal observed damage to the columns and piles indicating that much of the displacement demand was accommodated in the superstructure of each of these bridges.

#### **1.4.3. Behavior of Steel Superstructure during the Hyogoken-Nanbu ‘Kobe’**

##### **Earthquake**

The Hyogoken-Nanbu earthquake occurred near Kobe, Japan in January 1995 Extensive damage was suffered by numerous bridges in the area of severe shaking and, as a result, many major roads and rail lines were closed from Kobe to Osaka, due to damaged or collapsed bridges.

The concentration of steel bridges in the area of severe shaking was considerably larger than for any previous earthquake in recorded history. Damage was suffered by many steel piers, bearings, seismic restrainers, and superstructure components and some spectacular collapses resulted from this damage (Ministry of Construction, 1995, Shinozuka et.al., 1995, and Bruneau et al., 1996). This damage is particularly relevant to the Central and Eastern United States where steel bridges are more common than in Western United States, where bridges are mostly of concrete box girders. The damage suffered by short- and medium-span steel bridges can be grouped according to the following categories:

- *Superstructure*: The lateral displacements observed for bridge spans that were unseated from their bearings (but not from their supports) was often impressively large, sometimes producing localized severe lateral-bending of the steel girders and even rupture of the end cross frames. Tensile fracture of the bolts connecting end cross frames to the main girders, and fracture through the cross frame extension haunch near the tip of the haunch, was typical in such cases as shown in Figure 1-7
- *Bearings*: Bearings suffered a considerable amount of damage during this earthquake. Frequently they were the second structural element to fail following major substructure damage, but many also failed even though the substructure remained intact.
- *Seismic Restrainers*: While many restrainers worked effectively during this earthquake, and prevented simply-supported spans from being unseated, numerous restrainers showed signs of plastic yielding and/or buckling. Others were strained to their limit, often due to excessive sub-structure displacements, and failed.

## **1.5. Behavior of Steel Plate Girder Bridges under Lateral Loading**

Steel plate girder superstructures consist of several components that lie in the lateral seismic load path. These components are required to transmit the lateral forces to the supports. Any premature failure of these members may cause inadequate seismic response, and therefore, it is important to identify the load path in steel plate girder bridges for earthquake response in both the transverse and longitudinal directions. Subsequently, critical components in the load path should be modeled and designed to achieve optimal performance of the system during an earthquake.

### **1.5.1. Seismic Modeling of Steel Plate Girder Superstructures**

When calculating the lateral period of plate girder bridge, it is common practice (Priestley et. al. 1995, Buckle et. al. 1986) to model the superstructure (deck and girders) as an equivalent beam supported on columns, with or without foundation springs. The effective transverse stiffness of this equivalent beam is calculated considering that the deck and girders act as a single cross-section. While this approach is acceptable for concrete bridges and box-girder superstructures, it may not be adequate for some types of plate girder bridges. Typically in such bridges, the concrete deck is supported on I-shape beams interconnected by a few discrete cross frames, and the mechanism by which the seismically-induced inertia forces at the concrete slab level is transmitted to the bearings can be quite different from that assumed by the equivalent beam model. The magnitude of this difference is determined by the effectiveness of the cross frames, and can be quite large in bridges having flexible cross frames. It is important to represent the lateral stiffness of the superstructure correctly since it has a direct impact on the bridge period and consequently on the level of earthquake excitation in the superstructure, bearings and substructure.

A first step towards understanding the behavior of these bridges is to study a bridge without cross frames. Such a model would be valid for bridges having severely corroded cross frames, or with only nominal cross frames (such as single channels bolted along their web) as frequently

encountered in Eastern United States. Likewise, bridges having cross frames with non-ductile connection details could potentially become bridges without cross frames, once brittle failures develop in these connections.

The lateral behavior of such plate girder bridges of various span lengths was investigated by Zahrai and Bruneau (1998a). The calculated period of the first lateral mode of vibration, which gives rise to maximum drift in the superstructure, as well as spectral acceleration required to produce first yield, are presented by Zahrai and Bruneau (1998a), as a function of span length, along with comprehensive analytical expressions that capture that behavior. Although these response parameters vary non-linearly as a function of span length in a complex manner, the general trend is that the lateral periods and maximum lateral deflections are very large compared to values typically reported for plate girder bridges in the literature, reflecting the extreme flexibility of the superstructure in the absence of cross frames. The concrete deck displaces laterally nearly as a rigid body, while the flexible steel girders twist and deform laterally as necessary, spanning between the deck and the supports. Closer examination of the steel beams reveals that they are most severely distorted near the supports. Indeed, in each girder, the bearing supports are the only points which can counteract the lateral deformation of the web and hold the lower flange under the deck.

Analytical and experimental investigations have revealed the key role played by the end cross frames to ensure an adequate load-path in plate girder bridges. For bridges with cross frames, analyses have shown that even a set of frames with low lateral stiffness is sufficient to make the entire superstructure behave as a unit and remain in the elastic range. However, a dramatic shift in seismic behavior occurs once an end cross frame ruptures, involving a sizeable elongation of the lateral period and a corresponding increase in drift.

### **1.5.2. Lateral Load Path and Effect of Composite Action**

Earthquake loading in the transverse direction causes transverse bending of the superstructure, resulting in transverse reactions at the abutments and piers. Since the reinforced concrete deck and railings typically account for about 80% of the weight of a steel plate girder bridge, the majority of the inertia loads are generated in the deck slab. Furthermore, the bearings are attached to the bottom flange of the girders, therefore, the inertia loads must be transferred from the slab to the bearings through various components in the superstructure. Numerical analyses have shown that the loads are largely distributed through the superstructure at the ends of each span rather than along the length of each span. The forces are then distributed vertically through the cross frames at the piers and abutments to the bearings (Itani and Rimal 1995 and Zahrai and Bruneau 1998a). Since the primary function of the bearings is to allow the bridge to expand and contract longitudinally due to temperature variation, the bearings usually permit movement only in the longitudinal direction and are restrained in the transverse direction. Thus, the transverse shear forces in the bearings are transferred to the abutments and piers through these restraints (shear keys or guide bars). If the bearings are also restrained in the longitudinal direction, as in the case of rotation-only bearings (i.e., pinned bearings), then longitudinal forces may also be transmitted to the abutments and piers.

For longitudinal ground motion, the inertia forces are transferred from the deck into the girders using shear connectors along the length of the bridge. From the girders, the loads are transferred into the bearings and substructure. Longitudinal deformation in the bearings are typically limited by the abutment once the expansion joint has closed and, for longer span bridges, by restraints at the piers which are activated after the limit of the bearing deformation.

For earthquake ground motions in the longitudinal direction, the inertia forces can be distributed from the deck into the steel girders through the shear connectors along the entire length of the bridge since the shear connectors run parallel to the direction of loading. However, in the transverse direction, the distribution of forces in the shear connectors varies along the length of the bridge.

Numerical analyses have been performed on a typical four span, four girder, steel plate girder bridge in order to investigate the effect of composite action in the transverse response of a bridge. The bridge was modeled as fully composite along the entire length with shear connectors on the top flange of each girder in both positive and negative bending moment regions in accordance with the AASHTO LRFD Bridge Design Specifications (AASHTO, 2006). Application of transverse earthquake loads showed that the transverse shear forces in the shear connectors were very high within, approximately, 39 in. of the ends of each span but were negligible along the remaining length of each span. This behavior is consistent with observations made during an ultimate load test on a single span bridge model by Carden et al (2001), shown in Figure 1-8. It is apparent that most of the transverse loads are transferred from the deck to the substructure at the immediate ends of each span, highlighting the importance of composite action in this region. Although, for this bridge model, the finite element analyses showed that the maximum forces in the shear connectors were about 50% of their design strength at the ultimate limit state of the columns, the concentration of forces may be damaging in other bridges.

Many straight bridges have no shear connectors in the negative moment regions due to fatigue concerns when welding studs to the tension flange of a steel girder. A second numerical model was used to investigate the impact on the load path when there are no shear connectors in this region. In this model, large forces were found to occur in the shear connectors at the transition from positive to negative moment (i.e., at the points of contraflexure) where the composite region ended. Since additional shear connectors had been placed at these points to help make the transition from composite to non-composite action, the forces in the shear connectors were, in fact, below design levels. However, the load path from the contraflexure points to the piers was now through the girders and large weak-axis bending moments were induced in each non-composite girder. When combined with gravity load stresses, the resulting stresses caused nonlinear behavior in the girders before the plastic capacities of the columns were reached. When there is no composite action between the deck and the girder in the negative moment regions, the intermediate cross frames between the contraflexure points and the ends of each span become important elements in the lateral load path and should also be explicitly designed for earthquake loads.

To ensure a favorable load path, it is recommended that adequate composite action be provided between the girders and the deck for transverse earthquake loading along the full length of the girders and, if this is not possible in the negative moment regions, the top chord of the end cross frames should be made composite with the deck. As shown later, this technique can be very effective in transferring the earthquake loads directly from the deck into the cross frames and then to the bearings. Such a load path by-passes the intermediate cross frames, the girders between the contraflexure points, and the abutments or piers, and significantly reduces the demand on these elements. This connection should be designed to carry the full earthquake shear at the abutments or piers. Note that if the top chord of the cross frame is made composite in the negative moment regions, while the girders are non-composite with the deck; this chord is likely to be subjected to stresses in the longitudinal direction due to service loading on the bridge. These stresses should be accounted for in the design of the composite connection. Consequently, it is recommended that, in high seismic zones, the girders be made fully composite in both the positive and negative moment regions.

## **1.6. Behavior of End Cross Frame under Lateral Cyclic Loading**

### **1.6.1. Types and Configurations of Bridge Cross Frames**

#### **1.6.1.1. Introduction**

The AASHTO Specifications (AASHTO 2007) specify that cross frames or diaphragms may be placed at the ends of the structure, across interior supports, and intermittently along the span. Experimental and analytical investigations showed the importance of end cross frames in steel plate girder bridges in transferring the lateral seismic loads to the bearings. These results also showed that with proper attachment of the R/C deck to the cross frames over support locations, the intermediate cross frames along the span are not subjected to significant seismic forces.

AASHTO specifications define the cross frame as a transverse truss framework connecting adjacent flexural components used to transfer and distribute vertical and lateral load and provide stability to the compression flange. On the other hand, the diaphragm according to AASHTO is defined as vertically oriented solid transverse member connecting adjacent longitudinal flexural components to transfer and distribute vertical and lateral loads and provide stability to the compression flanges. The cross frames over support locations can be divided into two main types: 1) abutment cross frames and 2) bent/pier cross frames. The main difference between the two types is that the top chord of the abutment cross frame needs to support wheel loads due to the discontinuity of the R/C deck.

There are no standard specifications or details for the design of cross frames and diaphragms. Typical support cross frame consists of top chord, diagonal braces, and bottom chord. Variations exist between several parameters of cross frames:

- Pattern of diagonal braces: X, V, inverted V (chevron), or Z.
- Member cross section: single angle, double angles, T, or double channels.
- End connection detail: welded or bolted.

Figure 1-9 and Figure 1-10 show bent cross frames with V and X patterns for the diagonal braces, respectively. The diagonal members are made of single angles while the chord members are made of double angles. Figure 1-11 and Figure 1-12 show abutment cross frames with a V-pattern for the diagonal. The diagonal members are made of single angles while the top chord and the bottom chords are made of W-shape sections. Figure 1-13 shows diaphragms with a built I-sections and transverse stiffeners while Figure 1-14 shows a rolled shape section diaphragm.

Figure 1-15 to Figure 1-17 show the details of cross frames with inverted V-pattern for diagonal braces and their welded end connections. Figure 1-18 to Figure 1-20 show the details of cross frames with X-pattern for diagonal members and their welded end connections. Figure 1-21 to Figure 1-23 show details of cross frames with X-pattern for diagonal braces and their bolted connections.

All the above figures show that the cross frames and diaphragms can have large number of variations and end details. Based on discussions with many bridge designers and steel fabricators Gatti (Gatti 1993) compiled preferred details for various types and patterns of cross frames. Figure 1-24 shows preferred details for abutment cross frames, while Figure 1-25 shows preferred details for intermediate cross frames when they are subjected to large forces such as the case in tightly curved bridges. When intermediate cross frames are not subjected to large forces such as the case in straight bridges it is preferred to eliminate the gusset plate from the end connection and attach the cross frames directly to the transverse stiffener of the plate girder as shown in Figure 1-26. It is important to note here that in this case, many designer prefer not to use the top chord. Figure 1-27 shows the preferred details at bent locations which all the members of the cross frames are welded to gusset plates which in turn are bolted to the transverse stiffener of the plate girder.

Due that lack of information on the seismic response of cross frames bridge designers started to use R/C diaphragms that are monolithic to the R/C deck. This detail will transfer the seismic forces and does not subject the shear connectors on the plate girders to significant seismic forces. Figure 1-28 shows the diaphragm detail that was used on the steel alternative design of I5/SR14 interchange (Itani and Reno, 1994). Also, Figure 1-29 shows the detail that is used in the State of Tennessee in which steel cross frames are used during the erection of the steel plate girders then the R/C diaphragm will be cast at a later stage.

#### **1.6.1.2. Attachment of R/C Deck to Steel Plate Girders and Cross Frames**

To achieve composite action in the positive flexure regions shear connectors are used in that zone. These connectors are designed for fatigue and checked for strength based on the ultimate axial capacity of the plate girder and the effective width of the deck. The shear connectors are then spaced according to governing case. Analytical and experimental investigations by Carden

et al (Carden 2004) show the importance of shear connectors in transferring the seismic forces to the substructure. This investigation showed that the shear connectors at support locations will be subjected to shear and axial forces. If these connectors are not designed for such forces they may fracture and thus alter the load path. As mentioned earlier, it is interesting to note here that some state Department of Transportations do not allow shear connectors to be placed in negative moment zones due to presumed fatigue problems. This practice will have a detrimental effect on seismic force transfer to bents since the inertia forces in the deck will be transferred through the weak axis bending of the noncomposite plate girder. Furthermore, the intermediate cross frames will be subjected to significant seismic forces and may cause their failure if they are not designed for.

Figure 1-30 shows the kinematics of a support cross frame where the shear connectors are placed on the top of the plate girders under lateral loads. As the the plate girder undergoes lateral displacement the top and the bottom chords will be subjected to combined axial and bending effects. Furthermore, the shear connectors will be subjected to combined axial and shear. To facilitate the transfer of the lateral forces over bent locations, some bridge engineers connect the top chord to the R/C deck through shear connectors. Figure 1-31 shows the kinematics of a support cross frame where the shear connectors are placed on the top chord. As the plate girder undergoes lateral displacement, the shear connector of the top chord will be subjected to axial and shear forces. The chord member will be subjected mainly to flexure and axial forces.

## 1.6.2. Behavior of Shear Connectors under Shear and Axial Forces

### 1.6.2.1 Connectors under Shear Forces

The fatigue resistance and strength limit states of shear connectors are specified in the AASHTO LRFD Specifications (AASHTO 2004). The strength limit state of shear connectors was based on 48 two-slab push-out specimens that were conducted by Ollgaard et al (1971). Figure 1-32 shows one of the test specimens that was used for this investigation. The main purpose of their investigation was to evaluate the capacity and the behavior of stud shear connectors embedded in normal and light weight concrete. The main conclusion that was drawn from the study was that the shear strength of the stud embedded in normal and light weight concrete is influenced by the concrete compressive strength and the modulus of elasticity. The following empirical function described the test results:

$$Q_u = 1.106 A_s f_c'^{0.3} E_c^{0.4} \quad (3)$$

while the following the following simplified equation was used for design purposes in AASHTO Specifications:

$$Q_r = \phi_{sc} Q_n = 0.85 \times 0.5 A_{sc} \sqrt{f_c' E_c} \leq A_{sc} F_u \quad (4)$$

where  $A_{sc}$  is the area of the connector,  $f_c'$  is the concrete strength in ksi,  $E_c$  is the concrete modulus of elasticity in ksi, and  $F_u$  is the tensile strength of the connector. Also, the

specifications provide detailing requirements for minimum transverse and longitudinal spacing equal to  $4d_{sc}$  and  $6d_{sc}$  respectively. In addition, the specifications require that the clear depth of the concrete cover over the tops of the shear connector should not be less than 2.0 in. while the connector should penetrate at least 2.0 in. in the concrete deck.

### 1.6.2.2. Connectors under Axial loads and Combined Tension and Shear Forces

Section 6 of the AASHTO LRFD Specifications does not have any provisions for the tension capacity limit state of shear connectors. Appendix D of ACI 318-05 code (ACI 2005) provides the ultimate capacity of studs anchored in concrete. This document describes various modes of failure in both tension and shear of the stud-concrete joint. Depending on the size, length, spacing and edge distance, the failure mode may occur in the stud or in the concrete.

The limit states for a stud anchored in concrete under tension loading are:

- Steel strength of stud in tension
- Concrete breakout strength of stud in tension
- Pullout strength of stud in tension

The steel strength of stud in tension is:

$$N_{sa} = A_{sc} F_y \quad (5)$$

where  $F_y$  is the specified tensile strength of the anchor and  $A_{sc}$  is the cross sectional area of the stud.

The concrete breakout strength of a stud based on failure cone surface as shown in Figure 1-33 is calculated from the following equation:

$$N_b = 24\sqrt{f'_c} h_{ef}^{1.5} \quad (6)$$

where  $h_{ef}$  is the embedded length of the studs in inches and  $f'_c$  is the compressive strength of concrete in psi. For a group of studs the concrete breakout strength as calculated above is modified by the area of the overlapping failure cones.

The pullout strength of a stud in tension is expressed as:

$$N_p = 8A_{brg} f'_c \quad (7)$$

where  $A_{brg}$  is the bearing area of the stud head in units of  $\text{in}^2$ .

The ACI document also provides limit states for a stud anchored in concrete under shear loading, they are:

- Steel strength of stud in shear.
- Concrete breakout strength of stud in shear.
- Concrete pryout strength of stud in shear.

The steel strength of stud in shear is:

$$V_{sa} = A_{sc} F_u \quad (8)$$

where  $F_u$  is the specified tensile strength of the anchor and  $A_{sc}$  is the cross sectional area of the stud, which is similar to the AASHTO equation.

The concrete breakout strength of a stud is governed by the edge distance. Since the bridge shear connectors over the girder flanges are placed well away from the concrete edge. Therefore, the limit state of concrete breakout in shear failure will not govern the design of shear connectors. The concrete pry-out strength of a stud in shear is equal to concrete breakout strength in tension for studs 2.5 in. and shorter. For longer studs the concrete pryout capacity in shear is twice the concrete breakout strength in tension.

For combined tension and shear, the ACI document provides an interaction equation. The shear-tension interaction is expressed as:

$$\left( \frac{N_u}{N_{sa}} \right)^\zeta + \left( \frac{V_u}{V_{sa}} \right)^\zeta \leq 1.0 \quad (9)$$

where  $\zeta$  varies from 1 to 2. ACI recommends a trilinear curve that is a simplification of the above expression with  $\zeta = 5/3$ . It also states that for the combined effect of axial and shear forces, the sum of ratio of demand over capacity for shear and tension should not exceed 1.2 as:

$$\frac{N_u}{N_{sa}} + \frac{V_u}{V_{sa}} \leq 1.2 \quad (10)$$

### 1.6.2.3. Behavior of R/C Deck and Plate Girder Studded Joint

The shear connectors over the top flange of steel girders create a moment connection in the deck for the out-of-plane bending moment about the bridge longitudinal axis. Figure 1-34 shows a transverse section of the moment connection at the deck and plate girder joint. Since the transverse shear forces are higher than the longitudinal forces in the shear connectors near the ends, as shown in Figure 1-35 and Figure 1-36, the longitudinal shear forces in the studs are not considered here. In order to calculate the ultimate capacity of this moment connection per unit length of the span, the section included all the studs and concrete that are present over a strip of

unit length. The studed joint may be analyzed as a short reinforced concrete beam section with studs as reinforcement. Assuming the distance from the tension reinforcement to center of the concrete compression block is very close to the distance between the outer studs, then ultimate moment capacity of this section can be estimated by:

$$M_u = N_{sa}d \quad (11)$$

where d is the transverse spacing of the studs.

Referring to Figure 1-34 the moment that is developed in the studed connection as a result of the transferred shear F is:

$$M = F\left(h + \frac{t}{2}\right) = Td \quad (12)$$

where h is the haunch thickness, t is the deck thickness, T is the tensile force developed in the stud, and d is the stud spacing. Therefore, the ultimate shear force that would cause axial tension failure in the outer stud is:

$$F_{ult\_axial} = \frac{N_{sa}d}{\left(h + \frac{t}{2}\right)} \quad (13)$$

and the ultimate shear force on the connection to cause shear failure in the studs is:

$$F_{ult\_shear} = 2V_{sa} \quad (14)$$

In order for the axial failure in one of the studs to occur before the shear failure:

$$F_{ult\_axial} < F_{ult\_shear} \quad (15)$$

$$\frac{N_{sa}d}{\left(h + \frac{t}{2}\right)} < 2V_{sa} \quad (16)$$

Since due to stud size, length, and spacing concrete breakout failure does not occur and the ultimate axial ( $N_{sa}$ ) and shear ( $V_{sa}$ ) capacities of the studs are the same. Hence:

$$d < 2h + t \quad (17)$$

This requirement is almost always met in typical steel girder bridges for non-seismic loads. Therefore, if the concrete breakout strength as shown in Figure 1-33 is larger than the steel tensile strength of the stud, the tensile failure of studs will precede shear failure.

### 1.6.3. Behavior of Cross Frame under Lateral Loading

Support cross frames at abutments and bents transfer the seismic forces to the substructure. Therefore, it is important to understand the behavior of various components of cross frames, chords and diagonal members under lateral forces. Another advantage of the diagonal members of the cross frames is that they may act as a “fuse” by controlled buckling and yielding to dissipate the input energy. All the other components of the cross frames should be designed to stay elastic. Limit state analysis is normally used to for such system to protect the elastic members and limit the inelasticity to the diagonal members that are specially designed and detailed.

#### 1.6.3.1. Behavior of Special Diagonal Members

As discussed before, the diagonal members of cross frames can have several patterns and cross sections. The most common economical cross section of the diagonal members is the single angle section. These members are commonly used as braces in building construction in seismic zones. IBC 2006 and CBC 2007 recognize the Special Concentric Braced Frame System (SCBF) as an acceptable framing system that can be used in high seismic zones. The lateral response of SCBF can be similar to the end cross frames in plate girder bridges. During seismic events, the end cross frame will deflect through horizontal displacement creating axial forces in the diagonal members. Assuming that the lateral displacement is equal to  $\Delta$  and the axial displacement in the diagonal member is  $\delta$ , the yield displacement of the axial member is:

$$\delta_y = \frac{F_y L}{E} \quad (18)$$

where L is the length of the axial member.

Based on the depth of the girder, D, and the spacing of the girders, S, a relationship can be derived between  $\Delta$  and  $\delta$ . This relationship is assuming that the top and bottom chords are pin ended:

$$\delta = \Delta \cos \alpha \quad (19)$$

where  $\alpha$  is the inclination of the diagonal members. Assuming that the lateral drift in the end cross frame is equal to 4%, and using  $F_y = 36$  ksi and 50 ksi where the expected yield stresses are  $1.5 \times 36 = 54$  ksi and  $1.3 \times 50 = 65$  ksi, then the limitation on the girder depth to girder spacing for

various displacement ductility is shown in Figure 1-37. Figure 1-38 and Figure 1-39 show the free body diagrams of the two types of the cross frame where the R/C deck is attached to the top of the plate girders and the R/C deck is attached to the top chord of the cross frames.

The overall seismic behavior of cross frames is affected by the diagonal braces. Axial members under cyclic loading have been investigated by a number of researchers over the past thirty years. These members play an important role in braced frames since they significantly contribute to their strength and stiffness. Based on past experiments, the qualitative and the quantitative features of the seismic response of these members are well understood for building structures. However, the dimensions and the details that are used in building structures differ from those of bridge structures. Therefore, it important to study the behavior of diagonal members similar with aspect ratio (girder depth/girder spacing) that can be found in bridge structures.

Carden et al (2004) conducted cyclic axial experiments on 17 single angle members, with various dimensions and different end details. The angles came from three different batches of ASTM A36 steel, with ASTM coupon tests performed on a flat bar specimen from each of the three batches. Different lengths were used to represent the full and half lengths of the diagonal members in X-braces, resulting in specimens with different  $Kl/r$  and  $b/t$  ratios.

A 1.0 in. thick gusset plates were used in the experiments to promote formation of plastic hinges in the angles rather than the gusset plates during buckling. This was expected to more accurately represent the behavior diagonal members in bridge cross frames. The end conditions of the specimen varied between bolted and welded connections. The welded specimens used balanced welds, whereby the length of the weld on each side of the angle was equal to inverse of the relative distance from each edge to the centroid of the angle. The balanced welds resulted in the edge at the outstanding leg of the angle being connected with a full length weld between the gusset plate and the angle while the other edge was welded along approximately half of this length. These were designed to minimize stress concentrations in the connected leg when axial loads were applied to the member.

Each specimen was subjected to cycles of alternating tension and compression with amplitudes increasing by 0.25 in. increments of displacement, although, for some of the specimens the initial displacement cycle was larger than 0.25 in., as necessary to observe buckling or yielding of the member. Some of the members were first subjected to tensile actions while others were first subjected to compressive actions, as given in Table 1-2.

The experimental assembly used for the single angle experiments is shown in Figure 1-40. Axial forces were applied to the members using an actuator which was attached to slider to ensure axial loads. The variation in force due to friction in the slider was measured at less than 1 kip and was neglected in the analysis. Axial displacements and forces were measured by the actuator.

Force-displacement traces for each single angle experiment are shown in Figure 1-41 to Figure 1-45. The shape of the observed hysteresis loops is similar for each experiment and comparable to those observed in the past for single and double angles (Jain 1980, El-Tayem 1986, and Itani 1991). In tension, the members yielded followed by a post-yield increase in strength due to cyclic and strain hardening. In compression, the members buckled followed by immediate strength degradation. Stiffness degradation was also observed as the members elongated resulting in an increased displacement for the same tensile force with successive cycles. The number of cycles that each member was subjected to prior to failure differed with the failure mode for each member (Table 1-3) and depended largely on the type of connection. Bolted specimens with unreinforced connections each fractured in the region between the edge and first bolt hole of the connected leg, as illustrated in Figure 1-46. Failure was typically observed much earlier in members with this type of connection than in the other members. With the reinforced bolted connections, which had an increased  $A_n/A_g$  ratio, the failure was moved to outside the connection region. Failure in these members occurred in the plastic hinge formed during buckling at either end of the member (Figure 1-47) with a crack propagating from the edge of the connected leg. The welded connections resulted in an even further improvement in the performance of the angles. These members failed in the plastic hinges formed either at the end of the angle or at midspan as shown in Figure 1-48. The balanced weld appeared to delay the initiation of cracking at the edge of the connected leg due to an apparently lower stress concentration in this region compared to the bolted connections.

The maximum average axial strain is used to describe the maximum deformation in each specimen. The average axial strain was calculated using the axial displacement divided by the length of the member (Table 1-2). This measure of axial deformation, unlike ductility, is independent of the yield displacement which was shown to depend on the loading history and factors such as slippage in the connections and thus was difficult to determine. The maximum strain is also a useful measure as it can be converted to a maximum drift in X-brace assemblies. Table 1-3 shows that the maximum effective axial strain for each specimen ranged from 3% to 12%, indicating a large variation in the displacement capacity of the members. Even between theoretically identical members there was up to a 100% difference in their ultimate strains. While there was much variability, distinct factors had an effect on the maximum displacements. An increased  $A_n/A_g$  correlated to an increase in displacement due to prevention of premature failure around the bolt holes. For the welded members, and bolted members where fracture was prevented in the connection region using thickening plates, the maximum effective axial strain was at least 6%, while the bolted members where fracture occurred in the connections had a maximum strain below 6%. These details are recommended for the single angles in ductile end cross frames.

The cumulative plastic strain of each member was calculated to investigate the cumulative plastic deformation capacity. Cumulative plastic strain is defined as the absolute sum of the displacements in excess of the yield displacement divided by the member length for each cycle of deformation in the braces. This is quite different from the true strains in the brace due to the effects of buckling and elongation of the members. In order to define the cumulative plastic strain the yield displacement was calculated based on a theoretical value,  $\delta_y$ , given by:

$$\delta_y = \frac{F_{ye} l}{E} \quad (20)$$

where  $F_{ye}$  is the expected yield stress,  $l$  is the length between the centroid of the connections, and  $E$  is the elastic modulus of the steel member.

The cumulative plastic ductilities for each specimen are given in Table 1-3. Because of the increasing amplitude loading history there was a correlation between the maximum strains and the cumulative plastic capacity of the specimens. Those members with fracture observed in their connections resulted in cumulative plastic strains between 23 and 82%. All members for which fracture was prevented in the connections resulted in cumulative plastic strains between 113 and 201%, with the exception of Specimen O, which had an unusually high cumulative plastic strain of 596%. This was one of two members that violated the  $Kl/r$  limit of 120, which may explain the large cumulative strain as the buckled behavior was largely elastic resulting in less cyclic plastic deformation in the members, particularly localized deformation in the plastic hinges. Less localized plastic deformation allowed the member to undergo a larger number of cycles, however it made the member less effective as an energy dissipater than one that undergoes inelastic buckling. Furthermore, the slender properties resulted in a large variability in response as illustrated when Specimen O is compared to the theoretically identical Specimen N (Figure 1-45). The average cumulative strain for members without connection fracture, neglecting Specimen O, was 146%.

From these experiments it is recommended that single angle members in ductile end cross frames should be designed for a maximum deformation during an earthquake not exceeding 4.0%. Therefore, for the maximum considered earthquake a strain of no more than 6.0%, 1.5 times the design level earthquake, would be expected. This is consistent with the design of an isolation system which should be stable up to 1.5 times the design displacement (AASHTO, 1999) and also the buckling restrained braced frame guidelines which state that a brace should be capable of withstanding building drifts up to 1.5 times the design drift (SEAONC, 2003). The maximum strain limit of 6.0% is less than that for any of the members where fracture was avoided in the connection region, using thickened plates with bolted connections or balanced welded connections.

Tests were performed on coupons taken from single angle members of the same heat numbers as the members used in the bridge model in accordance with ASTM A370 standard coupon test for flat bars. Test 1 was for the heavy single angles with bolted connections, Test 2 was for the heavy single angles with welded connections and Test 3 was for the light single angles. Each set of angles came from a different heat number. The yield strengths from the three tests were 55%, 27% and 36% larger respectively than the minimum specified strength of 36 ksi for the ASTM A36 steel members. The ultimate strength was 50-52% larger than the measured yield stress for each specimen and the elongation at fracture was between 30-35% for each specimen.

The tensile yield point for the single angle specimens is defined as the point where the entire member yields. For a concentrically loaded member subjected to monotonic axial loads, this point can be clearly identified using such limits as the force at 0.2% offset strain. However, for the single angle members subjected to cyclic loads it was more difficult to identify the yield point, firstly; because there was an eccentricity in the connection between the single angles and the gusset plates with the resulting moment causing part of the member to yield before the entire member yielded. Secondly, there was slippage in the bolted connections that resulted in additional axial displacement, effectively reducing the stiffness of the member prior to yielding. In addition, some of the members buckled in compression before being subjected to tension; hence the properties of these members were modified by the formation of a plastic hinge due to buckling. These factors made it impossible to use a consistent method to identify the yield point. The yield point was subsequently identified by inspection at the point where the yield plateau was observed, indicating that the entire member had yielded. The yield force was relatively insensitive to variation in selection of the yield point and prior loading history. The estimated yield forces for each experiment are summarized in Table 1-4. In order to compare the measured yield and ultimate forces with predicted values the nominal yield forces, expected yield force based on the material strength from coupon tests, and the expected yield force based on AISC (2002), were each calculated. The nominal tensile strength is given by (AASHTO, 1998; AISC 2001):

$$P_{ny} = F_y A_g \quad (21)$$

where  $P_{ny}$  is the nominal yield force,  $F_y$  is the nominal yield stress of the material, and  $A_g$  is the gross area of the section, assuming the connections are designed to prevent net section fracture. The expected yield force based on the material strength from coupon tests was calculated by using the actual yield strength of the material from the coupon tests instead of the minimum specified strength in the above equation. The expected force based on AISC (2002) was calculated by multiplying the nominal force by an  $R_y$  factor of 1.5 as specified for A36 steel.

Each of these predicted values are given in Table 1-4. This table shows that the expected yield strength based on coupon tests was within 7% of the measured yield strength. The expected yield strength based on AISC (2002) was typically within 10% of the measured yield force with a maximum difference of 14%. Therefore, while coupon tests are useful to accurately define the expected yield force the  $R_y$  factor resulted in a good estimate for these members. In all cases the strength of the members was above their minimum specified values. The ultimate force or maximum force measured in each specimen was, on average, 21% larger than their measured yield strength, with the maximum difference being 28% (Table 1-3).

The buckling capacity, or maximum compression force, for each specimen is listed in Table 1-4. The buckling capacity was dependent on the material properties, cross sectional properties, effective length of the members and the loading history with members subjected to prior tensile yielding typically having a reduced buckling capacity. The buckling capacity,  $P_{nc}$ , was predicted using AASHTO (1998) (equivalent to AISC (2001)), for the slenderness parameter,  $\lambda$ , greater than 2.25, by:

$$P_{nc} = 0.66^{\lambda} F_y A_g \quad (22)$$

where the slenderness parameter is given by:

$$\lambda = \left( \frac{Kl}{r\pi} \right)^2 \frac{F_y}{E} \quad (23)$$

where  $K$  is the effective length factor and  $r$  is the radius of gyration about the minor principal axis of the angle.

The effective length was dictated by the end conditions. In practice there are two types of end condition which exist, those where plastic hinging due to buckling is expected in the gusset plates, such as for the detail shown in Figure 1-49 (a), and those where plastic hinging will occur in the angles, for example, as for the detail in Figure 1-49 (b) where the stiffener will be restrained by welds to the web and flange causing hinging in the angle member, or in Figure 1-49 (c) where the bottom chord will prevent bending of the gusset plate. The position of the plastic hinge is based on the relative stiffness and flexural strength of the connecting plate and angle members. In most practical cases, the location of the plastic hinges can be determined by inspection of the connection based on the conditions described above. For Specimen A, connected to 0.5 in thick gusset plates, plastic hinging due to buckling was observed in the gusset plates. For the remaining specimens, with the 1.0 in thick gusset plates to simulate the condition where the gusset plates are restrained to prevent bending, plastic hinging was observed in the angle members. While concentric braced frames are typically designed to allow hinging in the gusset plates due to buckling, comparison of Specimens A and B (Table 1-4) show that a rigid gusset plate causing a plastic hinge in the end of the angle resulted in a larger displacement and cumulative displacement capacity. In the past attempts have been made to quantify the effective length factor based on the relative stiffness of gusset plate components (El-Tayem 1986, Astaneh-Asl 1985). El-Tayem suggested an effective length factor of 0.85, with the length defined by the full length of the angles, is appropriate for typical single angle X-brace members with simple gusset plate connections. In that study the plastic hinges at the ends of the members formed during buckling occurred in the gusset plates. In the current study when the plastic hinge due to buckling occurred in the gusset plate an effective length factor of 1.0 was assumed with the length is defined between the centroid of the connections. This is comparable to an effective length factor of 0.85 using the full length of the member and so is consistent with the previous research. Alternatively, when gusset plates were sufficiently rigid or restrained, resulting in plastic hinges in the angles, an effective length factor of 0.7 was assumed. The resulting calculated buckling capacity for each specimen is given in Table 1-4, based on the yield strengths from coupon tests. For specimens not affected by prior tension yielding, the measured buckling strengths were within around 20% of the calculated strengths. As the buckling force was a relatively small part of the overall strength of and X-brace a 20% error in buckling force correlated to a 5 to 10% error in the overall X-brace strength. While more elaborate analyses could be performed for calculating the effective length factor, it is not be considered likely to result in improved accuracy given the variability resulting from the effects of different loading history and such factors. Prior tensile loading typically reduced the buckling capacity of the members by about 20%. Specimen N was the one member first subjected to compression that had a measured strength which differed from the calculated strength by more than 20%. This was

also one of two slender members with a  $Kl/r$  ratio of 181. All other members have a  $Kl/r$  ratio of less than 120. For slender members, the buckling capacity is more sensitive to the effective length factor, while, for non-slender members the capacity is relatively insensitive. Therefore, it is recommended that the cross frame members, being primary members for seismic loading, use the AASHTO (1998)  $Kl/r$  ratio limit of 120. This will prohibit the use of slender members such as Specimen N that have buckling strengths which are sensitive to the effective length. The  $b/t$  ratios defined by AISC Seismic Provisions (2002) for special concentric braced frames should also be satisfied to prevent local buckling.

The area enclosed by each cycle of the hysteresis loops was calculated using a simple algorithm for each specimen and was divided by the rectangular area enclosed by the maximum positive and negative forces and displacements to give the hysteretic area as a ratio of that for an “ideal” system. Analyses of the data show that early cycles have hysteretic energy dissipation of typically 40% of the “ideal” hysteretic area, while for subsequent cycles the equivalent energy dissipation is sometimes reduced to below 20% prior to failure (Figure 1-50). The reduction in energy dissipation can be explained by considering the two primary sources of hysteretic behavior. The first is tensile plastic deformations with increasing amplitude positive displacements. This deformation was largely irrecoverable and essentially only contributed to dissipating energy when positive displacement amplitudes exceeded previous amplitudes, resulting in pinched hysteresis loops and, consequently, a decrease in energy dissipation with repeated cycles. This property causes the amount of energy dissipation for a given cycle to be dependent on the prior loading history. The second, more minor, source of hysteretic energy dissipation in these types of members is from the plastic hinges formed during buckling of the members. The axial force resisted by plastic hinges is dependent on the displacement in the specimen, degrading as displacements increase in compression. Figure 1-50 shows that the members with the larger slenderness ( $Kl/r$ ) ratios have smaller energy dissipation ratios, which supports limiting the slenderness ratio to 120 as discussed in the previous section.

#### **1.6.4. Ductile End Cross Frames Design and Detail Requirements**

Ductile end frames cross are cross frames that are specially designed and detailed to limit the inelastic activity to the diagonal members where as all other components of the cross frames stays elastic. Based on the experimental testing of the diagonal members, the relative drift of the cross frame should be limited to 4% and the axial displacement ductility of the diagonal members should not exceed 12. The diagonal members of the cross frames should be configured either in an X-type or inverted V-type configurations with single or double angle cross section. Only welded connections should be used to connect the diagonal members to the end gusset plates.

In X-type configuration, the diagonal members shall be connected where the members cross by welds. The welded connection at that point should have a required resistance equal to 0.25 times the nominal tensile resistance of the diagonal member. Meanwhile, inverted V-type configuration, the top chord and the concrete deck at the location where the inverted diagonals intersect should be designed to resist the vertical component of the difference between the nominal tensile resistance of the diagonal member and the absolute value of the nominal post-

buckling compressive resistance of the diagonal member taken equal to  $0.3P_n$ , where  $P_n$  is the nominal compressive resistance.

Traditionally, diagonal cross frame member have shown little or no ductility during seismic events. The overall member buckling produces plastic hinges at the mid-point of the member and its two ends. At the plastic hinge, local buckling can cause large strains, leading to fracture at even small deformations. It has been found by many investigators that the diagonal cross-frame members with ultra-compact elements will be capable of achieving significant ductility by forestalling local buckling. Therefore, width thickness ratios of outstanding legs in single and double angles should be limited to:

$$\frac{b}{t} \leq 0.3 \sqrt{\frac{E}{F_y}} \quad (24)$$

In order to minimize the detrimental effect of local buckling and subsequent fracture due to repeated inelastic cycles, where  $b$  is the full length of the outstanding leg and  $t$  is the thickness of the outstanding leg.

The hysteresis loops for diagonal member with different slenderness ratio vary significantly. Loop areas are greater for stocky member than for a slender member, hence the slenderness ratio of diagonal member should limited to:

$$\frac{KL}{r} \leq 4.0 \sqrt{\frac{E}{F_y}} \quad (25)$$

where  $K$  is the effective length factor for in plane buckling which is equal to 0.7,  $L$  is the unbraced length measured between the gusset plates, and  $r$  is the minimum radius of gyration of the cross section. For members with X-type,  $L$  is taken as one-half the length of the diagonal member measured between the gusset plate and middle of the member.

The nominal resistance of the diagonal members is equal to  $R_y F_y A_g$  where  $R_y$  is a factor that is used convert the minimum yield stress to the expected yield stress, For A36 and A572 steels  $R_y$  is equal to 1.5 and 1.3, respectively. The end connection of the diagonal member should be design for 1.2 times the nominal resistance of the axial and flexural resistance of the diagonal member to ensure that the connection will stay elastic while strain hardening occurs in the diagonal member up to 4% drift.

## 1.7. Experimental Investigations on the End Cross Frame Subassembly

### Models

#### 1.7.1. Introduction

Analytical investigations showed that the variations of end cross frame details contribute to the lateral stiffness of steel bridge superstructures. However, these results were highly sensitive to the shear connector mathematical models. Based on these models, it was shown that the shear connectors at support locations are subjected to axial and bi-directional shear forces. Also, to accommodate large lateral drifts at the ductile end cross frames, several structural components of the steel bridge superstructures near the supports experience high displacement demand. Therefore, experimental investigations were required to determine the lateral behavior of the steel bridge superstructures at support locations and to calibrate the mathematical models.

#### 1.7.2. Description of Test Specimens

The three-girder bridge subassembly is a 50% scaled model of a superstructure bridge prototype outlined in the Caltrans Steel Girder Bridge Design Example (Caltrans 2007). Figure 1-51 shows a transverse cross section of the scaled bridge model. The width of the subassembly was equal to 3 ft. It represented a slice of a three-girder steel girder bridge superstructure over an interior bent. The girders were spaced at 6 ft on centers, and the deck overhangs were 2.5 ft. The R/C deck was 4.5 in. thick with a haunch of 1.06 in. The plate girders were built up sections of 1 in. thick by 9 in. wide flanges and webs of 5/16 in. thick by 39 in. deep. The bearing stiffener plates were 7/8 in. thick and 5 5/8 in. wide. The North, Middle, and South girders of Specimens F1A, F1B, F1B\_1, and F1C and their corresponding reactions in the subassembly specimens are called Girder 1, Girder 2, and Girder 3, respectively in this report. The girders for Specimens F1A, F1B, F1B\_1, and F1C were supported on rigid steel pedestals with 3/4 in. thick elastomeric bearings and washers to allow for rotation and steel shear keys to prevent translation.

The top chord of the prototype bridge was made of L2x2x3/8 and was designed to carry the horizontal component of the diagonal brace force. The tributary weight of the 3-span 3-girder prototype bridge supported on rigid substructure was 313 kips at the bent support. Based on the design chart shown in Figure 1-52 with a displacement ductility equal to 8, the required ratio of lateral yield force of the ductile end cross frame over the tributary weight of the bridge at the support is 0.4. Therefore, the required cross sectional area of diagonal bracing members at the end cross frames for the prototype was calculated to be 2.0 in<sup>2</sup>. This corresponds to single L2x2x1/2 braces. Therefore, the required cross sectional area of the bracing members for the model was 0.5 in<sup>2</sup>. This corresponds to single angle L 1 1/2 x 1 1/2 x 3/16 for diagonal bracing members.

### **1.7.2.1. Specimen F1A**

Figure 1-53 shows the details of Specimen F1A. Eight 3/8 in. diameter shear connectors were used on each girder. The shear connectors were 3 9/16 in. long and spaced at 6 in. and 5 in. in longitudinal and transverse directions, respectively, as shown in Figure 1-54. No shear connectors were placed over the top chord of the cross frames. In this Specimen the L1x1x1/8 diagonal braces were welded to 3/8 in. thick gusset plates and the gusset plates were connected to the bearing stiffeners through six 3/4 in dia. A490 bolts. The 2L1 1/4x1 1/4x3/16 cross frame top and bottom chords were also welded to the 3/8 in. gusset plates.

The specimen was supported on 3/4 in. elastomeric pads and connected to the pedestals using four 1 1/4 in. diameter oversized holes with 3/4 in. thick elastomeric washers. The bottom flange was laterally restrained against movements through steel brackets. The support detail is shown in Figure 1-55 and close-up view of the support is shown in Figure 1-56. Figure 1-57 shows Specimen F1A before the test.

### **1.7.2.2. Specimen F1B**

Figure 1-58 shows the details of Specimen F1B. There were six rows of two 3/8 in. diameter shear connectors on each cross frame top chord. The shear connectors were 5 in. long and spaced at 5 in. No shear connectors were present over the girder top flanges. The concrete deck thickness increased between the girders to 8 1/16 in. In this specimen, the L1x1x1/8 diagonal braces were welded to 3/8 in. thick gusset plates and the gusset plates were connected to the bearing stiffeners through six 3/4 in dia. A490 bolts. The 2L1 1/4x1 1/4x3/16 cross frame top and bottom chords were also welded to the 3/8 in. gusset plates. The concrete deck thickness and rebar arrangements were similar to Specimen F0B.

The specimen was supported on 3/4 in. elastomeric pads and connected to the pedestals using four 1 1/4 in. diameter oversized holes with 3/4 in. thick elastomeric washers. The support detail is shown in Figure 1-55 and close-up view of the support is shown in Figure 1-56. Figure 1-59 shows Specimen F1B before the test.

### **1.7.2.3. Specimen F1B\_1**

Due to a premature shear connector failure in specimen F1B, the top chord and shear connectors were modified in specimen F1B\_1. Figure 1-60 shows the details of Specimen F1B\_1. There were six rows of two 5/8 in. diameter shear connectors on each cross frame top chord. The shear connectors were 5 in. long and spaced at 5 in. No shear connectors were present over the girder top flanges. Similar to F1B, the concrete deck thickness increased between the girders to 8 1/16 in. In this specimen, the L1x1x1/8 diagonal braces were welded to 3/8 in. thick gusset plates and the gusset plates were connected to the bearing stiffeners through six 3/4 in dia. A490 bolts. The 2L1 1/4x1 1/4x1/4 cross frame top chords and 2L1 1/4x1 1/4x3/16 cross frame bottom chords

were also welded to the 3/8 in. gusset plates. The concrete deck thickness and rebar arrangements were similar to Specimen F0B.

The specimen was supported on 3/4 in. elastomeric pads and connected to the pedestals using four 1 1/4 in. diameter oversized holes with 3/4 in. thick elastomeric washers. The bottom flange was laterally restrained against movements through steel brackets. The support detail is shown in Figure 1-55 and close-up view of the support is shown in Figure 1-56. Figure 1-61 shows Specimen F1B\_1 before the test.

#### **1.7.2.4. Specimen F1C**

Figure 1-62 shows the details of Specimen F1C. There were no shear connectors on top of the girders. The overall view of Specimen F1C is shown in Figure 1-63. In this specimen, each chevron brace was directly attached to the deck. The L1x1x1/8 braces were welded to the 1/2 in. gusset plates that were welded to a horizontal plate with 9- 3/8 in. diameter shear connectors. The shear connectors were 3 in. long and spaced at 7 in. on centers as shown in Figure 1-64. The gusset plates at the deck were stiffened on either side by 1/2 in. stiffener plates.

The shear connectors were designed to resist the combined effects of lateral shear and the unbalanced tensile forces once the compressive brace buckles.

The haunch (1 1/16 in. thick) that was present over the girder in Specimen F1A and Specimen F1B was added to the deck thickness bringing its overall uniform thickness to 5 9/16 in. This added flexural and shear strength to the concrete deck and provided a flat surface at underside of the deck for sliding over top girder flanges. The actuator was connected to the end of the deck where the deck thickness was reduced to match the shape of the connecting steel piece. The deck was designed for the unbalanced bending moment and shear that would occur when the braces in compression buckle and the braces in tension resist the lateral load. 10 #4 rebar were used at the top and bottom for transverse reinforcements, as shown in Figure 1-65. The fabricated chevron bracing components are shown in Figure 1-66. Figure 1-67 shows the rebar as placed in the deck of Specimen F1C. The longitudinal reinforcements were #3 bars at 8 in. on centers. Additional rebar were placed at the locations of studded connection as shown in Figure 1-68. Figure 1-69 shows the additional rebar as they were placed in the deck at the location of the shear connectors in Specimen F1C. Figure 1-70 shows the completed rebar and formwork of Specimen F1C and Figure 1-71 shows the placement of concrete in the formwork. Figure 1-72 shows Specimen F1C before the experiment.

### **1.7.3. Material Properties of Test Specimens and Testing Protocol**

ASTM A36 steel was specified for all angle braces and chords. All steel plates including plate girder components and gusset plates were A572 Gr. 50 ksi steel. The specified ultimate strength

of the ASTM A108 3/8 in. and 5/8 in. diameter shear connectors was 60 ksi. The stress-strain traces for three coupons of 3/8 in. diameter shear connectors are shown in Figure 1-73. The ultimate strength of the 3/8 in. shear connectors, based on the coupon tests, was 80 ksi. The yield and ultimate strengths of the 5/8 in shear connectors, based on the Material Testing Report, was 72.8 and 77.9 ksi, respectively. The stress-strain traces for three coupons of the L 1x1x1/8 in. diagonals used in Specimen F1B\_1 are shown in Figure 1-74. The yield and ultimate strengths based on the coupons were 60 ksi and 82 ksi, respectively. The specified 28-day concrete strength for the deck was 4 ksi. The concrete slump for Specimens F1A, F1B, and F1C was 4 in., while for Specimen F1B\_1 the slump was 2 in. The maximum aggregate size was 3/8 in.

A displacement-controlled testing protocol was used for all experiments. The testing protocol was adapted from the loading history for qualifying cyclic test of buckling restrained braces as specified in Appendix T of the AISC Seismic Provisions (AISC 2005). The specimen would be subjected to two cycles at every specified drift level. The drift level was calculated based on the differential lateral displacement between the top and bottom flanges of the steel girders. Since the actuator force was applied at the deck level, the displacements that were measured from one of the diagonal displacement transducers were used to calculate the drift levels and fed into the actuator control program. Figure 1-75 show the number of cycles per drift level for all Specimens.

#### **1.7.4. Cyclic Response of Specimen F1A**

Figure 1-76 shows the lateral cyclic load-displacement response of the specimen in terms of total force versus the differential transverse displacement of the top and bottom flanges of the plate girders. The test showed that the lateral yield load capacity of the specimen was 24 kips and the lateral drift capacity was 7.5%. The elastic lateral stiffness of the specimens was 347 kips/in.

The hysteresis loops obtained from the test show good energy dissipation capability. This is the result of nonlinear axial behavior (yielding and buckling) of the bracing members as well as development of plastic moment hinges at the ends of top and bottom chords.

##### **1.7.4.1. Experimental Observations**

The diagonal braces showed signs of buckling at about 0.5% drift. At 1% drift, flexural cracks develop in the concrete deck. At 1.5% drift the concrete deck at the studded deck-to-girder connection starts to lift up over the top flange of Girder 2 as shown in Figure 1-77. At 2% drift, vertical cracks start to form at the interface of the flange and deck over the girders beginning from Girder 2. This is indicative of axial elongation (yield) of shear connectors in these regions. Figure 1-78 shows the deformed shape of a buckled brace at different drifts. A close-up view of the flexural cracks in the deck at 1.5% drift over Girder 2 is shown in Figure 1-79. Also, at 2%

drift, vertical cracks at the interface of flange and deck over the girders propagate upward toward the deck surface.

At 3% drift, the uplift of the deck over the girder was clearly noticeable since a major crack was developed along the width of specimen at the south side of Girder 2. At 3.5% drift diagonal cracking occurred in the studed deck-to-girder connection. The diagonal cracks, shown in Figure 1-80, indicated that the concrete breakout failure had occurred after yielding of the shear connector steel but before developing the ultimate tensile strength. Figure 1-81 shows diagonal crack formation at Girder 3. One of the diagonal braces ruptured at 5% drift near the gusset plate, as shown in Figure 1-82.

The specimen failed at 7.5% drift. The overall damaged state of the specimen is shown in Figure 1-83. Figure 1-84 shows the damaged concrete joint at Girder 2 while Figure 1-85 and Figure 1-86 shows the close up of the final damaged state of joints over Girder 3 and 1, respectively.

The rupture of another brace at the final damage state of the specimen is shown in Figure 1-87. The cross frames underwent significant plastic deformation before failure of the deck to girder connection of specimen at 7.5% drift. The specimen at the final damaged state at zero displacement is shown in Figure 1-88. The close-up view of one of the cross frames is shown in Figure 1-89.

#### **1.7.4.2. Sequence of Yielding and Failure Modes**

In order to better interpret the experimental data collected, the envelopes of some strains, displacements, and force measurements at peak positive displacement of each cycle were plotted. Figure 1-90 shows the base shear force and the deck displacement values at the end of each displacement cycle for Specimen F1A.

Figure 1-91 shows the strain gauge measurements at the end of the top chord near the gusset plate north of Girder 2. Figure 1-92 shows measurements at the top chord south of Girder 2. Figure 1-93 shows the strain gauge measurements at the end of the bottom chord near the gusset plate north of Girder 2 and Figure 1-94 shows measurements at the bottom chord south of Girder 2. These plots indicate that the ends of the chord members start to yield early on at about 0.5% drift. The strains in the chords start to plateau between 1% to 1.5% drift as the deck starts to resist the lateral force through bending. This led to the formation of visible flexural cracks in the deck. The strains start to increase again at about 1.5% to 2% drift as the moment connection over the middle girder fails and causes a redistribution of bending moments in the deck to joints over the outsider girders. Figure 1-95 shows the strain data at each side of top of bearing stiffeners. The bearing stiffeners remained elastic throughout the test.

Figure 1-96 shows bending behavior at mid height of the bearing stiffeners. Figure 1-97 shows the drift versus peak rotation of the base of the girders during the experiment. This plot shows that all three girders rotate equally. Figure 1-98, on the other hand, shows the drift versus peak rotation of the concrete deck joint over the girders. Due to spalling of concrete joint and removal of some instruments, the differential displacement reading is not accurate beyond 1.5% to 2 % drift.

The horizontal support forces versus peak girder differential displacement are shown in Figure 1-99. Due to construction tolerance of using 1/16 in shim plates around supports, the support points were engaged at different drifts. The vertical support reactions are plotted in Figure 1-100.

### **1.7.5. Cyclic Response of Specimen F1B**

Figure 1-101 shows the lateral cyclic load-displacement response of the specimen in terms of total force versus the differential transverse displacement of the top and bottom flanges of the plate girders. The experiment showed that the lateral yield force capacity of the specimen was 27 kips. The elastic lateral stiffness of the specimens was 215 kips/in.

The hysteresis loops obtained from the experiment show good energy dissipation capability up to 2.5% drift. This is the result of nonlinear axial behavior (yielding and buckling) of the bracing members as well as development of plastic moment hinges at the ends of the top and bottom chords. The specimen failed prematurely due to brittle fracture of the connection of studs to top chords. The failure of the studs was due to the combination of weld defect and thickness of the top chord.

#### **1.7.5.1. Experimental Observations**

Figure 1-102 shows Specimen F1B before testing. The diagonal braces showed signs of buckling at about 0.5% drift. Figure 1-103 and Figure 1-104 show the flexural deformation of the top chords with respect to the deck at 2% drift. Figure 1-105 shows the buckled braces at various drift levels. As shown in Figure 1-106, at 2.5% drift, the top chords were completely separated from the deck causing an immediate loss of lateral load carrying capacity. No damage to the concrete deck was observed up to the final drift of 2.5%. The failed specimen at zero displacement is shown in Figure 1-107. The concrete deck was lifted up off the steel girders and the failure surface of the studs was examined. Figure 1-108 shows the close-up views of the failure surface of the studs.

During the testing of this specimen, it was noticed that bending of the top chord was excessive. The edges of the top chord outstanding legs were flexible enough that they started to flex and hit

the R/C deck. This indicated the beginning of prying action due to the axial forces in the connectors. However, with the observed defect in the weld of the shear connector it was not definitive that the cause of failure was this excessive top chord bending.

In 1968, Caoble was among the first researchers to study the shear strength of thin flange composite specimens. Based on his work, the AISC Specifications specifies in Section I 3.2d.6 a stiffness requirement between the stud and flange that it is attached to. It states “The diameter of the stud shall not be greater than 2.5 times the thickness of the flange to which they are welded, unless located over web.” For this specimen the  $d_{sv}/t_f$  ratio was equal to 2.0. It is important to note here, that the recommended ratio by AISC is for connectors that are mainly dominated by shear and not by combined axial and shear. Due to the observed defect of the weld it is hard to quantify the main cause of failure in this specimen.

### **1.7.5.2. Sequence of Yielding and Failure Modes**

In order to better interpret the experimental data collected, the envelopes of some strains, displacements, and force measurements at peak positive displacement of each cycle were plotted. Figure 1-109 shows the base shear force and the deck displacement values at the end of each displacement cycle for Specimen F1B.

Figure 1-110 shows the strain gauge measurements at the end of the top chord near the gusset plate north of Girder 2. Figure 1-111 shows measurements at the top chord south of Girder 2. Figure 1-112 shows the strain gauge measurements at the end of the bottom chord near the gusset plate north of Girder 2 and Figure 1-113 shows measurements at the bottom chord south of Girder 2. These plots indicate that the ends of the chord members start to yield early on into the experiment at about 0.5% drift.

Figure 1-114 shows the strain data at either side of top of bearing stiffeners. The bearing stiffeners remained elastic throughout the test. Figure 1-115 shows bending behavior at mid height of the bearing stiffeners. Figure 1-116 shows the drift versus peak rotation of base of the girders during the experiment. This plot shows that all three girders rotate equally. Figure 1-117 shows the drift versus peak rotation of the concrete deck joint over the girders.

The horizontal support forces versus peak girder differential displacement are shown in Figure 1-118. The smaller gaps and construction tolerance due to using 1/8 in. shim plates around supports in this experiment caused equal distribution of lateral forces between the support points. The vertical support reactions are plotted in Figure 1-119.

## 1.7.6. Cyclic Response of Specimen F1B\_1

The main difference between specimens F1B\_1 and F1B is the cross section of the top chord and the diameter of the shear connectors. Figure 1-120 shows the lateral cyclic load-displacement response of the specimen in terms of total force versus the differential transverse displacement of the top and bottom flanges of the plate girders. The test showed that the lateral yield force capacity of the specimen was 45 kips. The elastic lateral stiffness of the specimens was 131 kips/in.

The hysteresis loops obtained from the test show good energy dissipation capability up to 7.0% drift. This is the result of nonlinear axial behavior (yielding and buckling) of the bracing members as well as development of plastic moment hinges at the ends of the top chords.

### 1.7.6.1. Experimental Observations

Figure 1-121 shows Specimen F1B\_1 before testing. The diagonal braces showed signs of buckling at about 0.5% drift, shown in Figure 1-122. Figure 1-123 shows yielding of the diagonal braces and the top chord between the gusset plate and the beginning of the studded deck-to-chord connection at 2.0% drift. Figure 1-124 shows the diagonals deforming at the gusset plate interface at 3.0% drift. Figure 1-125 shows separation between the deck and the girders at 3.0% drift. Figure 1-126 shows the top chord at 3.0% drift. There was no indication of elongation of the shear studs.

Buckling and yielding of the diagonal braces as well as yielding of the top cord and uplift of the deck from the girders continues, in increasing magnitude, until the beginning of the 7.0% drift run. Figure 1-127 shows deformations at 4.0% drift. Figure 1-128 shows the rotation of the Girder 2 at 5.0% drift. Figure 1-129 shows deformations at 6.0% drift. During the first cycle (push) at 7.0% drift, one of the diagonal braces ruptured halfway between the gusset plate and the intersection of the two braces between Girders 2 and 3, shown in Figure 1-130. Also during the first cycle (pull) at 7.0% drift, two more diagonal braces ruptured, one of the diagonal braces ruptured halfway between the gusset plate and the intersection of the two braces between Girders 2 and 3, shown in Figure, and the other ruptured at the gusset plate interface just south of Girder 2, Figure 1-131 (between Girder 1 and 2). Also, during the 7.0% drift run, all of the top cords fractured on their vertical legs at the gusset plate interface, shown in Figure 1-132, and a closed crack formed across the width of the deck on either side of the Girder 2, shown in Figure 1-133. There was permanent liftoff of the deck over all of the girders. Figure 1-134 shows Specimen F1B\_1 in the final state at 0% drift.

### 1.7.6.2. Sequence of Yielding and Failure Modes

In order to better interpret the experimental data collected, the envelopes of some strains, displacements, and force measurements at peak positive displacement of each cycle were plotted.

Figure 1-135 shows the base shear force and the deck displacement values at the end of each displacement cycle for Specimen F1B\_1.

Figure 1-136 shows the strain gauge measurements at the end of the top chord near the gusset plate south of Girder 2. Figure 1-137 shows measurements at the top chord north of Girder 2. Figure 1-138 shows the strain gauge measurements at the end of the bottom chord near the gusset plate south of Girder 2 and Figure 1-139 shows measurements at the bottom chord north of Girder 2. These plots indicate yielding in the chords after the 1.5% drift run.

Figure 1-140 shows the strain data at either side of top of bearing stiffeners. The bearing stiffeners remained elastic throughout the test. Figure 1-141 shows bending behavior at mid-height of the bearing stiffeners. Figure 1-142 shows the drift versus peak rotation of base of the girders during the experiment. This plot shows that Girder 1 experiences more rotation than Girders 2 and 3; Girders 2 and 3 rotate similarly. Figure 1-143 shows the total force versus peak rotation of the concrete deck joint over the girders. This plot shows that, during the same cycle on the same side of the girder as the plot of the base rotation, Girder 1 shows negative rotation, which is expected. Girders 2 and 3, on the other hand show positive displacements. This can be attributed to the plastic behavior of the top chords and the deck lifting off the girders.

The horizontal support forces versus peak girder differential displacement are shown in Figure 1-144. The smaller gaps and construction tolerance due to using custom cut 1/4 in. shim plates around supports in this test allowed for a more equal distribution of lateral forces between the support points. The vertical support reactions are plotted in Figure 1-145.

It is interesting to note here that although the ratio of  $d_{sc}/t_f = 2.5$  for this specimen, the top chord did not experience significant bending at the shear connector. This may be due to the fact that the axial forces in these connectors are less than forces in Specimen F1B by a factor almost 11 times  $[(5/8)/(3/16)]^2$ . This may suggest that the angle thickness of the top chord plays an important role in behavior of shear connectors under combined axial and bending. This observation needs further investigation.

### **1.7.7. Cyclic Response of Specimen F1C**

Figure 1-146 shows the actuator force versus deck displacement. The experiment showed that the ultimate lateral load carrying capacity of the specimen was 30.5 kips. The lateral drift capacity was 16%. The initial lateral stiffness of the specimens was 95 kips/in.

### **1.7.7.1. Experimental Observations**

Figure 1-147 shows Specimen F1C at 2% drift. The compression brace buckled before 0.1% drift in the experiment. Figure 1-148 shows that with increased drift the lateral deflection on the buckled braces increase and this caused distortion of the brace section near the welded connection at the gusset plates as shown in Figure 1-149. Due to bending in the deck as a result of unbalanced vertical component of the tension braces the deck experienced small rotations over outside girders as shown in Figure 1-150.

Once the friction between the deck and top flanges was overcome the deck was able to slide over the girders. Figure 1-151 shows movement of deck over the girders as indicated by the abrasion of the underside of concrete deck.

Figure 1-152 shows the Specimen F1C at the end of the experiment. Three of the four braces in the specimen had ruptured at 9% drift. Therefore, the cyclic testing stopped at this point and the specimen was pulled in the direction to develop tension in the remaining brace until the brace ruptured at the lateral drift of 16%. Figure 1-153 shows the large plastic axial deformation in a ruptured brace.

No visible damage to the concrete deck was observed during the entire experiment as shown in Figure 1-154.

### **1.7.7.2. Sequence of Yielding and Failure Modes**

In order to better interpret the experimental data collected the envelopes of some of the strain, displacement, and force measurements at peak positive displacement of each cycle were plotted. Figure 1-155 shows the base shear force and the deck displacement values at the end of each displacement cycle for Specimen F1C.

Figure 1-156 shows the axial strain gauge measurements for the chevron bracing members between Girders 1 and 2 while Figure 1-157 shows the axial strain measurements for the chevron bracing members between Girders 2 and 3. These plots show very high strains in the braces reaching 140,000 microstrains at 9% drift.

The plots in Figure 1-158 shows strain gauge measurements on the bottom chord of the cross frame on the left side of Girder 2 and Figure 1-159 shows the strain measurements on the bottom chord on the right side. These figures indicate bending moments being developed in the bottom chord members. This could be attributed to the small rotations (0.015 rad.) in the fixed supports due to construction tolerance as shown in Figure 1-160. The rotation of the deck is shown in

Figure 1-161. This plot shows the rotations of the deck over girders due to bending moments in the deck from the unbalanced vertical force of braces.

Figure 1-162 shows the strain measurements at the bottom of the bearing stiffeners. Figure 1-163 shows that the strains at the top of the bearing stiffeners are very small this is because there are no mending moment transferred from the deck except due to small eccentricity of the vertical force from the deck as point of contact of the changes due to rotates of deck over the top flange of the girders.

The support horizontal reactions are shown in Figure 1-164. This plot shows that the bottom chord helps distribute the total applied force among the supports. If the bottom chord had not been present, the horizontal reaction at Girder 3 would have been reduced to zero once compression braces buckled. Figure 1-165 shows the support vertical reaction forces. The low vertical reaction force at Girder 3 may be attributed to the effects from the actuator weight and its attachment to the specimen.

## **1.8. Seismic Performance of Plate Girder Bridges with Ductile End Cross**

### **Frames**

#### **1.8.1. General**

Since moderate-to-large earthquakes can impose very high loads, it is uneconomical to design conventional bridges to remain elastic in such events. Accordingly various members and components of these bridges are expected to behave inelastically during a large earthquake, provided the yielding is controlled and occurs in a ductile manner. In most bridges, it is the substructure that is designed to deform plastically, thereby reducing the foundation forces and the size and subsequent cost of the substructure itself. The inherent elastic strength of the superstructure for in-plane loads is assumed to be sufficient to exceed the plastic shear capacity of the substructures but an explicit check is not made for most bridges based, primarily, on the satisfactory behavior of monolithic concrete superstructures in past earthquakes.

However, as noted above, damage to superstructures has been observed in steel plate girder bridges during such earthquakes as the 1994 Northridge earthquake (Astaneh-Asl et al., 1994), 1995 Hyogo-Nanbu earthquake (Shinozuka et al., 1995; Bruneau et al., 1996) and the 2001 Nisqually earthquake, as illustrated in Figure 1-166 (WSDOT, 2001). This damage shows that the assumption all superstructure components remain elastic during earthquake loading is not necessarily valid.

The lateral load path in the longitudinal direction of a bridge is relatively straight-forward and typical superstructure damage includes pounding between adjacent spans or at the abutments, which can result in unseating of spans. Apart from using ductile columns, longitudinal seismic actions can be mitigated using seismic isolation (Buckle et. al., 2006), or a series of bearing restrainers which engage the capacity of the abutments, as described by Des Roches et al. (2004).

In the transverse direction, however, secondary members for gravity loading become primary members for seismic loads. End cross frames or diaphragms, which are members placed transversely between the girders at the supports of a plate girder bridge, have been identified analytically (Itani and Rimal, 1996; Zahrai and Bruneau, 1998) and experimentally (Carden et al, 2005a) as critical components in the transverse load path. It has also been recognized that these components in the superstructure could be designed as ductile members and thereby reduce the forces transmitted to the substructures during an earthquake (Zahrai and Bruneau, 1999a; 1999b). The advantages of this approach range from, protecting the foundations of bridges where damage is difficult to identify and repair, to reducing demand and damage in the substructure of a bridge. Furthermore, confining damage to purpose-built, replaceable, ductile elements which have a secondary role during normal operation of a bridge, is a desirable feature which potentially reduces the need for expensive substructure repair and bridge closure.

Previous investigators in this area (Zahrai and Bruneau, 1998; 1999a; 1999b) have proposed and performed experiments on three configurations of ductile end diaphragms, in which the inelastic components were principally subjected to flexural and shear deformations. The first configuration consisted of a steel shear panel (SPS) orientated in a vertical plane and designed to deform inelastically in shear. The second configuration used an eccentric braced frame (EBF), similar to the SPS but with the inelastic member orientated in the horizontal direction. The third system consisted of triangular plates that yield in flexure as ductile elements (TADAS). These systems were shown in subassembly experiments to perform with ductile behavior up to ultimate transverse drifts (at which fracture occurred) of about 3.0%, 3.0% and 3.8% of the girder height for frames fitted with the SPS, EBF and TADAS devices respectively. In order to reduce the effect of the girders in the transverse load path, these experiments used bearing stiffeners with reduced widths to lower their transverse flexural stiffness and capacity. The girder sections in the sub-assemblies had rotationally-fixed top and bottom flanges.

Single angle cross-braces (X-braces) are often used as cross frames in steel plate girder bridges, and whereas end cross frames have long been identified as critical components in the transverse load path, the nonlinear behavior of X-braces is not well understood. Concentrically braced frames have been used in buildings as ductile elements where it has been shown that the braces have a tendency towards strength and stiffness degradation due to buckling of the compression members when deformed inelastically (Jain et al., 1980; Astaneh-Asl et al., 1985; Sabelli, 2001). Provisions to minimize the impact of buckling and ensure adequate behavior in special, concentrically-braced, frames are defined by AISC (2002) for buildings. However, similar provisions are not available for the seismic design of special (inelastic) braces for bridges, such as those found in X-brace cross frames. To provide the information necessary to develop such a set of provisions an analytical and experimental research project has been undertaken as described in the following sections

## 1.8.2. Description of Bridge Model

In the experimental study, the transverse seismic performance of a plate girder superstructure was investigated using a single span model of a two-girder bridge, shown in Figure 1-167. This bridge model has been used for many experiments in recent years to investigate the effect of different components in the transverse load path (Carden et al., 2005a), but the focus of this section is the investigation of ductile end cross frames that use single angle X-braces. The overall girder dimensions for the bridge model were scaled down from a prototype by a factor of 0.4. Transverse seismic loads were simulated in the bridge model using two methods. The first method involved two actuators attached to the bridge model at the level of the deck, as shown in Figure 1-5, in order to apply reversed static loads. The actuators were attached at the one-third and two-third points along the length of the bridge model to approximate the distribution of inertia loads expected in the superstructure. Secondly, earthquake loading on the bridge model was simulated using shake table experiments as shown in Figure 1-168. Loads were simulated dynamically on the bridge model, with additional lead placed on the deck slab in order to satisfy mass similitude requirements.

The bridge model was 60 ft long, with the cross sectional properties shown in Figure 1-169. The web and flanges of the I-girders were built-up from plates that were welded with 3/8 in. fillet welds along the length of the girders. Transverse stiffeners, 3/8 in. thick, were placed at 10.0 ft centers on the exterior face of the girders and 5.0 ft centers on the interior face. The web and flanges were constructed from ASTM A709 Gr50 steel, while all other components were ASTM A36.

The thickness of deck slab and haunch, spacing of the girders, and length of overhang were scaled down from the prototype bridge, resulting in the cross sectional deck slab dimensions shown in Figure 1-170. Two rows of 3/8 in. diameter Nelson Headed Anchor studs were spaced at 18 in. centers along the length of each girder. During studies on the transverse load path in prior experiments (Carden et al., 2005a), some damage had occurred in several rows of the shear connectors at the north end of the bridge model. These connectors were not repaired for the experiments described in this section in order to enable the study of the pros and cons of a nominal (non-structural) connection between the plate girder and deck in the region of the end cross frame.

The intermediate cross frames in the prototype bridge were spaced at 24.9 ft based on the AASHTO Standard Specifications (AASHTO, 1996). After scaling, the intermediate cross frames in the bridge model were spaced 10.0 ft apart and were constructed from 1 3/4 x 1 3/4 x 1/4 in. single angles in an X-brace configuration with a double angle bottom chord (Figure 1-169).

The end cross frames were designed with lighter steel single angle members in order to provide a structural “fuse” to limit transverse forces during an earthquake. Single angles (1 x 1 x 3/16 in)

were selected for the cross frames, and were designed to yield with a strength below the theoretical strength of the substructure. These were the smallest available single angle members that satisfied the  $b/t$  and  $Kl/r$  ratios according to both the AASHTO LRFD Specifications (AASHTO 1998) for bracing members and AISC Seismic Design Specifications for special concentric braced frames (AISC 2002). The bridge model configuration with these X-braces is shown in Figure 1-170. They were welded directly to the bearing stiffeners, as shown, with connections designed to be stronger than the tensile capacity of the members, as specified by the AASHTO provisions, to prevent premature failure and promote optimal inelastic behavior.

In order to maximize the shear force in the diagonal members and allow them to deform inelastically at the design shear, it was necessary to minimize the transverse stiffness of the girders and other components at each end. Previous experiments (Zahrai and Bruneau, 1999b) showed that the bearing stiffeners had a considerable impact on the lateral stiffness and were likely to result in significant post-yield over-strength. In these earlier experiments, the stiffeners were trimmed in order to lower the lateral stiffness, which also resulted in a reduction in transverse girder strength. For the present bridge model an alternative method for reducing the effect of the bearing stiffeners was employed, whereby the girders were designed to “rock”, with resistance primarily due to the diagonal members of the cross frames (Figure 1-171). Rotations were allowed at the base of the girders using bearings with a relatively low rotational stiffness. Rotations between the deck and the girders were also permitted by having relatively few effective shear studs on top of the girders near the ends of the bridge, particularly at the north end due to prior damage. The top and bottom chords of the end cross frames were then pinned in order to further facilitate the rocking. The top chord was also used to provide connectivity between the deck slab and the steel superstructure. It was designed to carry the full end shear from the deck slab into the end cross frames based on the capacity of the diagonals. The top chord was designed to accommodate the small vertical relative displacements between the deck slab and girders that occur during transverse drift of the girders. Vertical movement was accommodated through flexure of the members in the bridge model, although vertically slotted holes could have also been used for this purpose. The double angle members and connections of the bottom chord were designed to transfer unbalanced forces caused by buckling of the cross frames evenly to the bearings. Both the top and bottom chords were designed to ensure development of the full capacity of the diagonal members.

During reversed static load experiments, the bridge model was placed on four reinforced elastomeric bearings. These were typical of those used to accommodate temperature fluctuations in the longitudinal direction of a bridge superstructure, and have previously been shown to be a relatively low maintenance, low cost option for bridge bearings with good resilience for extreme loading conditions (AISI, 1996). The elastomeric bearings consisted of three layers of neoprene (Figure 1-170) with a shear modulus of 124.7 psi. They were restrained in the transverse direction with stiffened angles as shown. Typically, in this type of bridge, there is a gap between the bearing and transverse restraint, but for these experiments this gap was minimized using custom fitted shims in an attempt to restrain the superstructure transversely without deforming the bearings. However, the bearings did allow rotation of the girder about an axis normal to the longitudinal axis of the superstructure. Rotation about the vertical axis was considered unrestrained as the rotational stiffness provided by the transverse restraint was relatively small. Similarly restrained elastomeric bearings were used in shake table experiments.

The weight of the superstructure was measured at 30.1 kips, within 6% of the expected weight based on geometry and material properties. The calculated additional weight required for similitude was 1.5 times the bridge weight and was added using lead bricks contained within six steel frames fixed to the deck slab of the bridge model (Figure 1-168). The total weight of the bridge including lead, as measured from load cells and checked using a dynamometer at each end of the bridge, summed to 76.7 kips.

The bridge model was supported on four load cells, one under each of the bearings, which were able to measure the vertical, axial and two horizontal shear components of force. Displacement transducers were used along the length of the bridge to measure the transverse displacement profile at deck slab and bottom flange of the superstructure. Vertical displacement transducers were also able to capture the vertical and torsional deformation of the bridge. Strain gages were used to check for yielding of the steel in deck slab and girders at critical locations and also to determine relative forces in the different cross frames while in the elastic range. In addition, for the dynamic shake table experiments, accelerometers were used to measure the response of the structure in the transverse, longitudinal and vertical directions.

### **1.8.3. Reversed Static Load Experiments**

The performance of the bridge model with ductile X-braces was first evaluated using reversed static transverse loading of the superstructure. The transverse shear force measured in the two load cells at each end of the bridge is plotted against the absolute displacement of the deck slab at each end in Figure 1-172. This figure shows considerable hysteretic behavior in the end cross frames, with large inelastic displacements. The cross frames also exhibit a clear yield point at which buckling and yielding of the diagonals occurs, indicating the transition between the elastic and inelastic response.

Comparison of the results for the two ends of the bridge (Figure 1-173) shows a large difference in forces and displacements between them. The yield force at the north end was 20.7 kips, much lower than at the south end, which had a yield force of 27.2 kips. These forces were measured at the observed yield point in the first plastic cycle in the end cross frames. The difference in forces between the two ends is attributed partly to a variation in the properties of the diagonal members, particularly the variation buckling strength as observed during component experiments. It is also attributed to the combination of the maximum compression force with the maximum tensile force in the corresponding diagonals. If buckling caused degradation in the strength of the compression diagonal before the yield tensile strength was reached, then overall yield strength of the cross frame would be less than found from a direct combination of maximum strengths. The shear studs on top of the girders at the north end of the bridge were less effective than those at the south end, based on relative levels of observed damage; therefore, the stiffness of the girders was lower at the north end. This can be observed by the north end having an apparently lower post-yield stiffness than the south end. Because the loading of the bridge model was controlled so that the

same forces were applied at each actuator, a difference in stiffness resulted in different displacements at the two ends.

The expected tensile capacity of the diagonals in the X-braces, with material strength based on a coupon test, was 16.7 kips. The expected buckling capacity, assuming an effective length equal to half of the diagonal length between the centroid of the connections to the stiffeners, an effective length factor of 0.7, and  $r$  defined about the minor principal axis, was 9.2 kips. This is similar to the assumptions used for design of the ductile members in special truss moment frames (Goel and Itani, 1994). The resulting shear strength of the end cross frame,  $V_{cf}$ , is calculated by:

$$V_{cf} = (P_c + P_t) \frac{h_{xb}}{h_g} \cos\theta \quad (1)$$

where:  $P_c$  is the axial strength of the compression diagonal,  $P_t$  is the axial strength of the tension diagonal,  $h_{xb}$  is the height between the lines of actions of the diagonals at the centerline of the girders (15.75 in.),  $h_g$  is the height of the girder between the centre of the girder flanges (23.23 in.), and  $\theta$  is the angle of the diagonals to the horizontal (17.0 degrees). Therefore, based on the dimensions of the bridge model, the shear in the cross frames was calculated to be 16.8 kips. As the girders also have some lateral stiffness, they also carry some force, increasing the yield and post-yield forces in the cross frames. Based on previous studies to investigate the forces in the girders (Carden et al., 2005a), the estimated capacity of the cross frames at each end was 21.8 kips and 22.7 kips at the north and south ends respectively. These are within 5% of the measured strength at the north end and 17% at the south end. The variation is attributed to the factors discussed above.

Degradation in stiffness of the cross frames with consecutive cycles, caused by buckling of the diagonal members during a compression half cycle and subsequent straightening during a tension half cycle is observed in Figure 1-172. While straightening, cross frame stiffness was comparatively low but once straightened their stiffness increased. Furthermore, the plastic tensile deformations were largely unrecoverable, hence the member elongated, adding to the stiffness degradation, with successive cycles. This behavior was not ideal as it resulted in reduced efficiency of the system for dissipating energy, where efficiency is defined by the area enclosed by the hysteresis loop relative to the area of the circumscribing rectangle. Despite this, the X-braces are shown to have relatively “full” hysteresis loops in the first excursion up to a given displacement. Hence, during a typical earthquake, which has the maximum acceleration early in the loading history, the cross frames can be expected to perform relatively efficiently.

The single angle component experiments exhibited not only stiffness degradation but also strength degradation due to a reduction in axial forces after buckling of the members. However, Figure 1-172 shows no apparent strength degradation in the X-brace system. This is because the increase in strength due to strain and cyclic hardening of the tensile members, along with the stiffness provided by the girders, offsets the decrease in strength observed in the compression members. The result is a system with a relatively low post-yield stiffness, which effectively acts a structural fuse limiting forces transferred into other superstructure components and the

substructure. Meanwhile the stability of the system is maintained due to the sources of post-yield stiffness. The maximum forces in the north and south ends of the bridge model were 1.9 and 1.6 times the measured yield forces respectively.

The maximum transverse displacement in the end cross frames was 1.25 in. Based on a girder height of 23.23 in. from the center of the top flange to the centre of the bottom flange, this corresponds to a drift of 5.3%. The axial deformation in the angles can be estimated using a similar transformation as that given in Equation 1 for the forces. In one diagonal the deformation is compressive and in the other diagonal the deformation is tensile. The axial deformation,  $\Delta_a$ , in a diagonal is given by:

$$\Delta_a = \Delta_{he} \frac{h_{xb}}{h_g} \cos \theta \quad (2)$$

where:  $\Delta_{he}$  is the horizontal end displacement and other variables are as previously defined. From the geometry of the bridge model the equivalent maximum deformation in the diagonal members of the cross frames would be 0.81 in. The deformations in the individual diagonal members were recorded across the length of the diagonals and the maximum measured diagonal deformation was 0.80 in., demonstrating that the deformations were highly compatible. This corresponds to an average axial strain of 1.6% which was about 27% of the maximum limit of 6%, established during component experiments. At this level of displacement, no fracture had occurred in the cross frames, as would be expected given the strain levels compared to the ultimate strains. If the ultimate strain based on component experiments were to be reached, then the drift in the end cross frames would be as high as 20%, illustrating the large displacement capacity of the cross frames. For other ductile end diaphragms previously discussed, including the SPS, EBF, and TADAS systems (Zahrai and Bruneau, 1998), the ultimate drifts were approximately 3.0, 3.0 and 3.8% respectively. Hence, the displacement capacity in the X-braces is calculated to be many times higher than in these other systems.

The drift in the bridge model was limited not by fracture of the cross frames but the drift limit of the girders (Carden et al, 2005a). Some damage was observed in the deck slab at the north end due to prior experiments, but no damage to the deck slab or the girder was observed at the south end, except minor cracking in the deck slab, as shown in Figure 1-168. In this figure a slight gap may be seen between the deck slab and the girder due to a small permanent drift in the end cross frames. By providing minimal connection between the deck slab and the girders at the end cross frame locations, large girder rotations were possible, with end shear transferred from the deck slab into the end cross frames through the composite top chord. The bridge model was not subjected to larger displacements at this stage to prevent potential damage to the deck slab so that it could be used for later experiments. It is however noted that girder drifts up to 7% were experienced during these later experiments without damage to the girders or deck slab (Carden et al., 2005b).

## 1.8.4. Shake Table Experiments

Ductile X-braces, with the same dimensions as those in the reversed static load experiments, were investigated in a series of shake table experiments on the bridge model (Figure 1-168). The north-south component of the 1940 El Centro earthquake was applied to the bridge model in the transverse direction and the amplitude of the excitation was increased by scaling the acceleration record from 0.25 up to 2.0 times the original recorded level.

Transverse shear forces, measured at each end of the bridge are plotted against the horizontal component of the deck slab displacements at each end, relative to the displacement of the bottom flange of the girders, in Figure 1-174 and Figure 1-175. The response for all simulations of increasing amplitude El Centro earthquake motions is shown, with the maximum response, at 2.0 times the El Centro earthquake, plotted in bold. In these figures, the envelopes for the hysteretic behavior at each end were almost elasto-plastic, demonstrating that X-braces provided an effective structural fuse for limiting forces in the bridge.

The measured yield forces were 27.9 and 25.0 kips at the north and south ends of the bridge, respectively. Based on a similar analysis as that described for the reversed static load experiments, the expected transverse strength of the X-braces alone was 16.8 kips. With the hysteretic properties of the girders, chords, and bearings, added to the strength of the diagonals, the yield force at each end was expected to be 22.1 and 22.2 kips which was within 11% and 20% of the measured strengths at the south and north ends, respectively. In the reversed static load experiments, the yield force at the south end was larger than that at the north end, while for the shake table experiments it was the reverse, indicating that the differences are largely due to variability in the members.

As in the reversed static load experiments, while there was likely to be some strength degradation observed in the diagonal members, the contribution of the girder stiffness the overall post yield stiffness in the shake table experiments was close to zero, with no overall strength degradation. The maximum force at the north end was 30.4 kips, 1.09 times the yield force. At the south end the maximum force was 27.9 kips, 1.12 times the yield force. Thus, the post-yield overstrength was less in the shake table experiments than for the reversed static load experiments, which was attributed to the elastomeric bearings used during the shake table experiments having a lower rotational stiffness than the elastomeric pads using during the reversed static load experiments. The response shown in bold in Figure 1-174 and Figure 1-175 illustrates that, while there was no strength degradation, there was stiffness degradation in the cross frames.

A comparison of Figure 1-174 and Figure 1-175 shows that although the end shears were comparable, the displacement at the north end was notably larger than that at the south end of the bridge, which is again similar to the response observed in reversed static load experiments. The

maximum displacement at the north end of the girders (0.92 in.) was equivalent to a drift of 4.0%. The maximum axial deformation in the diagonal was 0.60 in. corresponding to a strain of 1.2%. Again these measured deformations were well below the maximum calculated deformation for the cross frames. No further loading was applied to prevent potential damage to the girders and permit their use in future experiments.

The time histories for the horizontal end deck slab displacements relative to the bearings are shown in response to increasing amplitude excitations up to 2.0 times the El Centro earthquake in Figure 1-176. This figure shows a permanent offset was observed in the ends of the bridge model when the X-braces first buckled at an amplitude of 1.5 times the El Centro earthquake. This permanent offset could be a function of the earthquake excitation which favors displacements in the positive direction. It may also be explained because the X-braces, like other concentrically braced framing systems, favor biased buckling in which the system first buckles during loading in one direction, subsequently reducing its stiffness in that direction. On the other hand, the system is such that once deformed in one direction it takes relatively little force to return the system back to its centered position, since upon reversal of loading, the elongated tension member will easily buckle and the buckled compression member needs to straighten before carrying significant tension force. These self-centering characteristics help to explain why the permanent offset remained relatively constant before and after 2.0 times the El Centro earthquake, despite increasing amplitude excitation.

### **1.8.5. Response Comparison between Elastic and Ductile Cross Frames**

The maximum response of the bridge model with the ductile X-braces to 1.0, 1.5 and 2.0 times the El Centro earthquake is summarized in Table 1-1 and is compared to the response with “heavy” X-braces that remained elastic for the same earthquake excitations. The transverse displacements in Table 1-1 are based on the end deck slab displacement relative to the bottom flange displacements, and the forces are given by the load cells, with the values averaged between the two ends. As expected, the bridge model had the largest end shear forces with the elastic X-braces and the difference between the elastic and ductile response increased as the level of earthquake excitation increased. At 1.5 times the El Centro earthquake, the ductile X-braces only just yielded, therefore the base shear for the ductile X-braces was 78% of the elastic base shear. At 2.0 times the El Centro earthquake, the base shear for the ductile system was reduced to 61% of the elastic base shear. Extrapolating for larger excitations a further comparable reduction is expected. Parametric studies have shown that different cross frame configurations, without the limitations in section sizes associated with scale modeling, could result in even lower relative shear forces than those observed in the bridge model (Carden et al., 2005b).

## References

- Alfawakhiri, F. and Bruneau, M., 2000, *Flexibility of Superstructures and Supports in Seismic Analysis of Simple Bridges*. Earthquake Engrg. and Struct. Dyn. 29(5), 771-729.
- Alfawakhiri, F. and Bruneau, M., 2001, *Local versus Global Ductility Demands in Simple Bridges*. J. Struct. Engrg. 127(5), 554-560.
- American Association of State Highway and Transportation Officials (AASHTO), 1994, *Guide Specifications for Distribution of Loads for Highway Bridges*. AASHTO, Washington, DC.
- American Association of State Highway and Transportation Officials (AASHTO), 1996, *Standard Specifications for Highway Bridges*. AASHTO, Washington, DC.
- American Association of State Highway and Transportation Officials (AASHTO), 1998, *AASHTO LRFD Bridge Design Specifications*. AASHTO, Washington, DC.
- American Association of State Highway and Transportation Officials (AASHTO), 2006, *AASHTO LRFD Bridge Design Specifications*. AASHTO, Washington, DC.
- American Association of State Highway and Transportation Officials (AASHTO), 2007, *AASHTO Guide Specification for LRFD Seismic Bridge Design*. AASHTO, Washington, DC.
- American Association of State Highway and Transportation Officials (AASHTO), 1999, *Guide Specifications for Seismic Isolation Design, (Second Edition including 2000 Interim Revisions)*. AASHTO, Washington, DC.
- American Concrete Institute (ACI), 2005, *Building Code Requirements for Structural Concrete (ACI 318-05)*. ACI, Farmington Hills, MI
- American Iron and Steel Institute (AISI), 1996, *Steel Bridge Bearing Selection and Design Guide - Highway Structures Design Handbook - Vol. II, Chap. 4*. AISI, Washington, DC.
- American Iron and Steel Institute (AISI), 1997, *Four LRFD Design Examples of Steel Highway Bridges - Highway Structures Design Handbook - Vol. II, Chap. 1B*. AISI, Washington, DC.
- American Institute of Steel Construction (AISC), 2002, *Seismic Provisions for Structural Steel Buildings*. AISC, Chicago, IL.
- American Institute of Steel Construction (AISC), 2005, *Manual of Steel Construction – Load Factor and Resistance Design, 2nd Edition*. AISC, Chicago, IL.
- American Institute of Steel Construction (AISC), 2005, *Seismic Provisions for Structural Steel Buildings*. AISC. Chicago, IL.
- Applied Technology Council (ATC), 1996, *ATC 32-1 - Improved Seismic Design Criteria for California Bridges: Resource Document*. ATC, Redwood City, CA.
- Applied Technology Council (ATC), 1995, *ATC 19 - Structure Response Modification Factors*. ATC, Redwood City, CA.

- Applied Technology Council (ATC), 1992, *ATC 24 - Guidelines for Cyclic Seismic Testing of Components of Steel Structures*. ATC, Redwood City, CA.
- Astaneh-Asl, A., 1996, *Notes on the Cyclic Behavior and Design of Steel Bridges - Volume I - Response Modification Factor Based Design*. Report, American Iron and Steel Institute, Washington DC, November.
- Astaneh-Asl, A., 1982, *Cyclic Behavior of Double Angle Bracing Members with End Gusset Plates*. Ph.D. Dissertation, University of Michigan, Ann Arbor, MI.
- Astaneh-Asl, A., Bolt, B., McMullin, K.M., Donikian, R.R., Modjtahedi, D., and Cho, S., 1994, *Seismic Performance of Steel Bridges During the 1994 Northridge Earthquake*. Report UCB/CE-STEEL-94/01. Department of Civil Engineering, University of California, Berkeley, CA.
- Astaneh-Asl, A., Goel, S.C. and Hanson, R.D., 1985, *Cyclic Out-of-Plane Buckling of Double Angle Bracing*. Report UCB/CE-STEEL-94/01. Department of Civil Engineering, University of California at Berkeley, Berkeley, CA.
- Black, C., Makris, N., and Aiken, I., 2002, *Component Testing, Stability Analysis and Characterization of Buckling Restrained Unbonded Braces™*. PEER Report 2002/08, Berkeley, CA, September.
- Bruneau, M., Wilson, J.W., and Tremblay, R., 1996, *Performance of Steel Bridges during the 1995 Hyogoken-Nanbu (Kobe, Japan) Earthquake*. Canadian J. of Civil Engrg, 23(3), 678-713.
- Buckle, I.G., Constantinou, M.C., Dicleli, M., and Ghasemi, H., 2006, *Seismic Isolation of Highway Bridges*. Multidisciplinary Center for Extreme Events Research, Buffalo, NY.
- Buckle, I.G., and Mayes, R.L., 1990, *Seismic Retrofit of Bridges using Mechanical Energy Dissipators*. *Proc. of the Fourth U.S. Conf. on Earthquake Engrg - Vol. 3*. Palm Springs, CA, May 20-24.
- Buckle, I.G., Nagarajaiah, S., and Ferrell, K., 2002, *Stability of Elastomeric Isolation Bearings: Experimental Study*. J. of Struct. Engrg. 128(1), 3-11.
- Buckle, I.G. 1978, *Factors Affecting the Performance of Lead Rubber Energy Dissipators*. Road and Research Unit Bulletin 73, Transit New Zealand, Wellington, New Zealand.
- Buckle, I.G., Mayes, R.L., and Button, M. R., 1986, *Seismic Design and Retrofit Manual for Highway Bridge*, Rep. FHWA-IP-87-6, U.S. Department of Transportation, Federal Highway Administration, Washington, DC.
- Buckle, I. G. (Lead Author), Friedland, I., Mander, J., Martin, G, Nutt, R., and Power, M., 2006, *Seismic Retrofitting Manual for Highway Structures: Part 1 – Bridges*, MCEER-06-SP10, Multidisciplinary Center for Earthquake Engineering Research, State University of New York at Buffalo, Buffalo, NY.
- California Department of Transportation (CALTRANS), 1992, *PEQIT Report-Highway Bridge Damage – Petrolia Earthquakes No. 1, No.2, No. 3. of April 25-26, 1992*. California Department of Transportation, Sacramento, CA.

California Department of Transportation (CALTRANS), 1993, *Bridge Design Specifications*. California Department of Transportation, Sacramento, CA.

California Department of Transportation (CALTRANS), 2001, *Guide Specification for Seismic Design of Steel Bridges*. California Department of Transportation, Sacramento, CA.

California Department of Transportation (CALTRANS), 2001, *Seismic Design Criteria (Version 1.2)*. CALTRANS, Sacramento, CA.

California Department of Transportation (CALTRANS), 2007, *Steel Girder Bridge Design Example, AASHTO-LRFD 3<sup>rd</sup> Edition with California Amendments*. California Department of Transportation, Sacramento, CA.

Carden, L. P., 2004, *Seismic Performance of Steel Girder Bridge Superstructures with Ductile End Cross Frames and Seismic Isolation*, Ph.D. Dissertation, Department of Civil and Environmental Engineering, University of Nevada, Reno

Carden, L. P., F. Garcia-Alvarez, A. M. Itani, and I. B. Buckle, 2001, *Cyclic Response of Steel Plate Girder Bridges in the Transverse Direction*, Proc. 2001 CALTRANS Seismic Conf.(CD Rom), Sacramento, CA.

Carden, L.P., Itani, A.M., and Buckle, I. B., 2002, *Composite Action in Steel Girder Bridge Superstructures Subjected to Transverse Earthquake Loading*. Transportation Research Record, 1814, (02-2455), 245-252.

Carden, L.P., Itani, A.M., and Buckle, I.B., 2003, *Seismic Performance of Ductile End Cross Frames using Concentric X-Braces and Unbonded Braces*. Proc. 2003 World Steel Bridge Symposium, November 19-21, Orlando, FL.

Carden, L.P., Itani, A.M., and Buckle, I.B., 2005, *Seismic Performance of Steel Girder Bridge Superstructure with Ductile End Cross Frames and Seismic Isolators*. Center for Civil Engineering Earthquake Research, Department of Civil and Environmental Engineering, University of Nevada, Reno, Report No. CCEER 05-04 January 2005.

Carden, L.P., Itani, A.M., and Buckle, I.G., 2005a, *Seismic Load Path in Steel Girder Bridge Superstructures*. Report Center for Civil Engineering Earthquake Research 05-03, University of Nevada, Reno, NV.

Carden, L.P., Itani, A.M., and Buckle, I.G., 2005b, *Seismic Performance of Steel Girder Bridge Superstructures with Ductile End Cross Frames and Seismic Isolation*. Report Center for Civil Engineering Earthquake Research 05-04, University of Nevada, Reno, NV.

Carden, L. P., F. Garcia-Alvarez, A. M. Itani, and I. B. Buckle, 2006, *Cyclic Behavior of Single Angles for Ductile End Cross Frames*, AISC Engineering Journal. Second Quarter (2006), 111-125

Celik, C.C., Bruneau, M., 2007, *Seismic Behavior of Bidirectional-Resistant Ductile End Diaphragms with Unbonded Braces in Straight or Skewed Steel Bridges*, Multidisciplinary Center for Earthquake Engineering Research (MCEER), Technical Report MCEER-07-0003, Buffalo, NY.

Chopra, A.K., 1995, *Dynamics of Structures, Theory and Applications to Earthquake Engineering*, Prentice-Hall, Inc., Upper Saddle River, NJ.

Chung, R., 1996, *The January 17, 1995 Hyogoken-Nanbu (Kobe) Earthquake – Performance of Structures, Lifelines, and Fire Protection Systems*, NIST Special Publication 901. Building and Fire Research Laboratory, National Institute of Standards and Technology, Gaithersburg, MD.

Clark, P.W., Aiken, I.D., Tajirian, F.F., Kasai, K., Ko, E., Kimura, I., 1999, *Design Procedures for Buildings Incorporating Hysteretic Damping Devices*. International Post-SMiRT Conference Seminar on Seismic Isolation, Passive Energy Dissipation and Active Control of Vibrations of Structures, Cheju, Korea, August 23-25.

National Standard of Canada (CAN/CSA-S6-00), 2000, *Canadian Highway Bridge Design Code*. Toronto, ON.

CSI, Computers and Structures, Inc., 2007, *CSI Analysis Reference Manual*. Berkeley, CA.

DesRoches, R., Choi, E., Leon, R.T., Dyke, S.J., and Aschheim, M., 2004, *Seismic Response of Multiple Span Steel Bridges in Central and Southeastern United States. II:Retrofitting*. Journal of Bridge Engineering, 9(5), 473-479.

Duan, L., 2006, *Seismic Design Practice of Steel Bridges in California*, Fifth National Seismic Conference on Bridges and Highways, San Mateo, California

Federal Emergency Management Agency (FEMA) FEMA-356, 2000, *Prestandard and Commentary for the Seismic Rehabilitation of Buildings*, Federal Emergency Management Agency, Washington, D.C.

Fehling, E., Pauli, W., and Bouwkamp, J.G., 1992, *Use of Vertical Shear Links in Eccentric Braced Frames*. Proc. 10<sup>th</sup> World Conference on Earthquake Engineering, Vol. 9, Madrid, 4475-4479.

Gatti, W., *Typical Steel Details*. Tensor Engineering Company, September 1993.

Gasparini, D.A., and Vanmarcke, E.H., 1976, *SIMQKE - A Program for Artificial Motion Generation - Users Manual and Documentation*. Massachusetts Institute of Technology - Department of Civil Engineering, Cambridge, MA, November.

Goel, S.C. and Itani, A.M., 1994, *Seismic Resistant Special Truss Moment Frames*. Journal of Structural Engineering, 126(6), 1781-1797.

Hawkins, N.M. and Mitchell, D., 1984, *Seismic Response of Composite Shear Connections*. J. of Struct. Engrg., 110(1984), 2120-2136.

Imbsen, R., 2006, *Recommended LRFD Guidelines for the Seismic Design of Highway Bridges*. AASHTO, United States.

Itani A.M., and Reno, M.L., 1995, *Seismic Design of Modern Steel Highway Connectors*. Proc. Of the Structure Congress XIII - Vol II, Boston, MA, April 2-5, 1529-1531.

Itani, A.M., and Rimal, P.P., 1996, *Seismic Analysis and Design of Modern Steel Highway Connectors*. Earthquake Spectra, 12(2) 275-296.

- Itani, A.M. and Sedarat, H., 2000, *Seismic Analysis and Design of the AISI LRFD Design Examples for Steel Highway Bridges*. CCEER Report 00-8, University of Nevada, Reno,
- Itani, A. M. and J. Woodgate, 2000, *Displacement Ductility of Steel Members under Axial Tension*. J. of Testing and Evaluation, 28(1), 22-26.
- Jain, K.A., Goel, S.C., and Hanson, R.D., 1978. *Hysteresis Behavior of Bracing Members and Seismic Response of Braced Frames With Different Proportions*. Report No. UMEE-78R3. The University of Michigan, Ann Arbor, MN.
- Jain, K.A., Goel, S.C., and Hanson, R.D., 1980, *Hysteretic Cycles of Axially Loaded Steel Members*. Journal of Structural Engineering, 106(8),1777-1797.
- Japan Road Association, 2002, *Specifications for Highway Bridges, Part V, Seismic Design*, Japan.
- Kasai, K. and Popov, E.P., 1986, *Cyclic Web Buckling Control for Shear Link Beams*. Journal of Structural Engineering, ASCE, 112(3), 505-523.
- Kunde, M.C., and Jangid, R.S., 2003, *Seismic Behavior of Isolated Bridges: A State-of-the-Art Review*. Electronic J. of Struct. Engrg., 3, 140-170.
- Lloyd, R.M., and Wright, H.D., 1990, *Shear Connection between Composite Slabs and Steel Beams*. J. Construct. Steel Research, 15(4), 255-285.
- Maleki, S., 2002, *Effect of Deck and Support Stiffness on Seismic Response of Slab-Girder Bridges*. Engineering Structures, 24, 219-226.
- Malley, J.O. and Popov, E.P., 1983, *Design Considerations for Shear Links in Eccentric Braced Frames*. EERC Report 83-24, University of California, Berkeley, CA.
- McMullin, K.M. and Astaneh-Asl, A., 1994, *Cyclic Behavior of Welded Shear Studs*. Proc. Of Structures Congress XII, Atlanta, GA. April 24-28.
- Mertz, D. P., 2001, *Designer's Guide to Cross-Frame Diaphragms*. American Iron and Steel Institute, Washington, DC. [www.steel.org/infrastructure/bridges](http://www.steel.org/infrastructure/bridges).
- Ministry of Construction, 1995, *Investigation of Damage to Highway Bridges from the Hyogoken-Nanbu Earthquake – Preliminary Report (in Japanese)*. Report Ministry of Construction – Hyogoken-Nanbu Earthquake Committee on Highway Bridge Damage Prevention, Tokyo, Japan.
- Mouras, J.M., Sutton, J.P., Frank, K.H., and Williamson, E.B., 2008, *The Tensile Capacity of Welded Shear Studs*. Center for Transportation Research at the University of Texas, Austin, TX. Report 9-5498-R2, October 14, 2008.
- Multidisciplinary Center for Earthquake Engineering Research (MCEER) / Applied Technology Council (ATC) , 2004, *Recommended LRFD Guidelines for Seismic Design of Highway Bridges (2 Volumes)*. ATC/MCEER (joint venture), Redwood City, CA.
- Nakashima, M., 1995, *Strain Hardening Behavior of Shear Panels mad of Low-Yield Steel. I: Testing*. Journal of Structural Engineering, ASCE, 121(12), 1742-1749.

- Nippon Steel Corporation, 2002, *Seismic Behavior of Typical Steel (Unbonded Brace) - Tensile Test Report for Steel Material of LYP-225*. Nippon Steel Corporation, Japan.
- Oehlers, D.J., 1995, *Design and Assessment of Shear Connectors in Composite Bridge Beams*. J. of Struct. Engrg., 121(2), 214-224.
- Oehlers, D.J. and Coughlan, C.G., 1986, *The Shear Stiffness of Stud Shear Connections in Composite Beams*. J. of Construct. Steel Research, 6, 273-284.
- Oehlers, D.J. and Johnson, R.P., 1987, *The Strength of Stud Shear Connections in Composite Beams*. Struct. Engineer, 65B(2), 44-48.
- Ollgaard, J.G., Slutter R.G. and Fisher, J.W., 1971, *Shear Strength of Stud Connectors in Lightweight and Normal-Weight Concrete*. Engrg. J. Am. Inst. Steel Cons. 8, 55-64.
- Pekcan, G, Mander J., Chen S., 1999, *Fundamental Considerations of the Design of Nonlinear Viscous Dampers*, Earthquake Engng. Struct. Dyn. 28, 1405-1425
- Priestley, M.J.N., Seible, F., and Calvi, G.M., 1996, *Seismic Design and Retrofit of Highway Bridges*. John Wiley and Sons, Inc., NY.
- Robinson, W.H., 1993, *Seismic Isolation of Bridges in New Zealand*. Proc. of the Second USJapan Workshop on Earthquake Protective Systems for Bridges, Japan, 185-194.
- Sabelli, R., 2001, *Research on Improving the Design and Analysis of Earthquake-resistant Steelbraced Frames*. Report PF2000-9 - FEMA/EERI 2000 Professional Fellowship.
- Sabelli, R., and Aiken, I., 2003, *Development of Building Code Provisions for Buckling-Restrained Braced Frames*. Proc. of the 2003 SEAOC Convention, Squaw Creek, CA,
- Sabelli, R., Mahin, S., and Chang, C., 2003, *Seismic Demands on Steel Braced Frame Buildings with Buckling-Restrained Braces*. Engineering Structures, 25(5), 655-666.
- Saiidi, M., Maragakis, E., and Griffin, G., 1999, *Effect of Base Isolation on the Seismic Response of Multi-column Bridges*. Struct. Engrg. and Mech., 8(4), 411-419.
- Sarraf, M., and Bruneau, M., 1998a, *Ductile Seismic Retrofit of Steel Deck-Truss Bridges. I: Strategy and Modeling*. J. of Struct.Engrg., 124(11), 1253-1263.
- Sarraf, M., and Bruneau, M., 1998b, *Ductile Seismic Retrofit of Steel Deck-Truss Bridges. II: Design Applications*, J. of Struct. Engrg., 124(11), 1263-1271.
- Sarraf, M. and Bruneau, M., 1998a, *Ductile Seismic Retrofit of Steel Deck-Truss Bridges. I: Strategy and Modeling*. Journal of Structural Engineering, ASCE, 124(11), 1253-1263.
- Sarraf, M. and Bruneau, M., 1998b, *Ductile Seismic Retrofit of Steel Deck-Truss Bridges. II: Design Applications*. Journal of Structural Engineering, ASCE, 124(11), 1263-1271.

- Seracino, R., Oehlers, D.J. and Yeo, M.F., 2001, *Partial-interaction Flexural Stresses in Composite Steel and Concrete Bridge Beams*. *Engrg. Structures*, 23(2001), 1186-1193.
- Shinozuka, M. (ed), Ballantyne, D., Borchardt, R., Buckle, I.G., O'Rourke, T., and Schiff, A., 1995, *The Hanshin-Awaji Earthquake of January 17, 1995, performance of Lifelines*. Technical Report NCEER-95-0015, National Center for Earthquake Engineering Research, Buffalo, NY.
- Tsai, K.C., Chen, H.W., Hong, C.P., and Su, Y.F., 1993, *Design of Steel Triangular Plate Energy Absorbers for Seismic-Resistance Construction*. *Earthquake Spectra*, EERI, 9(3), 505-528.
- Washington State Department of Transportation (WSDOT), 2001. Personal communication.
- Wada, A., Saeki, E., Takeuchi, T., and Watanabe, A., 1989, *Development of Unbonded Brace. Column* (A Nippon Steel Publication), No 115, 12.
- Zahrai, S. M., and Bruneau, M., 1998a, *Impact of Diaphragms on Seismic Response of Straight Slab-on-Girder Steel Bridges*, *J. of Struct. Engrg.*, 124(8), 938-947.
- Zahrai, S. M., and Bruneau, M., 1998b, *Seismic Retrofit of Slab-on-Girder Steel Bridges using Ductile End Diaphragms*, Report OCEERC 98-20, University of Ottawa, Ottawa, Ontario.
- Zahrai, S. M., and Bruneau, M., 1999a, *Ductile End-Diaphragms for Seismic Retrofit of Slab-on-Girder Steel Bridges*, *J. of Struct. Engrg.*, 125(1), 71-80.
- Zahrai, S. M., and Bruneau, M., 1999b, *Cyclic Testing of Ductile End-Diaphragms for Slab-on-Girder Steel Bridges*, *J. of Struct. Engrg.*, 125(9), 987-996.
- Zahrai, S. M., and Bruneau, M., 2000, *Seismic Performance of Diaphragms in Slab-on-Girder Steel Bridges*. Proc. 12th World Conference on Earthquake Engrg., Paper No 2406, Auckland, New Zealand, January.

Table 1-1. Comparison of bridge model response with ductile X-braces and elastic X-braces.

System	1.0 El Centro Earthquake		1.5 El Centro Earthquake		2.0 El Centro Earthquake	
	Max. Shear/Weight	Max. Displ. (mm)	Max. Shear/Weight	Max. Displ. (mm)	Max. Shear/Weight	Max. Displ. (mm)
Elastic X-Braces	0.65	2.0	0.99	3.8	1.24	5.1
Ductile X-Braces	0.51	3.9	0.70	12.1	0.76	20.3

Notes: 1. Displacements are measured at the deck slab relative to the transverse bearing displacements.

2. Input record is the 1940 El Centro earthquake, amplitude scaled as shown.

Table 1-2. List of Cyclic Axial Single Angle Experiments

Specimen	Section	Coupon Test	Effective Length (in.)	Gusset Thickness (in.)	Connection (Reinforced)	First Cycle	$A_n/A_g$	$b/t^a$	$Kl/r^b$
A	1¼×1¼×¼	1	40.5	½	Bolted	Compression	0.81	7	119
B	1¼×1¼×¼	1	40.5	1	Bolted	Compression	0.81	7	83
C	1¼×1¼×¼	1	40.5	1	Bolted	Tension	0.81	7	83
D	1¼×1¼×¼	1	40.5	1	Bolted (x)	Tension	0.93	7	83
E	1¼×1¼×¼	1	40.5	1	Bolted (c)	Compression	1.00	7	83
F	1¼×1¼×¼	1	22.5	1	Bolted	Compression	0.81	7	46
G	1¼×1¼×¼	1	22.5	1	Bolted	Compression	0.81	7	46
H	1¼×1¼×¼	1	22.5	1	Bolted (x)	Tension	0.93	7	46
I	1¼×1¼×¼	1	22.5	1	Bolted (c)	Compression	1.00	7	46
J	1¼×1¼×¼	2	40.5	1	Welded	Compression	1.00	7	83
K	1¼×1¼×¼	2	40.5	1	Welded	Tension	1.00	7	83
L	1¼×1¼×¼	2	22.5	1	Welded	Compression	1.00	7	46
M	1¼×1¼×¼	2	22.5	1	Welded	Tension	1.00	7	46
N	1×1×x	3	50.5	1	Welded	Compression	1.00	5.33	181
O	1×1×x	3	50.5	1	Welded	Tension	1.00	5.33	181
P	1×1×x	3	25.4	1	Welded	Compression	1.00	5.33	91
Q	1×1×x	3	25.4	1	Welded	Tension	1.00	5.33	91

<sup>a</sup>The limiting  $b/t$  ratio for members of special concentrically braced frames in accordance with the AISC *Seismic Provisions* (2002) is 8.5 and for AASHTO (1998) is 12.8, and therefore satisfied by all members.

<sup>b</sup>The limiting  $Kl/r$  for special concentrically braced frames based on the AISC *Seismic Provisions* (2002) is 167 and for AASHTO (1998) is 120 for primary members, and therefore satisfied by all members, except Specimens N and O.  $K = 1.0$  for Specimen A and  $K = 0.7$  for the remaining specimens.

Table 1-3. Failure Mode, Maximum Effective Axial Strains, and Cumulative Effective Plastic Axial Strains in the Angles

Specimen	Failure Mode	Measured Ultimate Axial Strain (%)	Theoretical Yield Displacement (in.)	Cumulative Effective Plastic Strain (%)
A	At bolt hole	3.1	0.0754	23
B	At bolt hole	4.9	0.0754	77
C	At bolt hole	5.4	0.0754	82
D	At end plastic hinge	6.2	0.0754	127
E	At end plastic hinge	6.2	0.0754	115
F	At bolt hole	5.5	0.0419	52
G	At bolt hole	5.5	0.0419	57
H	At end plastic hinge	8.1	0.0419	127
I	At end plastic hinge	8.9	0.0419	144
J	At midspan plastic hinge	7.4	0.0754	176
K	At midspan plastic hinge	7.7	0.0754	190
L	At end plastic hinge	9.0	0.0419	146
M	At end plastic hinge	8.0	0.0419	128
N	At end plastic hinge	6.0	0.0940	142
O	At midspan plastic hinge	12.2	0.0940	596
P	At end plastic hinge	10.0	0.0473	201
Q	At midspan plastic hinge	7.0	0.0473	113

Table 1-4. Tensile and Compressive Strengths of Single Angle Specimens Compared with Expected Properties

Spec.	Tensile Strength					Compressive Strength		
	Measured Yield Strength (kips)	Measured Ultimate Force (kips)	Nominal Yield Force (kips)	Yield Force Coupon Tests (kips)	Expected Yield Strength (kips)	Measured Buckling Strength (kips)	Calculated Buckling Force 1 <sup>b</sup> (kips)	Calculated Buckling Force 2 <sup>c</sup> (kips)
A	*	43.4	29.3	45.5	43.9	15.9	12.2	14.3
B	44.9	50.8	29.3	45.5	43.9	27.7	12.2	25.8
C	44.6	49.2	29.3	45.5	43.9	20.4	12.2	25.8
D	44.8	56.0	29.3	45.5	43.9	17.8	12.2	25.8
E	43.8	54.6	29.3	45.5	43.9	29.9	12.2	25.8
F	45.2	47.8	29.3	45.5	43.9	33.7	18.8	38.2
G	45.1	47.7	29.3	45.5	43.9	33.9	18.8	38.2
H	45.0	54.9	29.3	45.5	43.9	31.3	18.8	38.2
I	44.8	56.8	29.3	45.5	43.9	30.5	18.8	38.2
J	38.5	48.6	29.3	37.2	43.9	20.2	12.2	23.4
K	38.6	49.2	29.3	37.2	43.9	20.8	12.2	23.4
L	40.0	51.9	29.3	37.2	43.9	28.5	18.1	32.3
M	40.2	52.0	29.3	37.2	43.9	28.7	18.1	32.3
N	16.3	18.6	12.2	16.7	18.4	6.3	1.4	2.6
O	17.4	20.8	12.2	16.7	18.4	4.6	1.4	2.6
P	16.6	20.7	12.2	16.7	18.4	12.0	4.4	9.2
Q	17.6	22.5	12.2	16.7	18.4	10.7	4.4	9.2

\*Yield strength not clearly identified.  
<sup>b</sup>Calculated based on AISC specifications (2005) with  $K =$  that calculated from Section E5(a)  
<sup>c</sup>Calculated based on AISC specifications (2005) with  $K = 1.0$  for Specimen A (plastic hinges observed in gusset plates) and 0.7 for all other specimens (plastic hinges observed in angles).



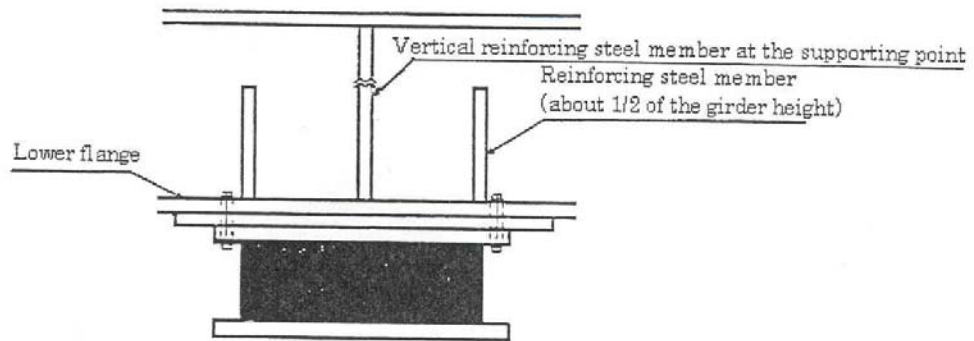


Fig.C-14.2.1 An Example of Reinforcing Abdominal Plate of a Steel Bridge above the Bearing Support by Using Vertical Reinforcing Steel Members

Figure 1-1. JRA Specifications, reinforcement at bearing support.

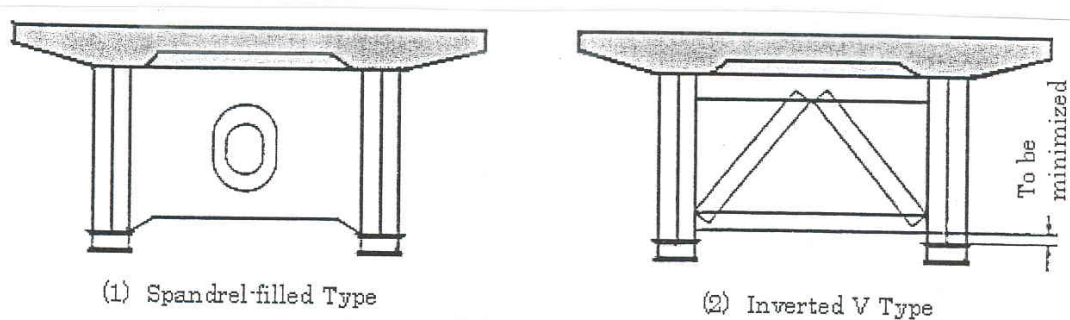


Fig.C-14.2.2 Structural Examples of Crossbeam in Steel Bridge

Figure 1-2. JRA Specifications, minimized space at lower ends of lateral support.

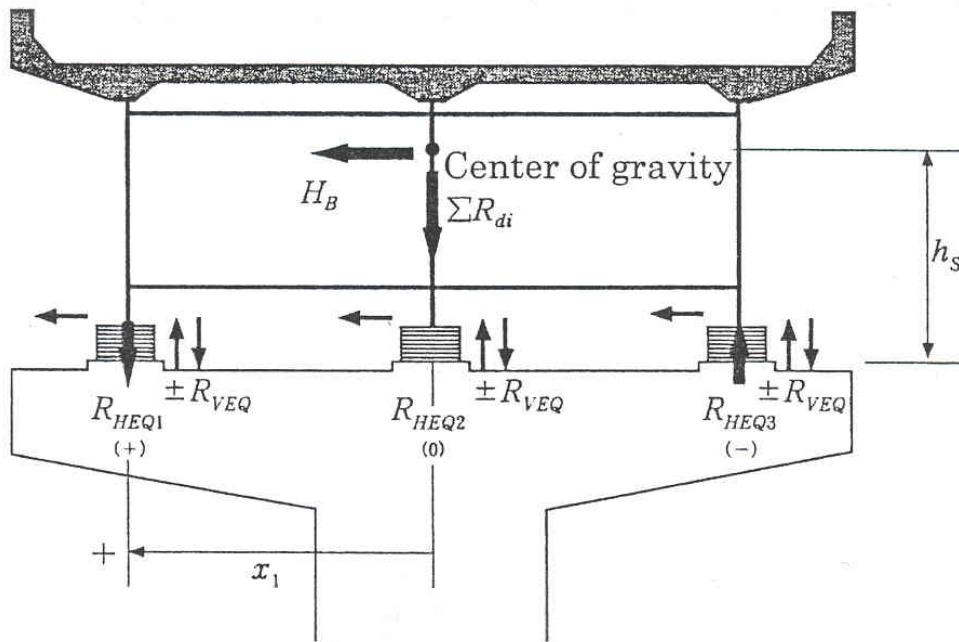


Figure 1-3. JRA Specifications, application of horizontal earthquake force.

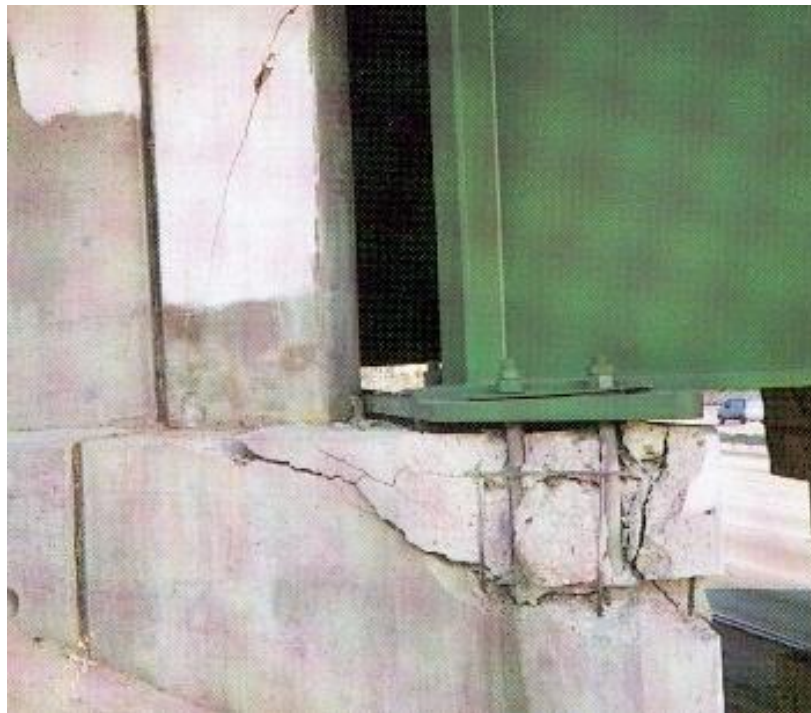


Figure 1-4. Damage to Bearing during the 1994 Northridge Earthquake.



Figure 1-5. Damage to End Cross Frames during the 1994 Northridge Earthquake



Figure 1-6. Damage to Web Stiffeners during the 1994 Northridge Earthquake.



Figure 1-7. Damage to End Cross Frames and Girders during 1995 Kobe Earthquake.



Figure 1-8. Failure of Shear Connectors in Bridge Model during Transverse Cyclic Loading.



Figure 1-9. Bent cross frames with V-pattern diagonals



Figure 1-10. Bent cross frames with X-pattern diagonals



Figure 1-11. Abutment cross frames with V-pattern diagonals



Figure 1-12. Abutment cross frames with V-pattern diagonals



Figure 1-13. Built up I-section diaphragm with transverse stiffener



Figure 1-14. Rolled shape diaphragm



Figure 1-15. Details of cross frames with inverted V-pattern diagonals



Figure 1-16. Details of cross frames with inverted V-pattern diagonals

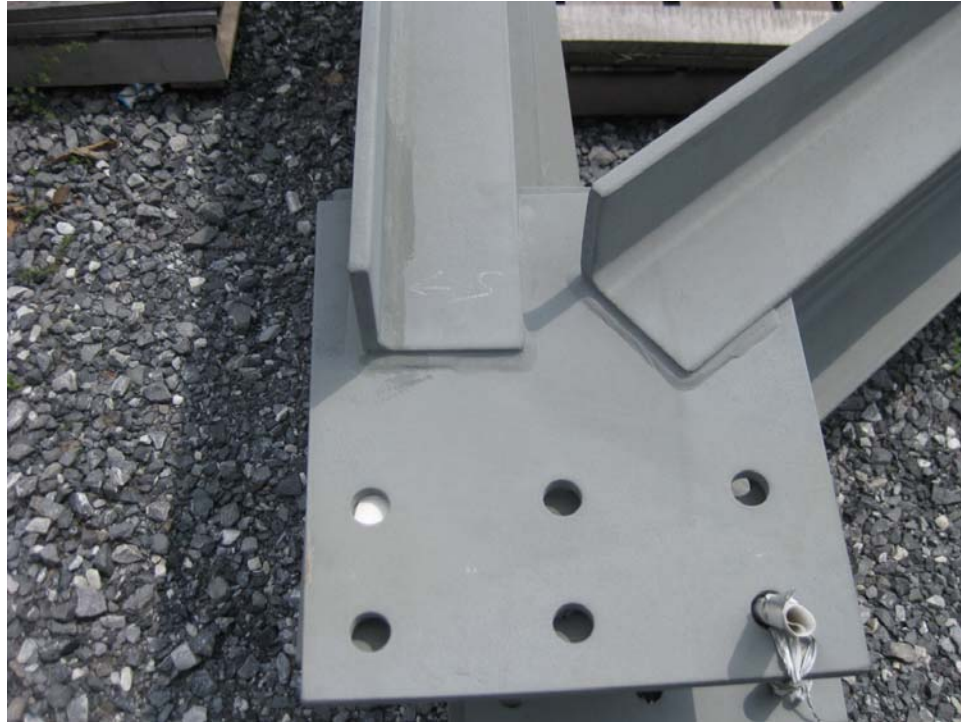


Figure 1-17. End details of cross frames with inverted V-pattern



Figure 1-18. Details of cross frames with X-pattern diagonals



Figure 1-19. End details of cross frames with X-pattern



Figure 1-20. End details of cross frames with X-pattern



Figure 1-21. Details of cross frames with X-pattern diagonals

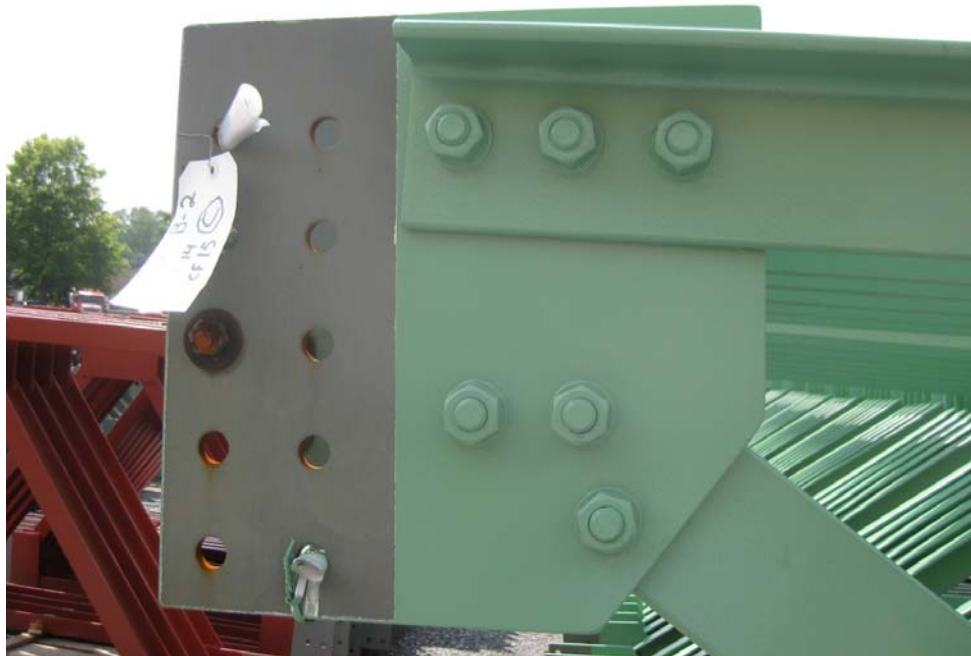


Figure 1-22. End details of cross frames with bolted members



Figure 1-23. Middle details of bolted cross frames with X pattern

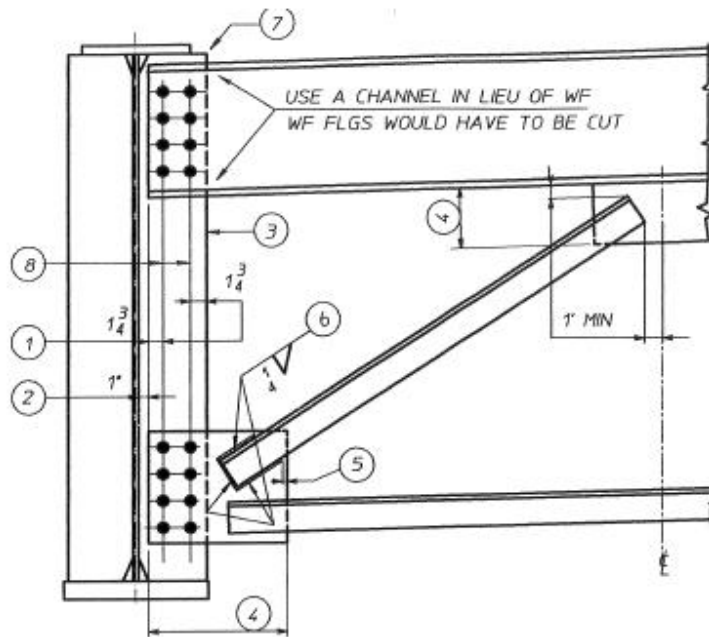


Figure 1-24. Preferred details for abutment cross frames

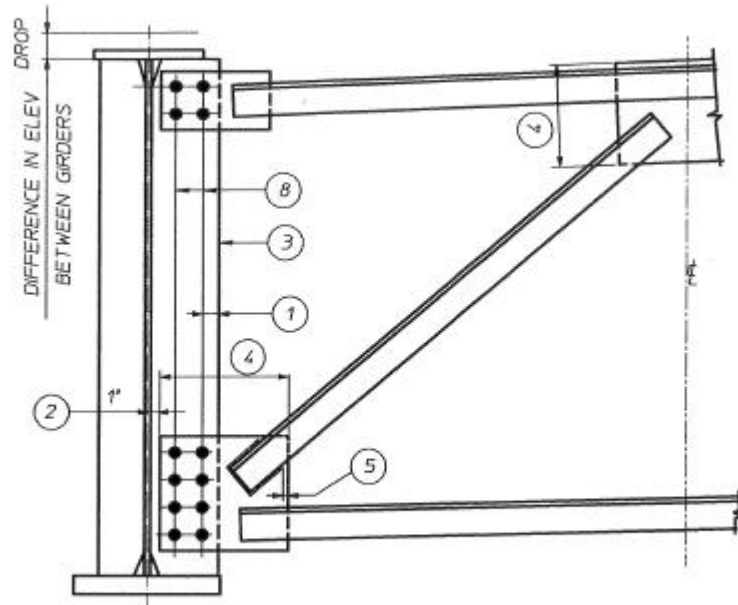


Figure 1-25. Preferred details for intermediate cross frames subjected to large forces

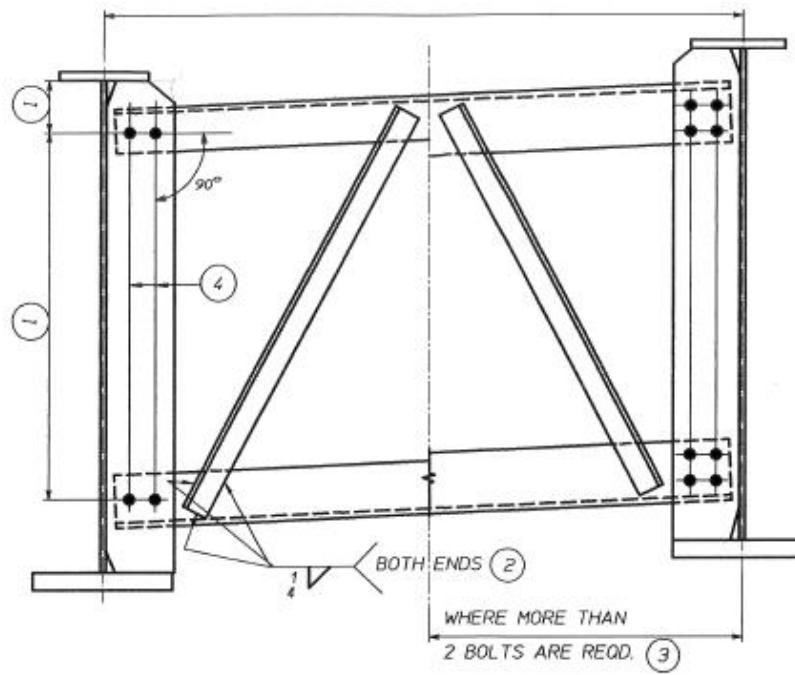


Figure 1-26. Preferred details for intermediate cross frame subjected to low forces



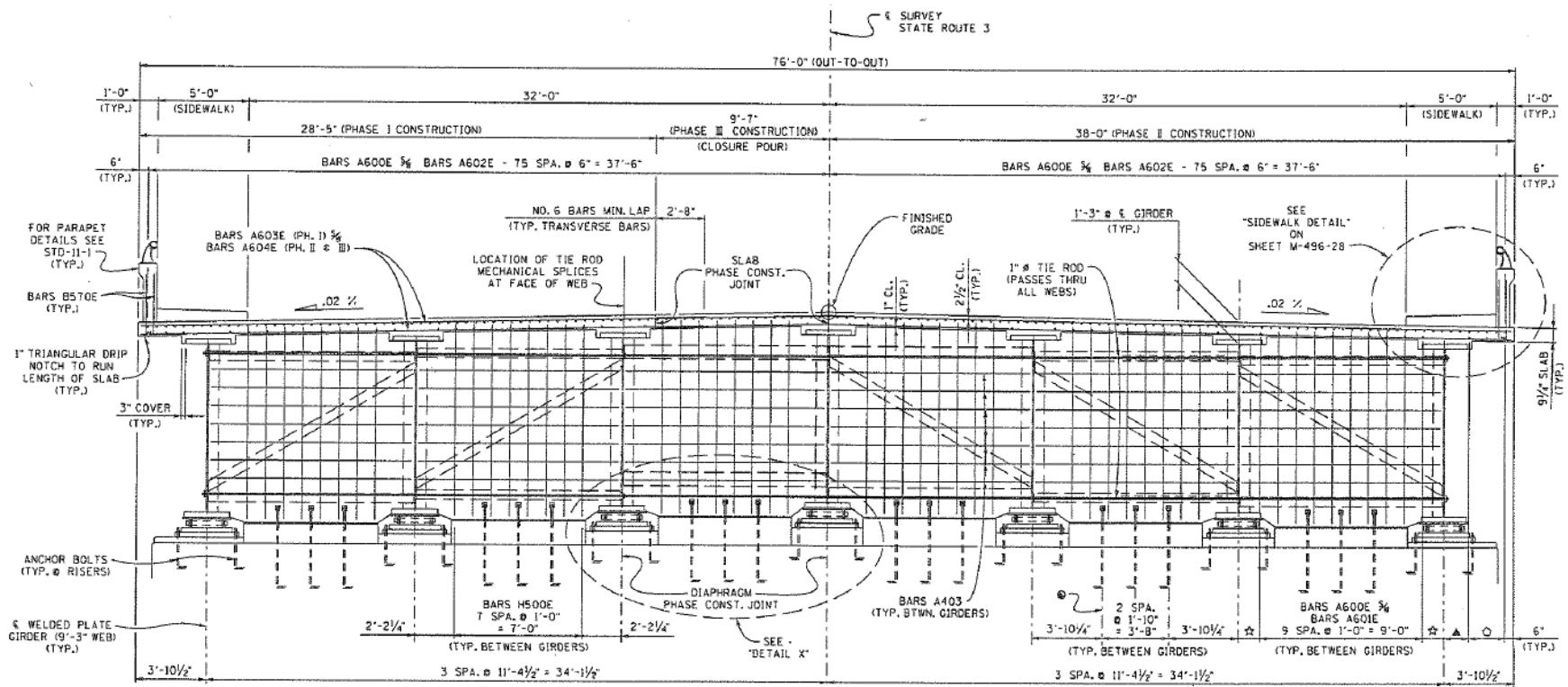


Figure 1-29. Detail used in the State of Tennessee where cross frames are used during erection

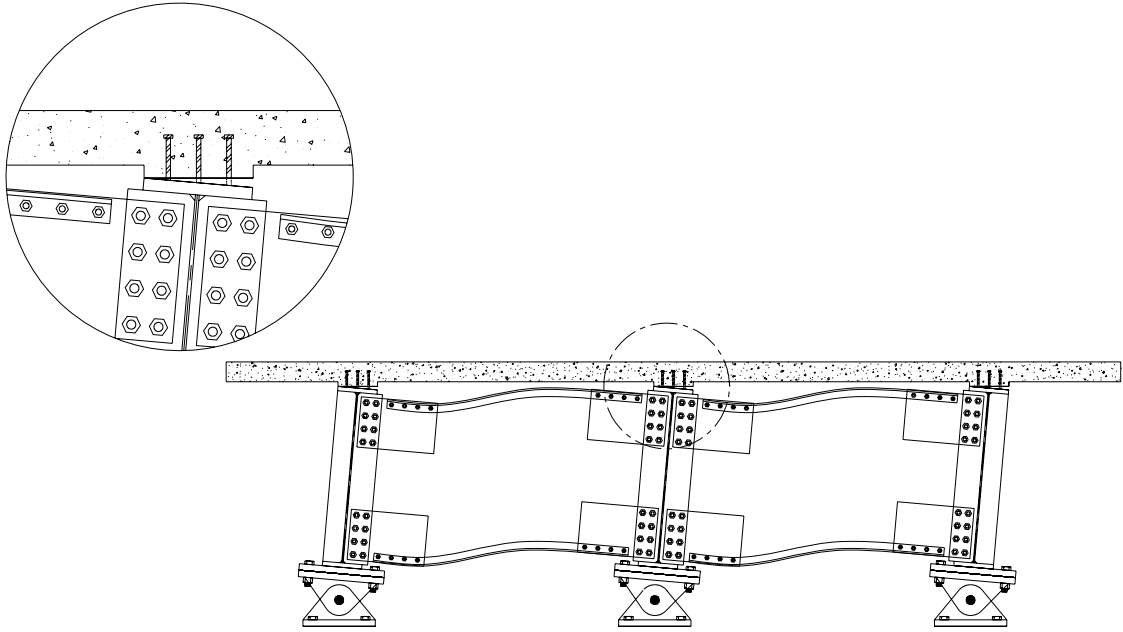


Figure 1-30. Kinematics of a support cross frame with shear connectors on the top girder flanges

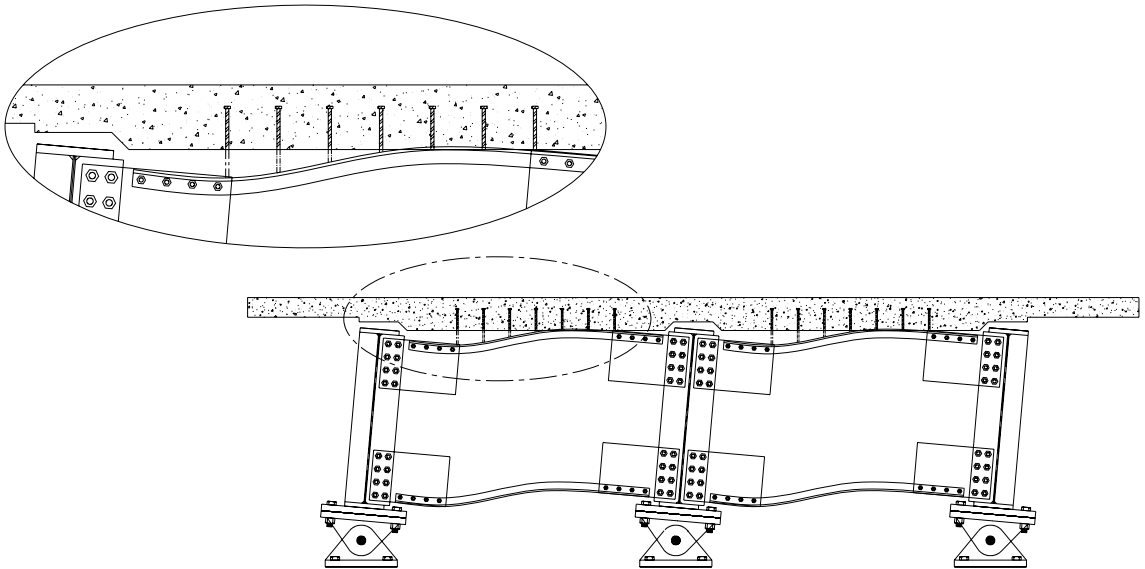


Figure 1-31. Kinematics of a support cross frame with shear connectors on the top chords

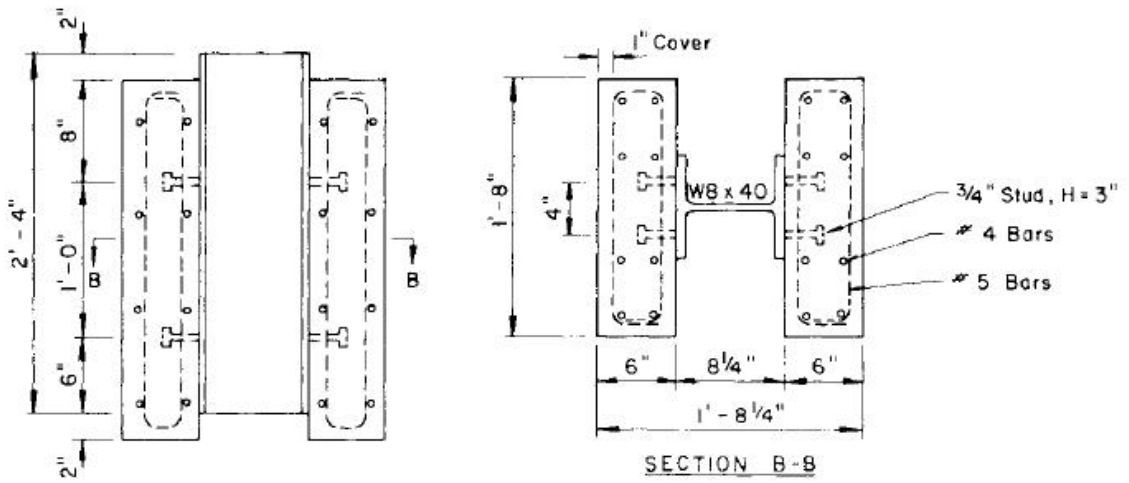


Figure 1-32. Test specimen used in two-slab push-out experiment

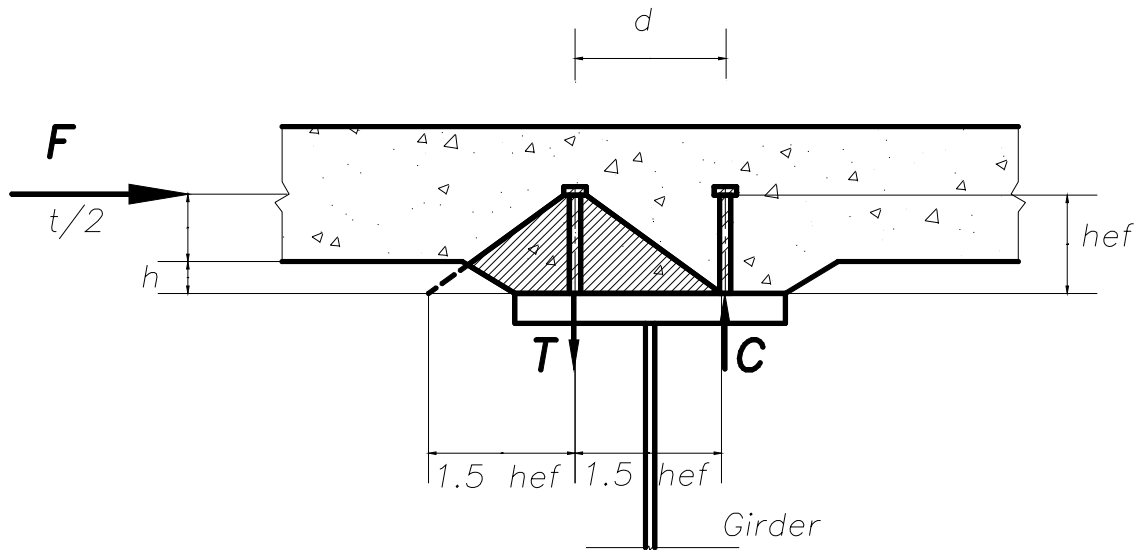


Figure 1-33. Deck-girder moment connection – concrete breakout failure in the stud in tension

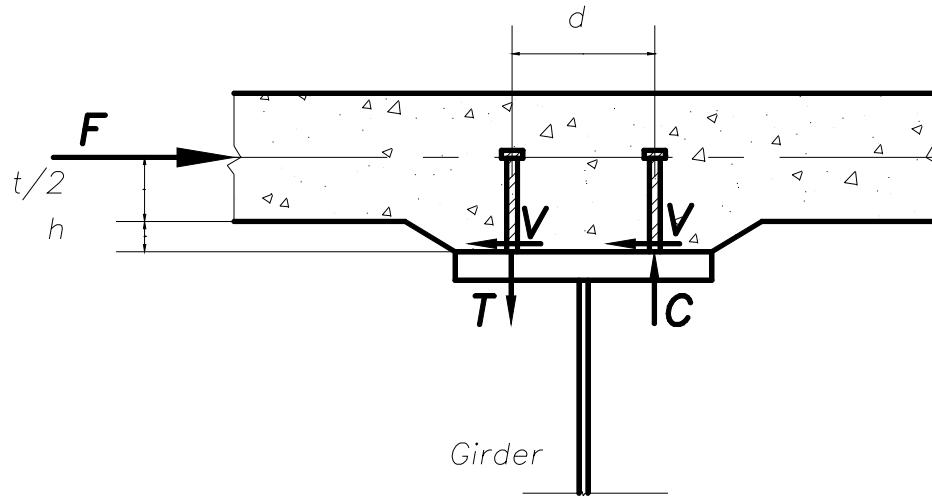


Figure 1-34. Moment connection of deck-girder studded joint

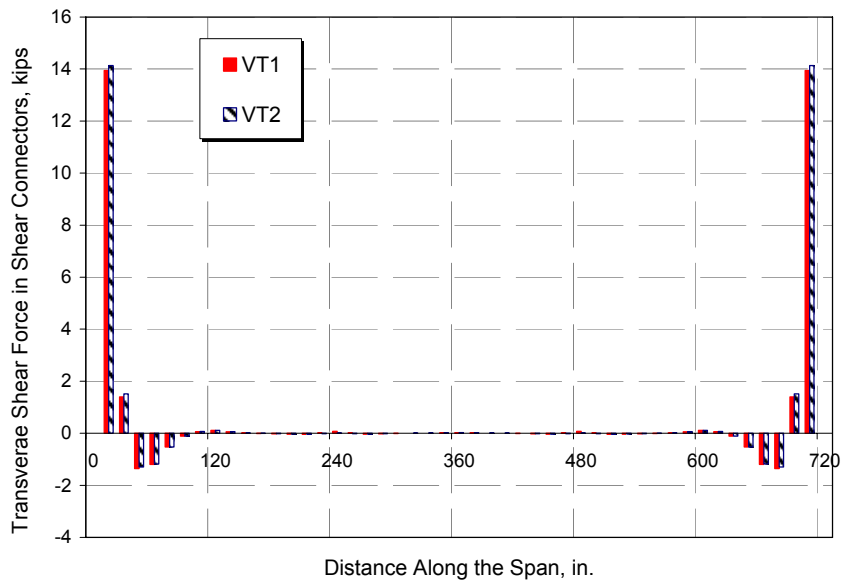


Figure 1-35. Transverse shear distribution in shear connectors on one girder for elastic superstructure without top chord attachment

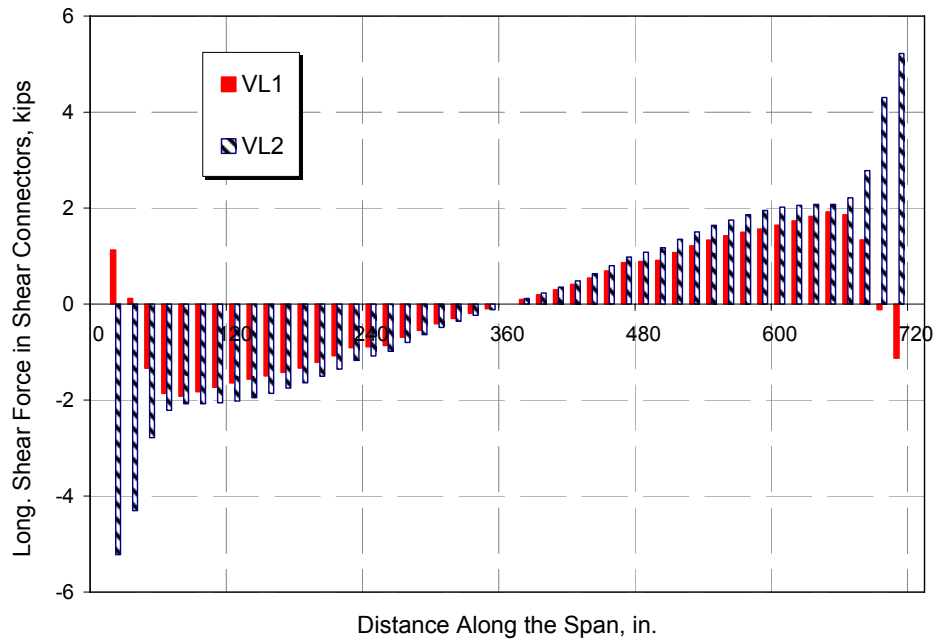


Figure 1-36. Longitudinal shear distribution in shear connectors on one girder for elastic superstructure without top chord attachment

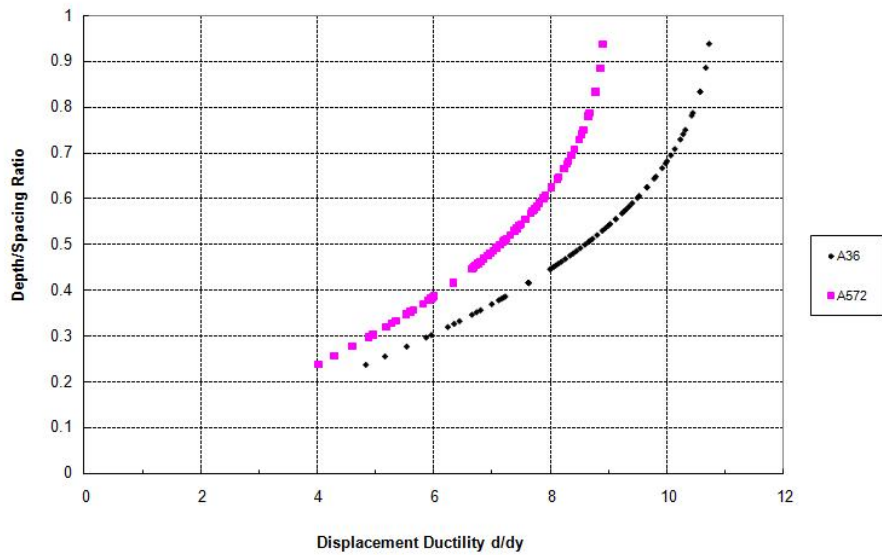


Figure 1-37. Limitation of D/S ratio for 4% drift limit

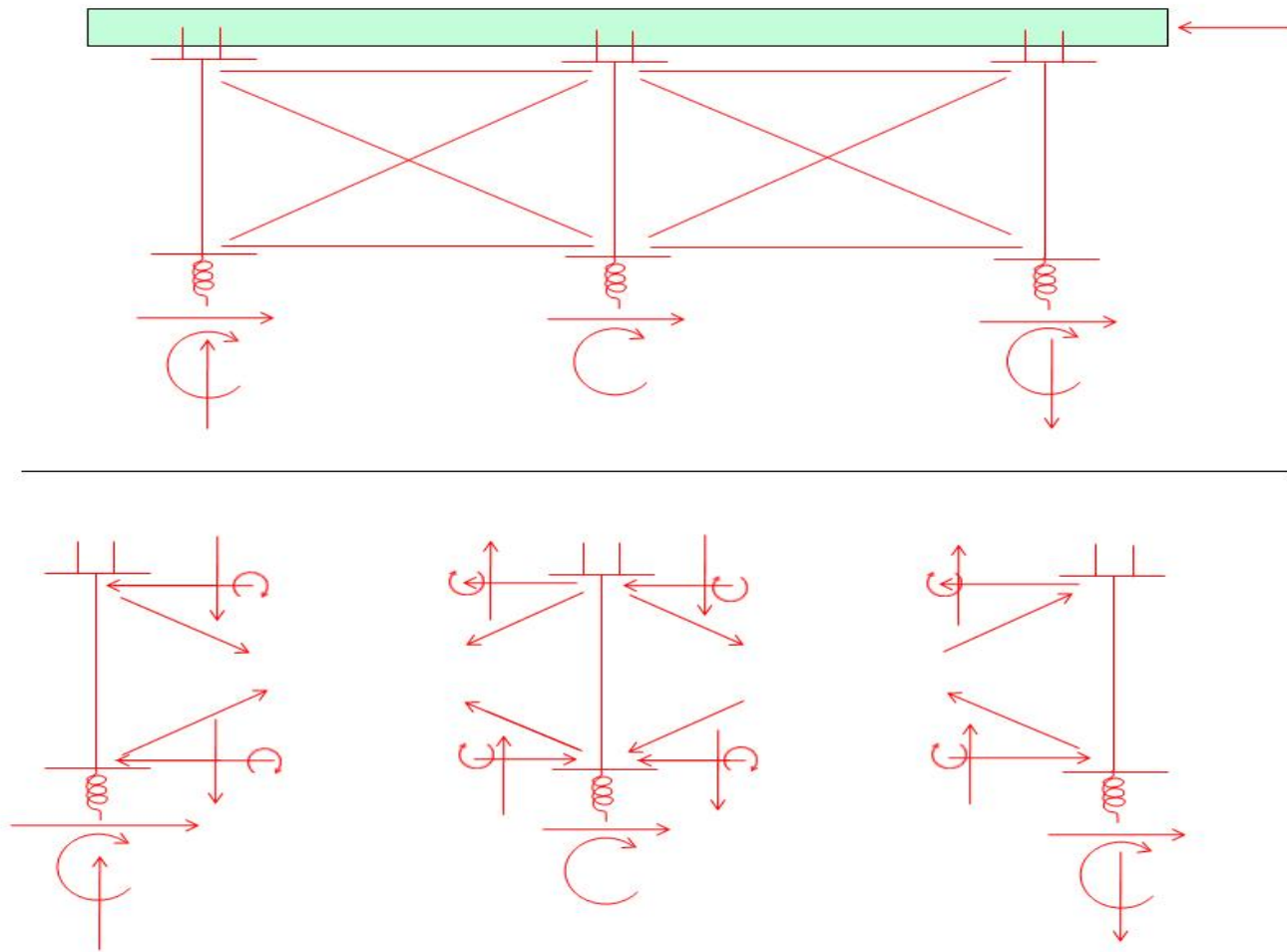


Figure 1-38. Free body diagram of internal forces due to lateral loading with connectors on top flange

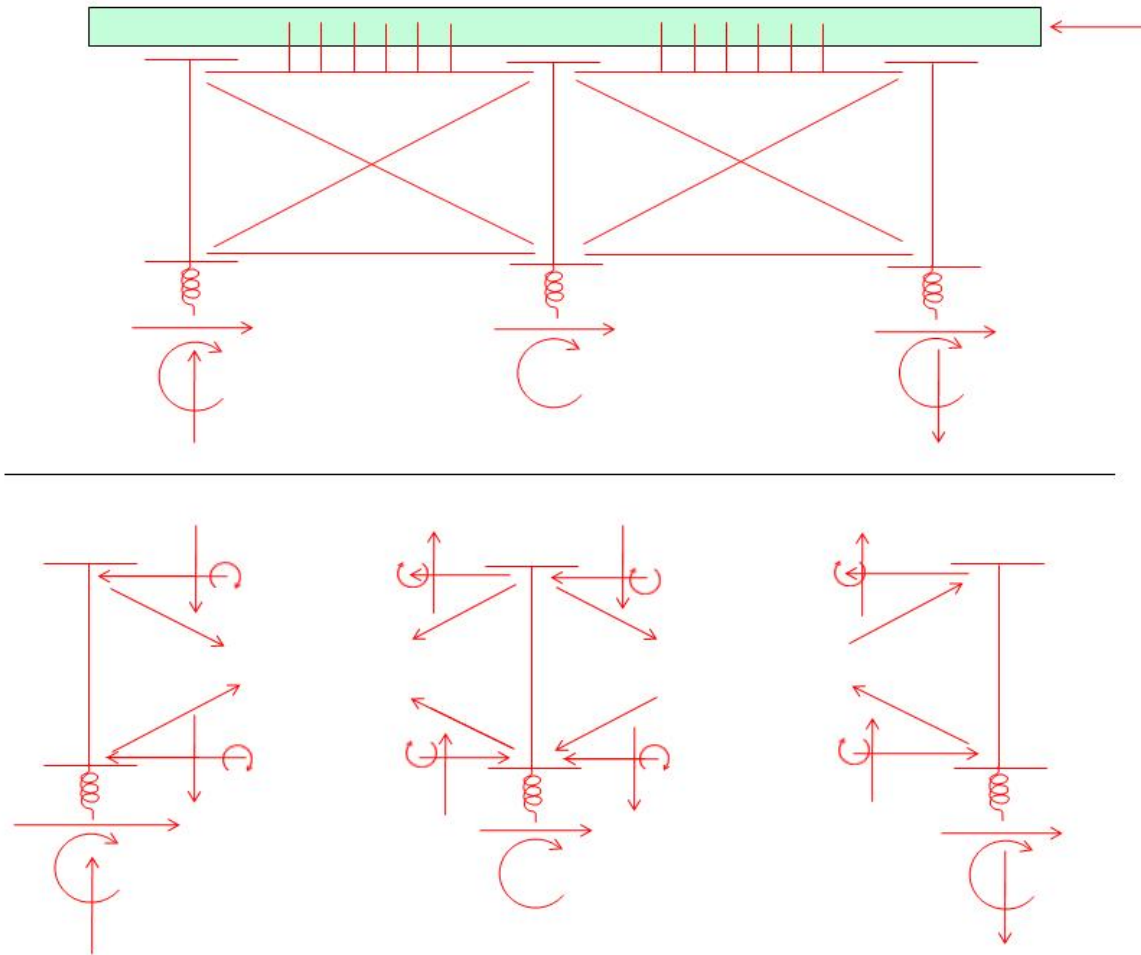


Figure 1-39. Free body diagram of internal forces due to lateral loading with connectors on top chord

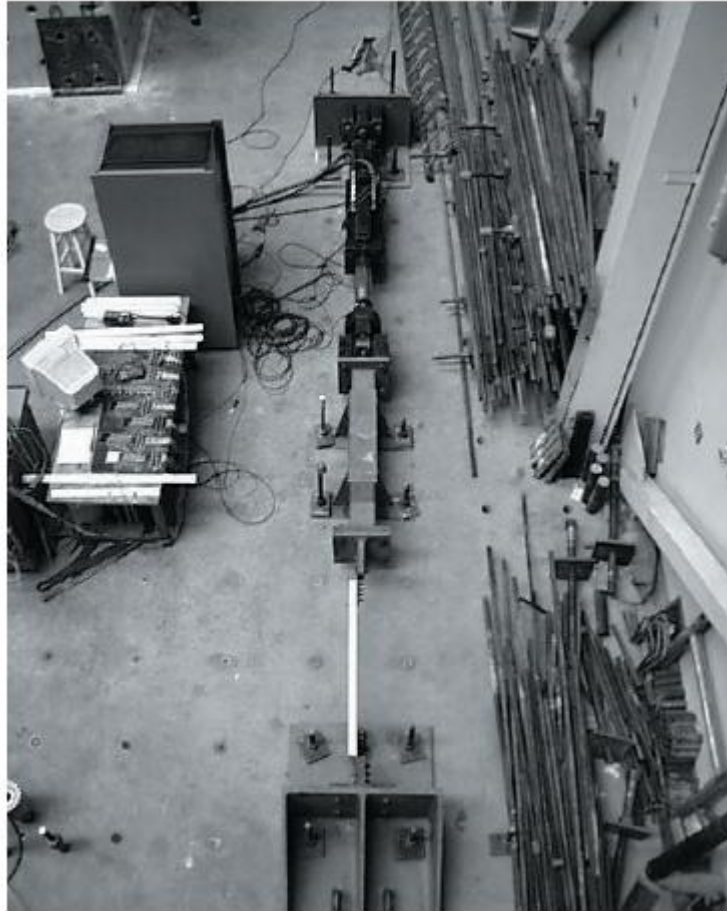


Figure 1-40. Experimental setup of cyclic axial experiments on angles

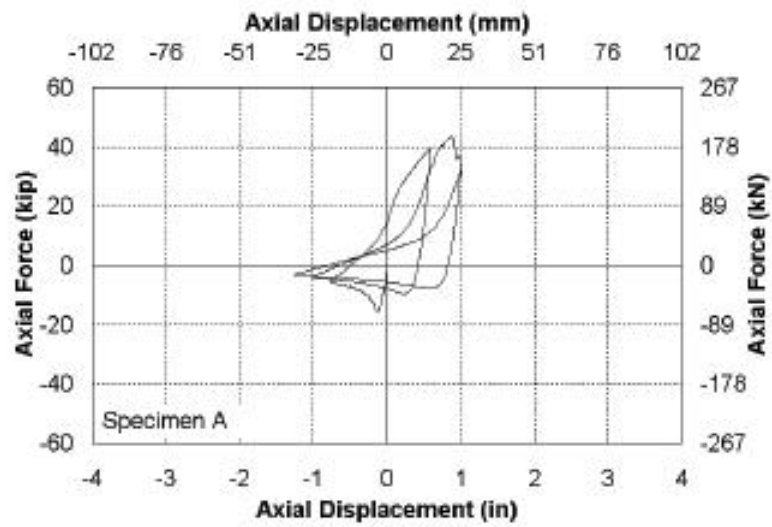


Figure 1-41. Hysteresis loops from single angle axial experiments

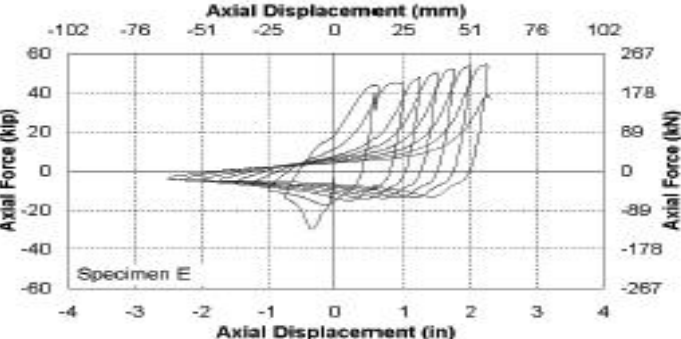
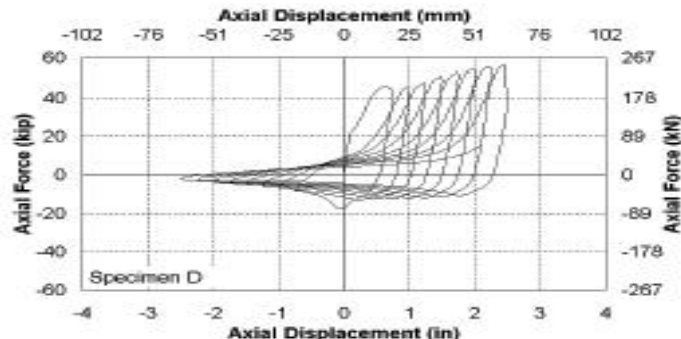
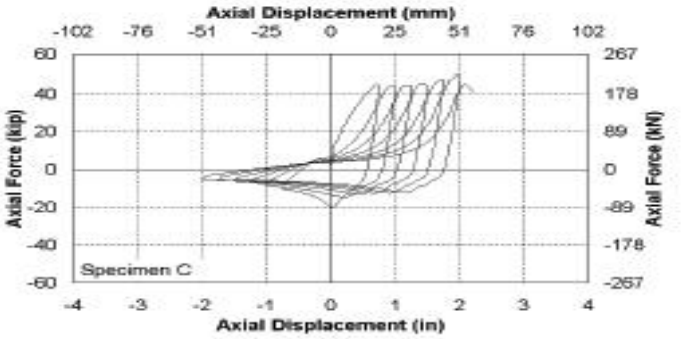
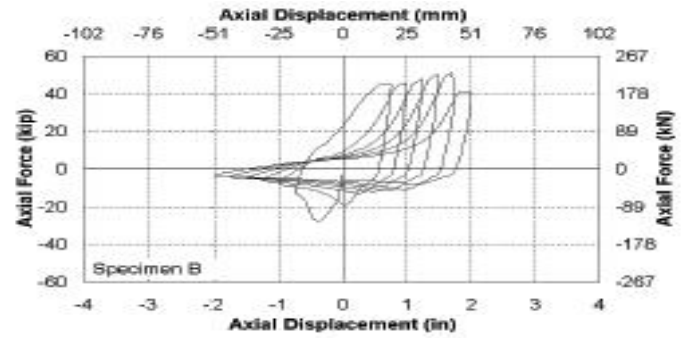


Figure 1-42. Hysteresis loops from single angle axial experiments

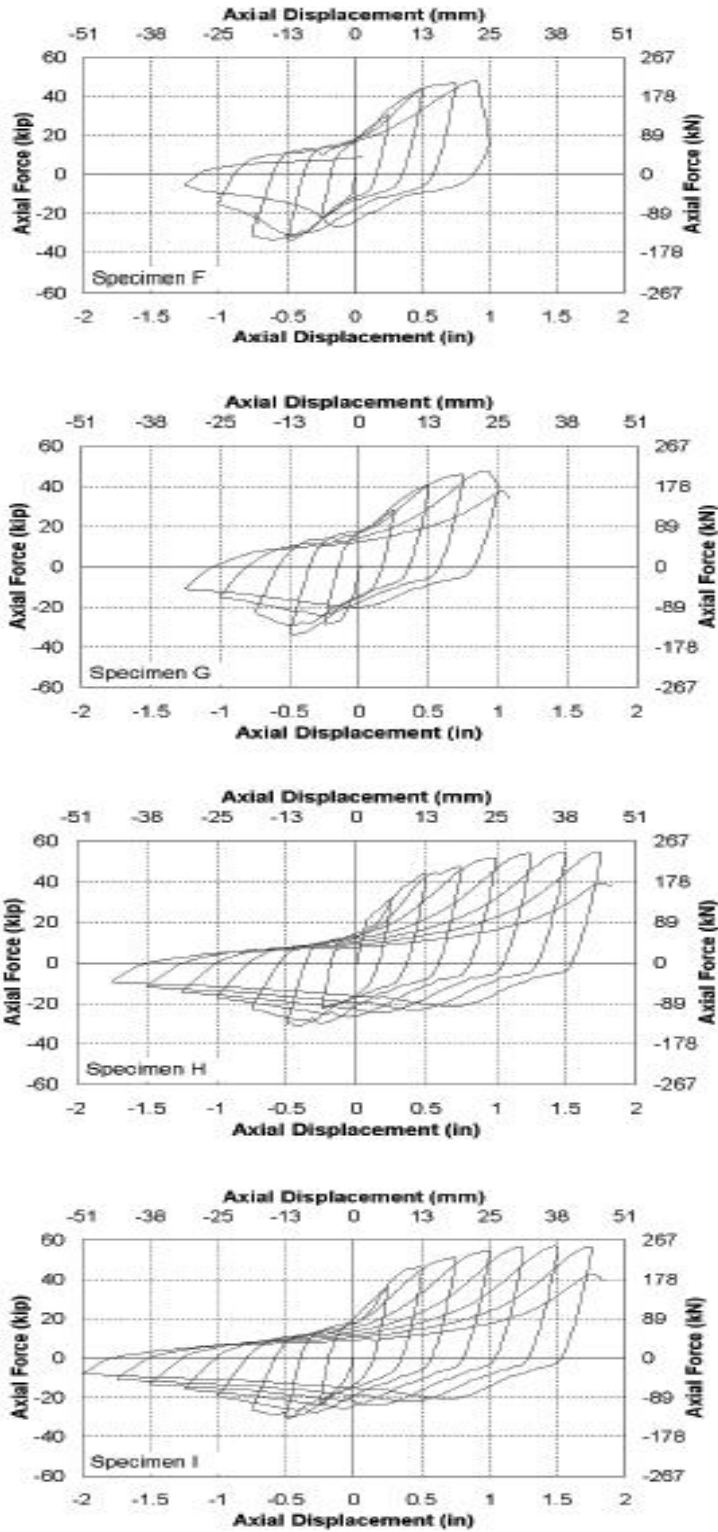


Figure 1-43. Hysteresis loops from single angle axial experiments

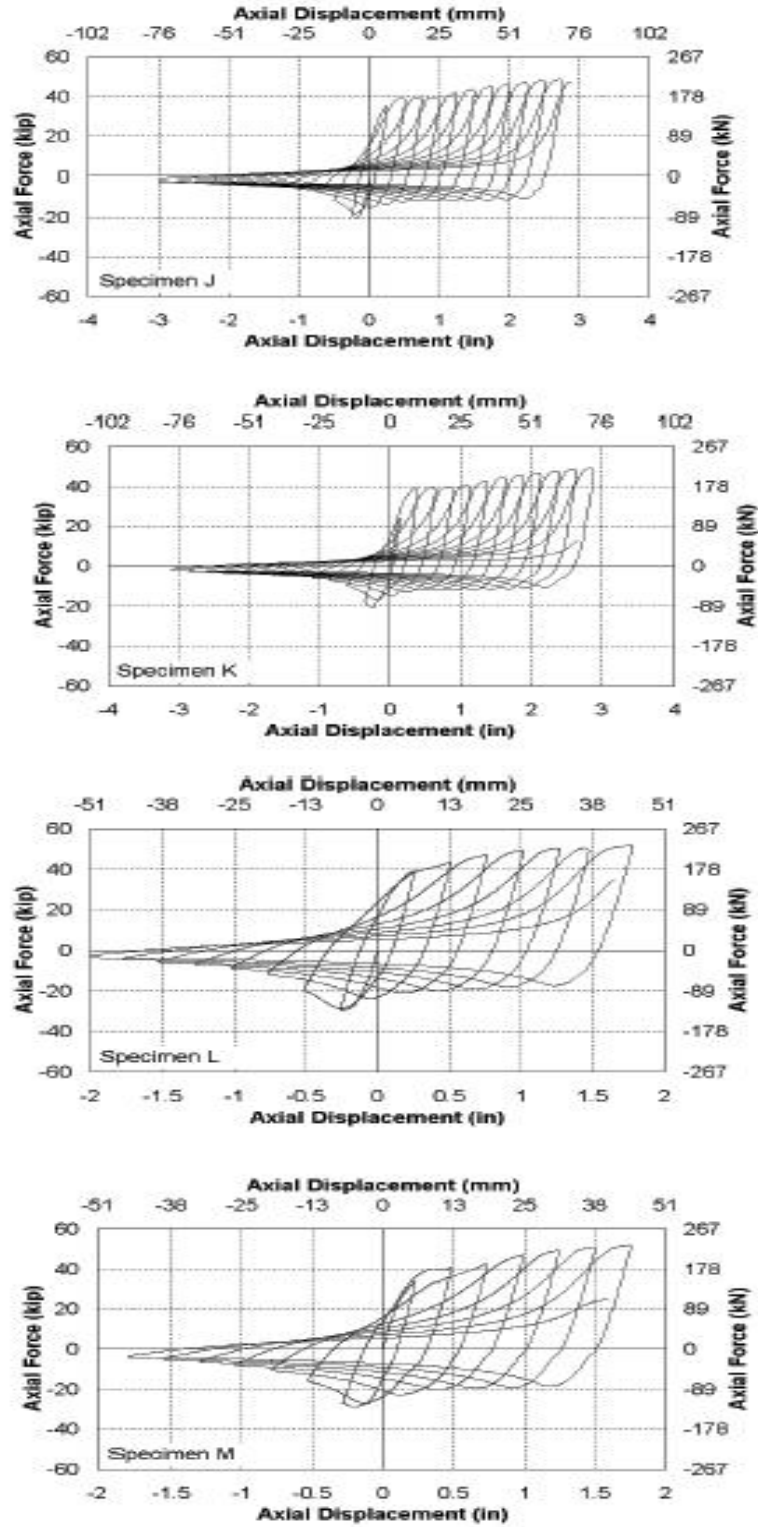


Figure 1-44. Hysteresis loops from single angle axial experiments

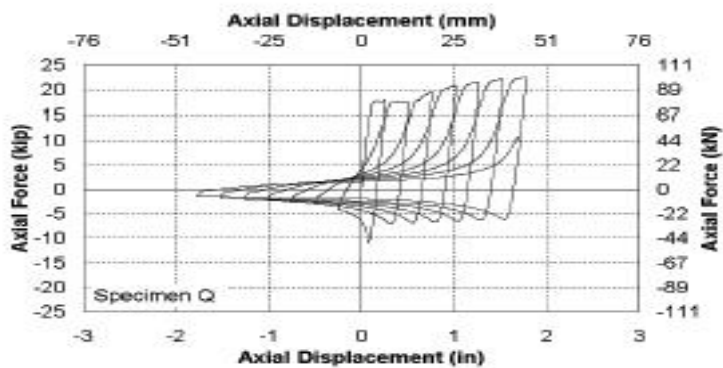
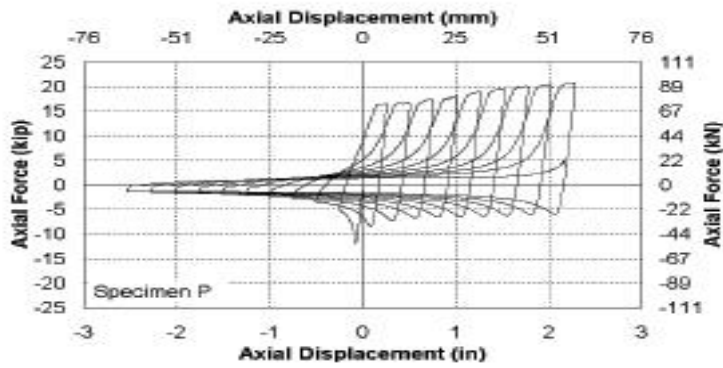
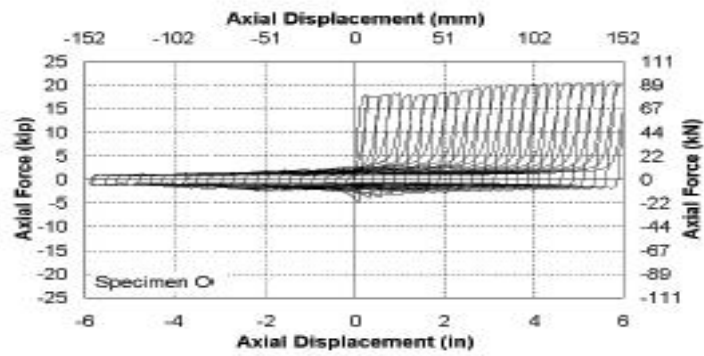
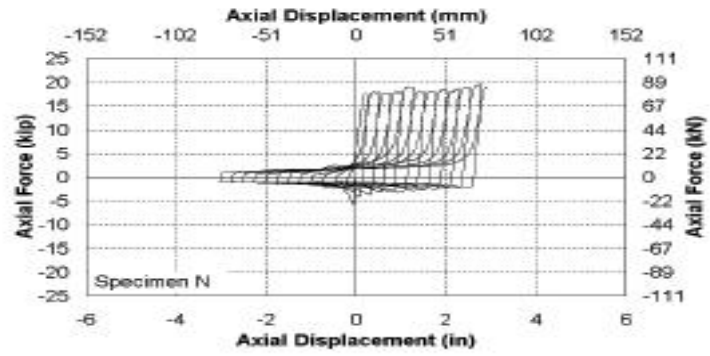


Figure 1-45. Hysteresis loops from single angle axial experiments

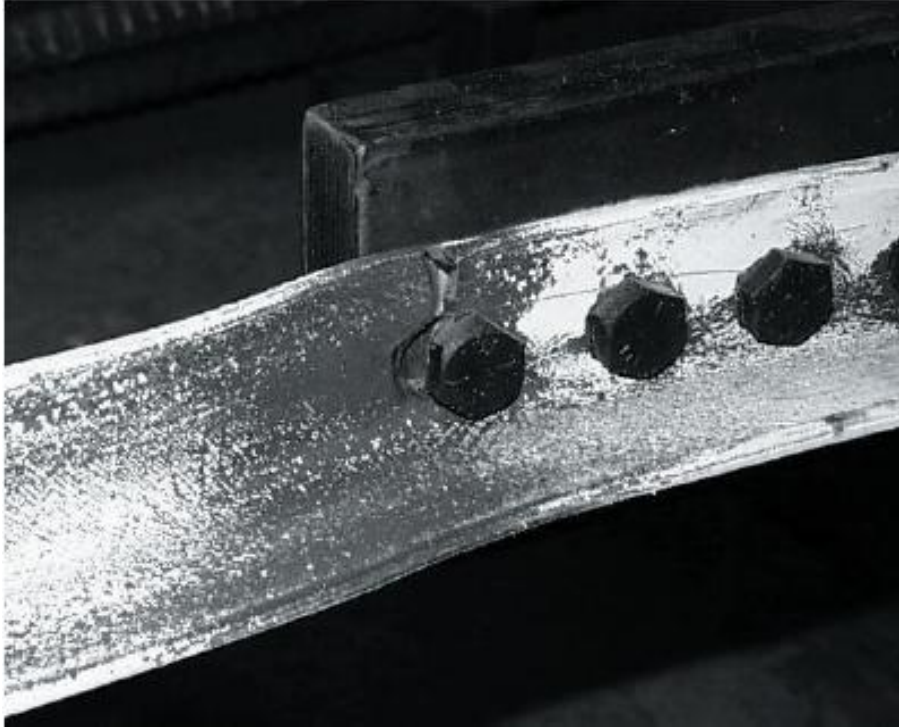


Figure 1-46. Fracture of bolted single angle specimen



Figure 1-47. Fracture of single angle specimen with thickened bolted connection

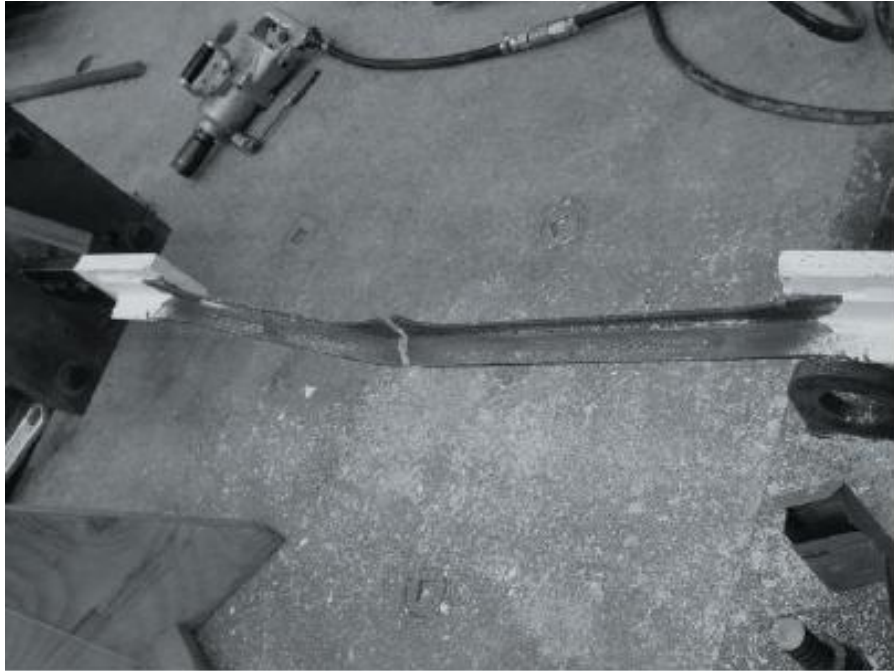


Figure 1-48. Fracture of single angle specimen with welded connections

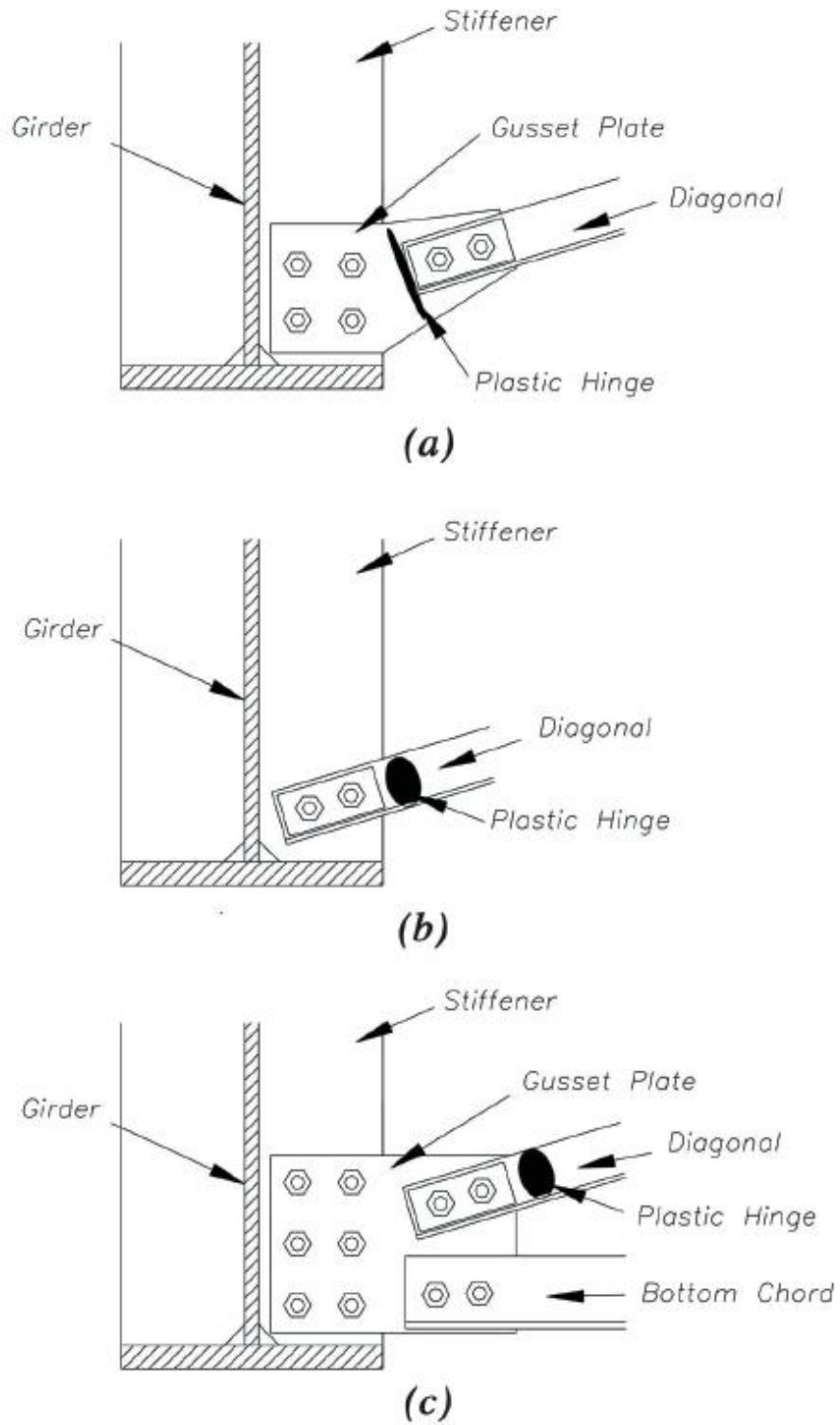


Figure 1-49. Different connection configurations for diagonal members of ductile end cross frames

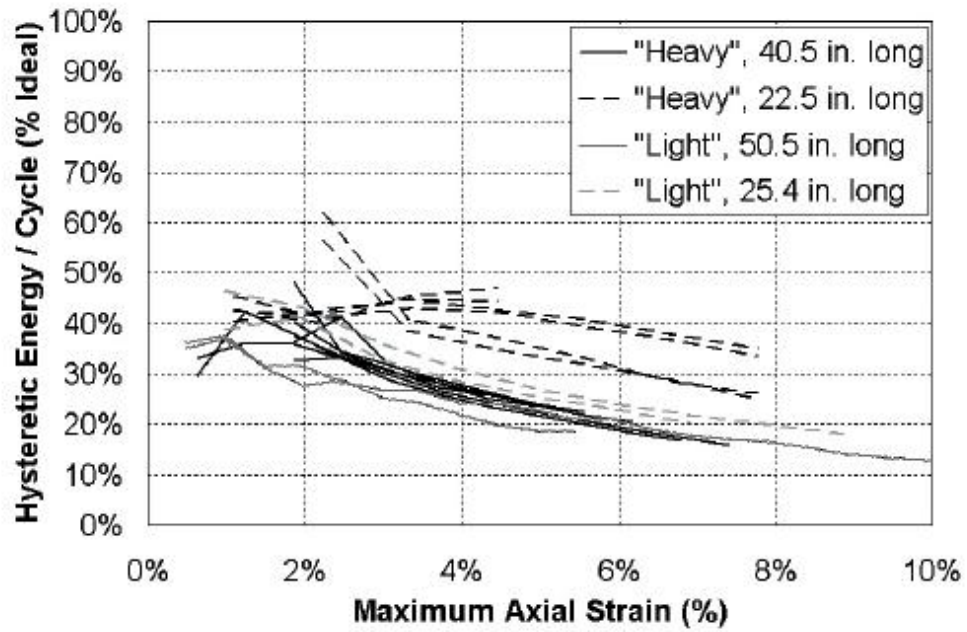


Figure 1-50. Energy dissipated per cycle as a percentage of "ideal" for single angle specimens

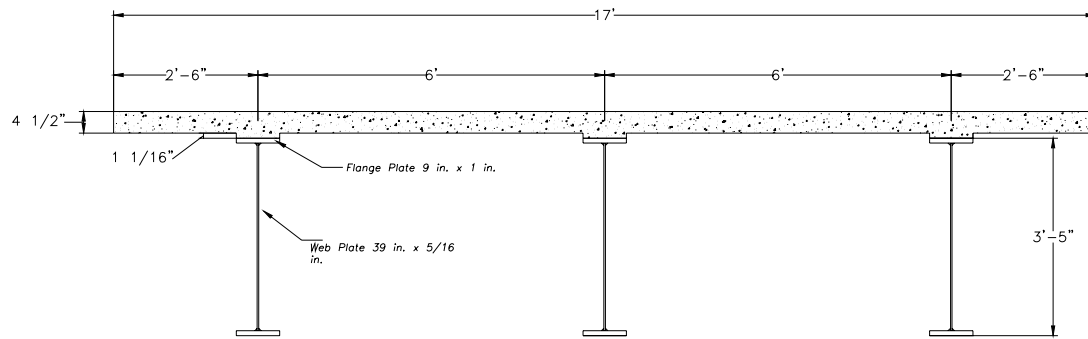


Figure 1-51. Dimension of transverse cross section of the bridge model

Flexible Substructure Design Chart  
 $K_d=0$ ,  $d_y=0.2$  in.,  $\mu=8.0$

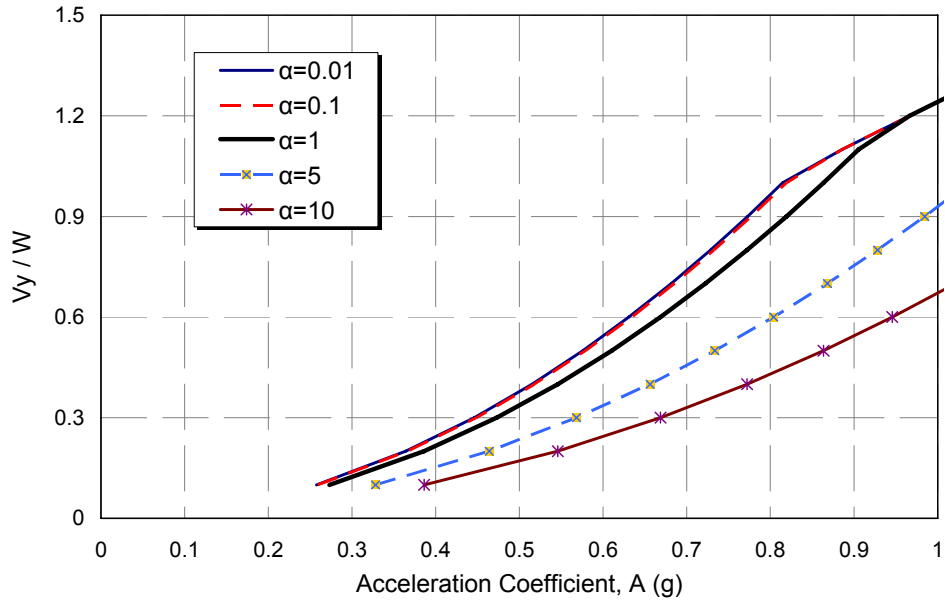


Figure 1-52. Single span design chart for displacement ductility of 8.0.

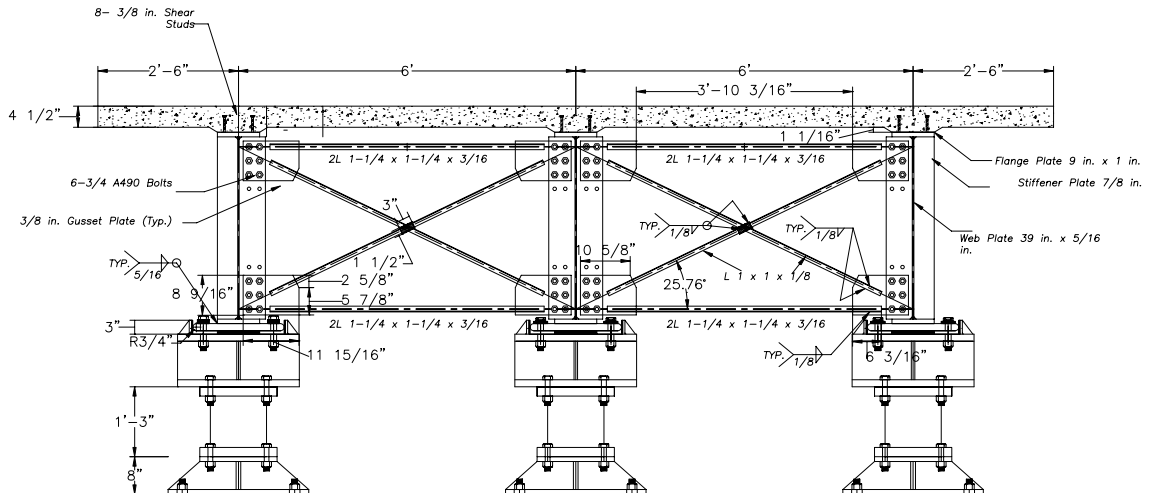


Figure 1-53. Dimensions and details of Specimen F1A

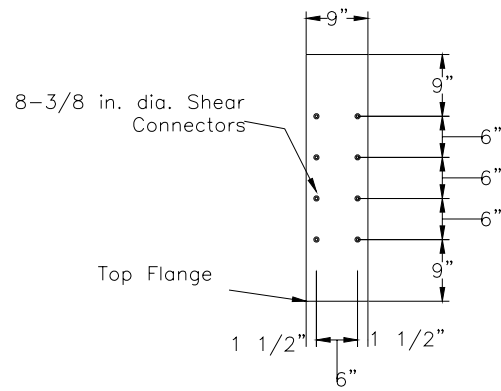


Figure 1-54. Plan view of top flange showing shear connector pattern for F1A

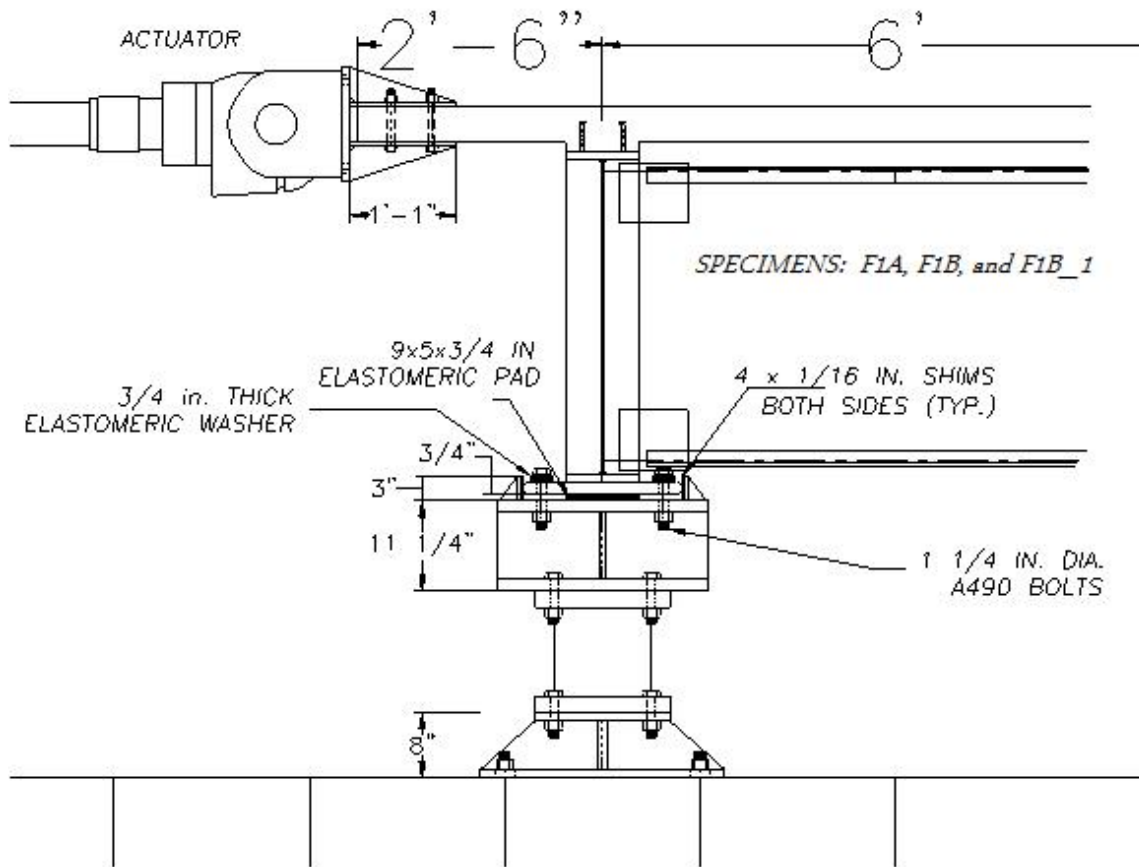


Figure 1-55. Support detail for Specimens F1A, F1B, and F1B\_1

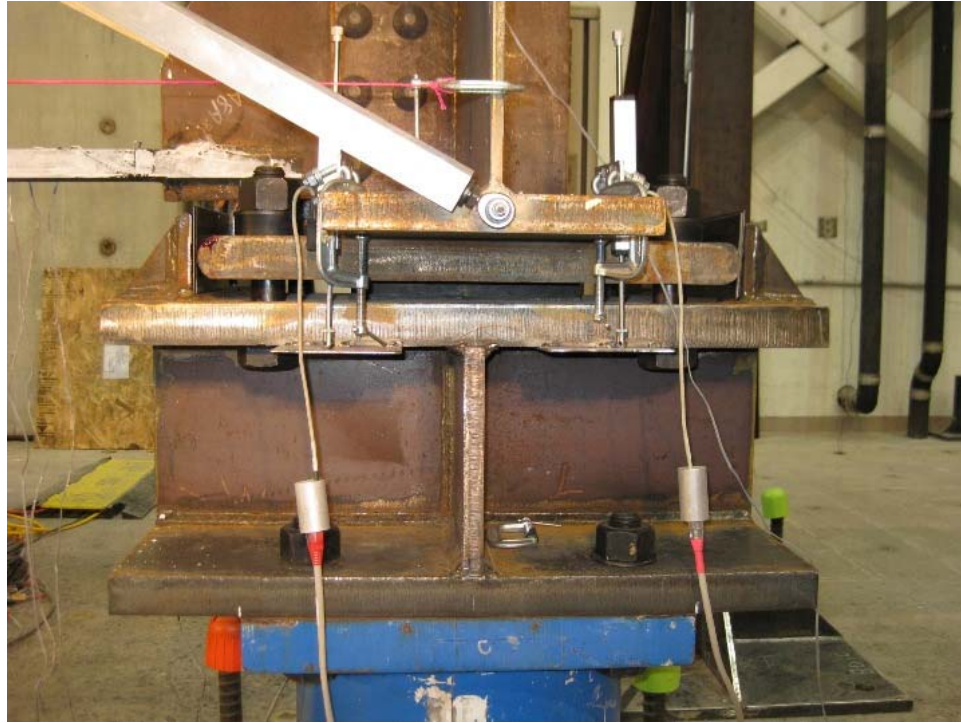


Figure 1-56. Close-up view of support detail for Specimens F1A, F1B, and F1B\_1

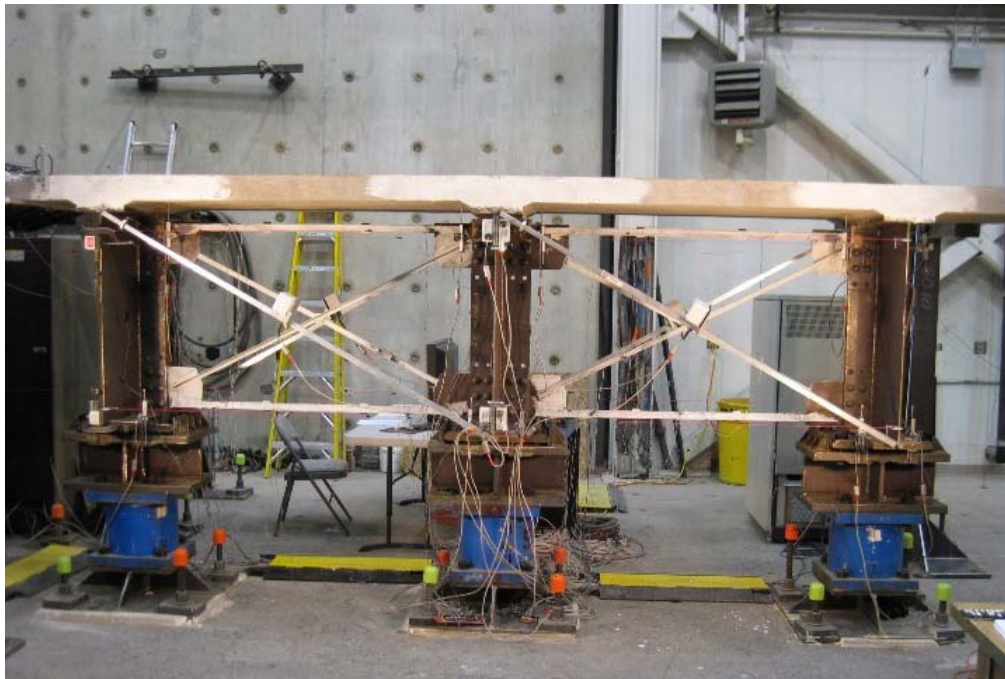


Figure 1-57. View of Specimen F1A before testing

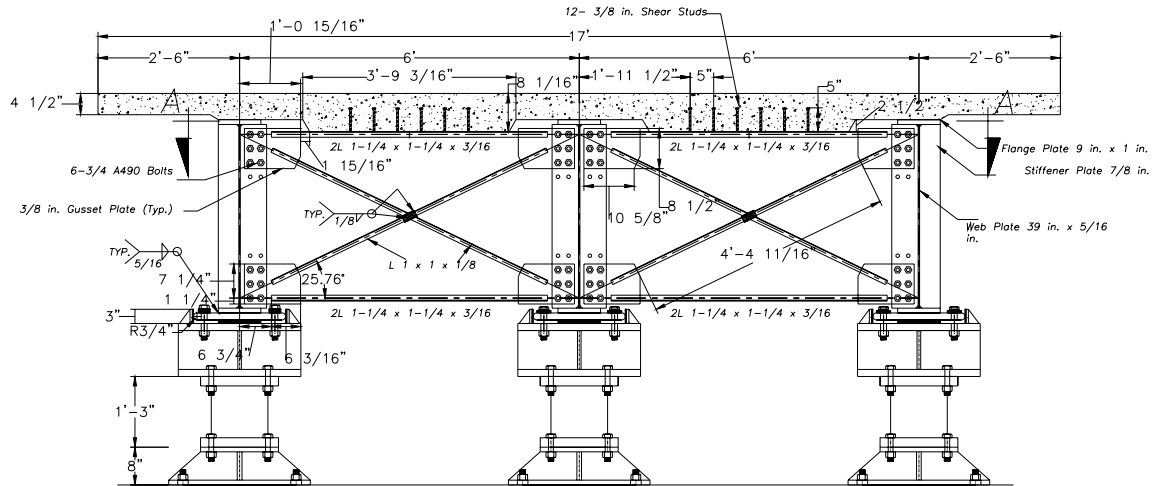


Figure 1-58. Dimensions and details of Specimen F1B

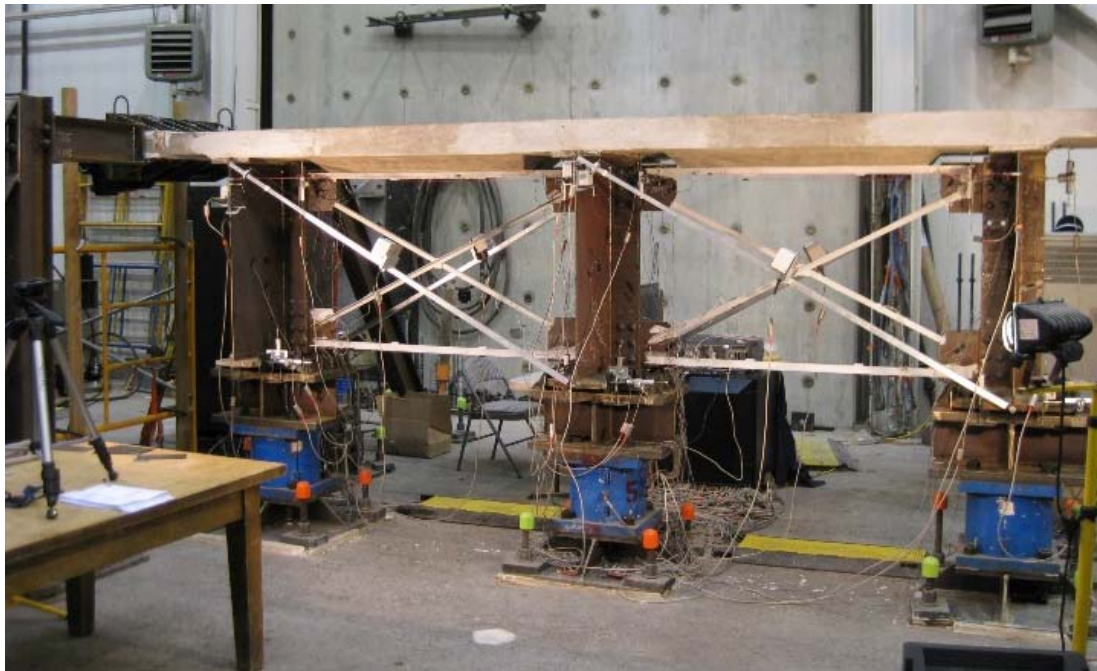


Figure 1-59. View of Specimen F1B before testing

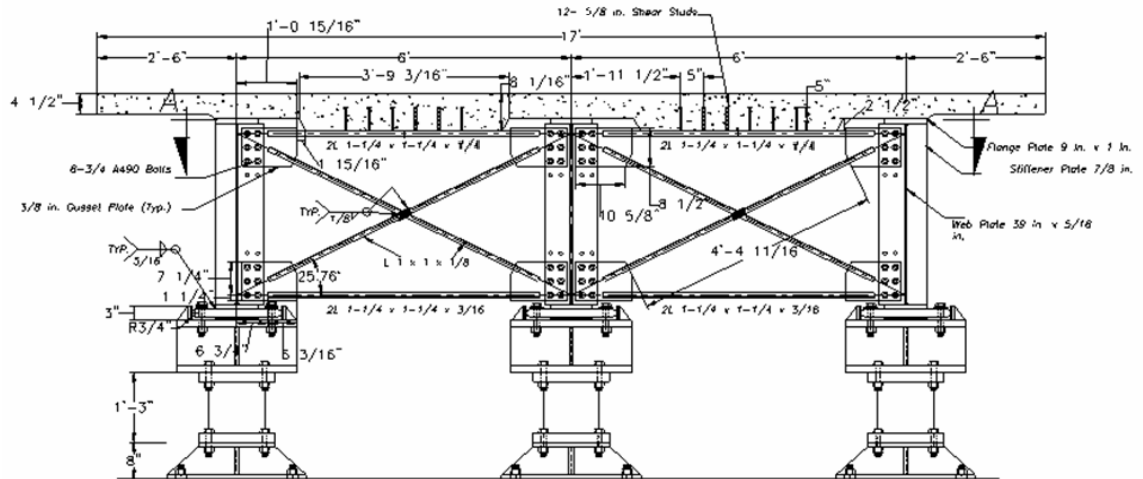


Figure 1-60. Dimensions and details of Specimen F1B\_1

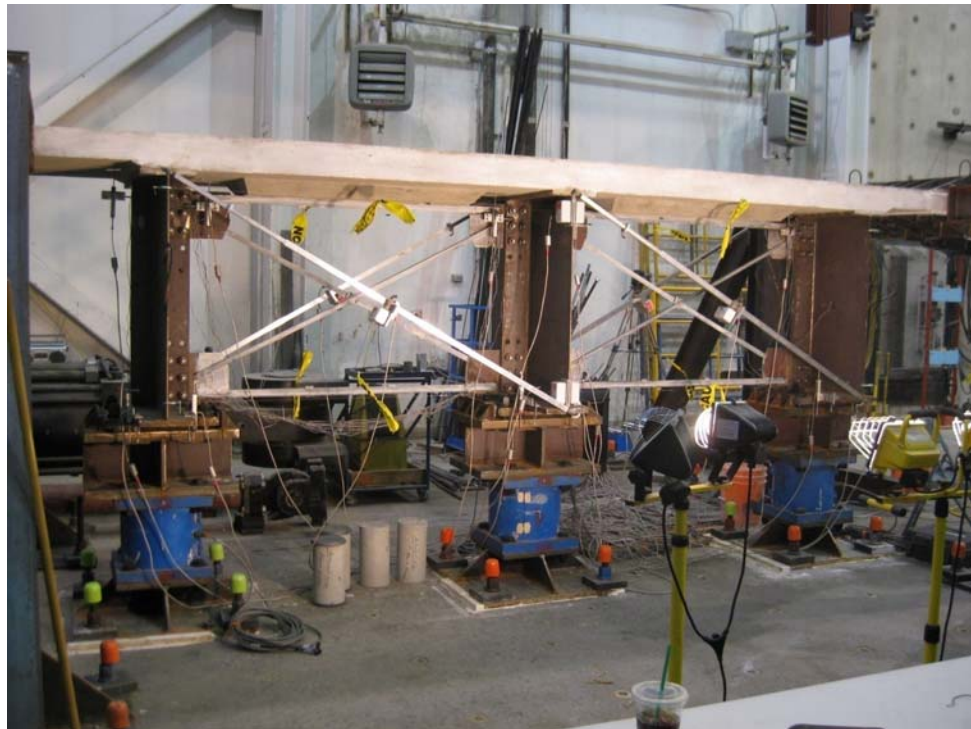


Figure 1-61. View of Specimen F1B\_1 before testing



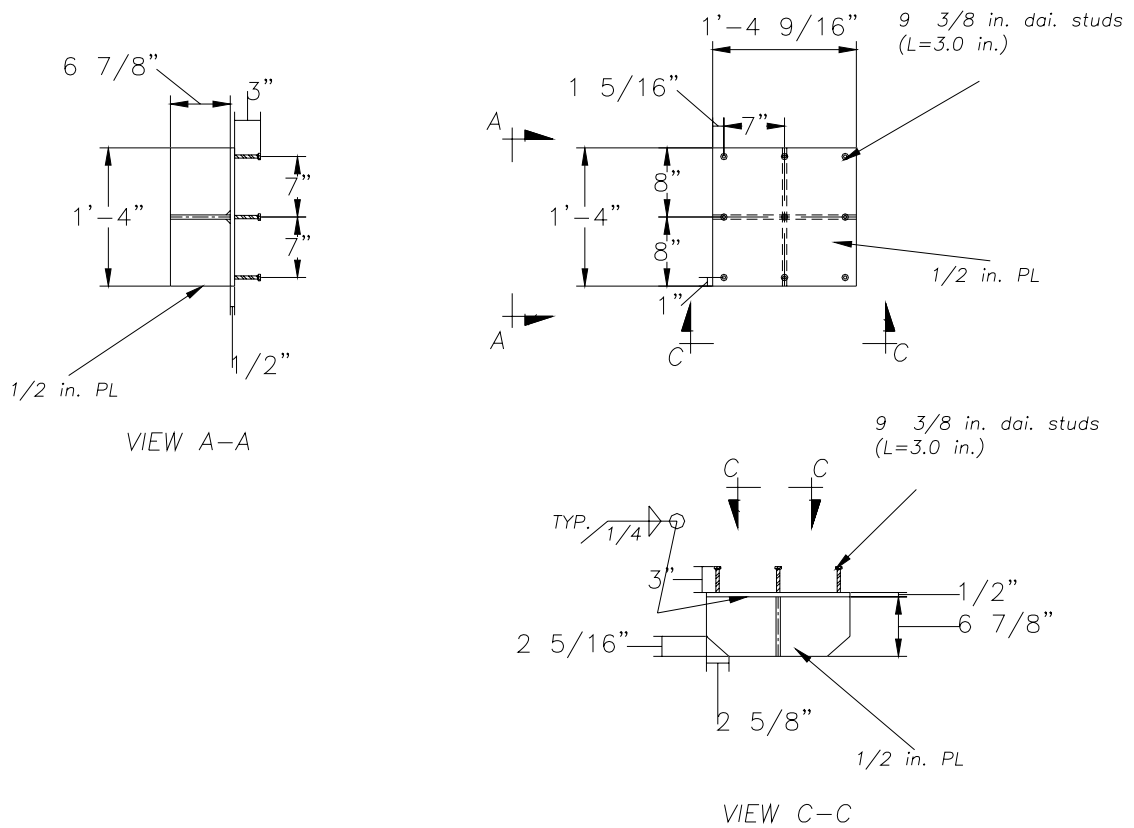


Figure 1-64. Shear connector detail for Specimen F1C

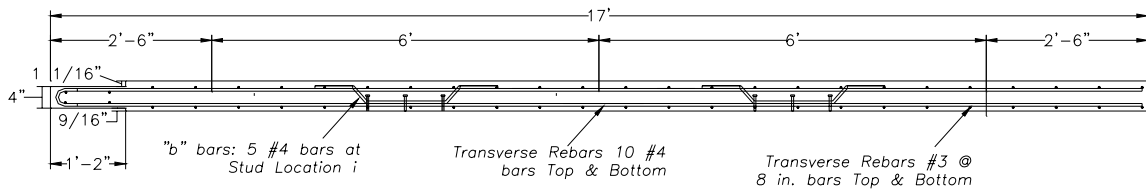


Figure 1-65. Specimen F1C deck reinforcement



Figure 1-66. Fabricated chevron bracing components before assembly in Specimen F1C



Figure 1-67. Rebar arrangement for Specimen F1C

"a" bars: 5 #4 bars at Stud Location

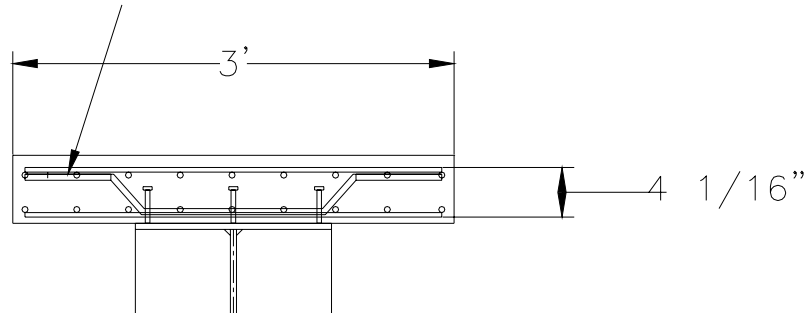


Figure 1-68. Transverse cross section of deck slab between girders for Specimen F1C



Figure 1-69. Specimen F1C: rebar detail near shear connectors



Figure 1-70. Specimen F1C: completed rebar and formwork



Figure 1-71. Pouring concrete for Specimen F1C

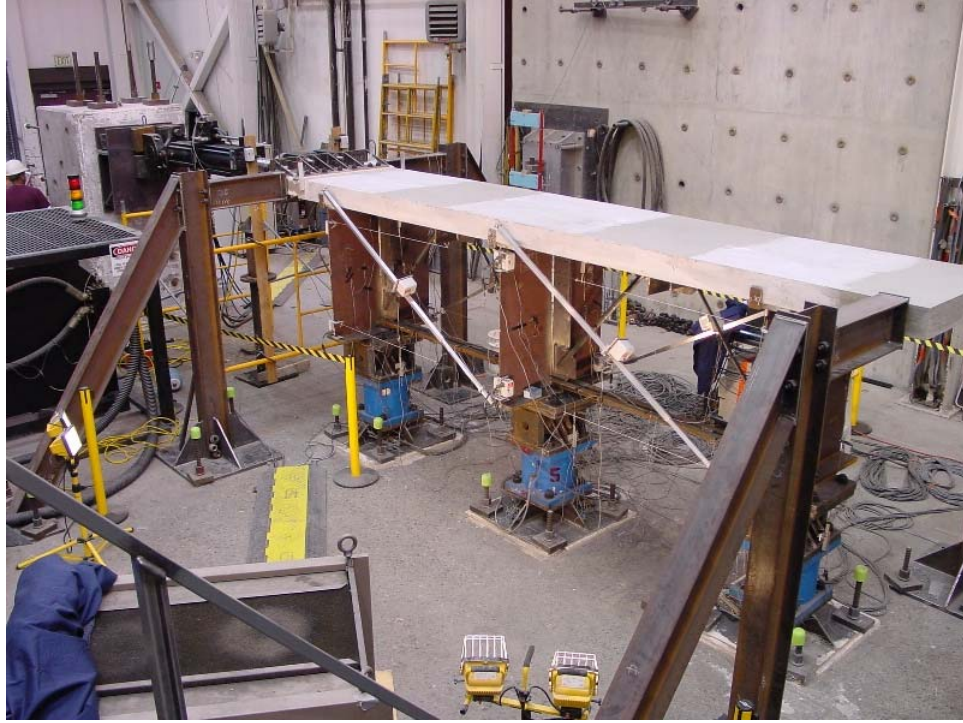


Figure 1-72. Specimen FIC before test

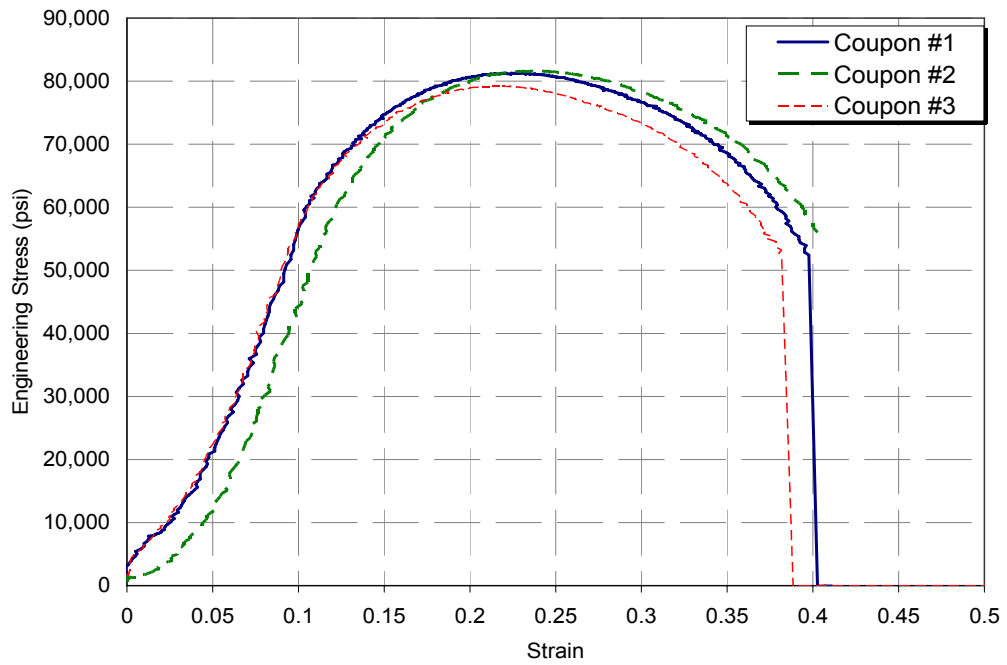


Figure 1-73. Shear connector coupon tests (3/8 in.)

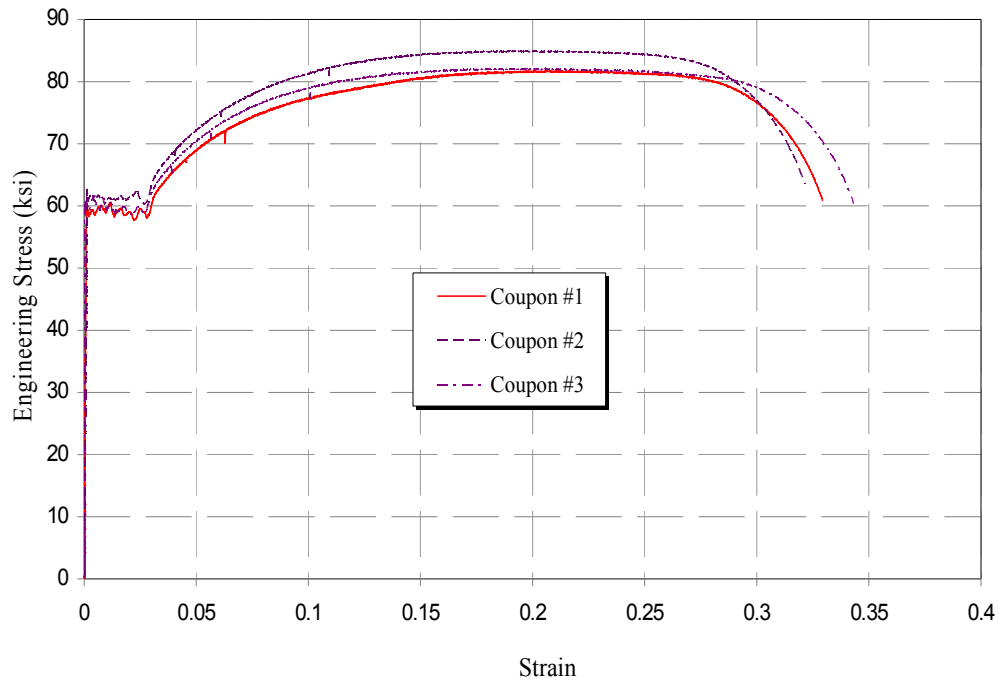


Figure 1-74. L 1x1x1/8 diagonal coupon test (Specimen F1B\_1)

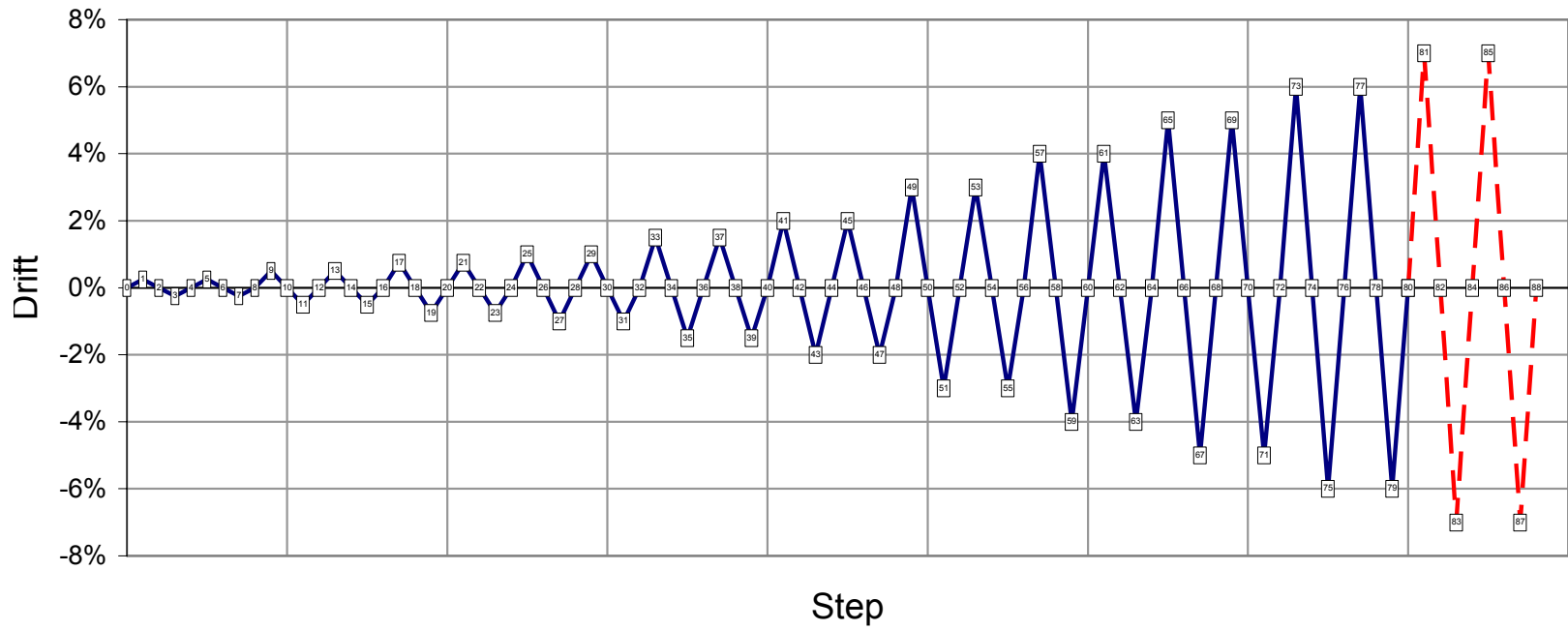


Figure 1-75. Displacement controlled testing protocol

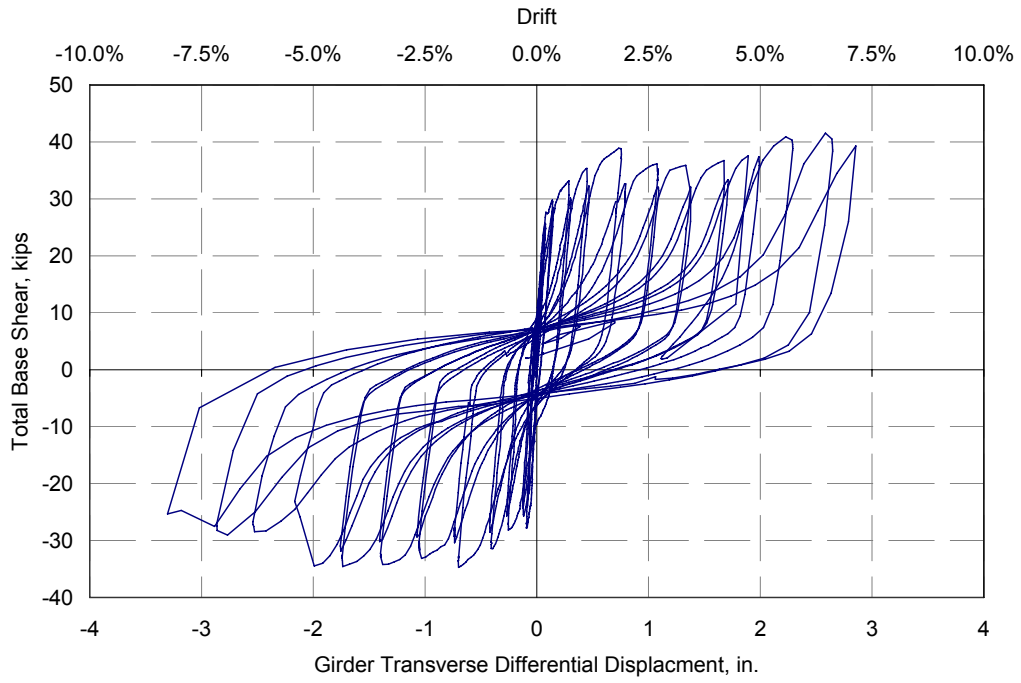


Figure 1-76. Specimen F1A: Actuator force versus differential girder displacement

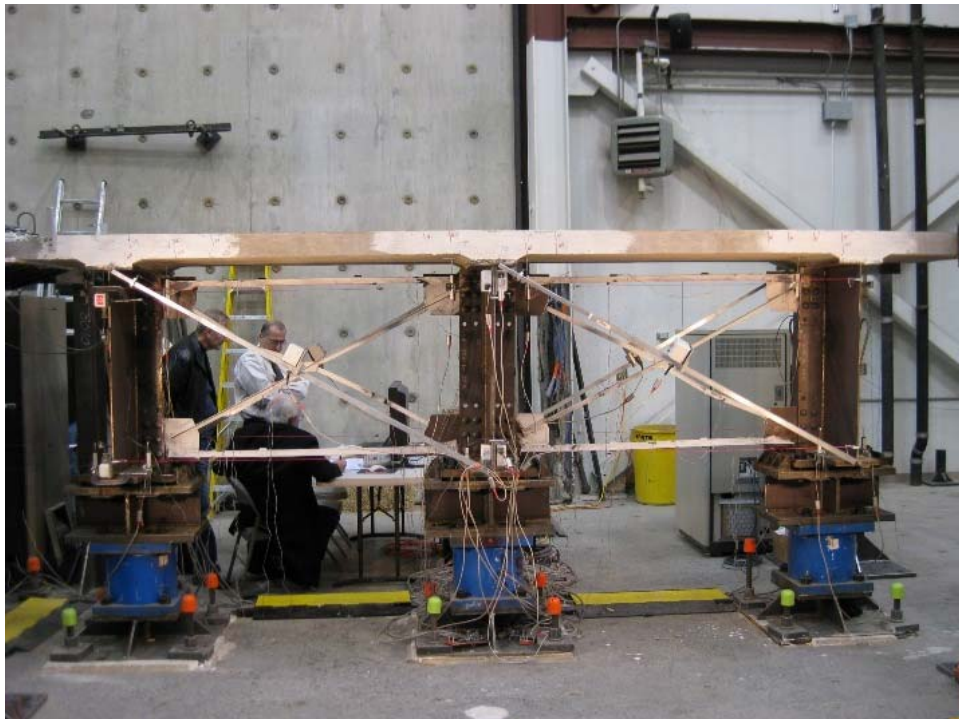


Figure 1-77. F1A at 1.5% drift showing flexural cracking in concrete deck

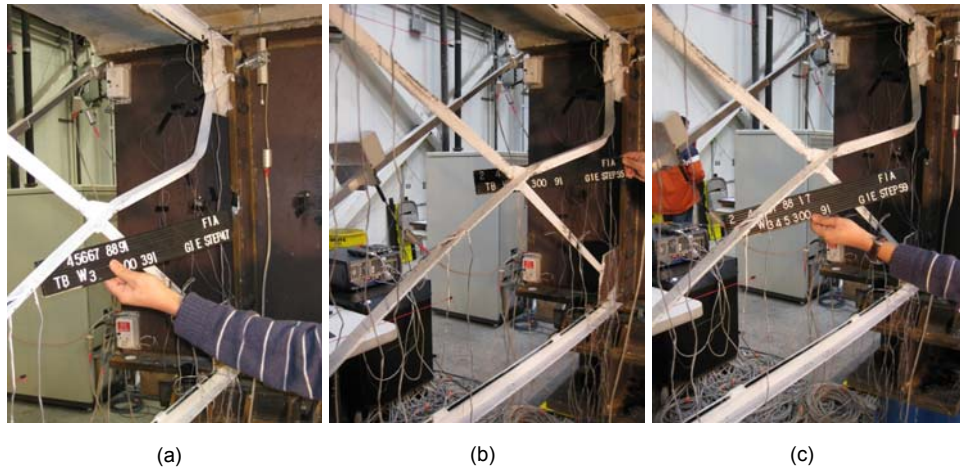


Figure 1-78. F1A Specimen, buckled brace at (a) 2% drift, (b) 3% drift, and (c) 4% drift

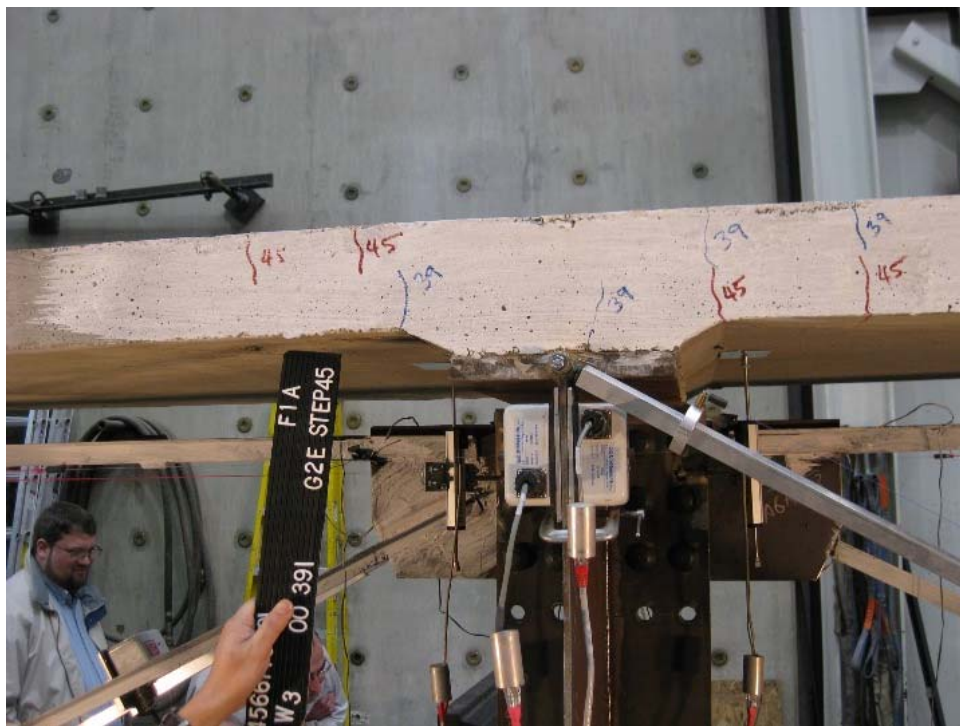


Figure 1-79. F1A Specimen, the studded connection over Girder 2 shows some uplift at 1.5% drift

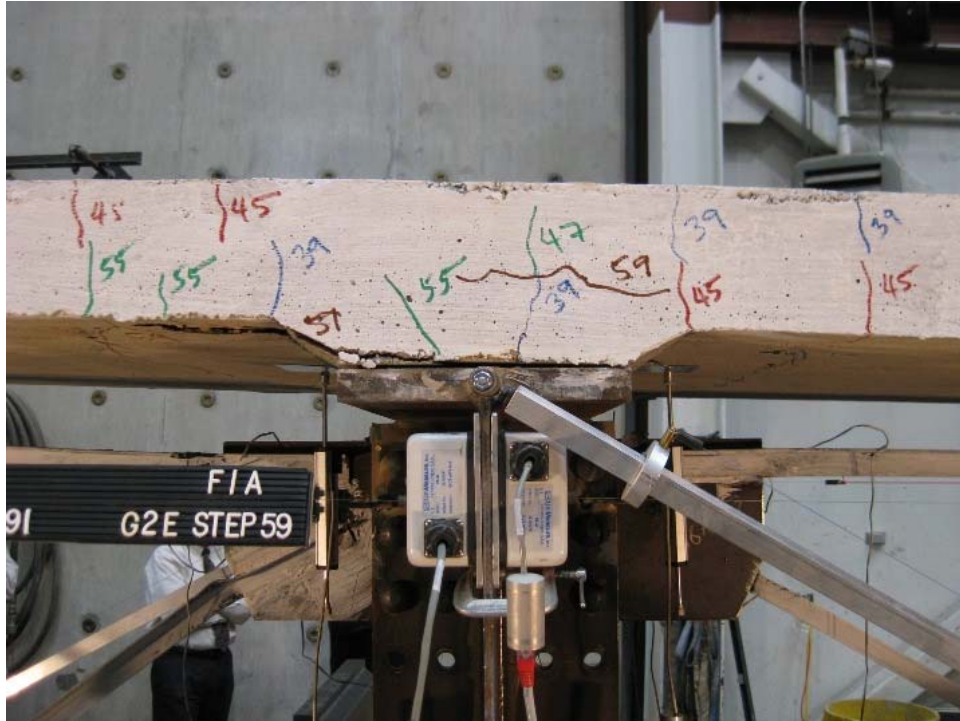


Figure 1-80. F1A Specimen, studded deck to girder connection over Girder 2 at 3.5% drift

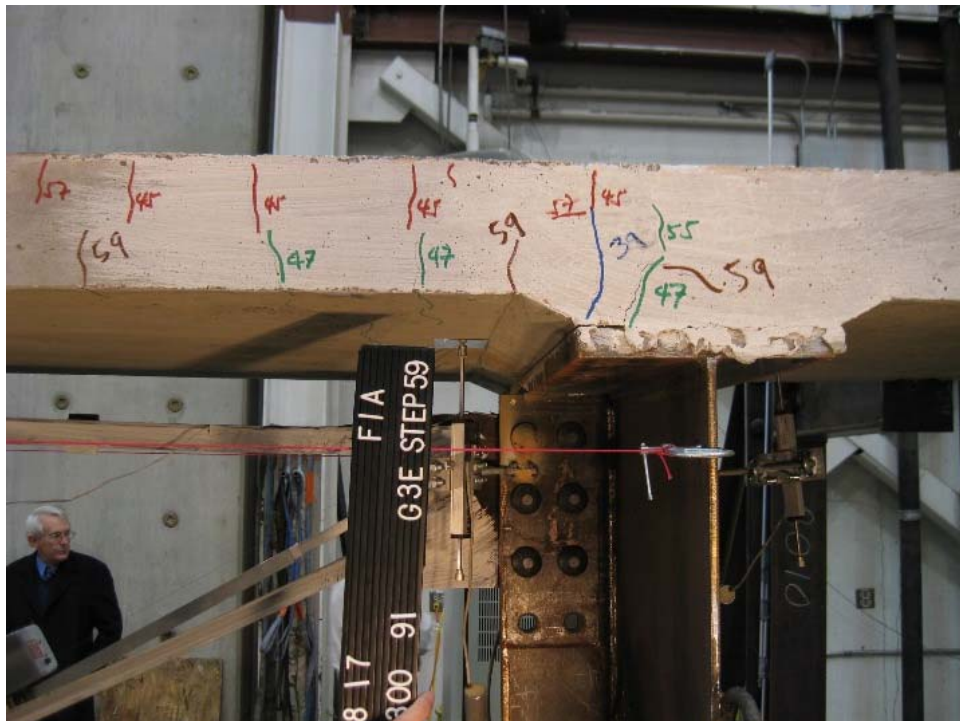


Figure 1-81. F1A Specimen, studded deck to girder connection over Girder 3 at 3.5% drift



Figure 1-82. F1A Specimen, rupture of one diagonal brace at 5% drift

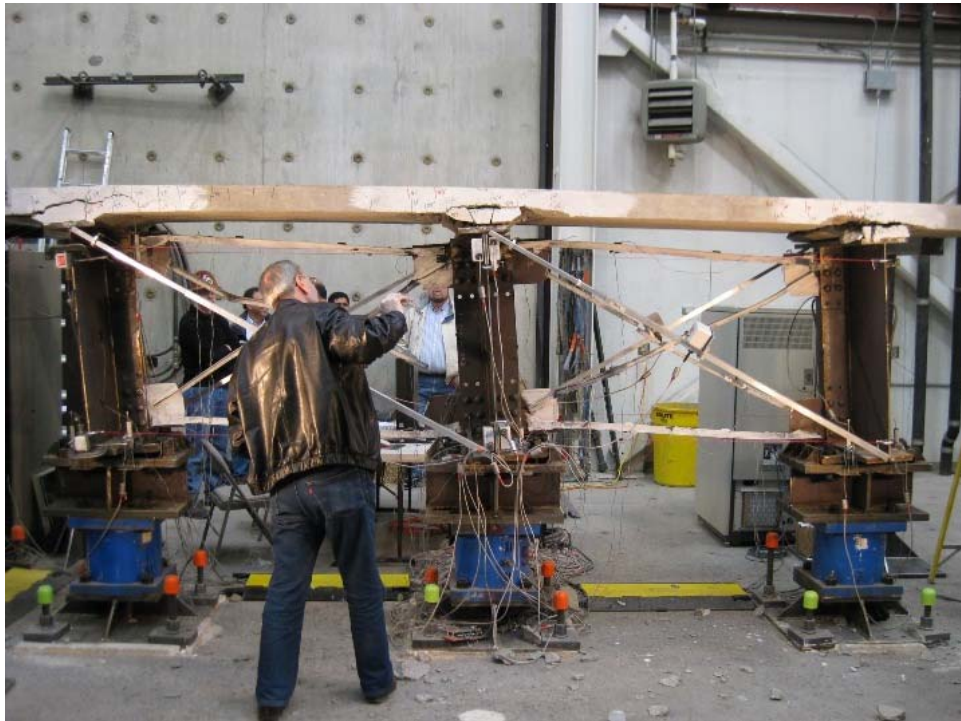


Figure 1-83. View of Specimen F1A at 7.5% drift



Figure 1-84. FIA Specimen, studded deck to girder connection over Girder 2 at 7.5% drift

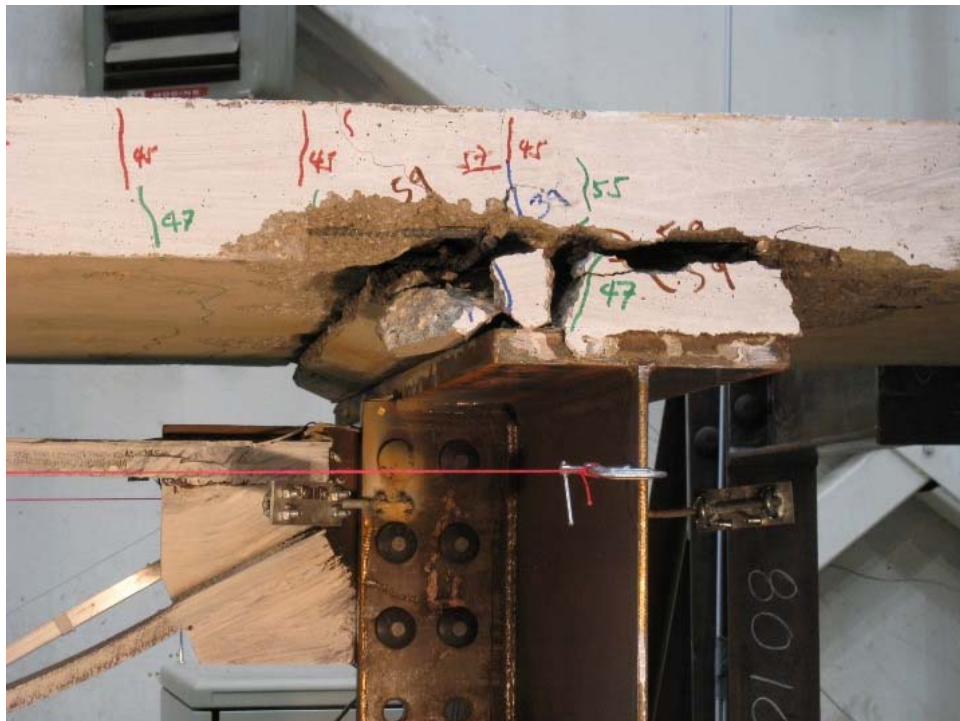


Figure 1-85. Studded deck to girder connection over Girder 3, Specimen FIA at 7.5% drift

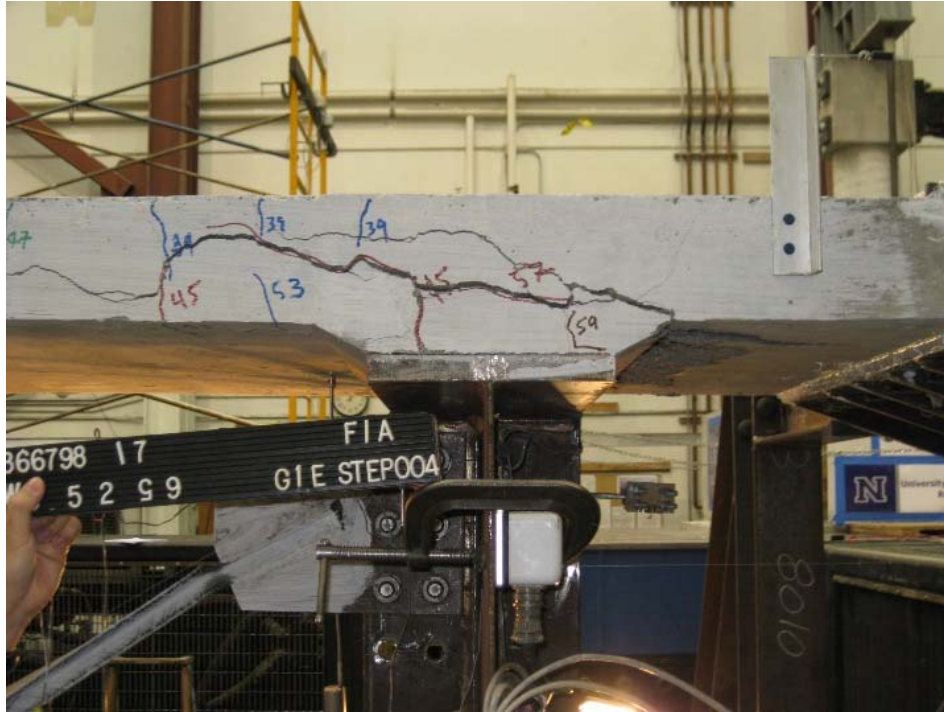


Figure 1-86. Studded deck to girder connection over Girder 1, Specimen F1A at 7.5% drift



Figure 1-87. View of Specimen F1A at 7.5% drift



Figure 1-88. Specimen F1A: final damage state at zero displacement



Figure 1-89. Specimen F1A: close-up of cross frame at final damage state at zero displacement

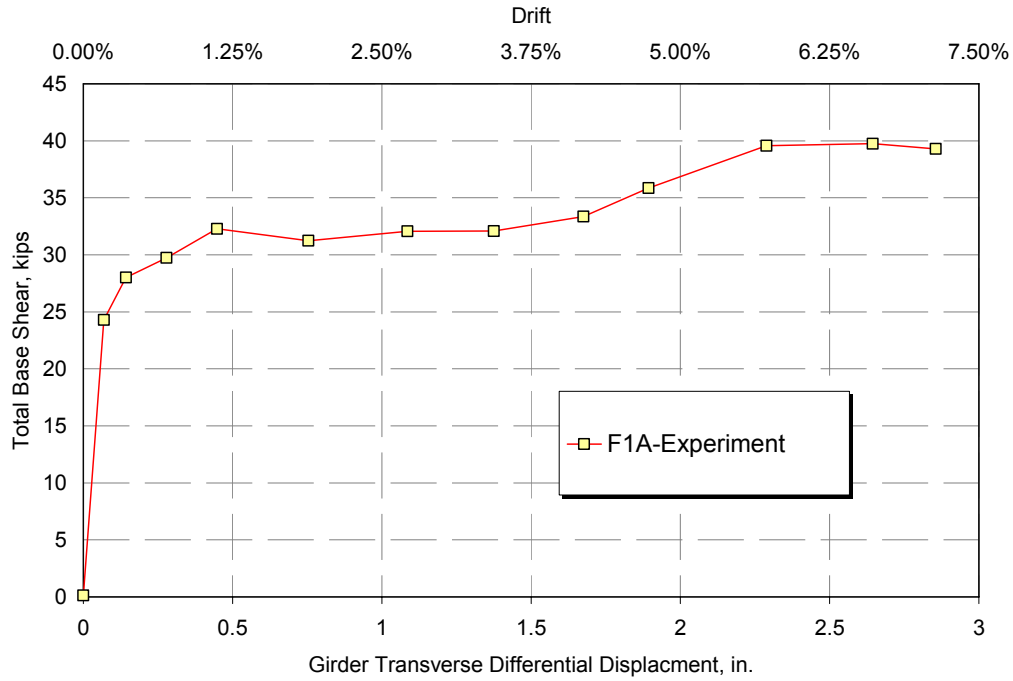


Figure 1-90. Specimen F1A: base shear at peak displacement cycles

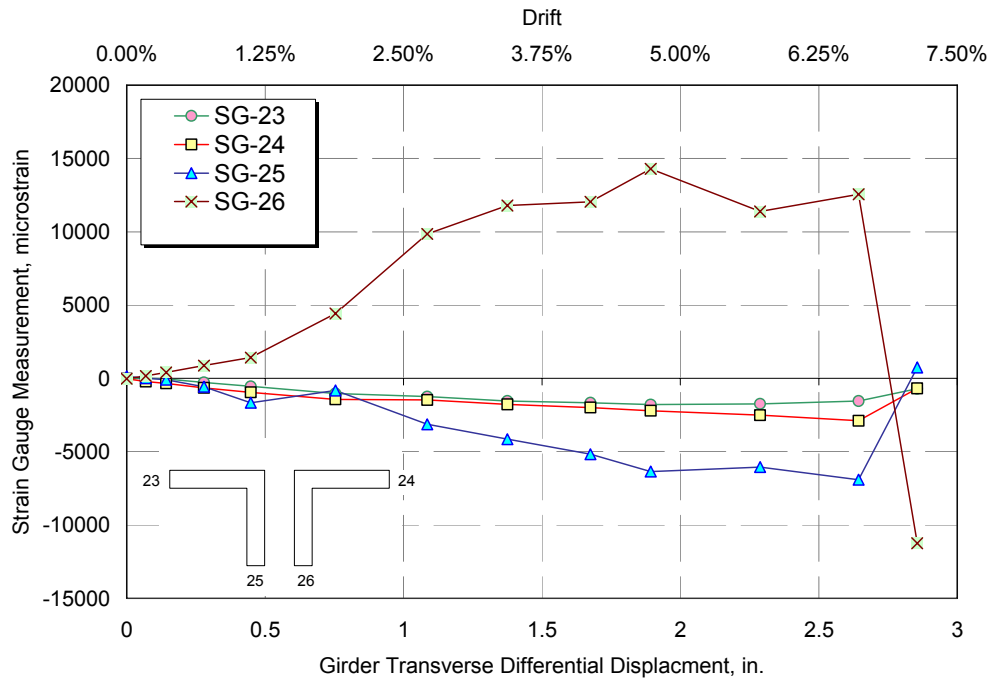


Figure 1-91. Specimen F1A: strain gauge measurement on top chord

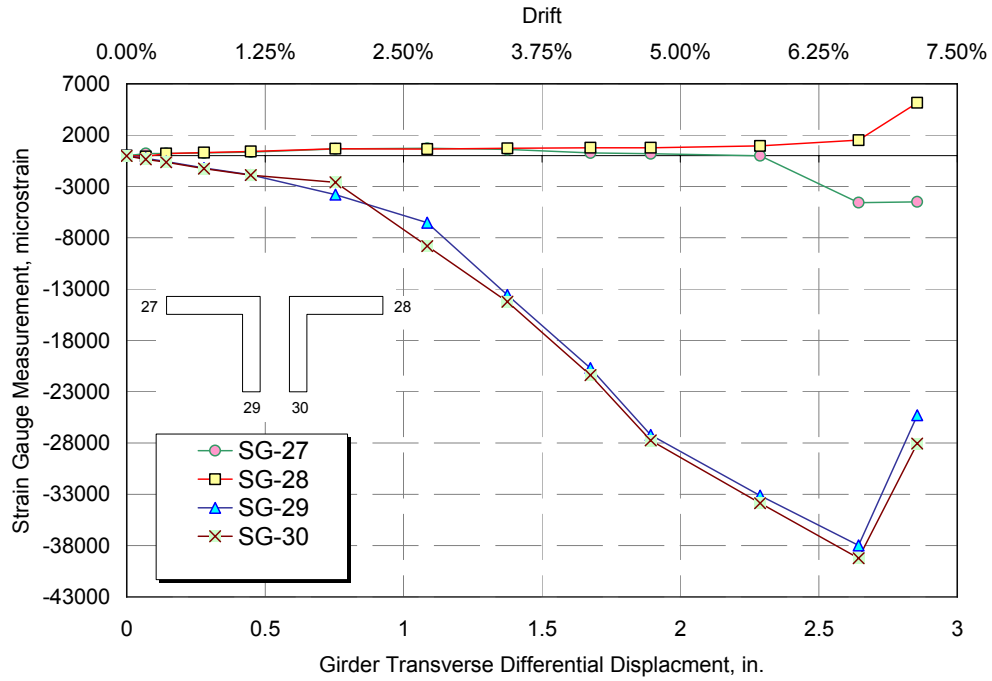


Figure 1-92. Specimen F1A: strain gauge measurement on top chord

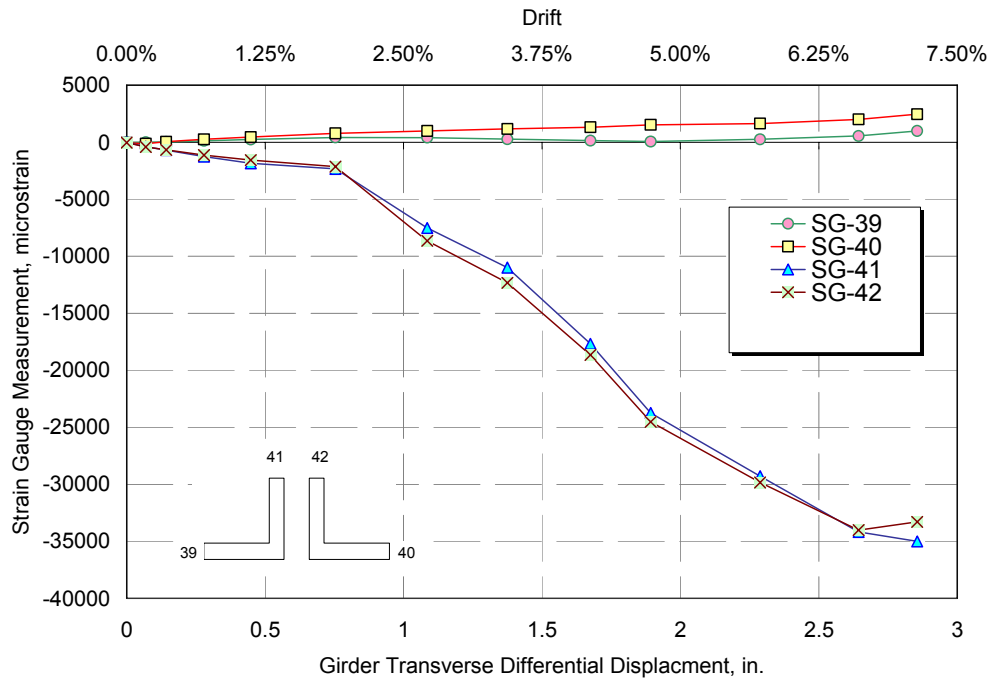


Figure 1-93. Specimen F1A: strain gauge measurement on bottom chord

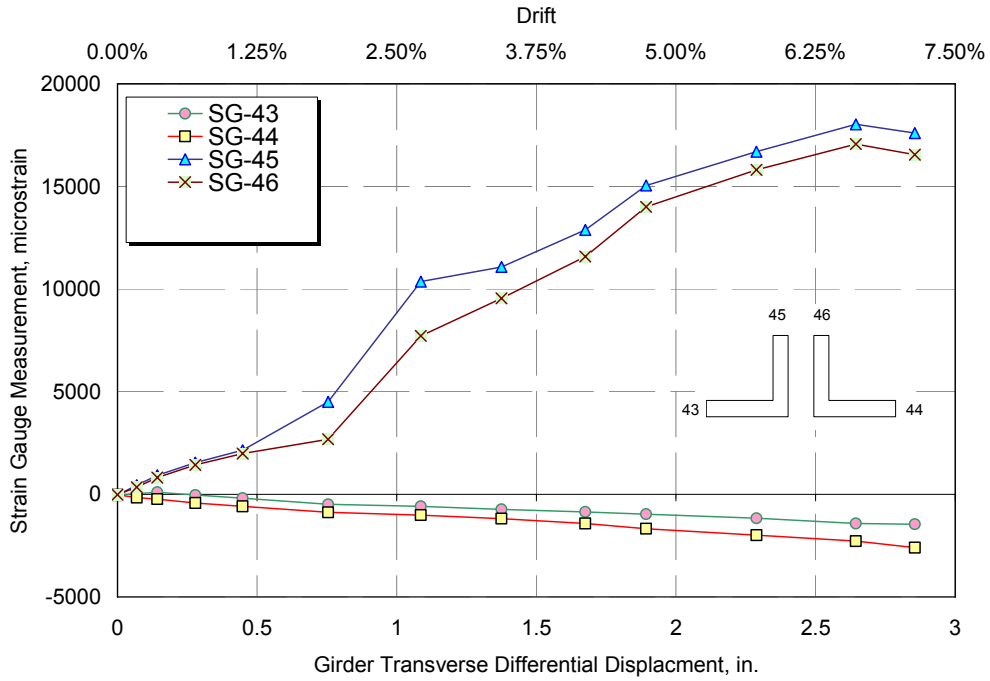


Figure 1-94. Specimen F1A: strain gauge measurement on bottom chord

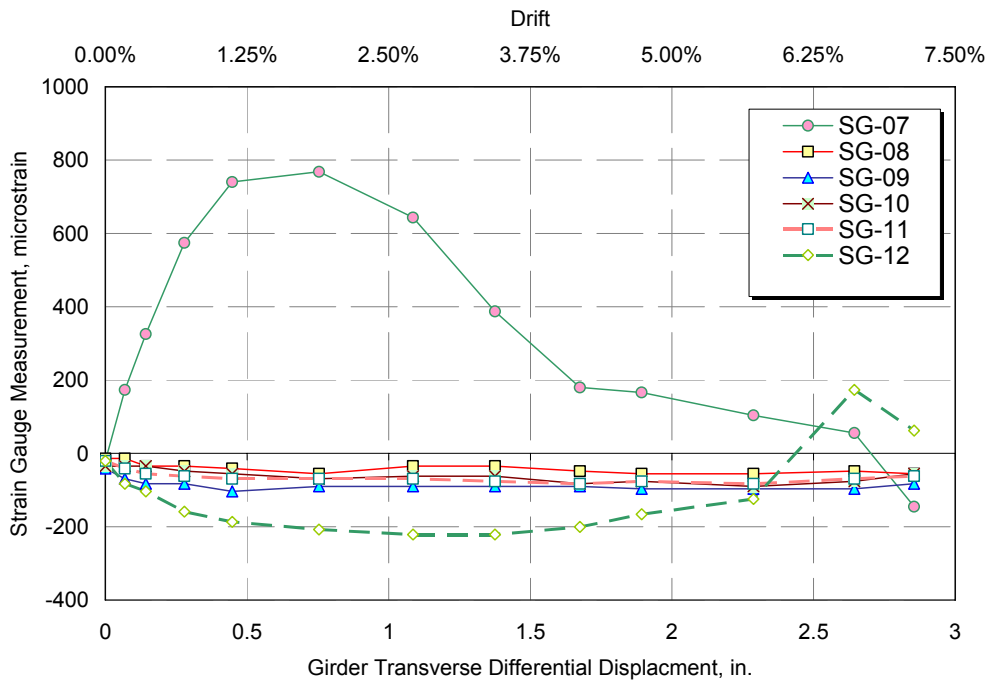


Figure 1-95. Specimen F1A: strain gauge measurement at top of bearing stiffeners

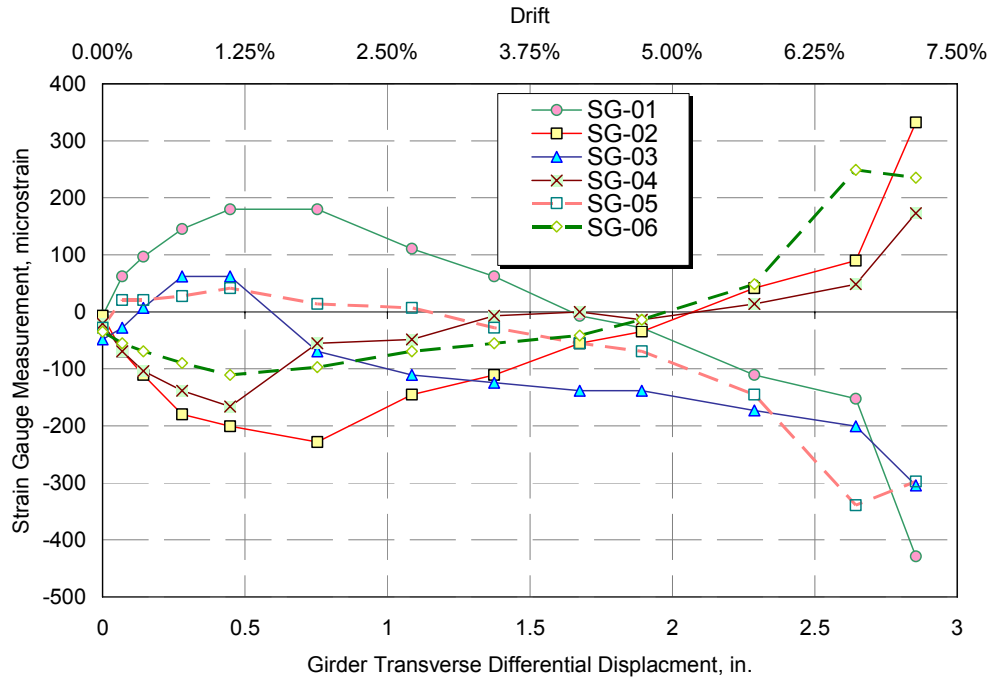


Figure 1-96. Specimen F1A: strain gauge measurement at mid-height of bearing stiffeners

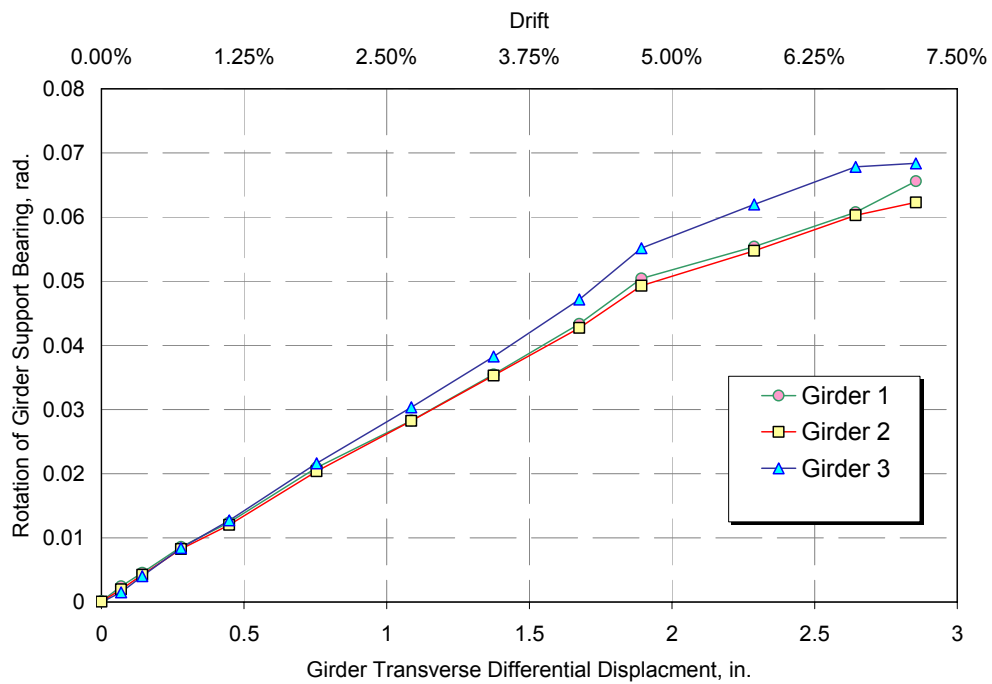


Figure 1-97. Specimen F1A: rotation of girder support bearings

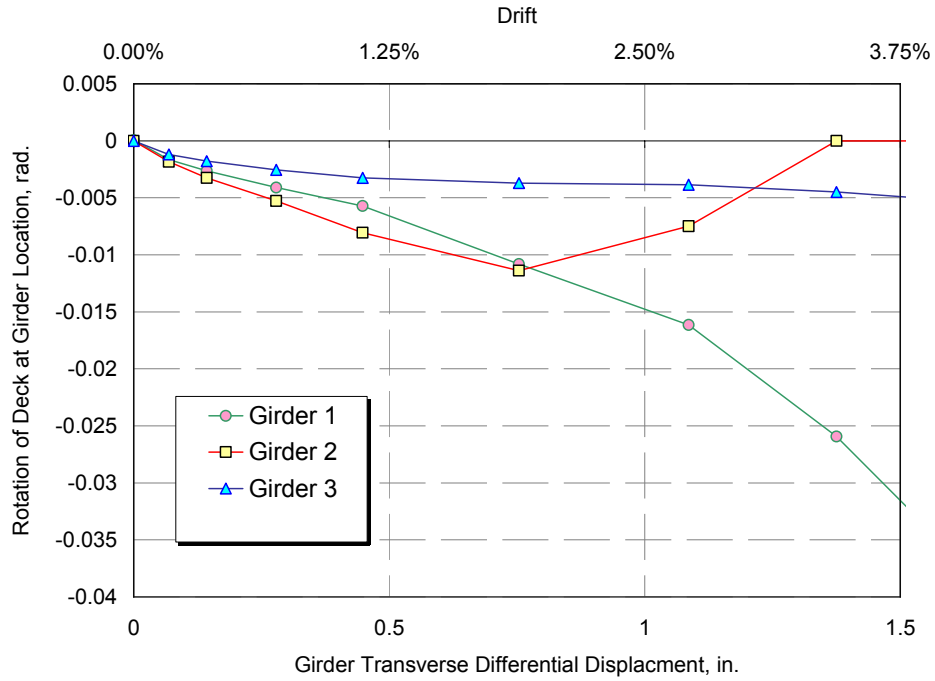


Figure 1-98. Specimen F1A: rotation of deck over girders

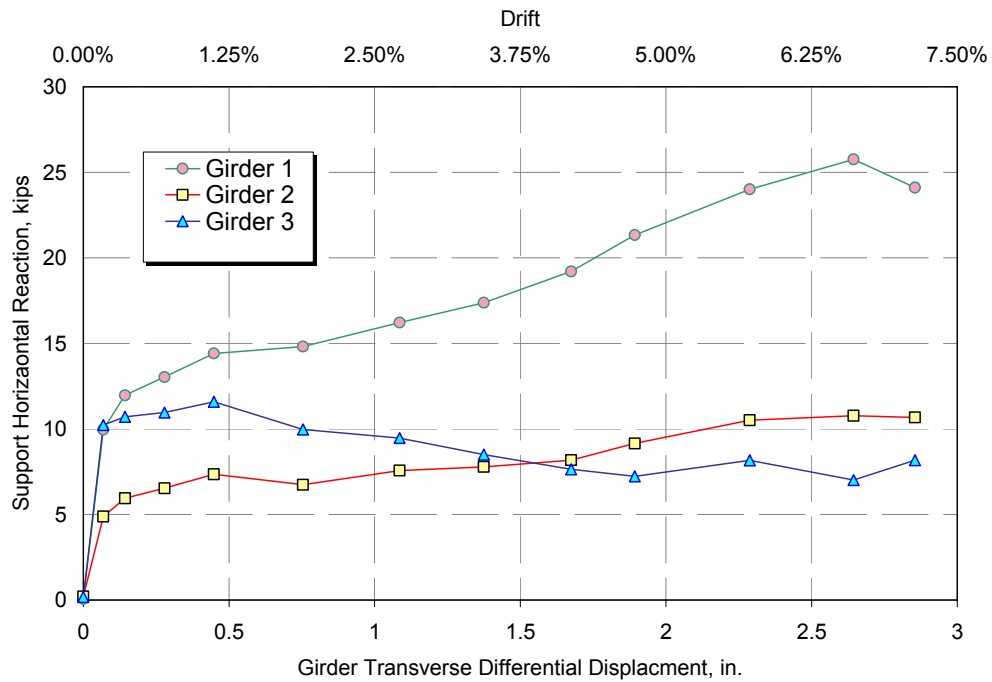


Figure 1-99. Specimen F1A: horizontal support reactions

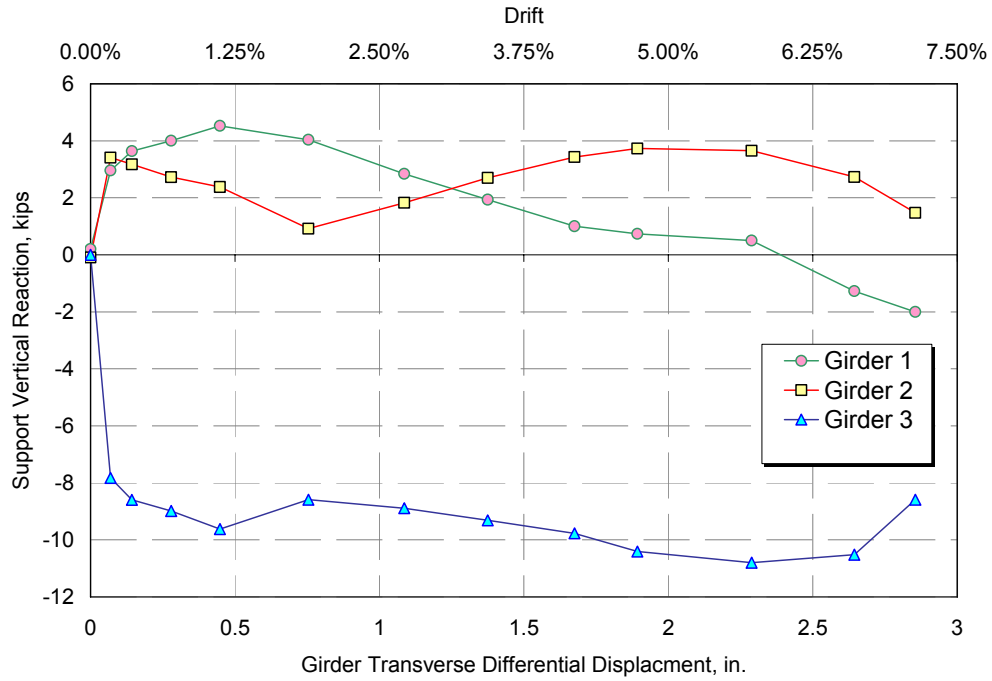


Figure 1-100. Specimen F1A: vertical support reactions

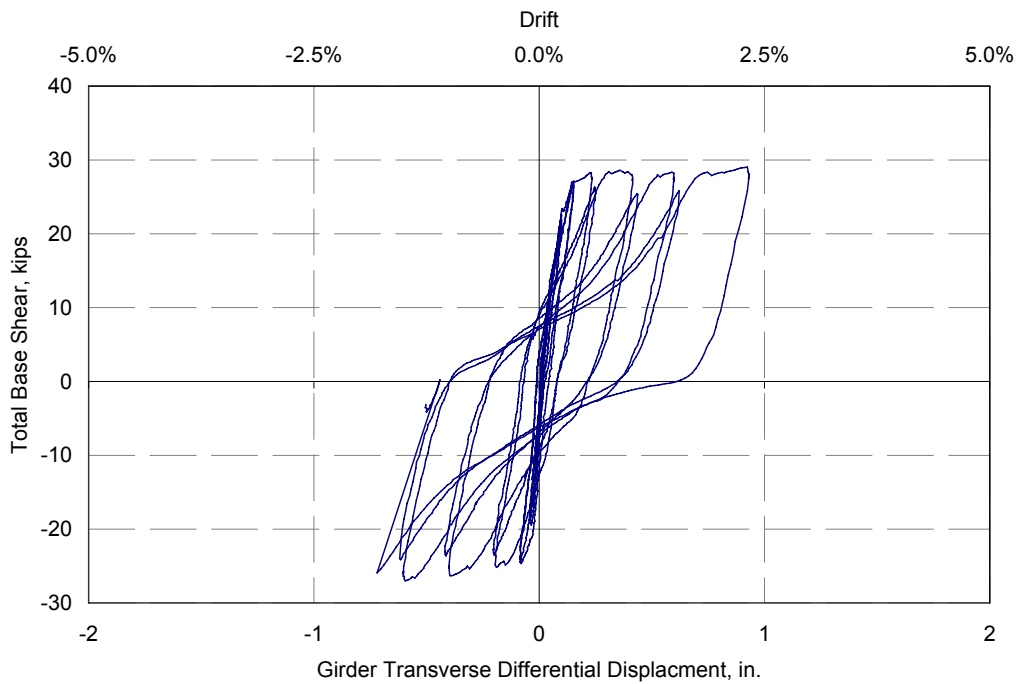


Figure 1-101. Specimen F1B: Actuator force versus differential girder displacement

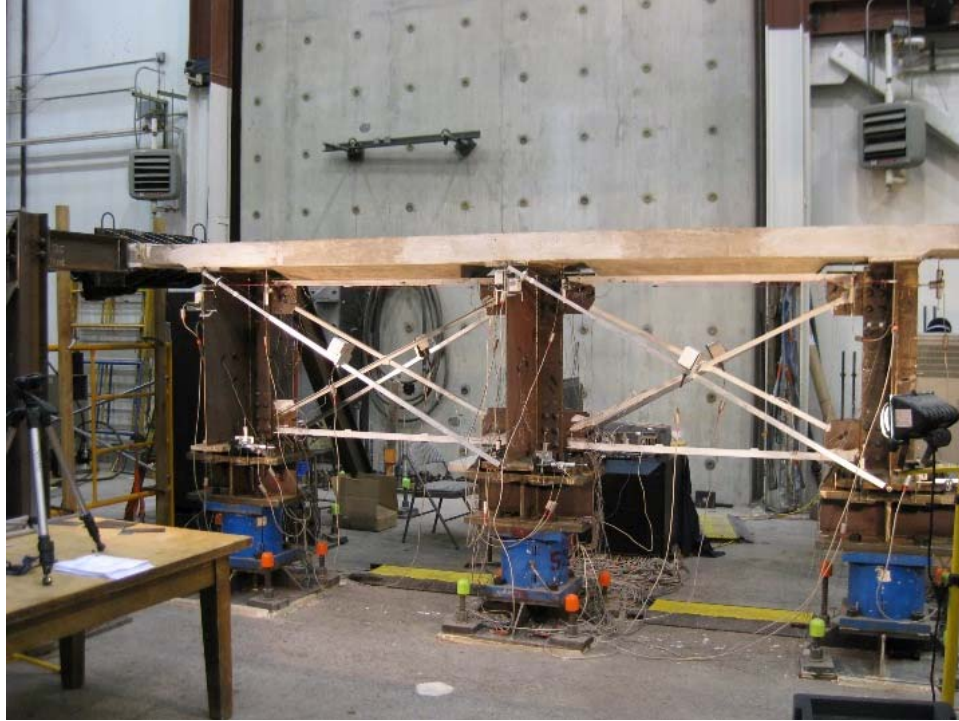


Figure 1-102. View of Specimen F1B before testing



Figure 1-103. Specimen F1B: relative deformation between top chord and deck at 2% drift



Figure 1-104. Specimen F1B: relative deformation between top chord and deck at 2% drift



(a)

(b)

(c)

Figure 1-105. Specimen F1B: buckled brace at a) 1.5% drift, b) 2% drift, and c) 2.5% drift



Figure 1-106. Specimen F1B: separation of top chord and deck at 2.5% drift



Figure 1-107. F1B Specimen: final damage state at zero displacement



Figure 1-108. F1B Specimen: close-up of underside of deck showing premature failure of stud connections

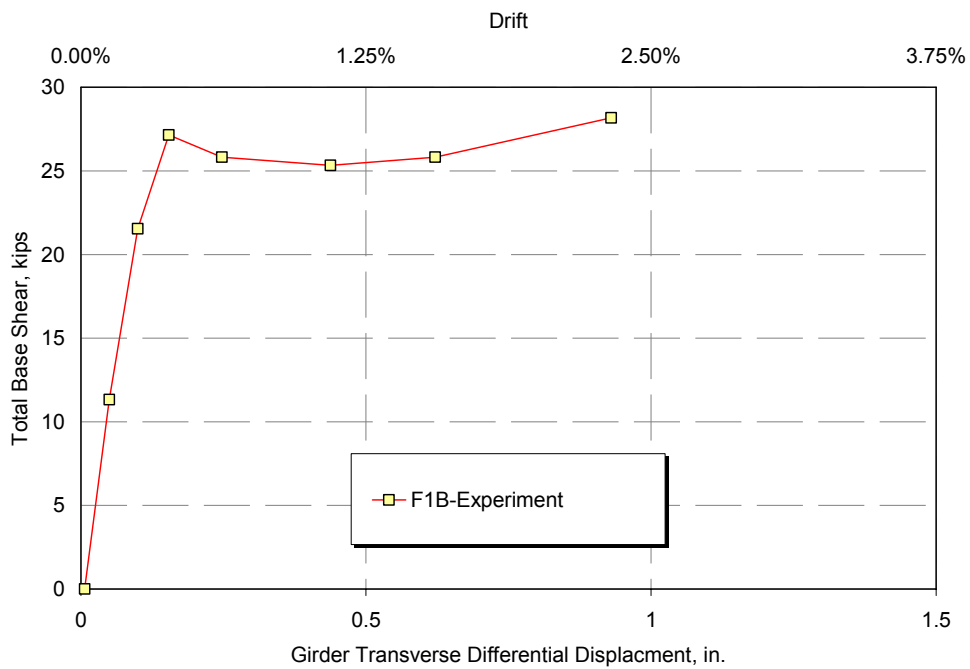


Figure 1-109. Specimen F1B: base shear at peak displacement cycles

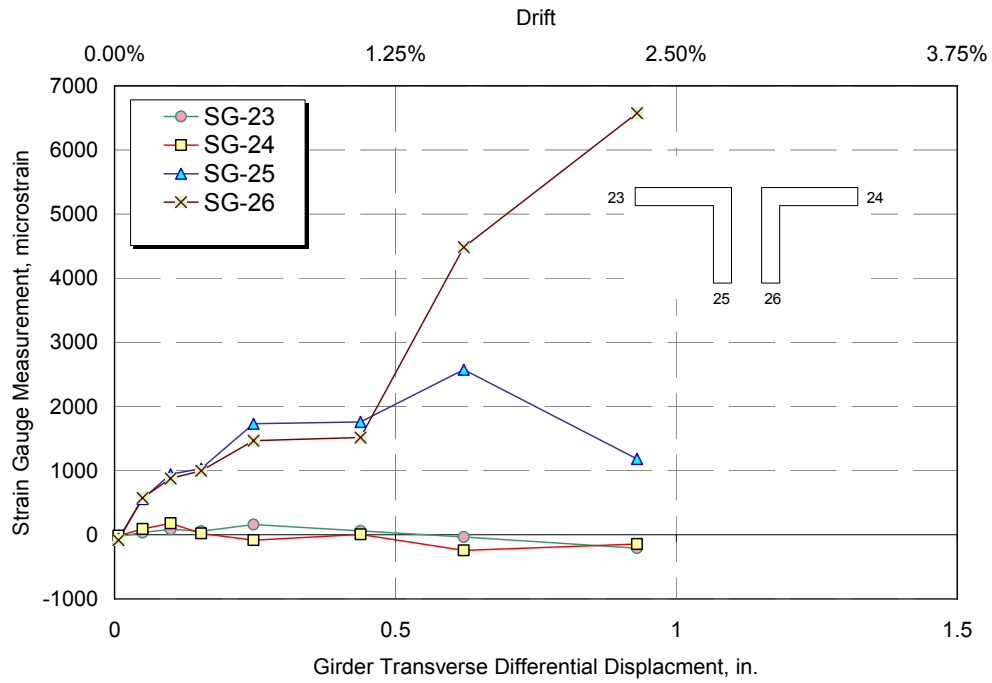


Figure 1-110. Specimen F1B: strain gauge measurement on top chord

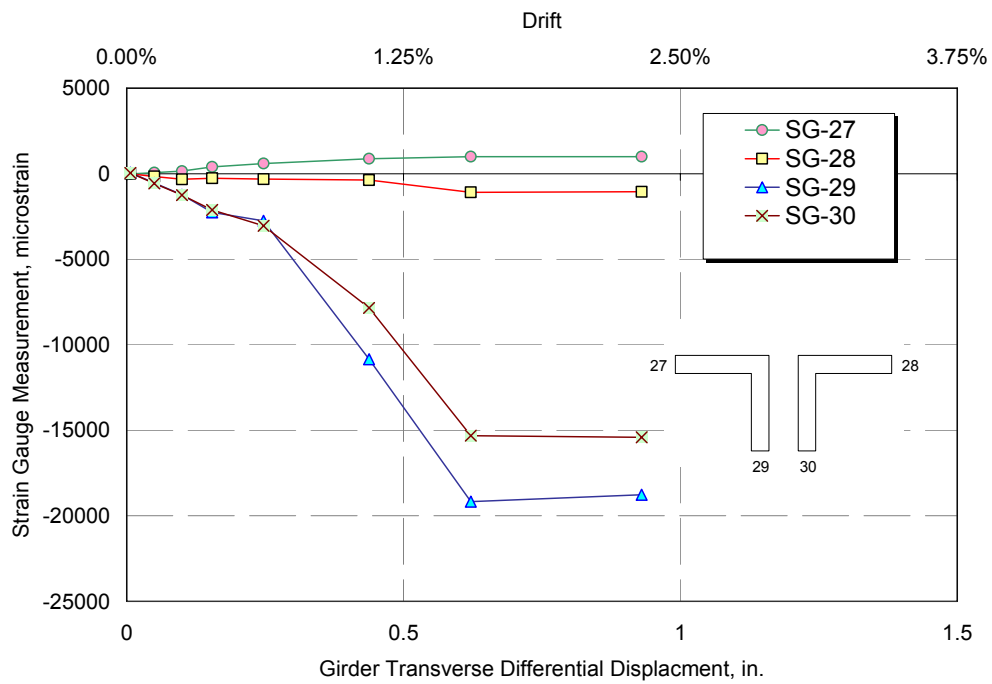


Figure 1-111. Specimen F1B: strain gauge measurement on top chord

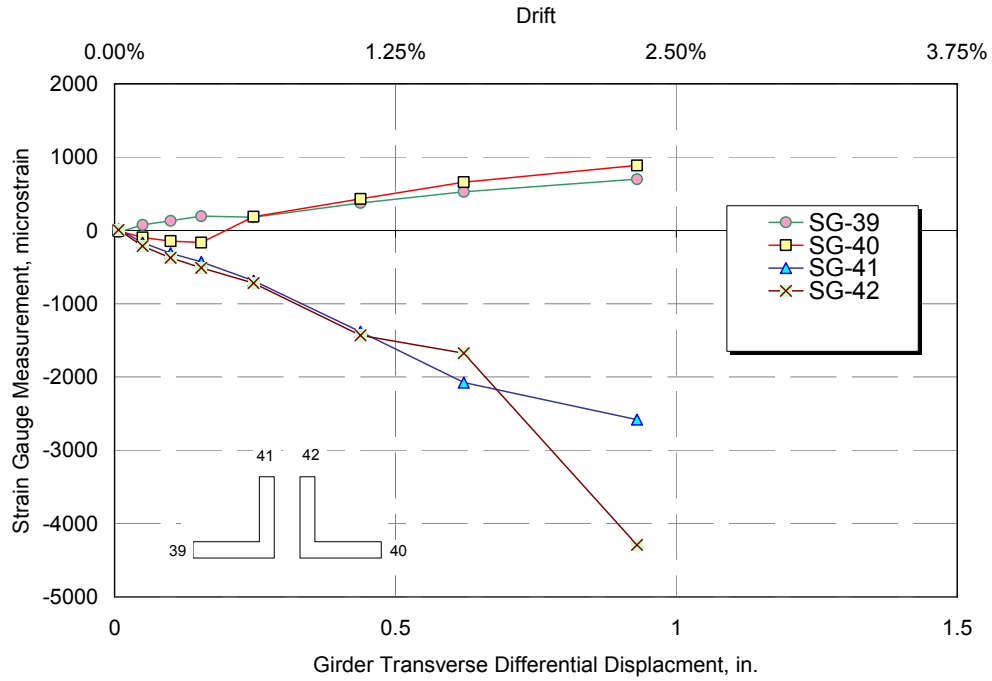


Figure 1-112. Specimen F1B: strain gauge measurement on bottom chord

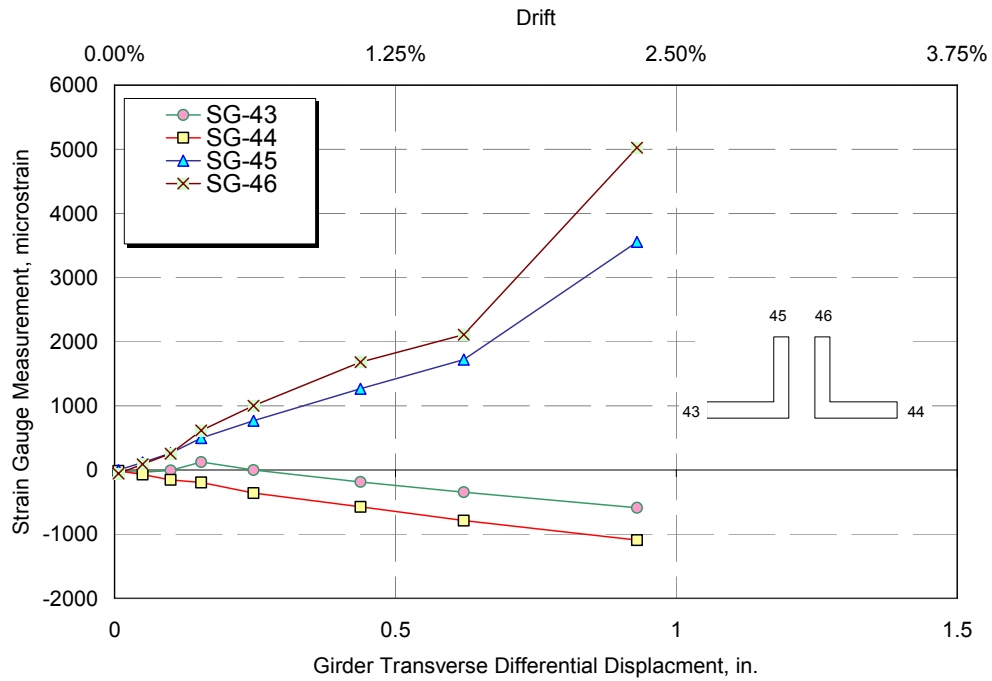


Figure 1-113. Specimen F1B: strain gauge measurement on bottom chord

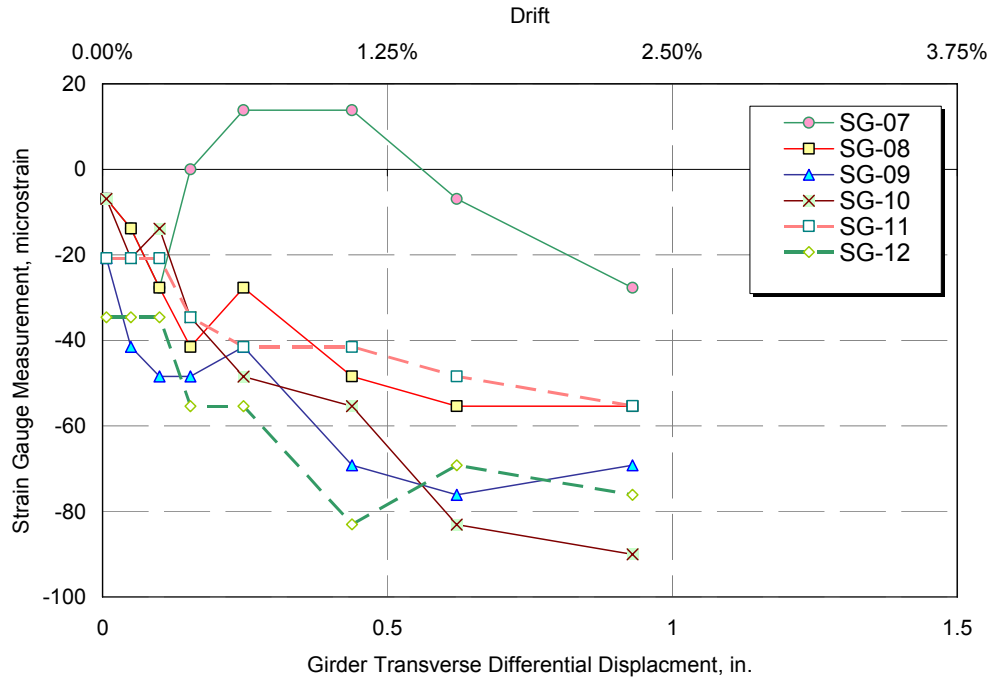


Figure 1-114. Specimen F1B: strain gauge measurement at top of bearing stiffeners

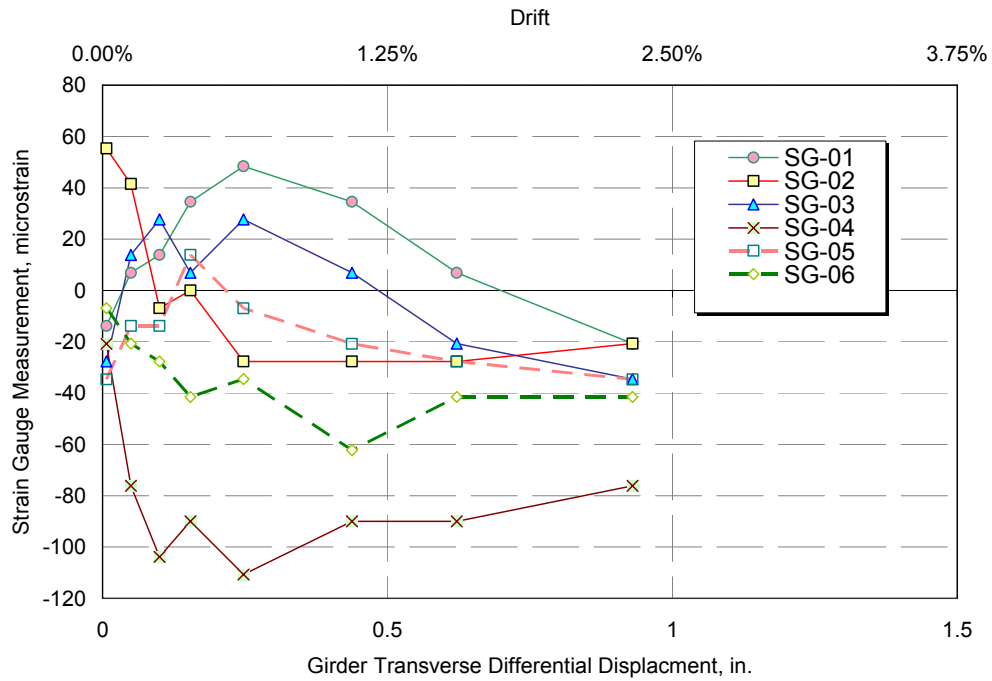


Figure 1-115. Specimen F1B: strain gauge measurement at mid-height of bearing stiffeners

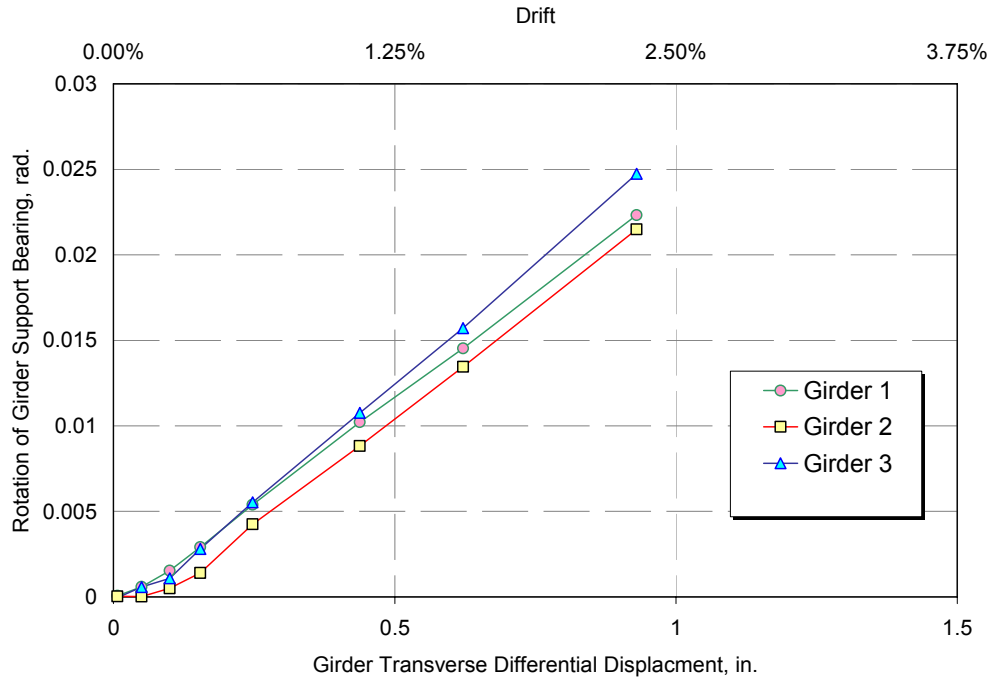


Figure 1-116. Specimen F1B: Rotation of girder support bearings

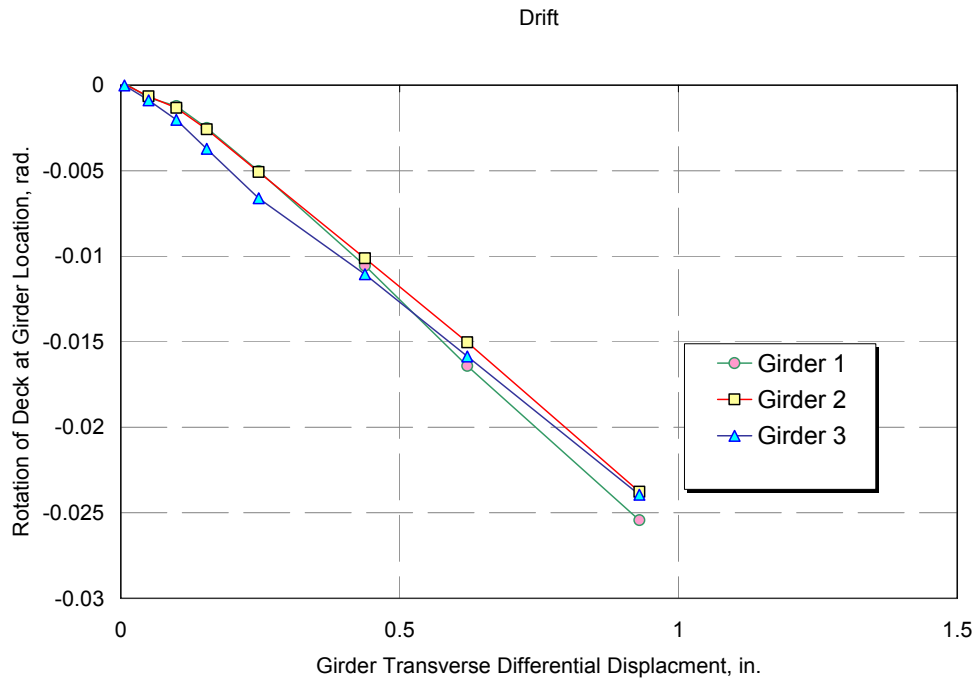


Figure 1-117. Specimen F1B: rotation of deck over girders

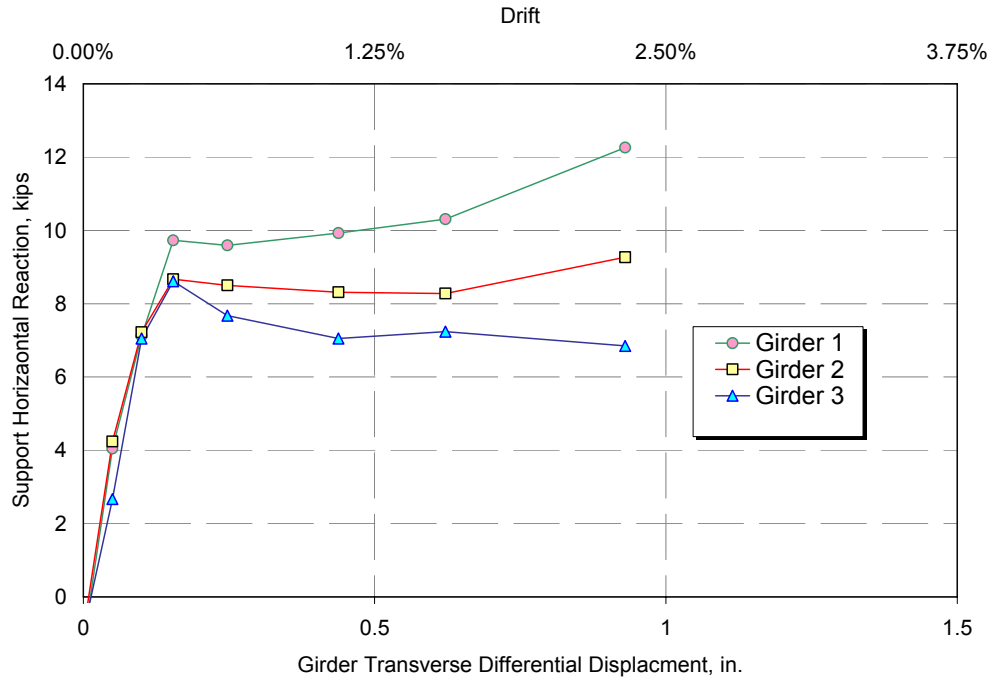


Figure 1-118. Specimen F1B: horizontal support reactions

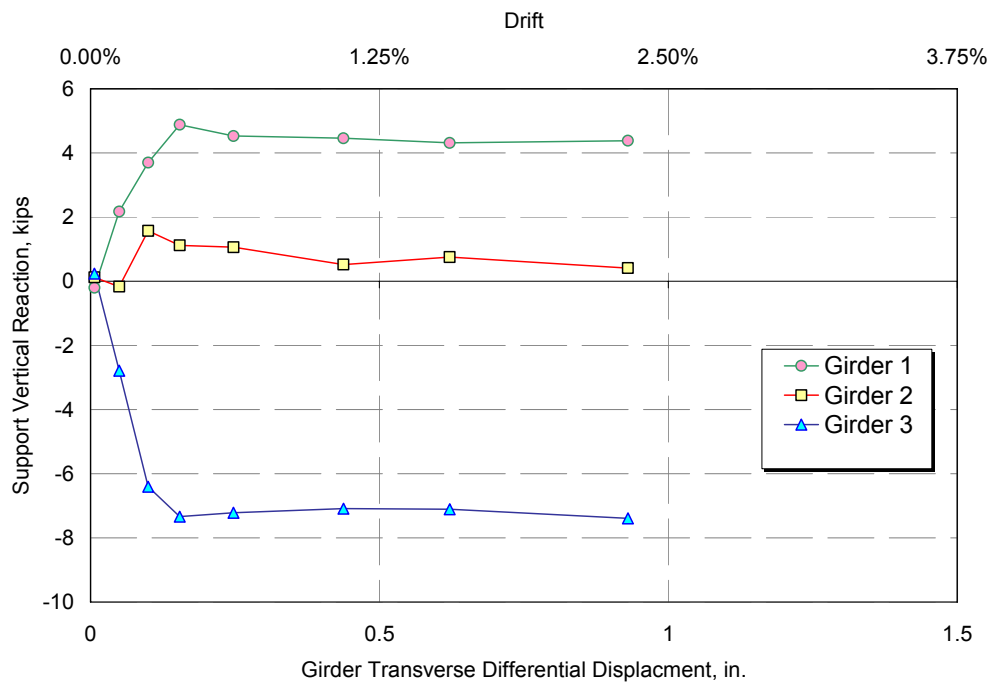


Figure 1-119. Specimen F1B: vertical support reactions

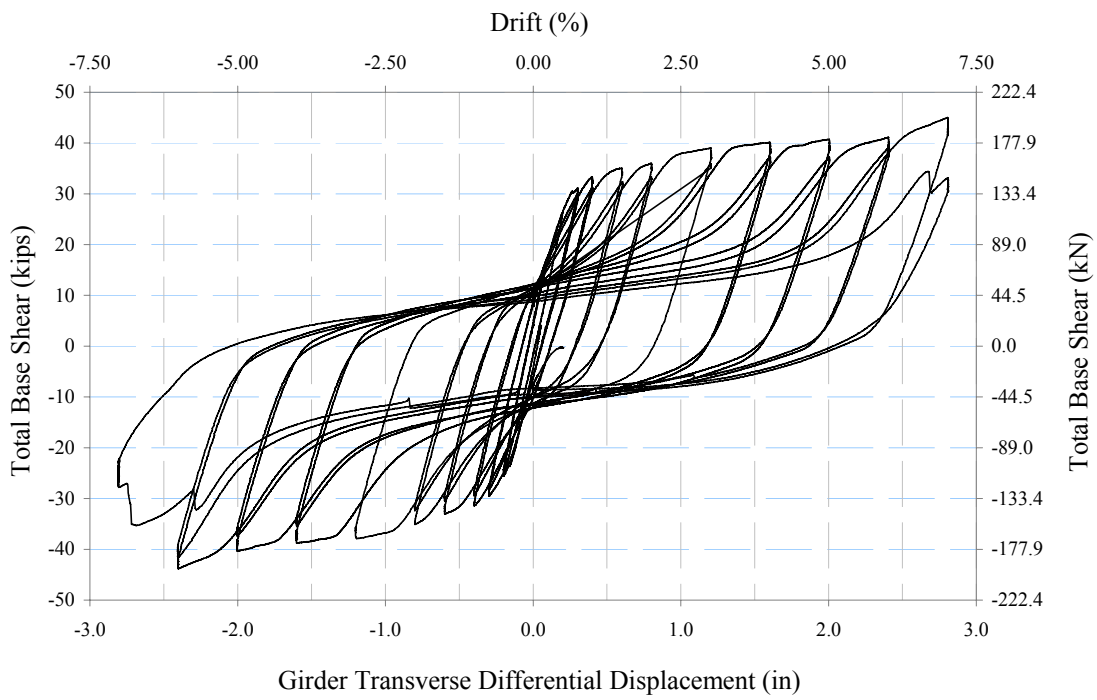


Figure 1-120. Specimen F1B\_1: Actuator force versus differential girder displacement

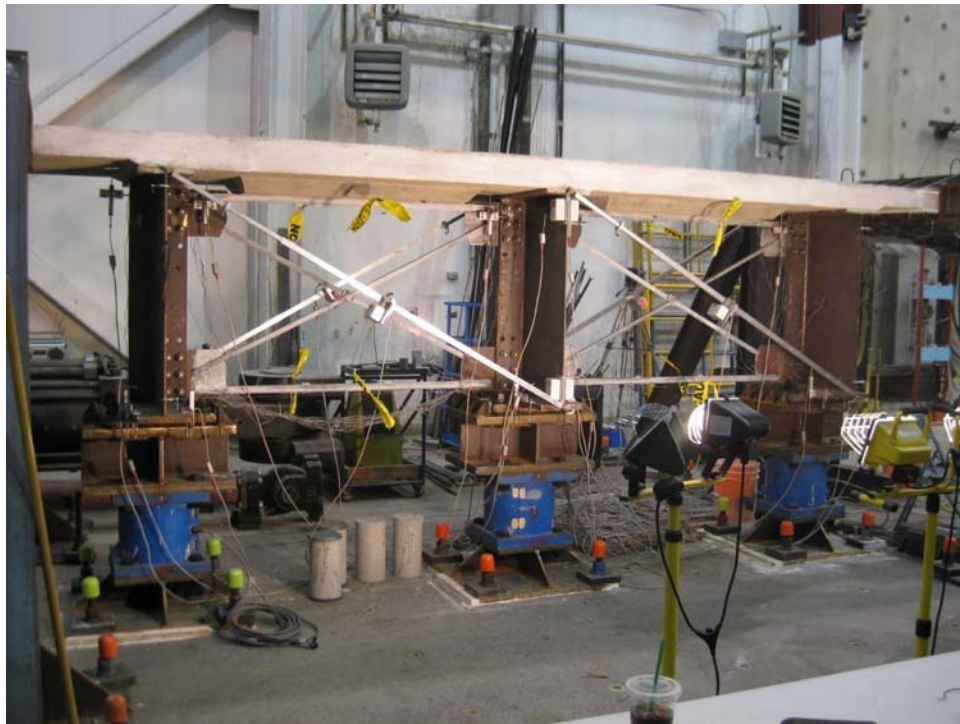


Figure 1-121. View of Specimen F1B\_1 before testing



Figure 1-122. Specimen F1B\_1: X-Frame buckling at 1% drift



Figure 1-123. Specimen F1B\_1: X-Frame yielding at 2% drift, top chord shows signs of yielding



Figure 1-124. Specimen F1B\_1: X-Frame deforming near gusset plate at 3% drift



Figure 1-125. Specimen F1B\_1: deck and girder separation at 3% drift



Figure 1-126. Specimen F1B\_1: top chord at 3% drift



Figure 1-127. Specimen F1B\_1: deformations at 4% drift



Figure 1-128. Specimen F1B\_1: Middle girder rotation at 5% drift



Figure 1-129. Specimen F1B\_1: deformations at 6% drift



Figure 1-130. Specimen F1B\_1: diagonal failure during 7% drift cycle



Figure 1-131. Specimen F1B\_1: diagonal failure during 7% drift cycle



Figure 1-132. Specimen F1B\_1: top chord failure during 7% drift cycle (typical)

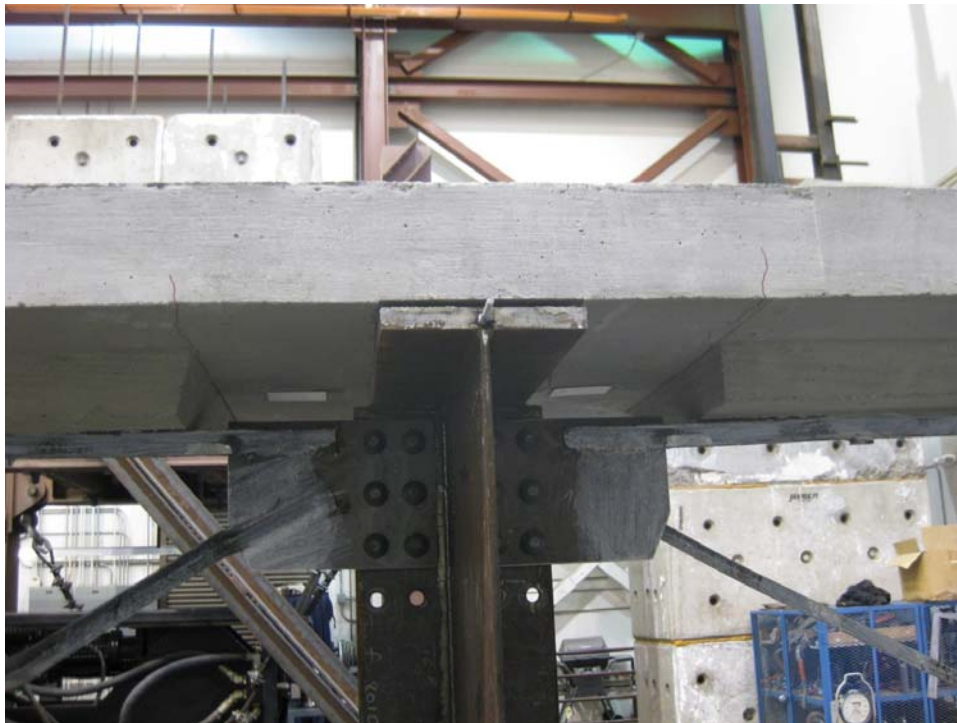


Figure 1-133. Specimen F1B\_1: deck cracks and permanent deck-girder separation – final state

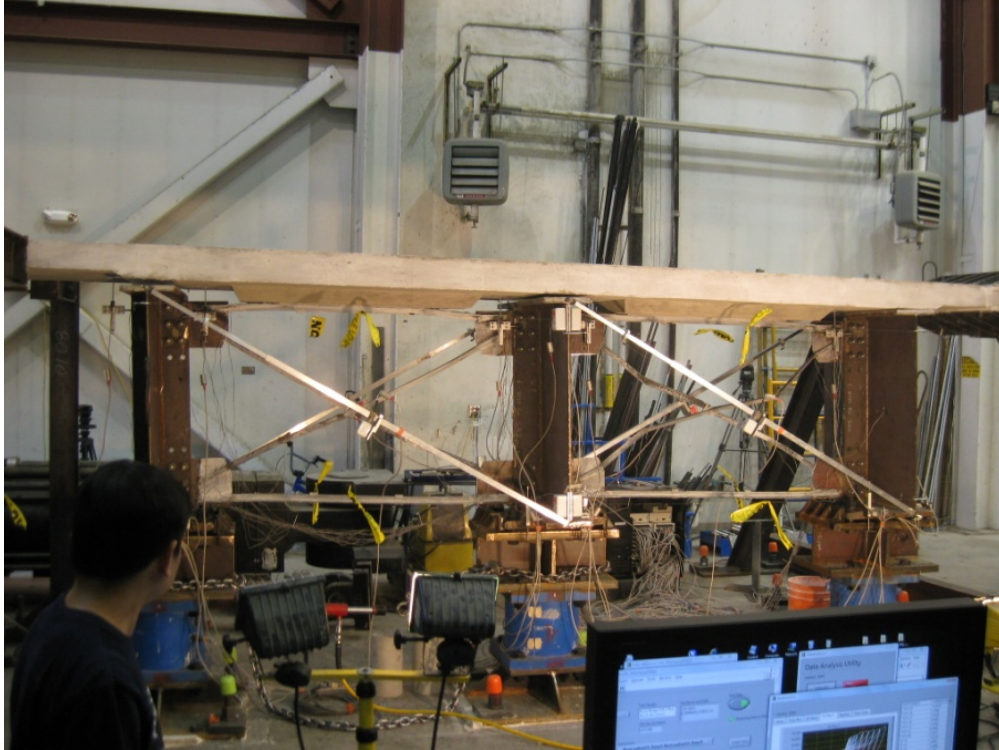


Figure 1-134. Specimen F1B\_1: final state - 0% drift

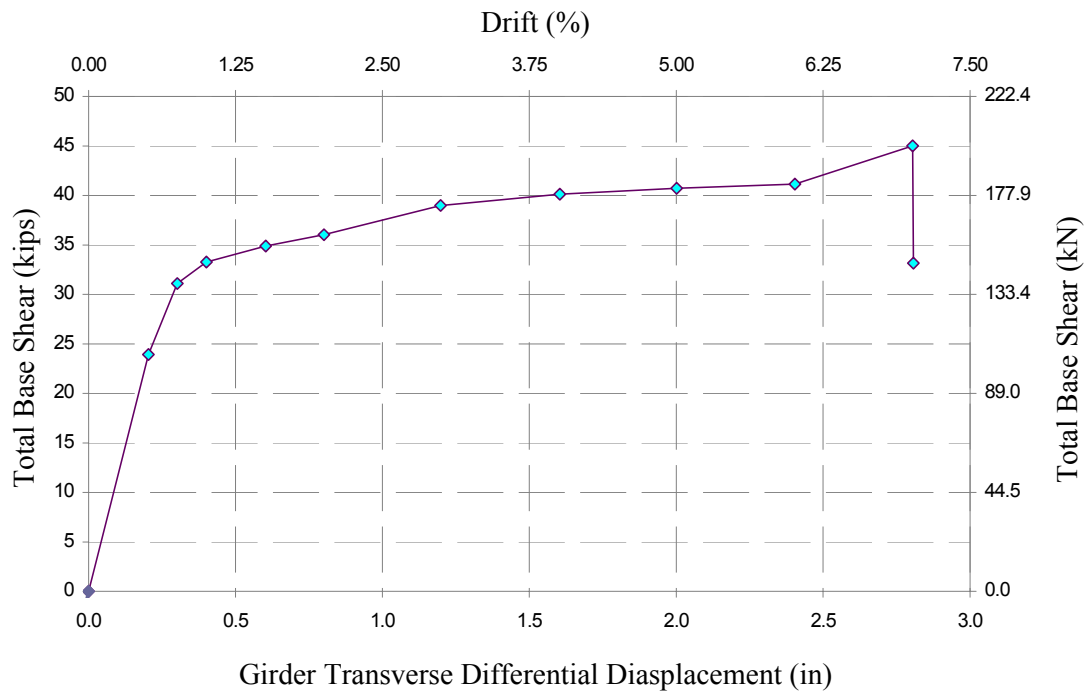


Figure 1-135. Specimen F1B\_1: base shear at peak displacement cycles

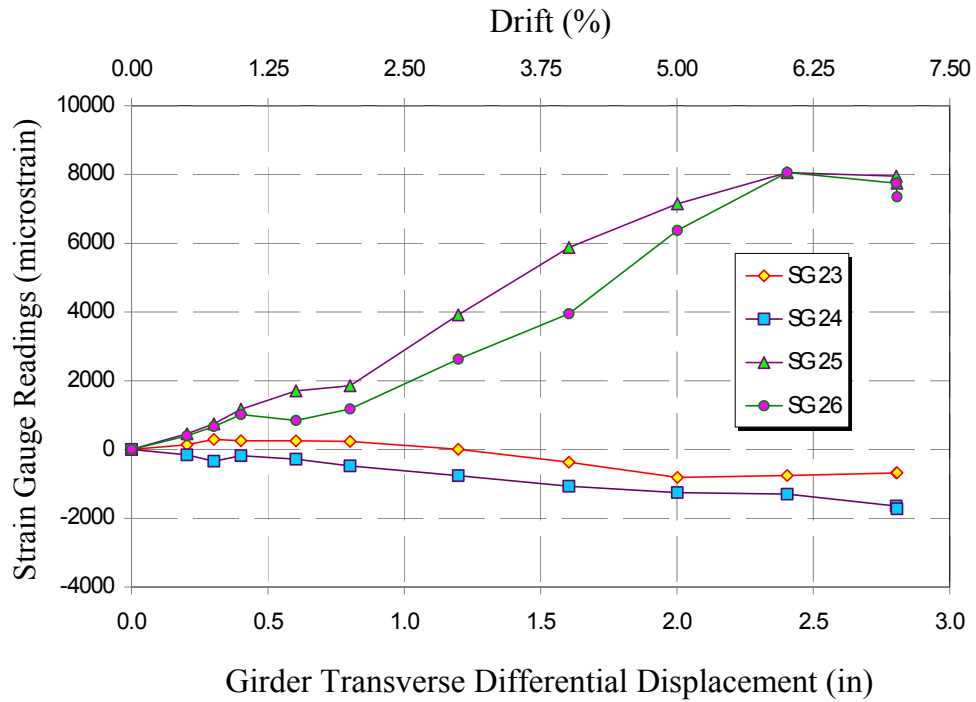


Figure 1-136. Specimen F1B\_1: strain gauge measurement on top chord

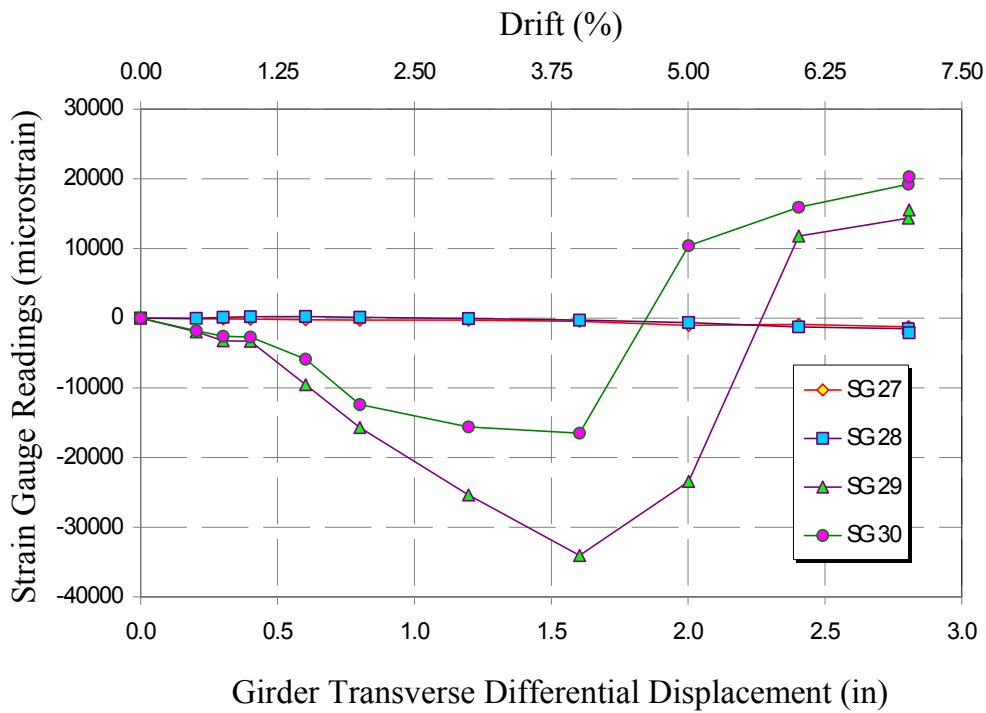


Figure 1-137. Specimen F1B\_1: strain gauge measurement on top chord

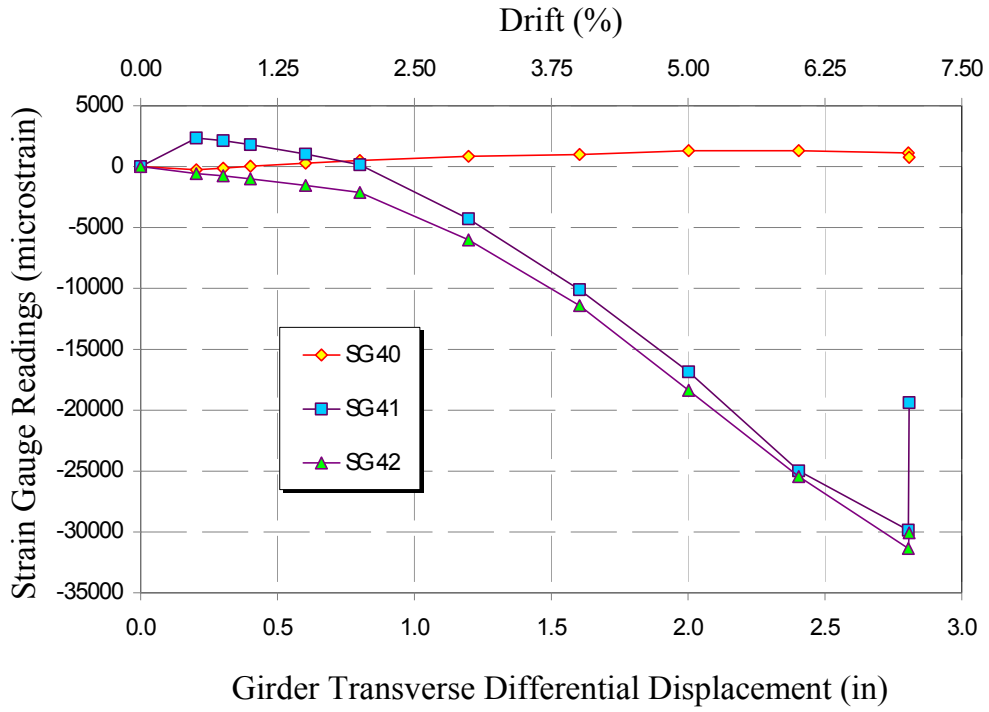


Figure 1-138. Specimen F1B\_1: strain gauge measurements on bottom chord

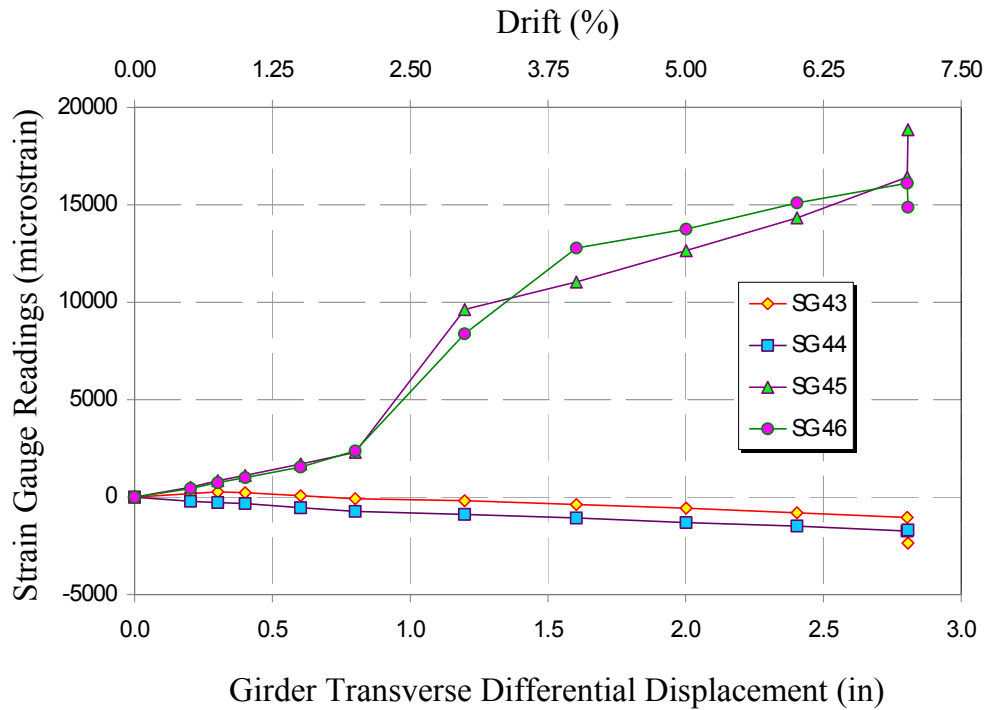


Figure 1-139. Specimen F1B\_1: strain gauge measurement on bottom chord

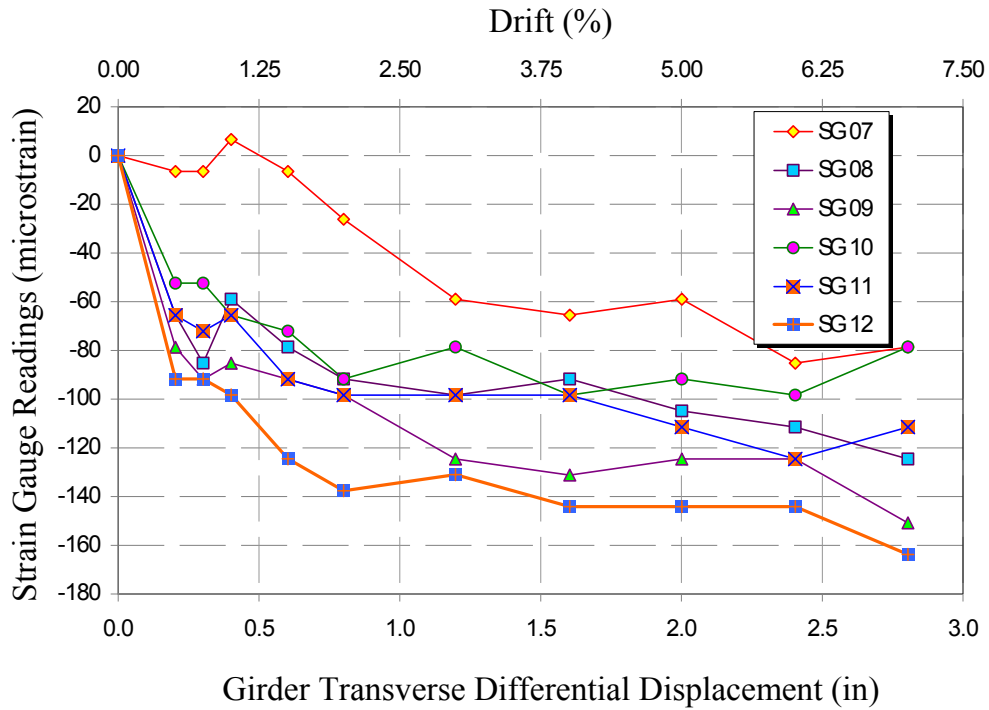


Figure 1-140. Specimen F1B\_1: strain gauge measurement at top of bearing stiffeners

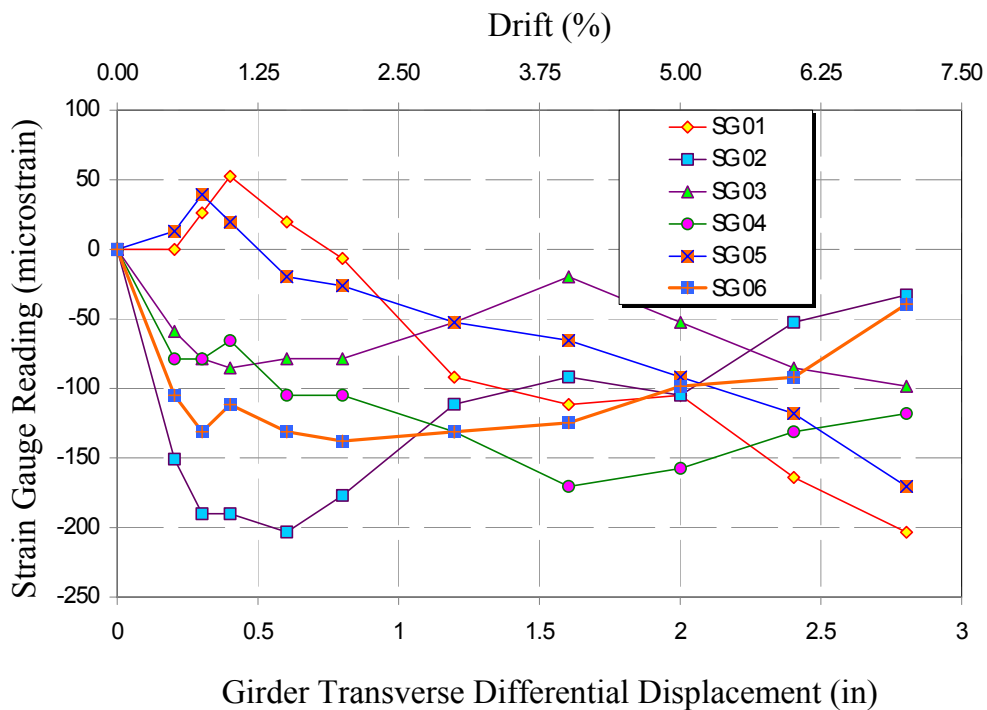


Figure 1-141. Specimen F1B\_1: strain gauge measurement at mid-height of bearing stiffeners

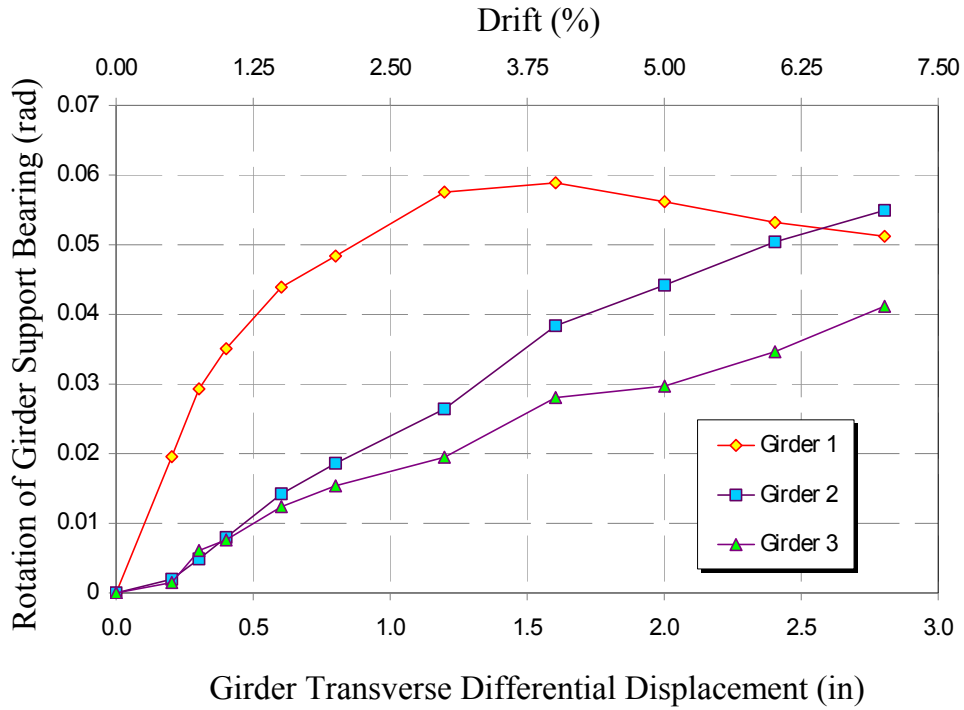


Figure 1-142. Specimen F1B\_1: Rotation of girder support bearings

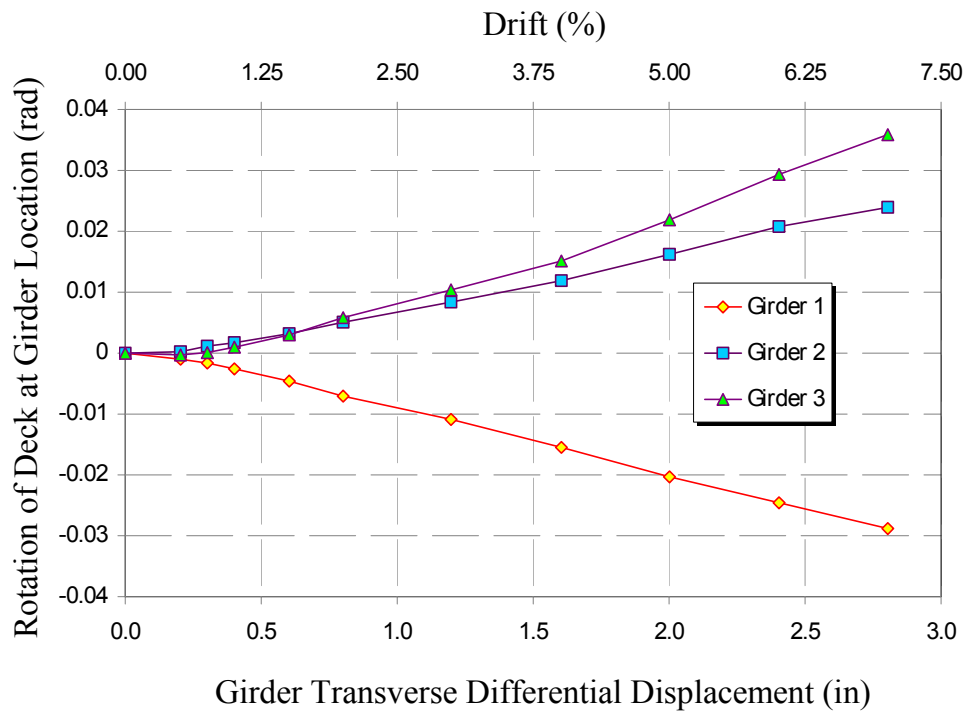


Figure 1-143. Specimen F1B\_1: rotation of deck over girders

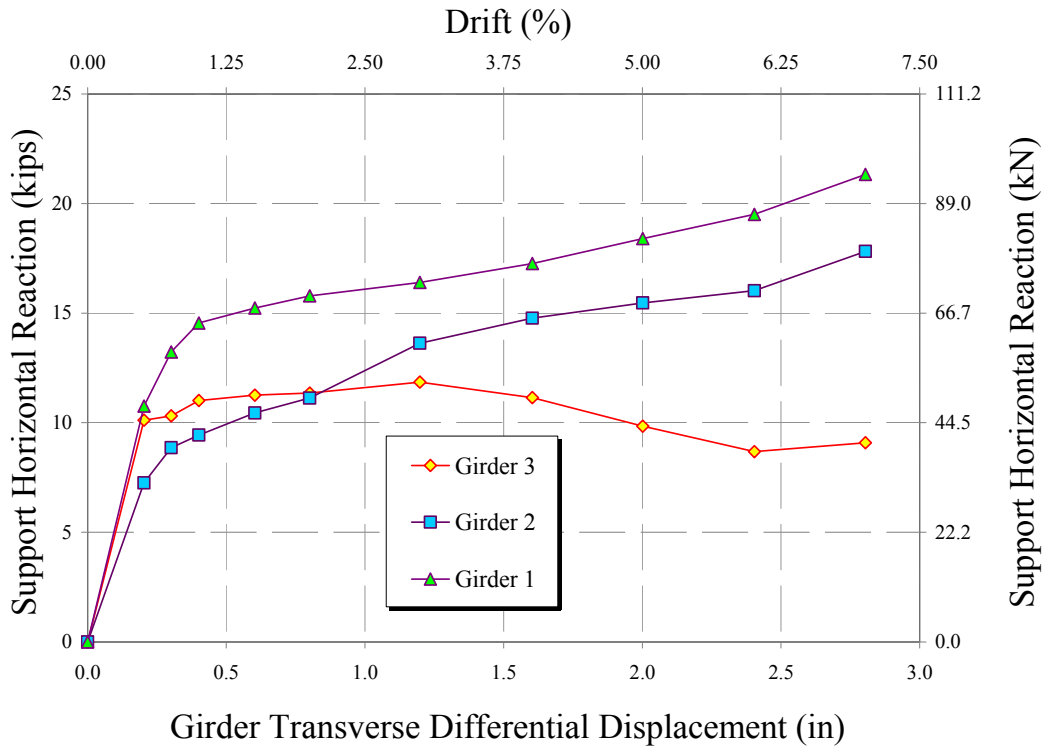


Figure 1-144. Specimen F1B\_1: horizontal support reactions

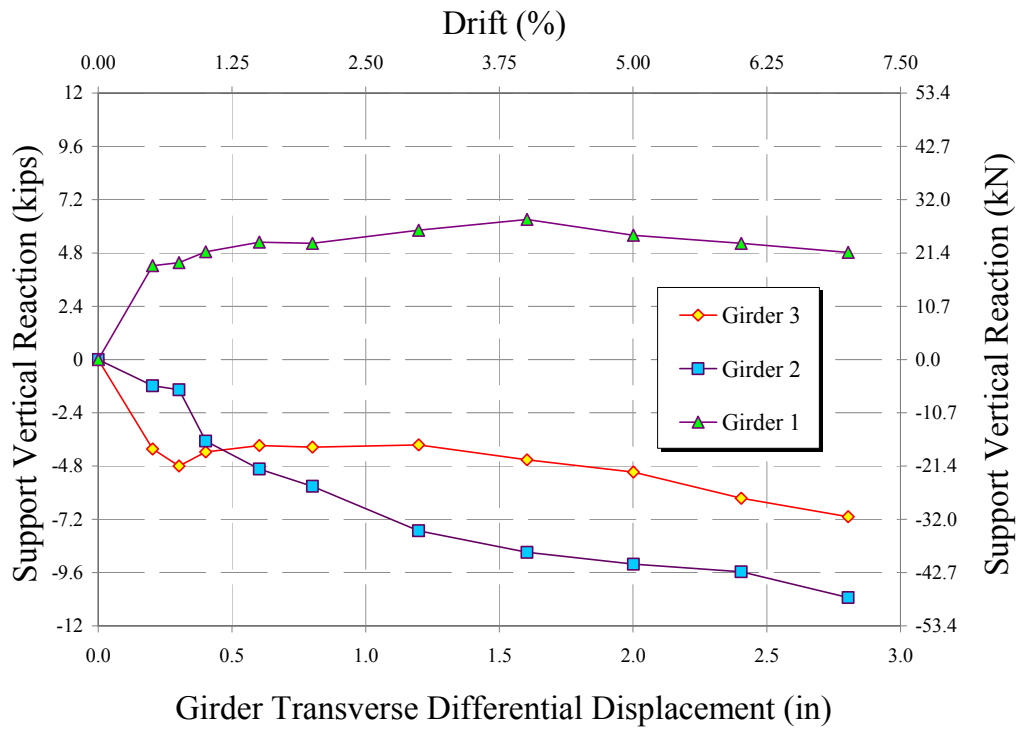


Figure 1-145. Specimen F1B\_1: vertical support reactions

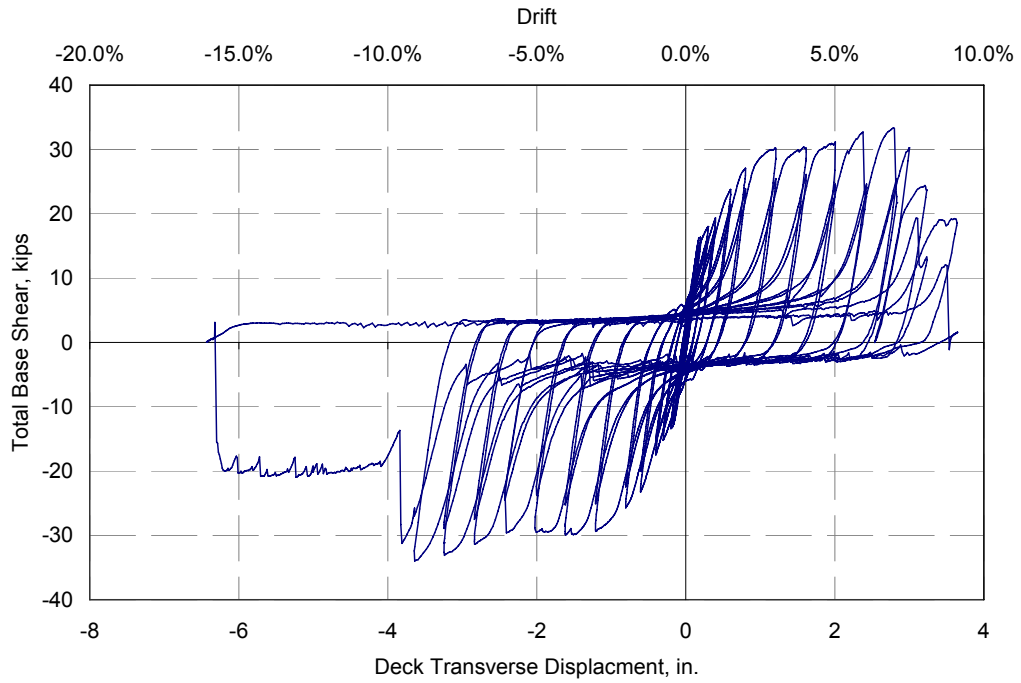


Figure 1-146. Specimen F1C: Actuator force versus actuator displacement (deck displacement)

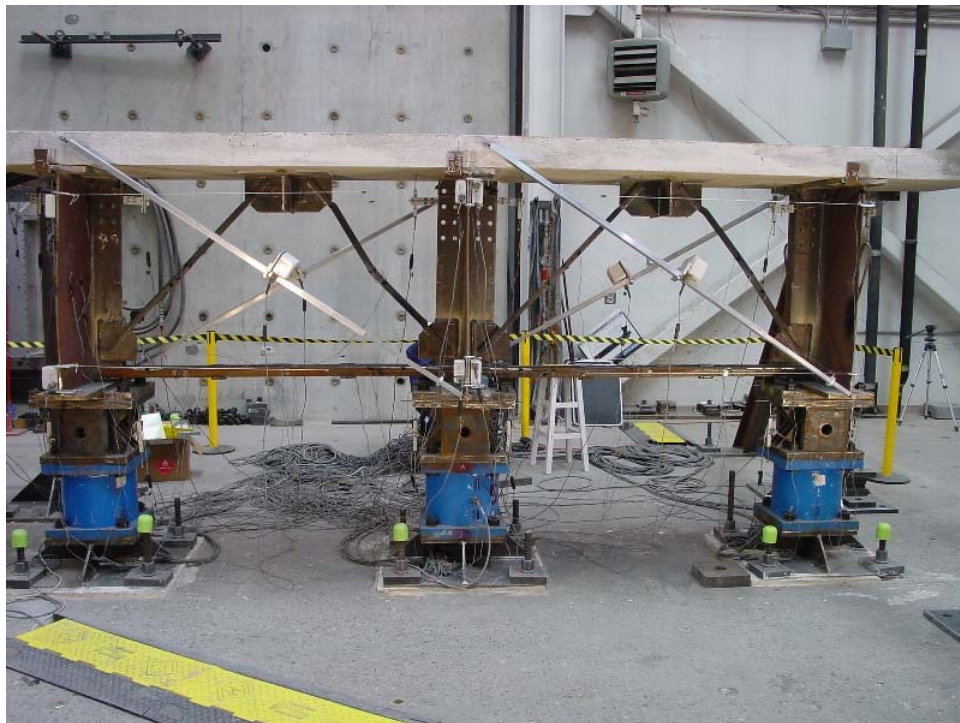


Figure 1-147. Specimens F1C: deformed shape at 2% drift

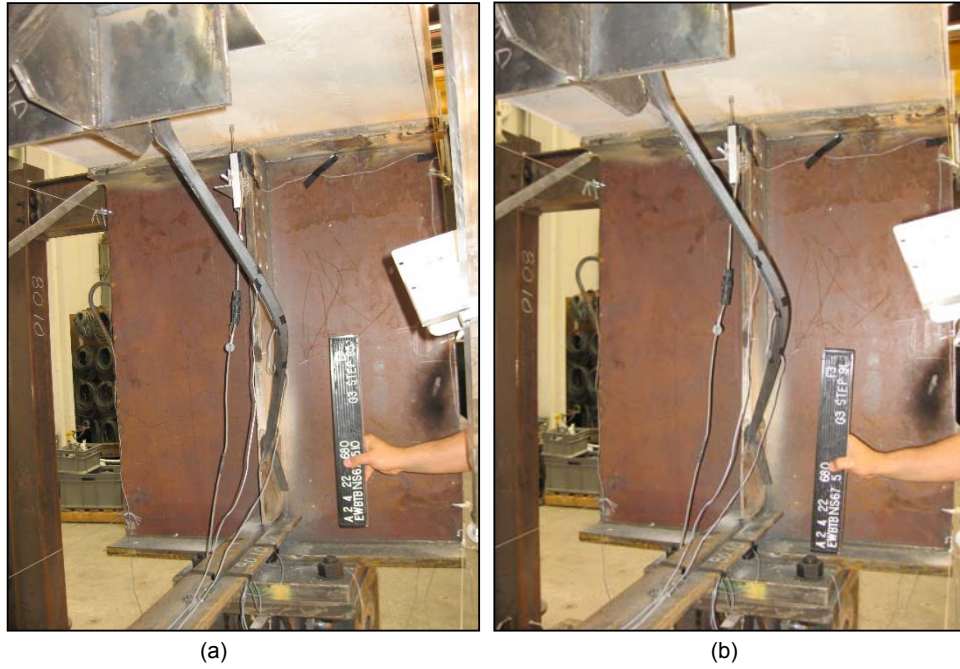


Figure 1-148. Specimen F1C: buckled brace at (a) 4% and (b) 5% drift



Figure 1-149. Specimen F1C: distortion of buckled angle bracing near the gusset at 2% drift



Figure 1-150. Specimen F1C: rotation of the deck over Girder 3 as a result of bending in the deck



Figure 1-151. Specimen F1C: abrasion of underside of deck shows sliding of the deck

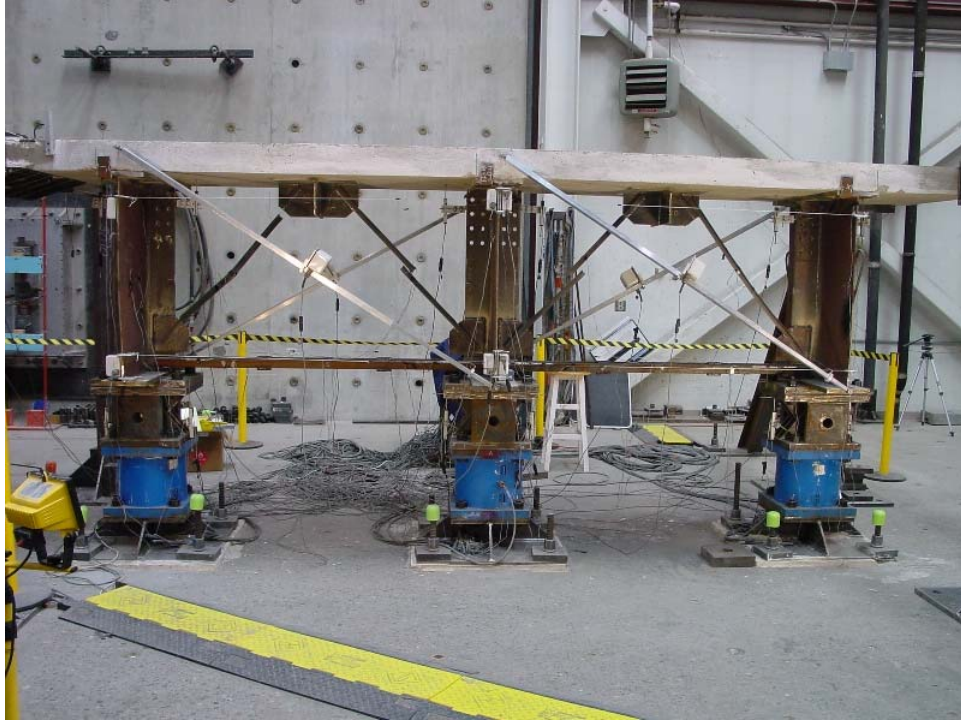


Figure 1-152. Specimen F1C after the test



Figure 1-153. Specimen F1C: large permanent axial deformations was observed in braces

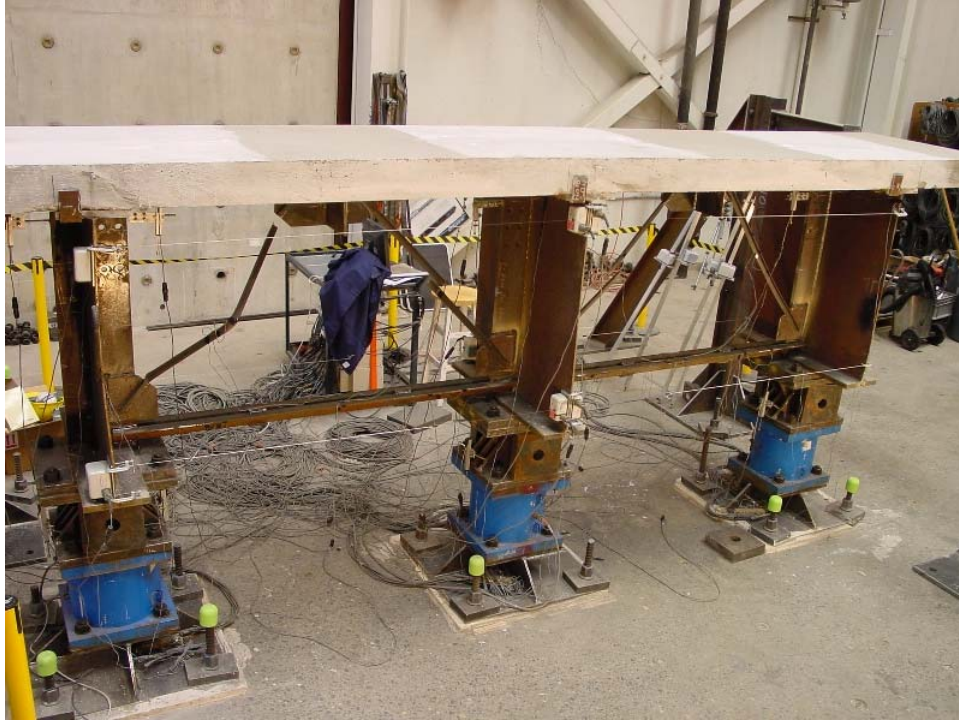


Figure 1-154. Specimen F1C: no damage in the concrete deck after the test

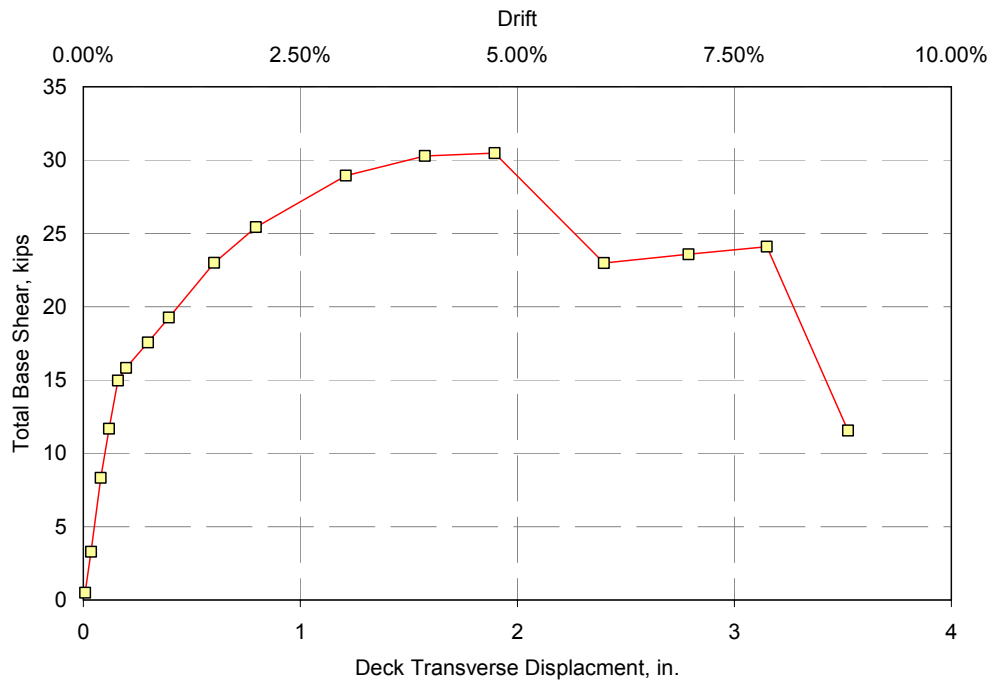


Figure 1-155. Specimen F1C: base shear at peak displacement cycles

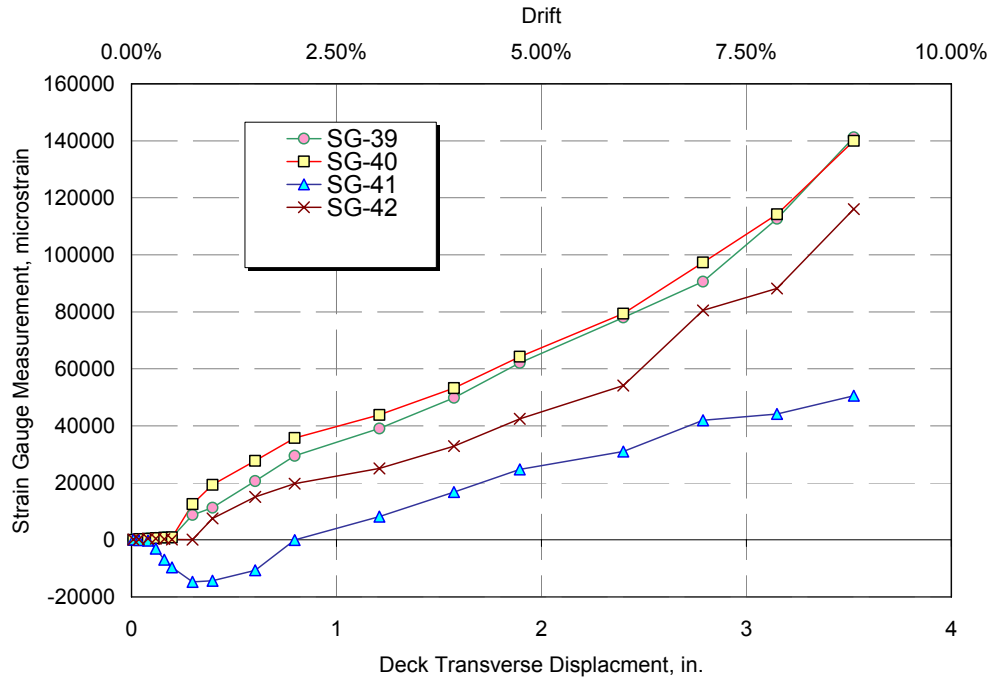


Figure 1-156. Specimen F1C: strain measurements on the chevron braces between G1 and G2

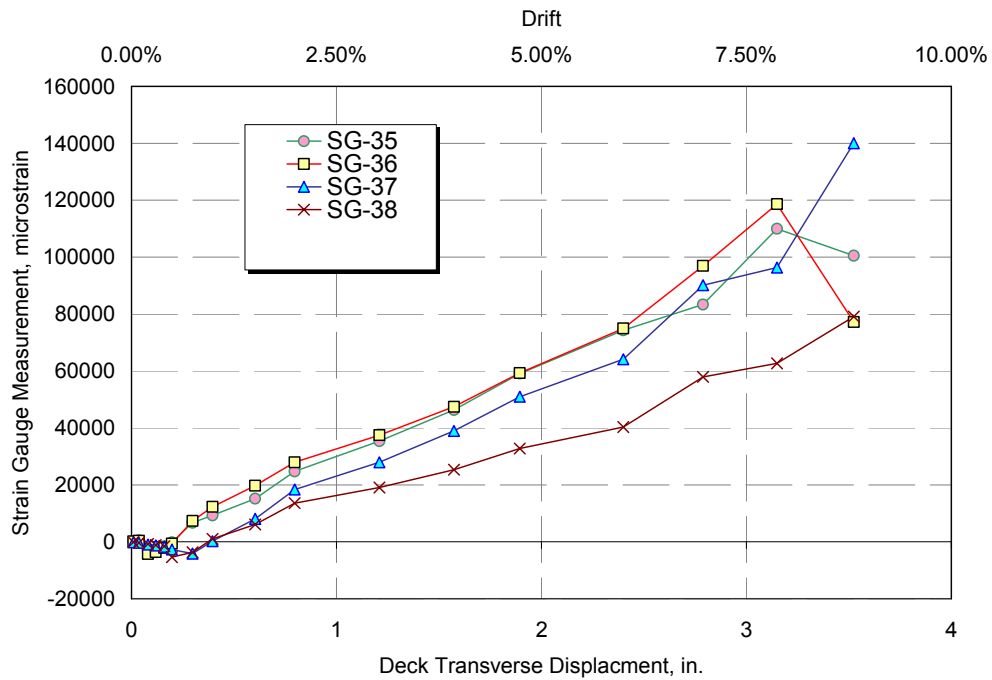


Figure 1-157. Specimen F1C: strain measurements on the chevron braces between G2 and G3

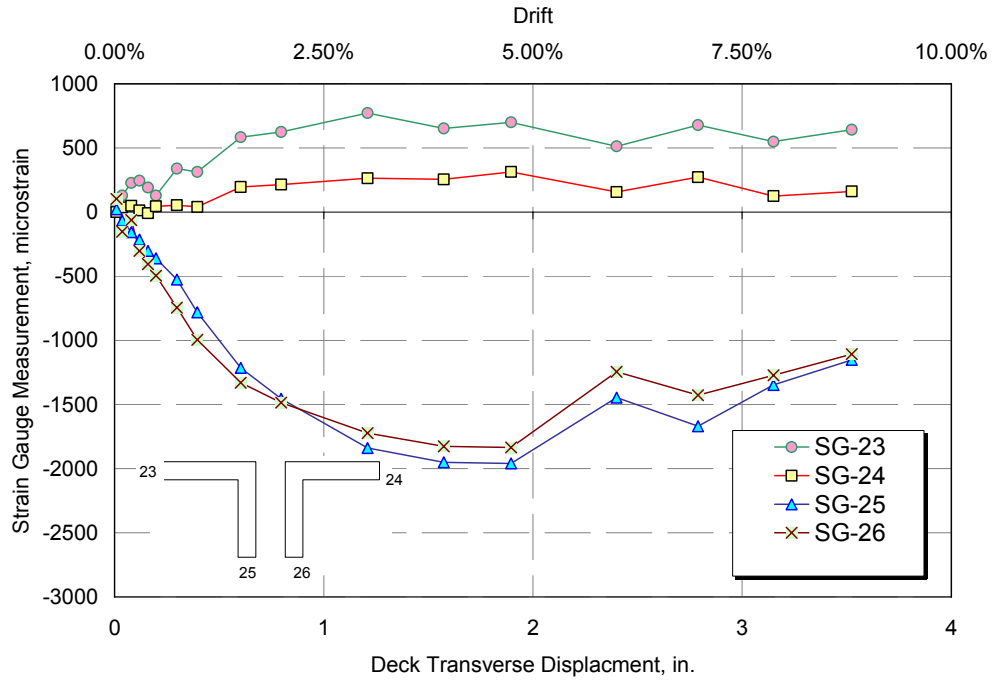


Figure 1-158. Specimen F1C: strain gauge measurement on bottom chord at Girder 2

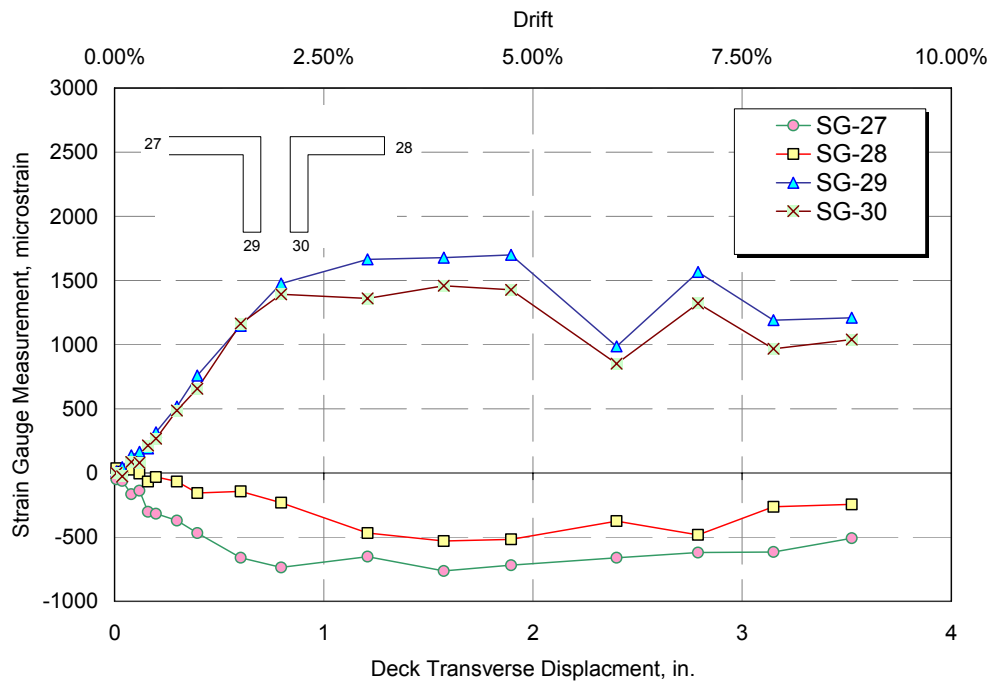


Figure 1-159. . Specimen F1C: strain gauge measurement on bottom chord at Girder 2

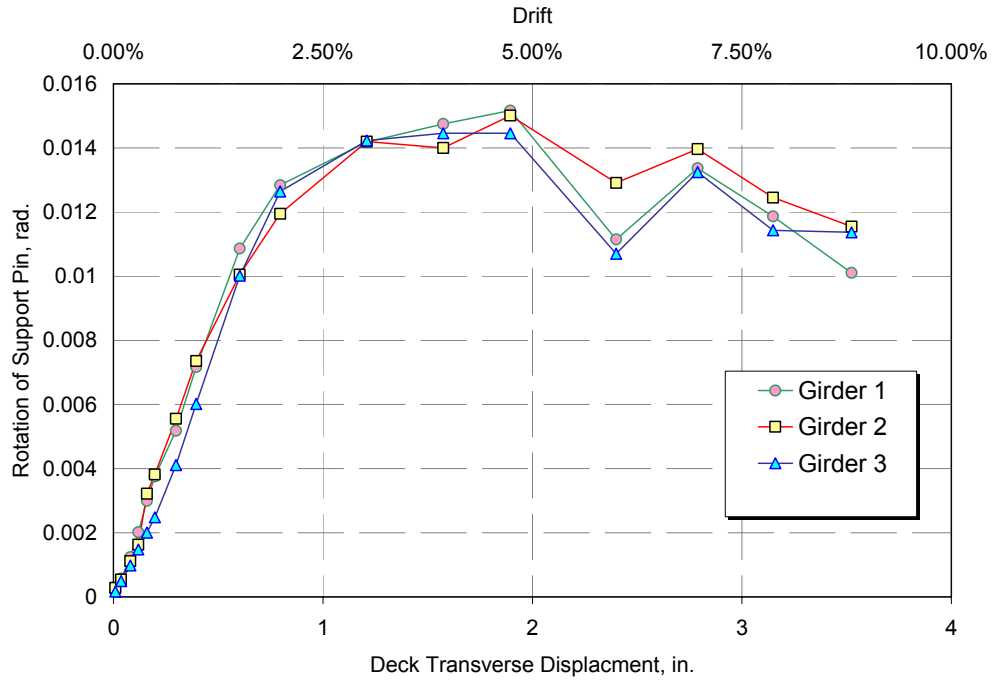


Figure 1-160. Rotation of the supports in Specimen F1C

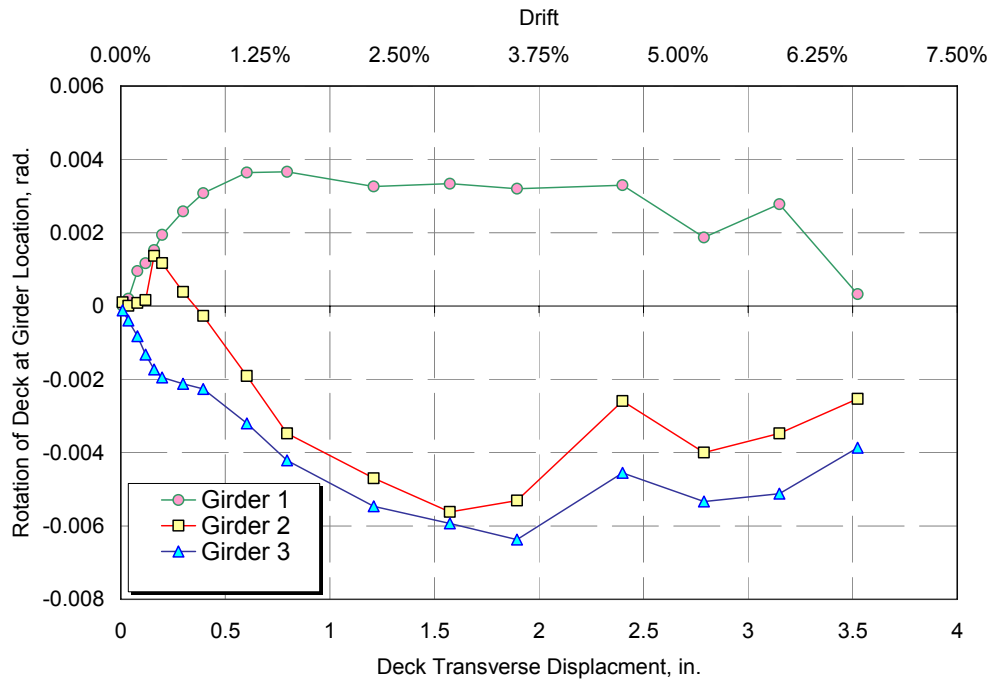


Figure 1-161. Rotation of the deck at girder locations in Specimen F1C

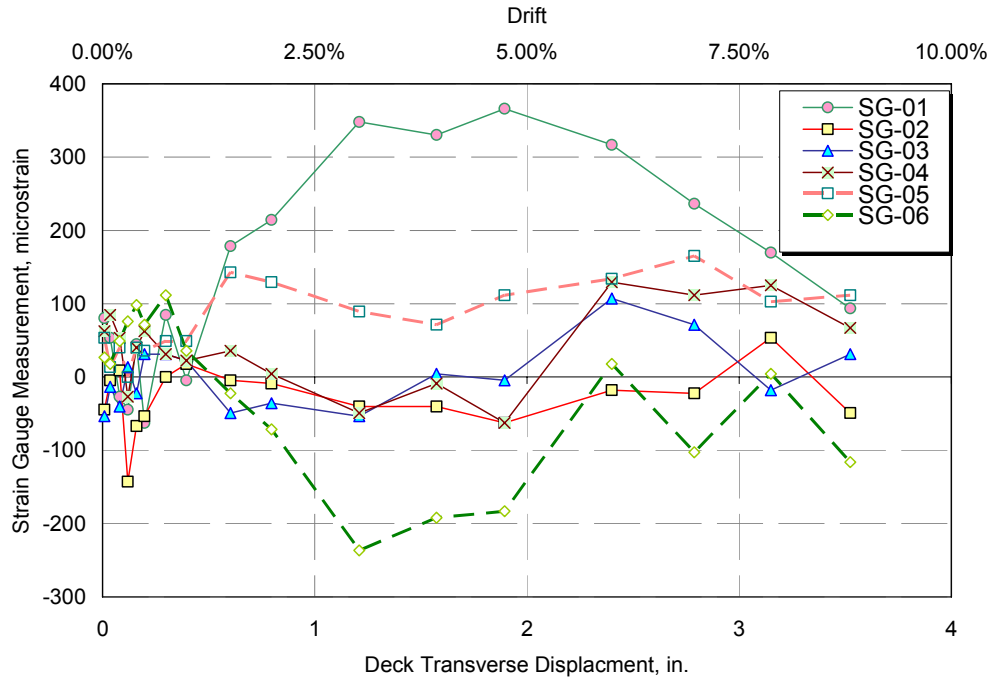


Figure 1-162. Specimen F1C: strain measurements at the bottom of the girders

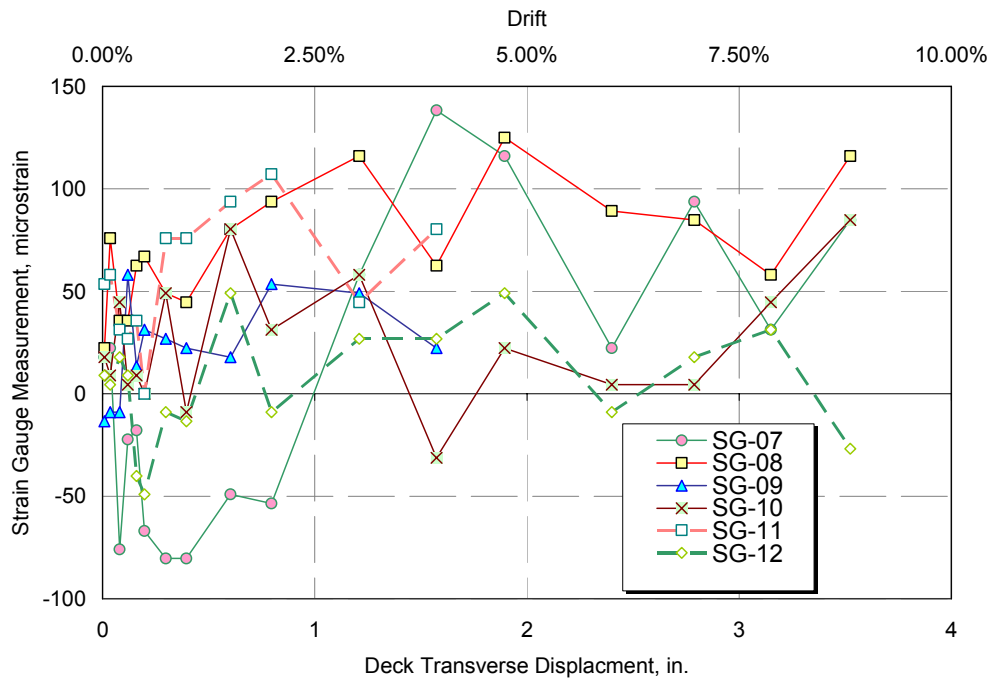


Figure 1-163. Specimen F1C: small strain measurements at the top of the girders

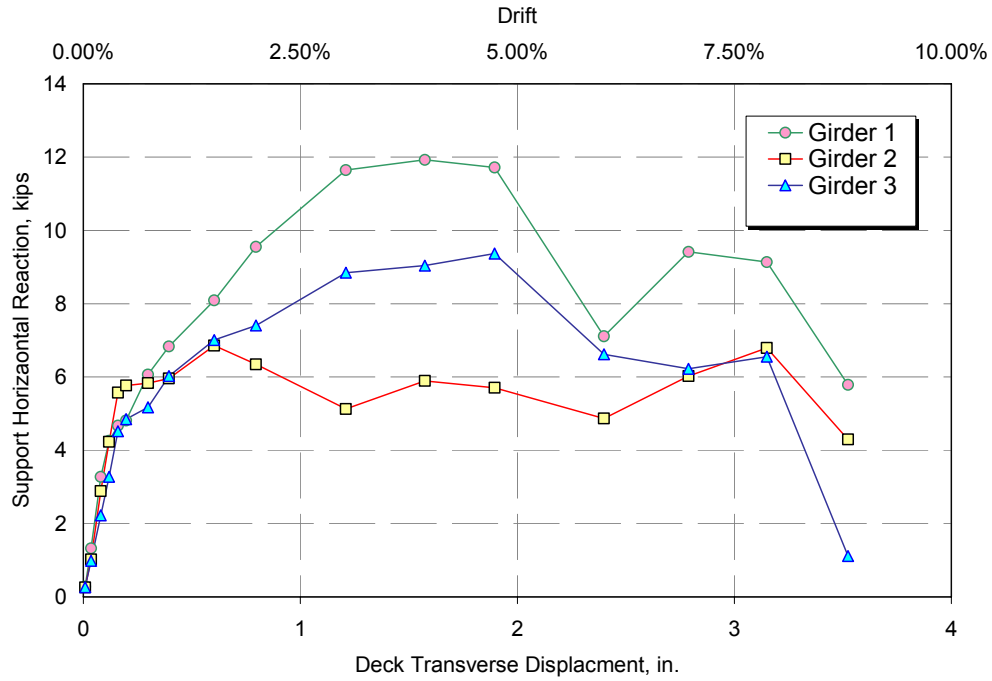


Figure 1-164. Specimen F1C: horizontal support reactions

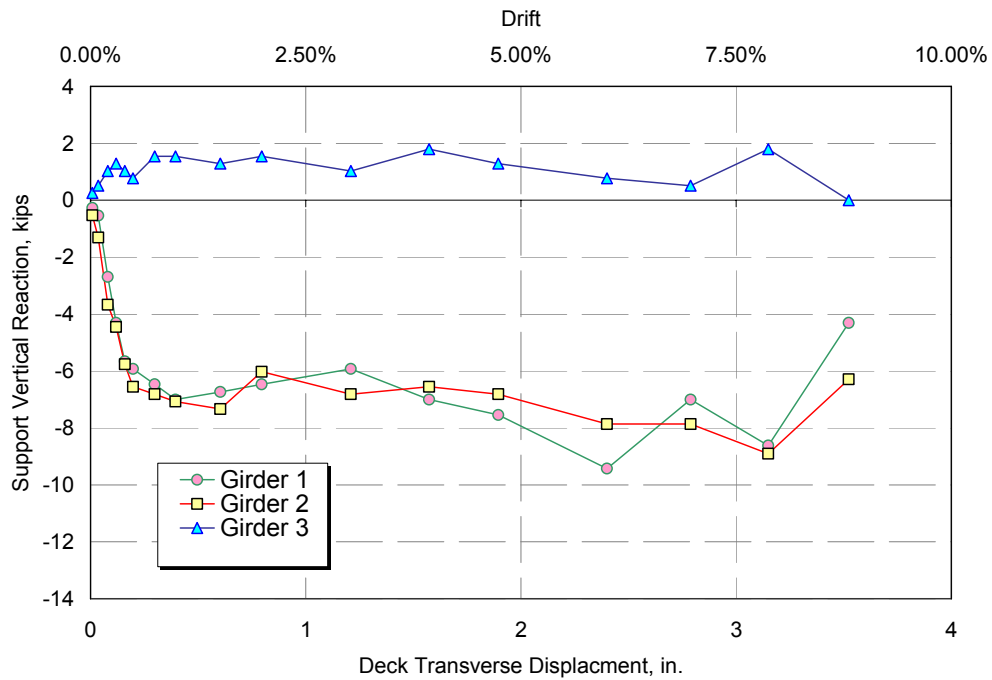


Figure 1-165. Specimen F1C: vertical support reactions



Figure 1-166. Buckled end cross frame member in Capitol Arch Bridge during the 2001 Nisqually Earthquake in Washington.



Figure 1-167. Two-girder steel bridge model subjected to reversed static load transverse loading.



Figure 1-168. Bridge model during shake table experiments with X-braces at the ends.



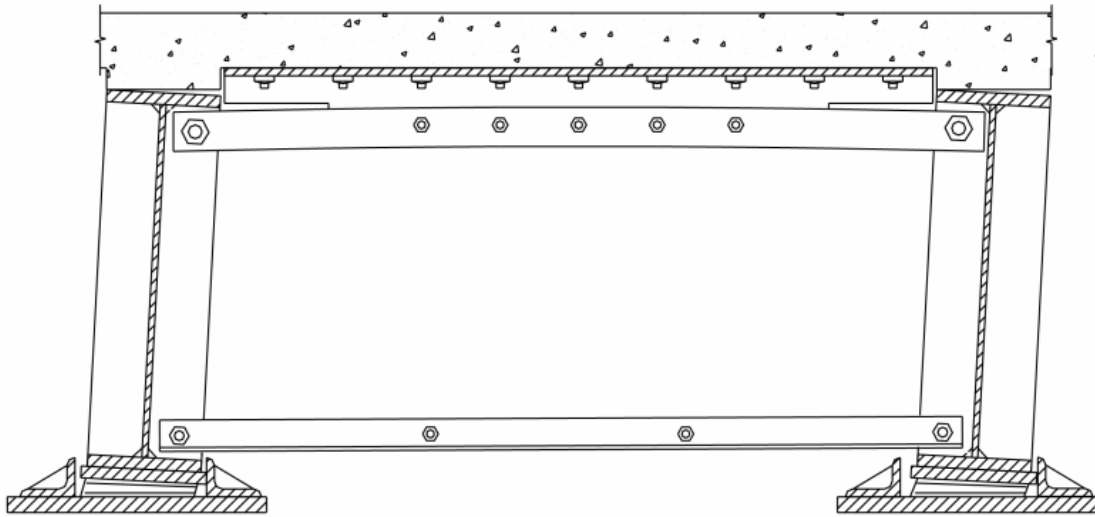


Figure 1-171. "Rocking" mechanism at the ends of the girders to allow relatively large girder drifts.

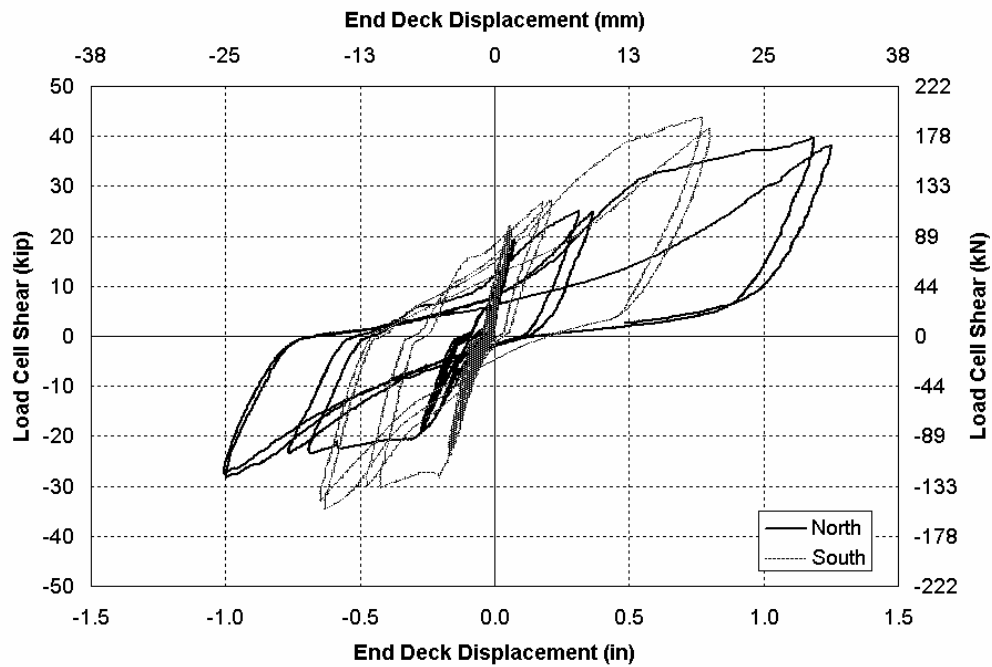


Figure 1-172. Hysteresis loops for each end of bridge model during the reversed static load experiment.

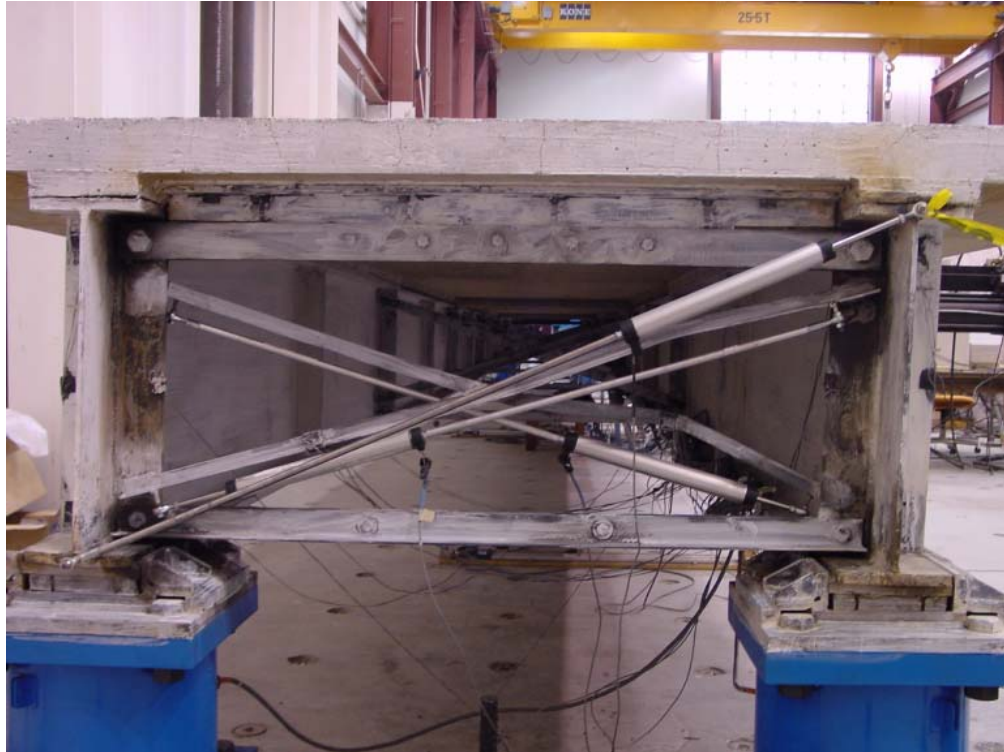


Figure 1-173. South end of bridge model after reversed static load experiment with ductile X-braces.

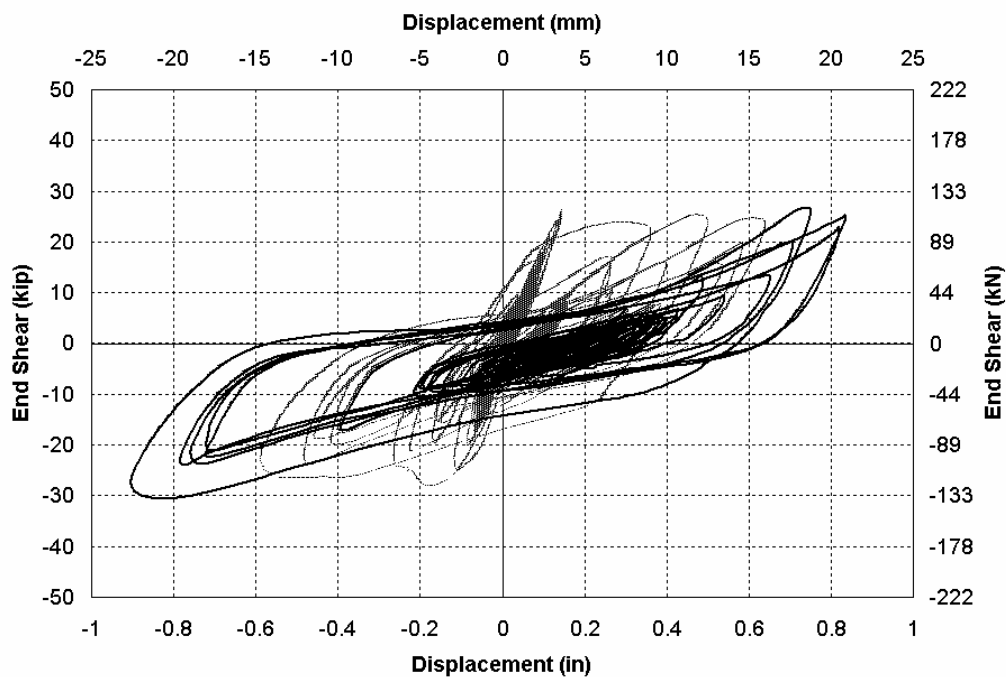


Figure 1-174. Hysteresis loops for north end of bridge model during shake table experiments while subjected to increasing amplitudes of the 1940 El Centro earthquake.

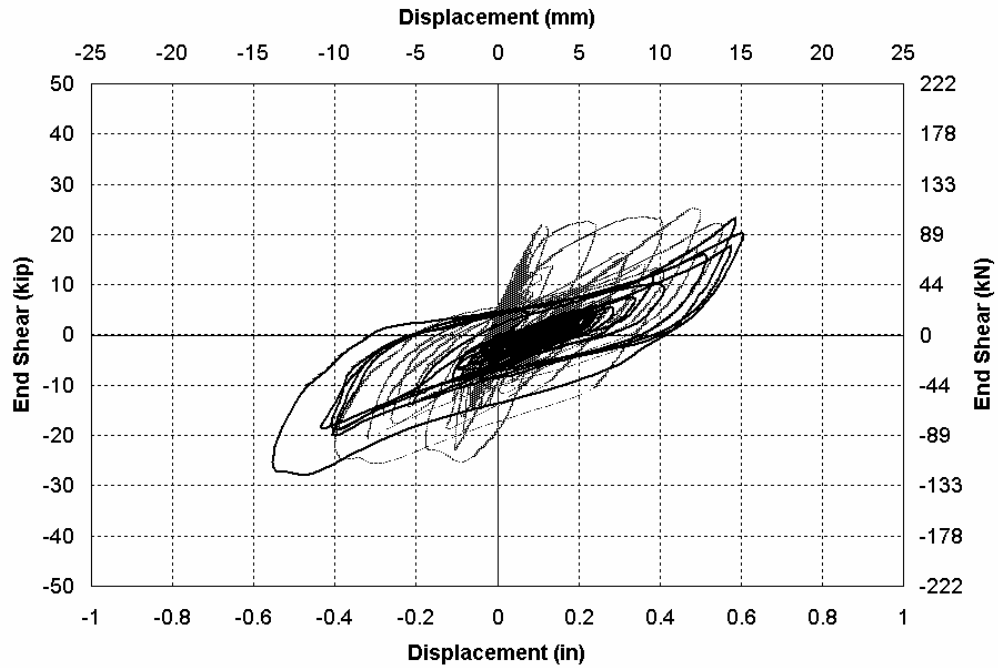


Figure 1-175. Hysteresis loops for south end of bridge model during shake table experiments while subjected to increasing amplitudes of the 1940 El Centro earthquake.

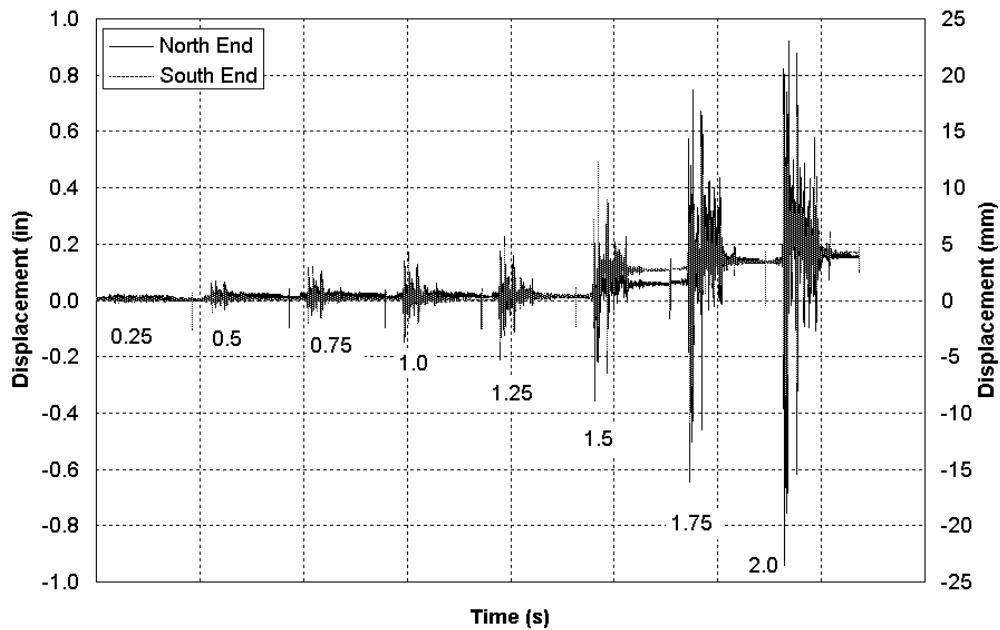


Figure 1-176. Displacement time histories at the ends of the bridge model in response to increasing amplitudes of the 1940 El Centro earthquake (eg. 0.25 = 0.25 times the El Centro earthquake).

# **Appendix 1**

## **Comparison between Various Specifications and Codes on the Seismic Analysis and Design of Steel Plate Girder Bridges**

No.	Description	MCEER / ATC 49	AASHTO LRFD	Canada S-6-00	Japan 2002	Guide Steel Spec. * SDC	Caltrans SDC	AASHTO 17th ed. 2002	AASHTO Guide Spec.
		Ref. Description	Ref. Description	Ref. Description	Ref. Description	Ref. Description	Ref. Description	Ref. Description	Ref. Description
1	Importance Classification (IC)	3.7 Operational/Immediate service under MCE and minimal damage under EE; Life safety: significant disruption of service and significant damage under MCE and immediate service and minimal damage under EE	3.3 Critical Bridges, Essential Bridges, Other Bridges	2.3 Life-Span Bridges, Emergency-closure bridges, Other bridges	2.3 Bridges of unspecified importance, Class A; Bridges with high importance (Class B)	Important and ordinary	Important and ordinary	Essential Bridges (CS), Other Bridges (C-III)	For a bridge to be classified as an Essential Bridge or Critical Bridge, one or more of the following items must be present: (1) bridge is required to provide secondary life safety, (2) sufficient time for restoration of functionality after closure creates a major economic impact, and (3) the bridge is normally used for emergency purposes. A bridge is classified as Critical, Essential or Normal as follows: Critical Bridges: Bridges that must be open to all traffic once inspected after the safety evaluation design earthquake (SEE) and be usable by emergency responders for security/defense purposes immediately after the safety evaluation design earthquake. Essential Bridges: Bridges that should, as a minimum, be open to emergency vehicles and for security/defense purposes after the safety evaluation
2	Acceleration Coefficient	3.7 4. Seismic Hazard Levels (I to IV) based on F <sub>s</sub> -S <sub>1</sub> or F <sub>s</sub> -S <sub>2</sub> values, see table 3.7-1	A	A	4.4 Modification Factors for Zone c <sub>2</sub> , Region A; 1.0, Region B; 0.85; Region C; 0.70. See table 4.4.1	Peak Rock Acceleration from Caltrans Seismic Hazard Map used in ARS curves	Peak Rock Acceleration from Caltrans Seismic Hazard Map used in ARS curves	A	4 SDCs based on F <sub>s</sub> or F <sub>s</sub> values.
3	Seismic Performance Category	3.6 Six Seismic Design Repair Categories based on Seismic Hazard Levels and Importance Category, see table 3.7-2	4.4 4 categories (1 to 4) based on Acceleration Coefficient(A)	4.4.4 4 categories based on Acceleration Coefficient(A) and Importance Category. See table 4.4.4.1	4.4 Seismic Performance 1: bridge keeps in sound functional condition under elastic, seismic motions. Seismic Performance 2: sustains limited damage; easy functional recovery; Seismic Performance 3: sustaining no critical damage. See tables C-5.3.1 and C-5.4.1	Based on importance category for two types of bridges: Functional Evaluation and Safety-Evaluation ground motions. See table 1 in MTD 20-1	Based on importance category for two types of bridges: Functional Evaluation and Safety-Evaluation ground motions. See table 1 in MTD 20-1	4 categories (A, B, C, D) based on Acceleration Coefficient(A) and Importance Category	5 SDCs based on F <sub>s</sub> or F <sub>s</sub> values.
4	Site Coefficient (S)	3.4.2 Site Classification (A to E) based on Table 3.4.2-1	4.4.6 Based on 4 soil types I to IV	4.4.6 Four types of soil profile; ranging from rock (type I) to soft clay or silt more than 12m (36 ft) deep (type IV). See table 4.4.6.1	3 types of ground (Type I, II, III), see table 4.5.1	5 types of soil (A to F) based on ATC 32 report used in ARS curves	5 types of soil (A to F) based on ATC 32 report used in ARS curves	Based on 4 soil types I to IV	Standard NEHRP soil types (A, B, C, D, E, and F)
5	Design Approach	Two-level design; design performance is implied for EE	Single level design	Single level design	Two-level design. An explicit functional evaluation is not required for Ordinary bridges if they meet safety-evaluation performance criteria	Single level design	Single level design	Single level design	Single level design
6	Return Periods	Maximum Considered EQ: 2500 years return period; Expected EQ: 150 years return period	475 years return	475 year return	2 level EQ	Maximum Creditable EQ	Maximum Creditable EQ	475 year return	Bridges shall be designed for the life safety performance objective considering a one level design for a 5% probability of exceedance in 50 years. Higher performance objectives, such as the operational objective, may be used with the authorization of the bridge owner.

No.	Description	MCEER / ATC 49	AASHTO LRF	Canada S-6-00	Japan 2002	Guide Steel Spec. + SDC	Caltrans SDC	AASHTO 17th ed. 2002	AASHTO Guide Spec.
7	Elastic Seismic Response Coefficient	3.4.1 Spectra based on 0.2s and 1.0s spectral response accelerations: <b>General Procedure:</b> For $T < T_{10}$ , $S_a = 0.60 \cdot S_{a1} / T$ ; for $T > 40 \cdot T_{10}$ , $S_a = S_{a1} / T$ . <b>Site-Specific Procedure:</b> for special types of ground conditions, important bridges, or closer than 10 km from fault. In lieu of a dynamic analysis use variations in: Col axial load = $(1+C_v) \cdot D_L$ axial force; superstructure bending moment (w/ or w/o structure); Shear = $(1+C_v) \cdot V(DL)$ Shear. See table 3.4.5-1 & table 3.4.5-2 for $C_v$ .	Specs based on PCA: C=1.2(ASTV(2/3); exceptions: for type III and IV for other than fundamental modes with $T < 0.3s$ use $C_s = A(0.8+4T)$ ; for $T > 4s$ use $C_s = 3AS(T^{1/4})^3$	Specs based on PCA: C=1.2(ASTV(2/3)=2.5A; I=3.0 for inline bridges but not greater than R factor I=1.5 for emergency-route bridges I=1.0 for other bridges	Based on ground types: Seismic Motion Level 2 Types I & II; table 4.3.182	GEE will recommend standard ARS, modified standard ARS, or site-specific ARS curve. Standard ARS curves in Appendix B of SDC	GEE will recommend standard ARS, modified ARS, or a site-specific ARS curve in Appendix B of SDC	Specs based on PCA: C=1.2(ASTV(2/3); exceptions: for type III and IV for other than fundamental modes with $T < 0.3s$ use $C_s = A(0.8+4T)$ ; for $T > 4s$ use $C_s = 3AS(T^{1/4})^3$	
8	Vertical Acceleration Effects	Ignore if farther than 50 km from fault. In lieu of a dynamic analysis use variations in: Col axial load = $(1+C_v) \cdot D_L$ axial force; superstructure bending moment (w/ or w/o structure); Shear = $(1+C_v) \cdot V(DL)$ Shear. See table 3.4.5-1 & table 3.4.5-2 for $C_v$ .		The effects of vertical ground motion are considered in the dead load factors in seismic load combinations: 1.2SD + EQ 0.8DD + EQ		For ordinary bridges include the effects of vertical ground acceleration when peak rock acceleration is greater than 0.6g as an equivalent vertical load of 7-25% of dead load on superstructure.	For ordinary bridges include the effects of vertical ground acceleration when peak rock acceleration is greater than 0.6g as an equivalent vertical load of 7-25% of dead load on superstructure.		
9	R-factor	Base Response Modification Factor, $R_B$ for substructures using SDAP D or E. Based on performance objective of the bridge, for MCE $R_B$ ranges from 1 to 6, and for EE from 0.9 to 1.3. See table 4.7-1 $R = 1 + (R_B - 1) \cdot \frac{T}{1.25T_c} = R_B$	Value ranges from 1.5 to 5 based on table 3.10.7.1-1	Value ranges from 2 to 5	Force Reduction Factor (equivalent to 1/R) applied to design horizontal seismic coefficient. $C_B = 1 / (2\mu - 1)$ ; $\mu =$ Allowable ductility ratio for component, RC Pier: $\mu = 1 + \frac{\delta_u - \delta_c}{\delta_c}$	Specified in terms of displacement ductility demand	Specified in terms of displacement ductility demand	Value ranges from 2 to 5	
10	Combination of orthogonal seismic forces	SRSS and 100%-40% rules	100%-30% rule	100%-30% rule		100%-30% rule	100%-30% rule	100%-30% rule	100%-30% rule

No.	Description	MCEER /ATC 49	AASHTO LRFD	Canada S-6.00	Japan 2002	Guide Steel Spec. + SDC	Caltrans SDC	AASHTO 17th ed. 2002	AASHTO Guide Spec.
11	Seismic Design and Analysis Procedures (SDAP) / Analysis	See (A1, A2, B, C, D, E) SDAP based on SHL and Importance Category see table 3.7.2; SDAP A1 & A2: No dynamic analysis needed; SDAP B: no seismic analysis needed but capacity design principles and min. design details needed for bridges requiring SDAP C; Capacity Spectra Method for regular bridges meeting 4.4.2 requirements; SDAP D: Elastic Response Spectrum Method; Uniform Load Method for bridges meeting Table 5.4.2.1-1 requirements, otherwise use Multi-mode Dynamic Response Method; SDAP E: Elastic Response Spectrum Method w/ Displacement Capacity Verification. <b>Where abutments resist lateral loads use SDAP D&amp;E</b>	Based on Seismic Zone and Importance Category one of the following methods of analysis should be used: UL = uniform load method SM = single mode spectral method MM = multimode spectral method TH = time-history method See table 4.7.4.3.1-1	Based on SPZ and Importance Category one of the following methods of analysis should be used: UL = uniform load method SM = single mode spectral method MM = multimode spectral method TH = time-history method See table 4.4.5.3.1	<b>Static Method:</b> Seismic Motion Level 1: seismic motion Level 2 Type I: use spectral table 6.4.1 & Seismic Motion Level 2 Type II: use spectral table 6.4.2. <b>Dynamic Methods:</b> 1) response spectrum method: Seismic Motion Level 1: spectra from table 4.3.1 & Seismic Motion Level 2 Type I: use spectral table 4.3.1 & Seismic Motion Level 2 Type II: use spectral table 4.3.2; 2) Time history analysis: adjust amplitude of past EQ to match the accelerations obtained from response spectra tables for the corresponding seismic motion. See table C.5.5.1 for the type of analysis required for different types of bridges.	Equivalent Static Analysis (ESA) using effective cross sectional properties; Elastic Dynamic Analysis (EDA); Inelastic Static Analysis (ISA)	Equivalent Static Analysis (ESA) for SPC A, for regular 2 to 6 span bridges with SPC B, C, D use ULM or SMSM; for not regular 2 to 6 span bridges with SPC B, C, D use MSM	No analysis needed for SPC A, for regular 2 to 6 span bridges with SPC B, C, D use ULM or SMSM; for not regular 2 to 6 span bridges with SPC B, C, D use MSM	Based on Seismic Design Category and 1.0 sec spectral acceleration, SDC A through D A site-specific procedure shall be used if any of the following apply: <ul style="list-style-type: none"> <li>• Soils at the site require site-specific evaluation (i.e., Site Class F soils, Article 3.4.2.1);</li> <li>• Unless a determination is made that the presence of such soils requires a significantly higher level of seismicity than that of the bridge.</li> <li>• The bridge is considered to be critical or essential according to Article 4.2.2, for which a higher degree of confidence of meeting the seismic performance objectives of Article 3.2 is desired.</li> <li>• The site is located within 6 miles of a major fault and its response could be significantly and adversely influenced by near-fault ground motion characteristics.</li> </ul>
12	Regular Bridge Requirements	bridges meeting Table 5.4.2.1-1 requirements	see table C4.7.4.3.1-1	Less than 7 spans. No abrupt or unusual changes in weight, stiffness, and geometry between adjacent spans. See table 4.4.5.3.2		Ordinary bridges see 1.1	Ordinary bridges see 1.1	see table 4.2.B	
13	Load Distribution	A viable load path shall be established based on stiffness of deck, girders, diaphragms. Continuous and clear load path is required. Welds designed as capacity-proceeded elements. Capacity effects to be considered.		Continuous and clear load path(s) required Full penetration welds at locations of inelastic deformation. Forces obtained from P-Delta analysis					
14	Damping	5% critical damping	5% critical damping	5% critical damping	5% critical damping	5% critical damping-10% w/ energy dissipators	5% critical damping	5% critical damping	5% critical damping- adjustment to 10% allowed



No.	Description	MCEER /ATC 49	AASHTO LRFD	Canada S-6-00	Japan 2002	Guide Steel Spec. + SDC	Caltrans SDC	AASHTO 17th ed. 2002	AASHTO Guide Spec.
Ref.	Description	Ref.	Description	Ref.	Description	Ref.	Description	Ref.	Description
17	Displacements	use cracked sectional properties	use cracked sectional properties	In modeling reinforced concrete sections, cracked cross-sectional properties shall be used when calculating the periods and force effects, while the effects of cracking shall be taken into account in calculating deflections.		use cracked sectional properties	use cracked sectional properties	from elastic analysis - no guidance	use cracked sectional properties
18	Bearings	SDR 1: Min horizontal design connection force in the restrained direction=0.10 (tributary permanent load and EQ live loads); SDR 2: Min horizontal design connection force in the restrained direction=0.25 (tributary permanent load and EQ live loads); SDR 3,4,5,6: Three alternatives: 1) Testing, 2) Positive restraint system to resist MCE, 3) Let bearings fail and displace-provide adequate seat	The criteria for seismic design is to minimize damage allow a certain degree of energy dissipation, movement, or plastic deformation in seismic load resisting system made of end connections, bearings and substructures. <b>Rigid Bearings</b> transmit seismic loads w/o movements. <b>Deformable Bearings</b> transmit limited loads by plastic deformation or restricted slippage-use this type when both superstructure and substructure are designed to support adjacent to bearing are	Connectors (bearings and shear keys) shall be designed to transmit in their restrained directions the maximum force effects determined from 1.25 x elastic seismic forces (R = 1.0), but these forces need not exceed the force that can be developed by the substructure element attaining 1.25 times its probable resistance.	122 <b>Type A:</b> Bearing with unseating prevention system to be designed for seismic motion level I - displacement stoppers to be designed to resist seismic motion level II, to be used for bridges on two abutments and on long spans. <b>Type B:</b> Self supporting bearings to be designed using forces from seismic motion level I & II. <b>Type C:</b> Bearings to be used in case of weak abutments. <b>Design forces:</b> Type B: force equal to lateral plastic strength of pier. Type A: forces from design seismic motion I for seismic motion I	For ordinary standard bridges bearings are considered sacrificial elements	For ordinary standard bridges bearings are considered sacrificial elements	Design for elastic forces or over-strength plastic hinging forces	
19	Shear Keys	For Zone 1 with A<0.025 and soil type I and II the connection force in the restrained direction shall not be less than 0.1 times vertical tributary dead load, for all other sites in Zone 1 use 0.05 times tributary dead load. Design for elastic forces or over-strength plastic hinging forces	Connectors (bearings and shear keys) shall be designed to transmit in their restrained directions the maximum force effects determined from 1.25 x elastic seismic forces (R = 1.0), but these forces need not exceed the force that can be developed by the substructure element attaining 1.25 times its probable resistance.	When supports have ample width to tolerate seismic displacements, shear keys may be designed as fuse elements in accordance with Article 7.8.4 of the SDC. When excessive seismic displacements must be prevented, shear keys shall be provided and designed as capacity-protection elements	7.8.4 Typically <b>Abutment shear keys</b> are expected to transmit the lateral shear forces generated by small earthquakes and service loads. The forces generated with elastic demand assessment models should not be used to size the abutment shear keys. Shear abutments shall be limited to the smaller of the following: 75% of lateral pile capacity or 30% of $F_{\text{axial}}$ abutments supported on spread footings are only designed to 0.3P <sub>axial}. <b>Column shear keys</b> shall be designed for the axial and shear forces</sub>				
20	Restraining Components	Friction not effective. Design for "A" (lighter adjoining spans)	Longitudinal Restrainers: Purpose: To ensure integrity movement without brittle failure, (lighter load of the two adjoining spans). Connection of the restrainer to be designed for 1.25* ultimate restrainer capacity	Excessive displacement stoppers to be designed for 3* (design seismic coefficient) dead load reaction not to exceed the ultimate strength	Hinge restrainers shall be designed as a secondary line of defense against unseating of girders in accordance with Article 7.2.6 of the SDC.	Hinge restrainers and shear keys needed to prevent excessive lateral movements. A satisfactory method of design requires a sufficient number of restrainers required at expansion joints is not currently available adequate seat shall be provided to prevent unseating as a primary requirement. Hinge restrainers are considered secondary members to			

No.	Description	MCEER /ATC 49	AASHTO LRFD	Canada S-6-00	Japan 2002	Guide Steel Spec. + SDC	Caltrans SDC	AASHTO 17th ed. 2002	AASHTO Guide Spec.	
Ref.	Description	Ref.	Description	Ref.	Description	Ref.	Description	Ref.	Description	
21	Min. seat width	11.6.5 n/A, 3.10	See Article 7.4.4	4.1.10 see 4.4, 10.5	10.2 Equation 10.2.1	See article 7.2.5.4		3.10 n/A, 3.10	All bridges shall meet the seat width requirements of SPC A&B: Max(6+0.02L+0.08'H); SPC C&D: Max(12+0.03L+0.12'H; 30.5+2.5'L+10'H)	
22	Hold-down Devices		In seismic performance zones 2, 3, and 4, where seismic forces are greater than 50% but less than 100% of the dead load reaction: - Design for 10% of dead load reaction, assuming simple span reaction, if seismic force results in net uplift, the hold-down device to be designed for the maximum of: a) 120% of the difference between vertical seismic force and dead load reaction b) 10% of dead load reaction as above	In seismic performance zones 2, 3, and 4, where uplift due to seismic forces is greater than 50% but less than 100% of the dead load reaction: - Design for 10% of dead load reaction, assuming simple span reaction, if seismic force results in net uplift, the hold-down device to be designed for the maximum of: a) 120% of the difference between vertical seismic force and dead load reaction b) 10% of dead load reaction as above				where uplift due to seismic forces is greater than 50% but less than 100% of the dead load reaction: - Design for 10% of dead load reaction, assuming simple span reaction, if seismic force results in net uplift, the hold-down device to be designed for the maximum of: a) 120% of the difference between vertical seismic force and dead load reaction b) 10% of dead load reaction as above	Abutment shear keys designed as sacrificial elements	
23	Abutments	8.5.3 11.6.5	Investigate the EQ effects using the extreme event limit state w/ resistance factor of 1.0 and an acceptable methodology (Mononobe Okabe); See 11.6.5	Seismically induced lateral soil pressures on the back of abutment and retaining walls shall be included in design, where appropriate. These pressures may be calculated by the Mononobe-Okabe method	Longitudinal direction: Ensure enough gap exist to avoid collision of superstructure with abutment at Seismic Motion Level 1. Verify that excessive strong force is not transmitted from Level 2, knock-off structure or absorption system may be used.	Longitudinal direction: Use effective abutment stiffness based on passive soil eq. 7.4.3, 4.4 & 4.5. For seat abutments backwall are designed to break off to protect foundation from inelastic action. Entire diaphragm above and below soffit is designed to engage the backfill. If diaphragm is not designed for backfill soil pressure, then the effective area of abutment is limited to the portion above soffit. Transverse direction: seat type abutments to resist moderate EQ loads elastically. Abutments should not be considered effective for MCE unless shown. Assume seat type abutments on piles and dense soil (ignoring wingwalls 40 kips/ft).	Longitudinal direction: Use effective abutment stiffness based on passive soil pressure eq. 7.4.3, 4.4 & 4.5. For seat abutments backwall are designed to break off to protect foundation from inelastic action. Entire diaphragm above and below soffit is designed to engage the backfill. If diaphragm is not designed for backfill soil pressure, then the effective area of abutment is limited to the portion above soffit. Transverse direction: seat type abutments to resist moderate EQ loads elastically. Abutments should not be considered effective for MCE unless shown. Assume seat type abutments on piles and dense soil (ignoring wingwalls 40 kips/ft).	7.8.1	Longitudinal direction: Use effective abutment stiffness based on passive soil pressure eq. 7.4.3, 4.4 & 4.5. For seat abutments backwall are designed to break off to protect foundation from inelastic action. Entire diaphragm above and below soffit is designed to engage the backfill. If diaphragm is not designed for backfill soil pressure, then the effective area of abutment is limited to the portion above soffit. Transverse direction: seat type abutments to resist moderate EQ loads elastically. Abutments should not be considered effective for MCE unless shown. Assume seat type abutments on piles and dense soil (ignoring wingwalls 40 kips/ft).	SPC A: No special seismic design requirements. Ensure vertical and lateral support to loads other than EQ. SPC B&C: Free-Standing Abutments: in case of sliding bearings use Mononobe Okabe for active soil pressure w/ K=0.5K <sub>1</sub> . For rigid acceleration, foundation should slide with it. Seismically induced soil pressures from wall inertia, and forces from bridge deck if on elastomeric bearings. If restrained from horizontal displ by means of anchors or batter piles, the magnitude of seismic soil pressures are higher than Mononobe Okabe, an appropriate use of K=0.5K <sub>1</sub> should be used. Design for maximum soil passive pressure being mobilized-usually is greater than the force from superstructure. SPC D: In addition to requirements for SPC C, consider longitudinal and transverse inertia forces to the abutment, soil-abutment interaction. To minimize potential loss of bridge access, use sacrificial elements for approach abutments. Settlement of approach slabs recommended.

# Chapter 2 PROPOSED SEISMIC PROVISIONS AND COMMENTARY

## **SECTION 6: STEEL STRUCTURES**

### PARTIAL TABLE OF CONTENTS – PROVISIONS FOR SEISMIC DESIGN

6.5.4.2 Resistance Factors.....	156
6.5.5 Extreme Event Limit State.....	156
6.13.2.1.2 Bearing-Type Connections.....	156
6.16 Provisions for Seismic Design.....	157
6.16.1 General.....	157
6.16.2 Materials.....	159
6.16.3 Design Requirements for Seismic Zone 1.....	159
6.16.4 Design Requirements for Seismic Zones 2, 3 or 4.....	160
6.16.4.1 General .....	160
6.16.4.2 Deck .....	161
6.16.4.3 Shear Connectors .....	162
6.16.4.4 Elastic Superstructures .....	164
6.16.4.5 Ductile Superstructures .....	165
6.16.4.5.1 Special Support Cross-Frames .....	165
6.16.4.5.1a Width-to-Thickness Ratio .....	167
6.16.4.5.1b Slenderness Ratio .....	167
6.16.4.5.1c Nominal Tensile and Compressive Resistance.....	168
6.16.4.5.1d Lateral Resistance.....	168
6.16.4.5.1e Double-Angle Compression Members.....	168
6.16.4.5.2 End Connections of Special Support Cross-Frame Members.....	169
6.16.4.4.2a Axial Resistance of the End Connections .....	169
6.16.4.4.2b Flexural Resistance of the End Connections.....	170
REFERENCES.....	170

**6.5.4.2–Resistance Factors**

- For shear connectors in tension  $\phi_{st} = 0.75$

**6.5.5–Extreme Event Limit State**

All applicable extreme event load combinations in Table 3.4.1-1 shall be investigated. For Extreme Event I,  $\gamma_p$  for DC and DW loads shall be taken to be 1.0.

All resistance factors for the extreme event limit state, except those specified for bolts and shear connectors, shall be taken to be 1.0.

All resistance factors for ASTM A 307 Grade C and ASTM F 1554 bolts used as anchor bolts for the extreme event limit state shall be taken to be 1.0.

~~Bolted joints not protected by capacity design or structural fuses may be assumed to behave as bearing-type connections at the extreme event limit state, and the values of resistance factors for bolts given in Article 6.5.4.2 shall apply.~~

The connections for a member that is part of a seismic load path shall be designed such that a ductile limit state in the member controls the design.

Bolted joints within a seismic load path shall be designed as bearing-type connections at the extreme event limit state, and the resistance factors for bolts specified in Article 6.5.4.2 shall apply. Standard holes or short-slotted holes normal to the line of force shall be used in such joints.

**C6.5.5**

During earthquake motion, there is the potential for full reversal of design load and inelastic deformations of members and/or connections. Therefore, slip of bolted joints located within a seismic load path cannot and need not be prevented. However, special consideration may be required for bolted joints in fracture critical members, as slip may affect their subsequent fatigue resistance. Close inspection of joints and connections in fracture critical members should be performed after a seismic event.

To prevent excessive deformations of bolted joints due to slip between the connected plies under earthquake motions, only standard holes or short-slotted holes normal to the line of force are permitted in bolted joints located within a seismic load path. For such holes, the upper limit of  $2.4dtF_u$  on the bearing resistance is intended to prevent elongations due to bearing deformations from exceeding approximately 0.25 in. It should be recognized, however, that the actual bearing load in a seismic event may be much larger than that anticipated in design and the actual deformation of the holes may be larger than this theoretical value. Nonetheless, the specified upper limit on the nominal bearing resistance should effectively minimize damage in moderate seismic events.

*6.13.2.1.2–Bearing-Type Connections*

Bearing-type connections shall be permitted only for joints subject to axial compression, joints within a seismic load path or joints on secondary members and shall satisfy the factored resistance,  $R_r$ , at the strength limit state specified in Article 6.13.2.2.

-----  
-----

-----  
-----

Insert the following Article 6.16 into Section 6 in its entirety.

## 6.16–PROVISIONS FOR SEISMIC DESIGN

### 6.16.1–General

The provisions of these Articles shall apply only to the design of steel-girder bridge superstructures at the extreme event limit state.

In addition to the requirements specified herein, minimum support length requirements specified in Article 4.7.4.4 shall also apply.

Bridges located in Seismic Zone 1 shall satisfy the requirements specified in Article 6.16.3. Bridges located in Seismic Zones 2, 3 or 4 shall satisfy the requirements specified in Article 6.16.4.

A clear seismic load path shall be established within the superstructure to transmit the inertia forces to the substructure based on the stiffness characteristics of the concrete deck, cross-frames or diaphragms, and bearings. The flow of the seismic forces shall be accommodated through all affected components and connections of the steel superstructure within the prescribed load path including, but not limited to, the longitudinal girders, cross-frames or diaphragms, steel-to-steel connections, deck-to-steel interface, bearings and anchor bolts.

### C6.16.1

These Specifications are based on the recent provisions published by NCHRP (2002, 2006), MCEER/ATC (2003), Caltrans (2006), and AISC (2005a and 2005b). The Loma Prieta earthquake of 1989, Petrolia earthquakes of 1992, Northridge earthquake of 1994, and Kobe earthquake of 1995 provided new insights into the behavior of steel details under seismic loads. The Federal Highway Administration, Caltrans, and the American Iron and Steel Institute initiated a number of research projects that have produced information that is useful for both the design of new steel-girder structures and the retrofitting of existing steel-girder structures.

This new information relates to all facets of seismic engineering, including design spectra, analytical techniques, and design details. Bridge designers working in Seismic Zones 2, 3 or 4 are encouraged to avail themselves of current research reports and other literature to augment these Specifications.

Steel-girder bridges are generally considered to perform well in earthquakes. However, the aforementioned earthquakes showed the vulnerability of steel-girder bridges to damage if they are not designed and detailed to resist the seismic motions (Roberts, 1992; Astaneh-Asl et al., 1994; Itani and Reno, 1995; Bruneau et al., 1996; Carden et al., 2005a). Typical damage included unseated longitudinal girders and failure of cross-frames and their connections, expansion joints and bearings. In a few cases, most notably during the Kobe earthquake, major gravity load-carrying members failed, triggered in some instances by the failure of components elsewhere in the superstructure. These earthquakes confirmed the vulnerability of steel-girder bridges during seismic events. New areas of concern that emerged included:

- Lack of understanding of the seismic load paths in steel-girder bridges;
- Damage to steel superstructure components; e.g. girders, shear connectors, end cross-frames, bearing stiffeners, bearings, and anchor bolts;
- Failure of steel substructures.

Seismic design specifications in the U.S. currently do not require the explicit design of bridge superstructures for seismic loads. The assumption is made that a superstructure that is designed for out-of-plane gravity load has sufficient strength, by default, to resist in-plane seismic loads. However, recent

earthquakes have shown the fallacy of this assumption and showed that a load path should be clearly defined, analyzed and designed for seismic loads.

Research on the seismic behavior of steel-girder bridge superstructures (Astaneh-Asl and Donikian, 1995; Itani, 1995; Dicleli and Bruneau, 1995a and 1995b; Itani and Rimal, 1996; Carden et al., 2005a and 2005b, Bahrami et al., 2009) further confirmed that seismically induced damage is likely in superstructures subjected to large earthquakes and that appropriate measures should be taken to ensure satisfactory seismic performance.

Limited research has been conducted on steel substructures and their connections to the superstructure. This lack of information makes the codification of seismic design provisions for steel substructures premature. It could be argued that a significant amount of the necessary information might be obtained from the seismic design provisions for steel building structures. However, the size of steel substructures and the general complexity of their details make it difficult to find the necessary parallels in building construction. Therefore, these specifications do not address the seismic design of steel substructures.

These specifications concentrate on the seismic design and detailing of steel-girder bridge superstructures. These types of superstructures have experienced moderate earthquakes and have been investigated analytically and experimentally in the aforementioned research. The common thread among these investigations was that these types of superstructures are vulnerable during earthquakes if they are not designed and detailed to resist the resulting seismic forces. A continuous and clearly defined load path is necessary for the transmission of the superstructure inertia forces to the substructure.

### 6.16.2–Materials

Structural steels used within the seismic load path shall meet the requirements of Article 6.4.1, except as modified herein.

Where a member or connection is protected by capacity design, the required nominal resistance of the member or connection shall be determined based on the expected yield strength,  $R_y F_y$ , of the adjoining member(s), where  $F_y$  is the specified minimum yield strength of the steel used in the adjoining member(s) and  $R_y$  is the ratio of the expected yield strength to the specified minimum yield strength. For AASHTO M 270M/M270 (ASTM A709/A709M) Grade 36,  $R_y$  shall be taken equal to 1.5. For AASHTO M 270M/M270 (ASTM A709/A709M) Grades 50 and 50W,  $R_y$  shall be taken equal to 1.1.

### 6.16.3–Design Requirements for Seismic Zone 1

For steel-girder bridges located in Seismic Zone 1, defined as specified in Article 3.10.6, no consideration of seismic forces shall be required for the design of the superstructure components, except that the design of the connections of the concrete deck to the girder at all support cross-frame or diaphragm locations, the connections of all support cross-frame or diaphragm members, and the connections of the superstructure to the substructure shall satisfy the minimum requirements specified in Articles 3.10.9 and 4.7.4.4.

### C6.16.2

Previous earthquakes have shown that cross-frames at support locations transfer the inertia forces of the superstructure to the substructure. Therefore, the connections of the diagonal cross-frame members must be protected during seismic events. This is achieved by utilizing a capacity-design methodology in which the cross-frame connections are designed based on the expected nominal resistance of the diagonal members. This methodology serves to confine the ductility demand to the members that have the available excess resistance to ensure ductile behavior. In the capacity-design methodology, all the components surrounding the nonlinear element are designed based on the maximum expected nominal resistance of that element. The capacity-design methodology requires a realistic estimate of the expected nominal resistance of the designated yielded members. To this end, the expected yield strength of various steel materials has been established through a survey of mill test reports and ratios of the expected to nominal yield strength,  $R_y$ , have been provided elsewhere (AISC, 2005b) and are adopted herein. The expected resistance of the designated member is therefore to be determined based on the expected yield strength,  $R_y F_y$ , which amplifies the nominal resistance to account for the effect of strain-hardening if the member is expected to undergo nonlinear response.

### C6.16.3

These requirements for Zone 1 are to ensure a clear load path for seismic forces.

## **6.16.4—Design Requirements for Seismic Zones 2, 3 or 4**

### **6.16.4.1—General**

Where base isolation is not utilized, steel-girder bridges located in Seismic Zones 2, 3 or 4, defined as specified in Article 3.10.6, shall be classified into one of the following two categories for seismic design:

- An elastic superstructure with a ductile substructure.
- A ductile superstructure with an essentially elastic substructure.

Provisions for the first category are specified in Article 6.16.4.4. Provisions for the second category are specified in Article 6.16.4.5. Only rolled or fabricated steel I-girder bridges with a composite reinforced concrete deck slab and special support cross-frames that are designed as specified in Article 6.16.4.5.1 shall be permitted in the second category. For bridges in either category, the deck and shear connectors shall satisfy the provisions of Articles 6.16.4.2 and 6.16.4.3, respectively. Support cross-frame members in either category shall be considered primary members for seismic design.

Structural analysis for seismic loads shall consider the relative stiffness of the concrete deck, girders, support cross-frames or diaphragms, and the substructure.

### **C6.16.4.1**

The implied seismic performance criterion for steel-girder bridges located in Seismic Zones 2, 3 or 4 is to provide an elastic superstructure in combination with a ductile substructure. In such cases, the support cross-frames are designed to transfer the seismic forces elastically and the inelasticity is limited to the concrete substructure, which is typically designed according to the provisions of Article 5.10.11. As used herein, an elastic component is one in which the demand-to-nominal capacity ratio is less than 1.5.

Previous earthquakes have demonstrated that inelastic activity at support cross-frames in some steel I-girder bridge superstructures has reduced the seismic demand on the substructure (Roberts, 1992; Astaneh-Asl and Donikian, 1995). This phenomenon has been investigated both analytically and experimentally by several researchers (Astaneh-Asl and Donikian, 1995; Itani and Reno, 1995; Itani and Rimal, 1996; Zahrai and Bruneau, 1998, 1999a and 1999b; Carden et al., 2005a and 2005b; Bahrami et al., 2009). Based on these investigations, it was concluded that the provision of a ductile superstructure, in which the diagonal members of the support cross-frames are permitted to undergo controlled inelastic activity, dissipates the input seismic energy limiting the seismic forces on the substructure; thereby providing an acceptable alternative strategy for the seismic design of rolled or fabricated steel I-girder bridges utilizing cross-frames at supports.

Note that providing an essentially elastic superstructure and substructure by utilizing response modification devices such as base isolation may also be a viable alternative strategy for designing steel-girder bridges in these seismic zones.

The design requirements for bridges located in Seismic Zone 2 have been included herein with the requirements for bridges located in Seismic Zones 3 and 4. Bridges located in Seismic Zone 2 have a reasonable probability of being subjected to significant seismic forces because the upper boundary for this zone in the current edition of the specifications is significantly higher than in previous editions due to the increase in the return period for the design earthquake from 500 to 1000 years.

In horizontally curved and/or skewed steel bridges, cross-frame forces due to gravity loads may govern over seismic loads depending on boundary conditions at abutments, pier flexibility, and degree of curvature and/or skew.

### 6.16.4.2–Deck

Reinforced concrete decks attached by shear connectors satisfying the requirements of Article 6.16.4.3 shall be designed to provide horizontal diaphragm action to transfer seismic forces to the supports as specified herein.

Where the deck has a span-to-width ratio of 3.0 or less, and the net mid-span lateral seismic displacement of the superstructure is less than twice the average of the adjacent lateral seismic support displacements, the deck within that span may be assumed to act as a rigid horizontal diaphragm designed to resist only the shear resulting from the seismic forces. Otherwise, the deck shall be assumed to act as a flexible horizontal diaphragm designed to resist shear and bending, as applicable, resulting from the seismic forces.

For an elastic superstructure, the total transverse seismic shear force on the deck,  $F_{px}$ , within the span under consideration shall be determined as:

$$F_{px} = \frac{W_{px}}{W} F \quad (6.16.4.2-1)$$

in which:

$$0.2S_{DS}W_{px} \leq F_{px} \leq 0.4S_{DS}W_{px} \quad (6.16.4.2-2)$$

where:

$F$  = total of the transverse base shears, as applicable, at the supports in the span under consideration (kip)

$S_{DS}$  = horizontal response spectral acceleration coefficient at 0.2-sec. period modified by the short-period site factor, determined as specified in Article 3.10.4.2

$W$  = total weight of the deck and steel girders within the span under consideration (kip)

$W_{px}$  = weight of the deck plus one-half the weight of the steel girders in the span under consideration (kip)

For a ductile superstructure, the total transverse seismic shear force on the deck,  $F_{px}$ , within the span under consideration shall be determined as:

### C6.16.4.2

In general, reinforced concrete decks on steel-girder bridges with adequate stud connectors have sufficient rigidity in their horizontal plane that their response approaches rigid-body motion. Therefore, the deck can provide a horizontal diaphragm action to transfer seismic forces to support cross-frames or diaphragms. The seismic forces are collected at the support cross-frames or diaphragms and transferred to the substructure through the bearings and anchor bolts. Thus, the support cross-frames or diaphragms must be designed for the resulting seismic forces. The lateral loading of the intermediate cross-frames in-between the support locations for straight bridges is minimal in this case, consisting primarily of the local tributary inertia forces from the girders. Adequate stud connectors are required to ensure the necessary diaphragm action as previous earthquake reconnaissance showed that for some bridges in California in which the shear connectors at support locations were damaged during a seismic event, the deck in fact slid on the top of the steel girders (Roberts, 1992; Carden et al., 2005a).

During a seismic event, inertia forces generated by the mass of the deck must be transferred to the support cross-frames or diaphragms. The seismic forces are transferred through longitudinal and transverse shear forces and axial forces.

$F_{px}$  in Eqs. 6.16.4.2-1 and 6.16.4.2-3 represents the total transverse seismic shear force that the deck is subjected to within a particular span. At skewed supports,  $F_{px}$  is taken as the sum of the components of the transverse and longitudinal base shears parallel to the skew as shown in Figure C6.16.4.2-1.

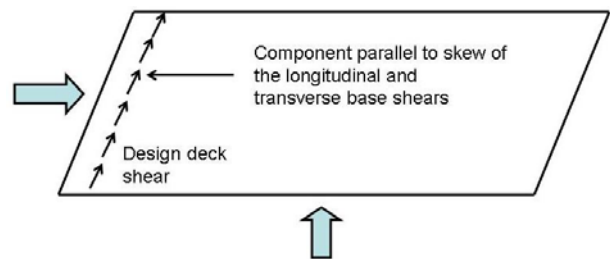


**Figure C6.16.4.2-1–Design Deck Shear,  $F_{px}$ , at Skewed Supports**

In cases where the deck may be idealized as a rigid horizontal diaphragm,  $F_{px}$  is distributed to the supports based on their relative stiffnesses. In cases where the

$$F_{px} = \frac{W_{px}}{W} F_{lat} \quad (6.16.4.2-3)$$

where:

$F_{lat}$  = total lateral resistance of the special support cross-frames in the span under consideration determined as specified in Article 6.16.4.5.1d (kip)

The limits given by Eq. 6.16.4.2-2 shall not apply in the case of a ductile superstructure.

#### 6.16.4.3–Shear Connectors

Stud shear connectors shall be provided along the interface between the deck and the steel girders, and along the interface between the deck and the top of the support cross-frames or diaphragms, to transfer the seismic forces.

The shear connectors on the girders assumed effective at the support under consideration shall be taken as those spaced no further than  $9t_w$  on each side of the outer projecting element of the bearing stiffeners at that support. In the case of a ductile superstructure, either no shear connectors, or at most one shear connector per row, shall be provided on the girders at the supports.

Shear connectors on support cross-frames or diaphragms shall be placed within the center two-thirds of the top chord of the cross-frame or top flange of the diaphragm. The diameter of the shear connectors within this region shall not be greater than 2.5 times the thickness of the top chord of the cross-frame or top flange of the diaphragm.

At support locations, shear connectors on the girders, as applicable, and on the support cross-frames or diaphragms shall be designed for ultimate strength to resist the combination of seismic shear and axial forces. The seismic shear demand shall be taken as the governing orthogonal combination of seismic shears at the support under consideration.

For ductile superstructures, the seismic shears and axial forces shall be scaled by the following factor:

$$\Omega = \frac{V_{lat}}{V} \quad (6.16.4.3-1)$$

deck must be idealized as a flexible horizontal diaphragm,  $F_{px}$  is distributed to the supports based on their respective tributary areas. Decks idealized as rigid diaphragms need only be designed for shear. Decks idealized as flexible diaphragms must be designed for both shear and bending as maximum in-plane deflections of the deck under lateral loads in this case are more than twice the average of the lateral deflections at adjacent support locations. Concrete decks may be designed for shear and bending moments based on strut and tie models (STM), as defined in Article 5.6.3.

The upper and lower bounds on the total seismic shear force on the deck,  $F_{px}$ , in an elastic superstructure given in Eq. 6.16.4.2-2 are based on the 2006 International Building Code (IBC, 2006).

In cases where the deck cannot provide horizontal diaphragm action, the Engineer should consider providing lateral bracing to serve as a horizontal diaphragm to transfer the seismic forces.

#### C6.16.4.3

Stud shear connectors play a significant role in transferring the seismic forces from the deck to the support cross-frames or diaphragms. These seismic forces are transferred to the substructure at support locations. Thus, the shear connectors at support locations are subjected to the largest seismic forces. Failure of these shear connectors will cause the deck to slip on the top flange of the girder, and thus, alter the seismic load path (Caltrans, 2001; Carden et al., 2005a, Bahrami et al., 2009).

The shear center of composite steel-girder superstructures is located above the deck. Therefore, during a seismic event, the superstructure will be subjected to torsional moments along the longitudinal axis of the bridge that produce axial forces on the shear connectors in addition to the longitudinal and transverse shears. In the case of a ductile superstructure, buckling and yielding of the special support cross-frame diagonals resulting from the lateral deformations during a seismic event produces double curvature in the top chord of the cross-frame creating axial forces in the shear connectors on that member that must be considered. Experimental and analytical investigations (Carden et al., 2004; Bahrami et al., 2009) showed that the seismic demand on shear connectors that are placed only on the girders at support locations will cause significant damage to the connectors and the deck. Improved cyclic behavior can be achieved by instead placing the shear connectors along the central two-thirds of the top chord of the support cross-frames. It was shown experimentally that this detail minimizes the axial forces on the shear connectors thus improving their cyclic response.

In order to reduce the moment transfer at the steel

where:

$V_{lat}$  = total lateral resistance of the special support cross-frames at the support under consideration determined as specified in Article 6.16.4.5.1d (kip)

$V$  = seismic base shear at the support under consideration obtained from a modal response spectrum analysis (kip)

The ultimate strength of stud shear connectors subject to combined shear and axial forces shall be evaluated according to the tension-shear interaction equation given as follows:

$$\left(\frac{N_u}{N_r}\right)^{5/3} + \left(\frac{Q_u}{Q_r}\right)^{5/3} \leq 1.0 \quad (6.16.4.3-2)$$

in which:

$N_r$  = factored tensile resistance of a single stud shear connector (kip)

$$= \phi_{st} N_n \quad (6.16.4.3-3)$$

$N_n$  = nominal tensile resistance of a single stud shear connector (kip)

$$= \frac{A_{nc}}{A_{nco}} N_b \leq A_{sc} F_u \quad (6.16.4.3-4)$$

$A_{nc}$  = projected area of concrete failure for a single stud shear connector based on the concrete breakout resistance in tension (in.<sup>2</sup>)

$$= 9h_{eff}^2 \quad (6.16.4.3-5)$$

$N_b$  = concrete breakout resistance in tension of a single stud shear connector in cracked concrete (kip)

$$= 0.76\sqrt{f'_c} h_{eff}^{1.5} \quad (6.16.4.3-6)$$

where:

$\phi_{st}$  = resistance factor for shear connectors in tension specified in Article 6.5.4.2

$A_{nc}$  = projected area of concrete for a single stud shear connector or group of connectors approximated from the base of a rectilinear geometric figure

girder-deck joint in a ductile superstructure, it is recommended that either no shear connectors, or at most one shear connector per row, be provided on the steel girder at the supports. Thus, in the case of a ductile superstructure, all or most of the shear connectors should be placed on the top chord of the special support cross-frames within the specified region.

For ductile superstructures, the factor,  $\Omega$ , insures that the shear connectors are designed according to a capacity-design philosophy to maintain integrity of the bridge during a seismic event.

Mouras et al, 2008 investigated the effect of haunches in decks, stud length, number of studs and arrangement of studs on the vertical resistance of stud shear connectors. Based on this investigation, the tension-shear interaction equation for stud shear connectors given by Eq. 6.16.4.3-2 was recommended for inclusion in ACI Appendix D (ACI 2005). Experimental investigation by Bahrami et al., (2009) showed that this equation may be used to satisfactorily determine the ultimate strength of stud shear connectors under the combined loading effects.

For the seismic design of continuous composite spans, shear connectors should be provided throughout the length of the bridge. Should shear connectors be omitted in regions of negative flexure, positive attachment of the deck to the support cross-frames or diaphragms located at interior piers must still be provided. Analytical investigation (Carden et al., 2004) showed that a lack of shear connectors in regions of negative flexure caused the seismic forces to be transferred into the steel girders at points of permanent load contraflexure, causing large weak-axis bending stresses in the girders. In addition, the intermediate cross frames were subjected to large seismic forces, while the support cross-frames were subjected to smaller forces. This indicated that the seismic load path had been significantly altered.

that results from projecting the failure surface outward  $1.5h_{eff}$  from the centerline of the single connector, or in the case of a group of connectors, from a line through a row of adjacent connectors (in.<sup>2</sup>)

$A_{sc}$  = cross-sectional area of a stud shear connector (in.<sup>2</sup>)

$F_u$  = specified minimum tensile strength of a stud shear connector determined as specified in Article 6.4.4 (ksi)

$h_{eff}$  = effective embedment depth of a stud shear connector (in.)

$N_u$  = seismic axial force demand per stud at the support cross-frame or diaphragm location under consideration (kip)

$Q_u$  = seismic shear demand per stud at the support cross-frame or diaphragm location under consideration due to the governing orthogonal combination of seismic shears (kip)

$Q_r$  = factored shear resistance of a single stud shear connector determined as specified in Article 6.10.10.4.1 (kip)

#### 6.16.4.4—Elastic Superstructures

For an elastic superstructure, support cross-frame members or support diaphragms shall be designed according to the applicable provisions of Articles 6.7, 6.8 and/or 6.9 to remain elastic during a seismic event.

The lateral force for the design of the support cross-frame members or support diaphragms shall be determined based on the lesser of:

- The governing orthogonal force combination obtained from a linear elastic seismic analysis;

and:

- At a pier, the force,  $V_{po}$ , corresponding to plastic hinging of the substructure as specified in Article 3.10.9.4.3, including an overstrength factor,  $\lambda_{mo}$ ;

or:

- At an abutment, the force,  $V_{as}$ , corresponding to the lateral resistance of shear keys, including an overstrength factor,  $\lambda_{mo}$ .

#### C6.16.4.4

To achieve an elastic superstructure, the various components of the support cross-frames or the support diaphragms, as applicable, must be designed to remain elastic under the forces that are generated during the design earthquake according to the applicable provisions of Articles 6.7, 6.8 and/or 6.9. No other special seismic requirements are specified for these members in this case.

The overstrength factor,  $\lambda_{mo}$ , accounts for material strength variations between adjacent members, and column moment capacities greater than idealized plastic moment capacities.

The overstrength factor,  $\lambda_{mo}$ , shall be taken equal to 1.2 and 1.4 for ASTM A706 and ASTM A615 grade 60 reinforcement, respectively.

#### 6.16.4.5–Ductile Superstructures

For a ductile superstructure, special support cross-frames, designed as specified in Article 6.16.4.5.1, shall be provided at all supports.

The response modification factor,  $R$ , to be considered in the design of the special support cross-frame members shall be taken as specified in Table 6.16.4.5-1.

**Table 6.16.4.5-1–Response Modification Factors for Special Support Cross-Frames and Drift Limits for Ductile Superstructures**

Special Support Cross-Frames	Importance Category		
	Critical	Essential	Other
$R$	1.5	2.0	3.0
Superstructure Drift Limit	Critical	Essential	Other
$\Delta$	1%	2%	4%

Drift shall be calculated as the ratio of the relative lateral displacement of the girder flanges to the total depth of the steel girder, and shall not exceed the applicable drift limit specified in Table 6.16.4.5-1. For ductile superstructures, the calculated drift shall be multiplied by the scale factor,  $\Omega$ , determined from Eq. 6.16.4.3-1.

##### 6.16.4.5.1–Special Support Cross-Frames

Special support cross-frames shall consist of top and bottom chords and diagonal members. The diagonal members shall be configured either in an X-type or an inverted V-type configuration. Only single angles or double angles with welded end connections shall be permitted for use as members of special support cross-frames.

In an X-type configuration, diagonal members shall be connected where the members cross by welds. The welded connection at that point shall have a nominal resistance equal to at least 0.25 times the nominal tensile resistance of the diagonal member determined as specified in Article 6.16.4.5.1c.

In an inverted V-type configuration, the top chord and the concrete deck at the location where the

#### C6.16.4.5

A ductile superstructure with an essentially elastic substructure may be used as an alternative to an elastic superstructure in combination with a ductile substructure. Ductile superstructures must be specially designed and detailed to dissipate seismic energy. In ductile superstructures, special support cross-frames are provided and must be detailed and designed to undergo significant inelastic activity and dissipate the seismic input energy without premature failure or strength degradation. This concept has been analytically and experimentally validated using subassembly and shake table experiments.

Ideally ductile superstructures have shown the most effectiveness when utilized in conjunction with stiff substructures. Flexible substructures will attract smaller seismic forces, and thus, the special support cross-frames will also be subjected to smaller seismic forces and will be less effective (Alfawakhiri and Bruneau, 2001). Bridge dynamic analyses conducted according to the provisions of Article 4.7.4 can provide insight on the effectiveness of special support cross-frames utilized in conjunction with flexible substructures.

##### C6.16.4.5.1

Concentric support cross-frames are those in which the centerlines of members intersect at a point to form a truss system that resists lateral loads. Concentric configurations that are permitted for special support cross-frames in ductile superstructures are X-type and inverted V-type configurations. The use of tension-only bracing in any configuration is not permitted. V-type configurations and solid diaphragms are also not permitted. Members other than single-angle or double-angle members are not permitted, as other types of members have not yet been studied for potential use in special support cross-frames.

The required resistance of the welded connection at the point where the diagonals cross in X-type configurations is intended to permit the unbraced length

diagonals intersect shall be designed to resist the vertical component of the difference between the nominal tensile resistance of the diagonal member taken equal to  $R_y P_{ny}$  and the absolute value of the nominal post-buckling compressive resistance of the diagonal member taken equal to  $0.3P_n$ , where  $R_y$  is taken as specified in Article 6.16.2,  $P_{ny}$  is determined as specified in Article 6.8.2 and  $P_n$  is determined as specified in Article 6.9.4.1.

In both configurations, the top chord shall be designed for the an axial force taken as the larger of the elastic seismic force divided by the appropriate response modification factor specified in Table 6.16.4.5-1, or the horizontal component of the nominal tensile resistance of the diagonal member taken as  $R_y P_{ny} \cos \theta$ .  $\theta$  is the angle of inclination of the diagonal member with respect to the horizontal.

Members of special support cross frames in either configuration shall satisfy the requirements specified in Articles 6.16.4.5.1a through 6.16.4.5.1e. The end connections of the special support cross-frame members shall satisfy the requirements specified in Article 6.16.4.5.2.

for determining the compressive buckling resistance of the member to be taken as half of the full length (Goel and El-Tayem, 1986; Itani and Goel, 1991; Carden et al., 2005a and 2005b, Bahrami et al., 2009).

Inverted V-type configurations exhibit a special problem that sets them apart from X-type configurations. Under lateral displacement after the compression diagonal buckles, the top chord of the cross-frame and the concrete deck will be subjected to a vertical unbalanced force. This force will continue to increase until the tension diagonal starts to yield. This unbalanced force is equal to the vertical component of the difference between the nominal tensile resistance of the diagonal member and the absolute value of  $0.3P_n$ .  $0.3P_n$  is taken as the nominal post-buckling compressive resistance of the member.

During a moderate to severe earthquake, special support cross-frames and their end connections are expected to undergo significant inelastic cyclic deformations into the post-buckling range. As a result, reversed cyclic rotations occur at plastic hinges in much the same way as they do in beams. During severe earthquakes, special support cross-frames are expected to undergo 10 to 20 times the yield deformation. In order to survive such large cyclic deformations without premature failure, the elements of special support cross-frames and their connections must be properly designed (Zahrai and Bruneau, 1999a and 1999b; Zahrai and Bruneau, 1998; Carden et al., 2006, Bahrami et al., 2009).

The requirements for the seismic design of special support cross-frames are based on the seismic requirements for Special Concentric Braced Frames (SCBFs) given in AISC (2005b). These requirements are mainly based on sections and member lengths that are more suitable for building construction. However, Carden et al. (2006) and Bahrami et al., (2009) tested more typical sections and member lengths utilized in bridge construction and verified that the AISC seismic provisions for SCBFs can be used for the seismic design of special support cross-frames. These studies, in addition to other analytical and experimental investigations conducted by numerous researchers, have identified three key parameters that affect the ductility of cross-frame members:

- Width-to-thickness ratio;
- Slenderness ratio; and
- End conditions.

During earthquake motions, the cross-frame member will be subjected to cyclic inelastic deformations. The plot of the axial force versus the axial deformation of the inelastic member is often termed a hysteresis loop. The characterization of these loops is highly dependent on the aforementioned parameters. Satisfaction of the

requirements related to these parameters specified in Articles 6.16.4.5.1a through 6.16.4.5.1e will help to ensure that the diagonal members of special support cross-frames can undergo large inelastic cyclic deformations without premature fracture and strength degradation when subjected to the design seismic forces.

*6.16.4.5.1a–Width-to-Thickness Ratio*

Members of special support cross-frames shall satisfy the following ratio:

$$\frac{b}{t} \leq 0.3 \sqrt{\frac{E}{F_y}} \quad (6.16.4.5.1a-1)$$

where:

$b$  = full width of the outstanding leg of the angle (in.)

$t$  = thickness of the outstanding leg (in.)

*6.16.4.5.1b–Slenderness Ratio*

Members of special support cross-frames shall satisfy the following ratio:

$$\frac{K\ell}{r} \leq 4.0 \sqrt{\frac{E}{F_y}} \quad (6.16.4.5.1b-1)$$

where:

$K$  = effective length factor in the plane of buckling = 0.85

$\ell$  = unbraced length (in.). For members in an X-type configuration,  $\ell$  shall be taken as one-half the length of the diagonal member.

$r$  = radius of gyration about the axis normal to the plane of buckling (in.)

*C6.16.4.5.1a*

Traditionally, diagonal cross-frame members have shown little or no ductility during a seismic event after overall member buckling, which produces plastic hinges at the mid-point of the member and at its two ends. At a plastic hinge, local buckling can cause large strains, leading to fracture at small deformations. It has been found that diagonal cross-frame members with ultra-compact elements are capable of achieving significantly more ductility by forestalling local buckling (Astaneh-Asl et al., 1985, Goel and El-Tayem, 1986). Therefore, width-to-thickness ratios of outstanding legs of special support angle cross-frame members are set herein to not exceed the requirements for ultra-compact elements taken from AISC (2005b) in order to minimize the detrimental effect of local buckling and subsequent fracture during repeated inelastic cycles.

*C6.16.4.5.1b*

The hysteresis loops for special support cross-frames with different slenderness ratios vary significantly. The area enclosed by these loops is a measure of that component's energy dissipation capacity. Loop areas are greater for a stocky member than for a slender member; hence, the slenderness ratio of diagonal members in special support cross-frames subject to compression is limited accordingly herein to the requirement for stocky members in SCBFs given in AISC (2005b).

*6.16.4.5.1c–Nominal Tensile and Compressive Resistance*

The nominal tensile resistance of diagonal members of special support cross-frames shall be taken as  $R_y P_{ny}$  where  $R_y$  is taken as specified in Article 6.16.2 and  $P_{ny}$  is determined as specified in Article 6.8.2.

The nominal compressive resistance of diagonal members of special support cross-frames shall be taken as  $P_n$ , where  $P_n$  is determined as specified in Article 6.9.4.1.

*6.16.4.5.1d–Lateral Resistance*

The lateral resistance a special support cross-frame in a single bay between two girders shall be taken as the sum of the following:

- The sum of the horizontal components of the nominal resistances of the tension and compression diagonal members taken as  $(R_y P_{ny} + 0.3 P_n) \cos \theta$ , where  $R_y$  is taken as specified in Article 6.16.2,  $P_{ny}$  is determined as specified in Article 6.8.2,  $P_n$  is determined as specified in Article 6.16.4.5.1c and  $\theta$  is the angle of inclination of the diagonal member with respect to the horizontal;
- The sum of the shear contributions due to bending of the top and bottom chord members. The shear contribution of each chord member shall be taken as  $2R_y M_p / h$ , where  $R_y$  is taken as specified in Article 6.16.2,  $M_p$  is the plastic moment of the chord member under consideration and  $h$  is taken as the vertical distance between the centerline of the bearing and the centerline of the chord member under consideration.

*6.16.4.5.1e–Double-Angle Compression Members*

Double angles used as diagonal compression members in special support cross-frames shall be interconnected by welded stitches. The spacing of the stitches shall be such that the slenderness ratio,  $\ell/r$ , of the individual angle elements between the stitches does not exceed 0.4 times the governing slenderness ratio of the member. Where buckling of the member about its

*C6.16.4.5.1c*

Since diagonal members of special support cross-frames are designed to act as “fuses” during seismic events to dissipate the input energy, the nominal tensile and compressive resistances of the resistance of the members must not be taken less than the nominal resistances determined using an actual expected yield stress,  $R_y F_y$ , which is taken to be larger than the specified nominal yield stress,  $F_y$  (AISC, 2005b).

*C6.16.4.5.1d*

The lateral resistance of special support cross-frames is based on the contribution of the diagonal members and the top and bottom chords.

*C6.16.4.5.1e*

More stringent spacing and resistance requirements are specified for stitches in double-angle diagonal members used in special support cross-frames than for conventional built-up members subject to compression (Aslani and Goel, 1991). These requirements are indented to restrict individual element buckling between the stitch points and consequent premature fracture of

critical buckling axis does not cause shear in the stitches, the spacing of the stitches shall be such that the slenderness ratio,  $\ell/r$ , of the individual angle elements between the stitches does not exceed 0.75 times the governing slenderness ratio of the member. The sum of the nominal shear resistances of the stitches shall not be less than the nominal tensile resistance of each individual angle element.

The spacing of the stitches shall be uniform. No less than two stitches shall be used per member.

#### *6.16.4.5.2–End Connections of Special Support Cross-Frame Members*

End connections of special support cross-frame members shall be welded to a gusset plate. The gusset plate may be bolted or welded to the bearing stiffener. The gusset plate and gusset plate connection shall be designed to resist a vertical shear taken equal to  $1.1R_yP_{ny}\sin\theta$  acting in combination with a moment taken equal to the design shear times the horizontal distance from the working point of the connection to the centroid of the bolt group or weld configuration, where  $R_y$  is taken as specified in Article 6.16.2,  $P_{ny}$  is determined as specified in Article 6.8.2 and  $\theta$  is the angle of inclination of the diagonal member with respect to the horizontal. The end connections of the special support cross-frame members shall satisfy the requirements of Articles 6.16.4.5.2a and 6.16.4.5.2b.

#### *6.16.4.5.2a–Axial Resistance of the End Connections*

The axial resistance of the end connections of special support cross-frame diagonal members subject to tension or compression shall not be taken less than  $1.1R_yP_{ny}$ , where  $R_y$  is taken as specified in Article 6.16.2 and  $P_{ny}$  is determined as specified in Article 6.8.2.

The axial resistance of the end connections of special support cross-frame top chord members subject to tension or compression shall not be taken less than  $1.1R_yP_{ny}\cos\theta$ , where  $\theta$  is the angle of inclination of the diagonal member with respect to the horizontal.

#### *6.16.4.5.2b–Flexural Resistance of the End*

these members during a seismic event.

#### *C.6.16.4.5.2*

Due to the size of the gusset plate and its attachment to the bearing stiffener in typical support cross-frames, the diagonal members tend to buckle in the plane of the gusset (Astaneh-Asl et al., 1985; Carden et al., 2004, Bahrami et al., 2009). During a seismic event, plastic hinges in special support cross-frames are expected at the ends of the diagonal members next to the gusset plate locations. It has been found experimentally (Itani et al., 1991; Carden et al., 2004, Bahrami et al., 2009) that bolted end connections of special support cross-frame diagonal members may suffer premature fracture at bolt-hole locations if the ratio of net to gross area,  $A_n/A_g$ , of the member at the connection is less than 0.85. Therefore, the use of welded end connections is conservatively required for special support cross-frame members in order to ensure ductile behavior during a seismic event.

The welded end connections of the diagonal members are to be designed as a minimum for the full axial and flexural yield resistance of the member based on the expected yield strength,  $R_yF_y$ . The resistances are each conservatively increased by 10 percent in Articles 6.16.4.5.2a and 6.16.4.5.2b to help ensure that a ductile limit state in the member controls the design.

#### *C6.16.4.5.2a*

The specified axial resistance of the end connections of special support cross-frame members ensures that the connections are protected by capacity design; that is, that the member is the weaker link.

#### *C6.16.4.5.2b*

### Connections

The flexural resistance of the end connections of special support cross-frame diagonal members shall not be taken less than  $1.1R_yF_yZ$ , where  $R_y$  is taken as specified in Article 6.16.2 and  $Z$  is the plastic section modulus of the diagonal member about the axis of bending.

The specified flexural resistance of the end connections of special support cross-frame diagonal members ensures that the connections are protected by capacity design.

## REFERENCES

### (TO BE ADDED TO THE SECTION 6 REFERENCE LIST)

American Concrete Institute (ACI), 2005, "Building Code Requirements for Structural Concrete (ACI 318-05)," ACI, Farmington Hills, MI.

AISC. 2005a. "Specifications for Structural Steel Buildings," American Institute of Steel Construction, Chicago, IL.

AISC. 2005b. "Seismic Provisions for Structural Steel Buildings," American Institute of Steel Construction, Chicago, IL.

Alfawakhiri, F., and M. Bruneau. 2001. "Local Versus Global Ductility Demands in Simple Bridges," *Journal of Structural Engineering*, American Society of Civil Engineers, Reston, VA.

Aslani, F., and Goel, S.C. 1991. "An Analytical Criteria for Buckling Strength of Built-Up Compression Members," *Engineering Journal*, AISC, 28 (4):159-68.

Astaneh-Asl, A., Bolt, B., McMullin, K.M., Donikian, R., Modjtahedi, D., and Cho, S. 1994. "Seismic Performance of Steel Bridges During the 1994 Northridge Earthquake," *Report UCB/CESTEEL-94/01*, Department of Civil Engineering, University of California at Berkeley, Berkeley, CA.

Astaneh-Asl, A., Goel, S.C. and Hanson, R.D., 1985, "Cyclic Out-of-Plane Buckling of Double Angle Bracing," *Report UCB/CE-STEEL-94/01*. Department of Civil Engineering, University of California at Berkeley, Berkeley, CA

Astaneh-Asl, A., and Donikian, R. 1995. "Seismic Behavior and Design of Steel Bridges, Volume I-Response Modification Factor Based Design," American Iron and Steel Institute, Washington, DC.

Bahrami, H., Itani, A.M., and Buckle, I.G., 2009, "Guidelines for the Seismic Design of Ductile End Cross-Frames and Diaphragms in Steel Girder Bridge Superstructures," Report Center for Civil Engineering Earthquake Research 09-04, University of Nevada, Reno, NV

Bruneau, M., J.W. Wilson, and R. Tremblay. 1996. "Performance of Steel Bridges During the 1995 Hyogoken-Nanbu Earthquake," *Canadian Journal of Civil Engineering*.

California Department of Transportation (Caltrans). 2001. "Seismic Design Criteria (Version 1.2)," Caltrans, Sacramento, CA.

- California Department of Transportation (Caltrans). 2006. "Seismic Design Criteria (Version 1.4)," Caltrans, Sacramento, CA.
- Carden, L.P., A.M. Itani, and I. Buckle. 2002. "Composite Action in Steel Girder Bridge Superstructures Subjected to Transverse Earthquake Loading," *Transportation Research Record No. 1814*, Transportation Research Board, Washington, DC.
- Carden, L.P., Itani, A.M., and Buckle, I.G., 2005a, "Seismic Load Path in Steel Girder Bridge Superstructures," Report Center for Civil Engineering Earthquake Research 05-03, University of Nevada, Reno, NV.
- Carden, L.P., Itani, A.M., and Buckle, I.G., 2005b, "Seismic Performance of Steel Girder Bridge Superstructures with Ductile End Cross Frames and Seismic Isolation," Report Center for Civil Engineering Earthquake Research 05-04, University of Nevada, Reno, NV.
- Carden, L.P., A.M. Itani, and I. Buckle. 2006. "Seismic Performance of Steel Girder Bridges with Ductile End Cross Frames Using Single Angle X Braces," *Journal of Structural Engineering*, American Society of Civil Engineers, Reston, VA.
- Carden, L.P., F. Garcia-Alvarez, A.M. Itani, and I. Buckle. 2006. "Cyclic Behavior of Single Angles for Ductile End Cross Frames," *Engineering Journal*, American Institute of Steel Construction, Chicago, IL.
- Dicleli, M., and Bruneau, M. 1995a. "Seismic Performance of Multispan Simply Supported Slab-on-Girder Highway Bridges," *Engineering Structures*, Vol. 17, No. 1, 4-14.
- Dicleli, M., and Bruneau, M. 1995b. "Seismic Performance of Simply Supported and Continuous Slab-on-Girder Steel Bridges," *Structural Journal of the American Society of Civil Engineers*, Vol. 121, No. 10, 1497-1506.
- Goel, S.C., and El-Tayem, A. 1986. "Cyclic Load Behavior of Angle X-Bracing," *Journal of Structural Engineering*, 112(11):2528-2539.
- IBC. 2006. "2006 International Building Code (IBC)," International Code Council, Falls Church, VA.
- Imbsen, R.A. 2007. "Proposed AASHTO Guide Specifications for LRFD Seismic Bridge Design," AASHTO Subcommittee for Seismic Effect on Bridges-T3.
- Itani, A. M. 1995. "Cross Frame Effect on Seismic Behavior of Steel Plate Girder Bridges," *Proceedings of the SSRC Annual Technical Session*, Kansas City, MO, Structural Stability Research Council, University of Missouri, Rolla, MO.
- Itani, A.M., and Goel, S.C. 1991. "Earthquake Resistant Design of Open Web Framing Systems," Research report No. UMCE 91-21, University of Michigan, Department of Civil and Environmental Engineering, Ann Arbor, MI.
- Itani, A. M., and H. Sedarat .2000. "Seismic Analysis and Design of the AISI LRFD Design Examples of Steel Highway Bridges," Report N. CCEER 00-08, Center for Civil Engineering Earthquake Research, University of Nevada, Reno, NV.
- Itani, A. M., and M. Reno. 1995. "Seismic Design of Modern Steel Highway Connectors," *Proceedings of the ASCE Structures Congress XIII*, Boston, MA, American Society of Civil Engineers, Reston, VA.
- Itani, A. M., and P.P. Rimal. 1996. "Seismic Analysis and Design of Modern Steel Highway Bridges," *Earthquake Spectra*, Earthquake Engineering Research Institute, Volume 12, No.2.
- Itani, A.M., M. Bruneau, L. Carden, and I. Buckle. 2004. "Seismic Behavior of Steel Girder Bridge Superstructures," *Journal of Bridge Engineering*, American Society of Civil Engineers, Reston, VA.

Mouras, J.M., Sutton, J.P., Frank, K.H., and Williamson, E.B., 2008, "The Tensile Capacity of Welded Shear Studs," Center for Transportation Research at the University of Texas, Austin, TX. Report 9-5498-R2, October 14, 2008

Multidisciplinary Center for Earthquake Engineering Research (MCEER)/Applied Technology Council (ATC). 2003. "Recommended LRFD Guidelines for Seismic Design of Highway Bridges (2 Volumes)," *ATC/MCEER Joint Venture*, Redwood City, CA.

NCHRP. 2002. *Comprehensive Specification for the Seismic Design of Bridges*. NCHRP Report 472, Transportation Research Board, Washington DC.

NCHRP. 2006. *Recommended LRFD Guidelines for the Seismic Design of Highway Bridges*. Draft Report NCHRP Project 20-07, Task 193, TRC Imbsen & Associates, Sacramento, CA.

Roberts, J.E. 1992. "Sharing California's Seismic Lessons," *Modern Steel Construction*, American Institute of Steel Construction, Chicago, IL.

Zahrai, S.M., and M. Bruneau. 1998. "Impact of Diaphragms on Seismic Response of Straight Slab-on-Girder Steel Bridges," *Journal of Structural Engineering*, American Society of Civil Engineers, Reston, VA.

Zahrai, S. M., and M. Bruneau. 1999a. "Ductile End-Diaphragm for Seismic Retrofit of Slab-on-Girder Steel Bridges," *Journal of Structural Engineering*, American Society of Civil Engineers, Reston, VA.

Zahrai, S. M., and M. Bruneau. 1999b. "Cyclic Testing of Ductile End-Diaphragms for Slab-on-Steel Girder Bridges" *Journal of Structural Engineering*, American Society of Civil Engineers, Reston, VA.

# Chapter 3 SEISMIC DESIGN EXAMPLES

## 3.1 Introduction

This chapter illustrates the application of the proposed seismic provisions to the seismic design of the deck, shear connectors, cross-frames and connections. The design examples covered here represent a straight single-span and a straight two-span composite steel I-girder bridge. Two design cases were considered for the single-span bridge – (a) elastic superstructure where there is no yielding and buckling in the support cross-frames, and (b) ductile superstructure where there is yielding and buckling in the support cross-frames. Only the ductile superstructure was considered for the two-span bridge. It was assumed that these bridges are located in a zone with high seismicity but at different particular locations. The two-span bridge is located in a site with higher ground acceleration. The design of the steel girders is not covered here but literature can be found elsewhere.

## 3.2 Single-Span Bridge

The single-span bridge is designed with elastic and ductile superstructures. Detailed calculations are shown in Appendix 3-A and 3-B, respectively.

### 3.2.1 Description

This design example represents a straight single-span composite steel I-girder bridge with a span length equal to 165 ft and a total out-to-out width of 58 ft. The superstructure is composed of a 4,000 psi concrete deck and five identical steel girders spaced 12 ft on centers. The deck thickness is  $9\frac{1}{8}$  in with a haunch thickness equal to  $2\frac{1}{2}$  in throughout the whole span. The girders are composed of 2 in x 18 in plates as top and bottom flanges and a  $\frac{5}{8}$  in x 78 in web plate.

The cross-frames are arranged in an X-type configuration and are uniformly spaced at 27.5 ft. For the case of the elastic superstructure, the support cross-frames are composed of  $2L6x6x\frac{7}{8}$  top chords,  $2L2x2x\frac{3}{16}$  bottom chords and  $L8x4x\frac{3}{4}$  diagonals. For the case of the ductile superstructure, the support cross-frames are composed of  $2L6x6x\frac{7}{8}$  top chords,  $2L2x2x\frac{1}{4}$  bottom chords and  $L4x4x\frac{1}{2}$  diagonals. The intermediate cross-frame members in both cases are all composed of  $L2x2x\frac{1}{4}$ .

### 3.2.2 Analytical Model

The analytical model (Figure 3-1) was developed using the computer program SAP2000. The deck was modeled as shell elements while the girders and cross-frames were modeled as frame elements. Shear connectors connecting the deck, cross-frame top chords and/or girder top flanges were represented by rigid link elements. In the case of the elastic superstructure, the shear connectors were located on the girder top flanges and on the top chords of the support cross-frames. In the case of the ductile superstructure, the shear connectors were located only on the top chords of the support cross-frames. Between the support locations, the shear connectors in both cases were located on the girder top flanges only. At one end of the bridge, pin supports were used where translation was restrained in all directions. At the other end of the bridge, pin-roller supports were used where vertical and transverse translations were restrained but longitudinal translation was unrestrained.

### 3.2.3 Seismic Analysis

The dynamic properties (modal periods and modal mass participation ratios) of the single-span bridges with elastic and ductile superstructures are tabulated in Appendices 3-A and 3-B, respectively. In the bridge with an elastic superstructure, the 1<sup>st</sup> mode (T = 0.549 sec) is the dominant vertical translational mode while the 8<sup>th</sup> mode (T = 0.132 sec) is the dominant transverse translational mode. In the bridge with a ductile superstructure, the 1<sup>st</sup> mode (T = 0.561 sec) is also the dominant vertical translational mode while the dominant transverse translational mode is the 5<sup>th</sup> mode (T = 0.207 sec). The bridge with an elastic superstructure is stiffer in the transverse direction because of the larger cross-frame members.

Seismic forces and displacements were obtained through multimode response spectrum analysis. Complete Quadratic Combination (CQC) was used to combine the modal responses. The seismic parameters are:

$$PGA = 0.572 \text{ g}$$

$$S_s = 1.36 \text{ g}$$

$$S_1 = 0.641 \text{ g.}$$

It was assumed that the bridge was located on Site Class D soil. The design spectra are shown in Appendices 3-A and 3-B. The bridge was assumed to be under the Importance category “Other”.

### 3.2.4 Seismic Design of a Single-Span Bridge with Elastic Superstructure

The 2007 AASHTO LRFD Specifications, the proposed seismic provisions, and the AISC Specifications (2005) were used in the design of the components. The design forces were obtained by dividing the

seismic forces by the response modification factor, which is equal to 1.0. Appendix 3-A shows the output of the spreadsheet developed for the design calculations. The first part shows the seismic parameters including the design response spectrum. The second part shows the result of the modal response spectrum analysis, which includes the modal periods and base shears. The third part covers the seismic design of the reinforced concrete (R/C) deck, shear connectors, cross-frame members and connections.

### Seismic Design of R/C Deck

The seismic design of the R/C deck was done according to Article 6.16.4.2 of the proposed seismic provisions. Detailed calculations are shown in Appendix 3-A under “Seismic Design of R/C Deck”.

Article 6.16.4.2 specifies that the deck can be considered to act as a rigid horizontal diaphragm if the following criteria are met:

- (a) span-to-width ratio is not more than 3.0
- (b) net mid-span lateral superstructure displacement is less than twice the average of the adjacent lateral support displacements.

Otherwise, the deck is considered to act as a flexible diaphragm and must be designed to resist shear and bending stresses. Rigid diaphragms, on the other hand, require no special seismic design, but must have sufficient shear resistance to transfer the seismic shear to the supports.

In this design example,

$$Length / Width = 165 / 58 = 2.84 < 3.0$$

$$\Delta_{av} = (\Delta_1 + \Delta_2) / 2 = 0.090in$$

$$\Delta_{3net} = \Delta_3 - \Delta_{av} = 0.161in$$

where  $\Delta_1$  is the lateral superstructure displacement at support 1,  $\Delta_2$  is the lateral superstructure displacement at support 2, and  $\Delta_3$  is the lateral superstructure displacement at mid-span. Since

$$\Delta_{3net} < 2\Delta_{av} = 0.18in$$

the deck can be considered to act as a rigid diaphragm.

The deck is then designed (or checked) for the lateral seismic shears. For the case of an elastic superstructure, the design forces were calculated in accordance with Eqns. 6.16.4.2-1 and 6.16.4.2-2.

From response spectrum analysis, the base shears at Supports 1 and 2 are 842 kips and 680 kips, respectively. The difference is due to the difference in support conditions at the ends of the bridge as discussed in Section 3.2.2. The total transverse seismic force,  $F_{px}$ , on the deck is:

$$F_{px} = \frac{W_{px}}{W} F = \frac{1,261}{1,430} (1,522) = 1,342 \text{ kips}$$

$F_{px}$  is then distributed to the supports based on their relative stiffnesses. Ratio-and-proportion, in lieu of distribution according to relative stiffness, with the base shears coming from response spectrum analysis can be also used. For example, the lateral shear at Support 1 ( $F_{px1}$ ) is calculated as follows

$$F_{px1} = \frac{V_{y1}}{F} F_{px} = \frac{842}{1,522} (1,342) = 742 \text{ kips}$$

where,  $V_{y1}$  is the lateral shear at Support 1 from response spectrum analysis. The above lateral shear, however, must be checked against the upper and lower bounds seismic shear given by Eqn. 6.16.4.2-2.

$$(F_{px})_{\min} = 0.2 S_{DS} W_{px} = 343 \text{ kips}$$

$$(F_{px})_{\max} = 0.4 S_{DS} W_{px} = 686 \text{ kips.}$$

Therefore, the design deck shear should be 686 kips and the shear demand at Support 1 is

$$F_{px} / \text{Width} = 11.83 \text{ kip} / \text{ft.}$$

This will be resisted by the combined shear resistance of concrete and steel reinforcement. No additional reinforcement is required if the concrete shear resistance is larger than the shear demand. The shear resistance provided by concrete is

$$\phi V_c = 0.75 (12 t_s) \left( 2 \sqrt{f'_c, \text{psi}} \right) / 1000 = 10.39 \text{ kip} / \text{ft.}$$

This is less than the shear demand of 11.83 kip/ft thus steel reinforcement should be provided. Using #5 reinforcement at a spacing of 18 in, the shear resistance provided by steel reinforcement is

$$\phi V_s = 0.75 [A_b (12 / s) f_y] = 9.3 \text{ kip} / \text{ft.}$$

Combining with that from concrete, the total shear resistance is

$$V_u = \phi (V_c + V_s) = 19.69 \text{ kip} / \text{ft} > 11.38 \text{ kip} / \text{ft.}$$

The spreadsheet also shows the calculation to determine how far along the span the steel reinforcement is required. The deck design at Support 2 follows the same procedure as that at Support 1.

### Seismic Design of Shear Connectors

The shear connectors at support locations were designed according to Article 6.16.4.3. Detailed calculations are shown in Appendix 3-A under “Seismic Design of Shear Connectors”. The shear connectors in this example are located on the girder top flanges and on the top chords of the support cross-frames. Over the top chords, the shear connectors are located on the center two-thirds of the top chord length, and are divided into three groups (for example, along the top chord of the support cross-frame between Girders 1 and 2, the shear connectors are divided into groups A, B and C).

The axial forces and longitudinal and transverse shears ( $N$ ,  $Q_L$ , and  $Q_T$ , respectively) obtained from the response spectrum analysis are tabulated as shown.  $Q_u$  in this table is the vector sum of  $Q_L$  and  $Q_T$ , which is taken as the design shear. The capacity of each group of shear connectors is then evaluated using the tension-shear interaction equation given by Equation 6.16.4.3-2.

$$\left(\frac{N_u}{N_r}\right)^{5/3} + \left(\frac{Q_u}{Q_r}\right)^{5/3} \leq 1.0$$

where  $N_u$  and  $Q_u$  are the axial and shear demands from the response spectrum analysis, and  $N_r$  and  $Q_r$  are the factored tensile and shear resistances of the shear connectors. Demand-capacity (D/C) ratios are shown in the table for each group of shear connectors.

### Seismic Design of Top Chord

The cross-frame members were designed according to Article 6.16.4.4 of the proposed seismic provisions, Articles 6.7, 6.8 and 6.9 of 2007 AASHTO LRFD Specifications and the AISC Specifications (2005). Detailed calculations for top chord design are shown in Appendix 3-A under “Seismic Design of Top Chord”.

The top chord was designed to resist the axial compression and/or tension force transmitted from the deck and the girder. From the response spectrum analysis, the design axial force on the top chord is

$$Q_E / R = 69.52 \text{ kips.}$$

The selected preliminary section based on Strength I analysis and design is 2L6x6x7/8 stitched at quarter points (48 in). The width-to-thickness ( $b/t$ ) ratio of the outstanding legs was checked against the limits set in Article 6.9.4.2 for local buckling.

$$\frac{b}{t} = 6.86 \leq 0.45 \sqrt{\frac{E}{F_y}} = 12.77$$

Slenderness ratio was calculated as the larger of  $KL/r$  from in-plane buckling and out-of-plane buckling. For in-plane buckling, the buckling length is the length between the stitches, which is 48 in. The slenderness ratio is therefore given by

$$\left(\frac{KL}{r}\right)_x = \frac{0.85 * 48}{1.81} = 22.54$$

For out-of-plane buckling,  $KL/r$  is calculated based on the modified slenderness ratio given by Equation 6.9.4.3.1-1

$$\left(\frac{KL}{r}\right)_m = \sqrt{\left(\frac{KL}{r}\right)_o^2 + 0.82\left(\frac{\alpha^2}{1 + \alpha^2}\right)\left(\frac{a}{r_{ib}}\right)^2} = 45.80$$

The governing  $KL/r$  ratio is therefore equal to 45.80.

The factored compressive resistance was then determined as specified in Article 6.9.4 where the resistance factor  $\phi$  is taken equal to 1.0 at the extreme event limit state.

$$\lambda = \left(\frac{KL}{r\pi}\right)^2 \frac{F_y}{E} = 0.26 < 2.25$$

$$P_n = 0.66^\lambda F_y A_s = 629 \text{ kips}$$

$$\phi P_n = 629 \text{ kips} > 69.52 \text{ kips.}$$

The factored tensile resistance was calculated according to Article 6.8.2 where the resistance factor  $\phi$  is again taken equal to 1.0.

$$\phi P_{ny} = \phi F_y A_g = 702 \text{ kips} > 69.52 \text{ kips.}$$

The design of the bottom chord is not shown here, as the forces are usually small due to the assumption of pinned supports.

### **Seismic Design of Diagonal Member**

Detailed calculations are shown in Appendix 3-A under “Seismic Design of Diagonal Member”.

The compressive force in the diagonal member is the result of seismic loads transmitted by the top chord and the girder. The design axial force from the response spectrum analysis is

$$Q_E / R = 118.54 \text{ kips.}$$

The selected preliminary section according to Strength I analysis and design is L8x4x3/4. The  $b/t$  ratio for this section is 10.67 and is less than the limit of 12.77 calculated above (see Seismic Design of Top Chord). For single angle compression members, the buckling length is equal to the distance between the working points and the effective slenderness ratio is given by

(a) for  $0 \leq L/r_x \leq 80$

$$\frac{KL}{r} = 72 + 0.75 \frac{L}{r_x}$$

(b) for  $L/r_x > 80$

$$\frac{KL}{r} = 32 + 1.25 \frac{L}{r_x} \leq 200$$

$KL/r$  for this section is 112.

The factored compressive resistance was then calculated according to the provisions of Article 6.9.4 where the resistance factor  $\phi$  is taken equal to 1.0

$$\lambda = \left( \frac{KL}{r\pi} \right)^2 \frac{F_y}{E} = 1.59 < 2.25$$

$$\phi P_n = \phi 0.66^\lambda F_y A_s = 157 \text{ kips} > 118.54.$$

The factored tensile resistance was calculated according to Article 6.8.2 where the resistance factor  $\phi$  is again taken equal to 1.0.

$$\phi P_{ny} = \phi F_y A_g = 304 \text{ kips} > 118.54 \text{ kips.}$$

### **Connection Design**

The connections were designed according to the provisions of Article 6.13. The response modification factor  $R$  for connections is 0.8 (amplification factor  $\Omega = 1/R = 1.25$ ) as specified in Article 3.10.7. The

cross-frame members are welded to the gusset plates while the gusset plates are bolted to the stiffeners. Detailed calculations are shown in Appendix 3-A under “Connection Design”.

### End Connections (Member to Gusset Plate Connections)

The design force for the end connection of the cross-frame members is calculated as

$$F = Q_E / R = Q_E \Omega.$$

where,  $Q_E$  is the axial force in the member under consideration.

The factored fillet weld resistance per unit length is given by

$$R_r = \phi(0.6F_{EXX})(0.707s)$$

where,  $\phi = 0.80$ ,  $F_{EXX} = 70$  ksi, and  $s =$  weld size in inches. The required weld length is then calculated from

$$L_w = F / \phi R_w.$$

### Gusset Plate and Gusset Plate to Stiffener Connection

The shear demand in the gusset plate and its connection to the bearing stiffener is equal to the vertical component of the amplified diagonal design force

$$V = \frac{(Q_E)_{diagonal}}{R = 0.8} \sin \theta = 67.73 \text{ kips}$$

where  $\theta$  is the angle of inclination of the diagonal member. The moment demand ( $M = 294.19$  kip-in) is equal to the shear demand calculated above multiplied by the horizontal distance from the working point to the centroid of the bolt group.

The bolts connecting the gusset plate to the bearing stiffener are designed based on the combined shear and moment calculated above. The bolt resistance is determined from either the bolt shear resistance

$$\phi R_n = \phi(0.48A_b)F_u$$

or the plate bearing resistance

$$\phi R_n = \phi(2.4d_b t_p)F_u$$

with resistance factors  $\phi$  taken equal to 0.8.

The gusset plate resistance at the gross and net sections was then evaluated against the combined shear and moment using the von Mises criterion

$$F_y = \sqrt{f_b^2 + 3f_v^2}$$

$$f_v = V / A$$

$$f_b = M / Z$$

At the gross section, the plastic section modulus is given by

$$Z_g = \frac{td^2}{4}$$

and at the net section it is given by

$$Z_n = Z_g \left( 1 - \frac{d_h}{s} \right)$$

where  $A$  = area at gross or net section,  $t$  is the gusset plate thickness,  $d$  is the height of gusset plate, and  $d_h$  is the bolt hole diameter ( $d_b + 1/16$  in).

### 3.2.5 Seismic Design of a Single-Span Bridge with Ductile Superstructure

Detailed design calculations are shown in Appendix 3-B.

Only the tensile diagonal members of the support cross-frames are included in the analytical model. This was done to get a realistic stiffness at the supports after the diagonal member in compression was assumed to have buckled. The design spectrum used in the analysis was the same as that for the single-span bridge with an elastic superstructure (Section 3.2.4). Dynamic properties and results of the modal response spectrum analysis are shown in Appendix 3-B.

Capacity design methodology is employed where the components other than the diagonal members are designed based on the resistance of the diagonal member. The diagonal members act as a “fuse” by controlled buckling and yielding, which in turn dissipates the seismic input energy. The chord members

of the support cross-frames, as well as the connections, are specially designed and detailed to remain elastic and limit the inelasticity to the diagonal members only.

The following is the step-by-step design procedure:

1. Perform a modal response spectrum analysis to obtain the elastic base shear and component forces ( $Q_E$ ).
2. Design the diagonal member by dividing the force obtained in Step 1 by the response modification factor,  $R$ , specified in Table 6.16.4.5-1. Nominal compressive and tensile resistances of the diagonal member are calculated based on the expected yield strength  $R_y F_y$  as specified in Article 6.16.4.5.1c.
3. Design the top chord members with the design force equal to the larger of either  $(Q_E)_{top\ chord} / R$  or the horizontal component of the nominal tensile resistance of the diagonal member taken as  $R_y P_{ny} \cos \theta$  (Article 6.16.4.5.1). The bottom chord forces are usually small due to the assumption of pinned supports. The nominal tensile and compressive resistances of the chord members are determined as specified in Articles 6.8 and 6.9, respectively, since they are to remain elastic.
4. Calculate the lateral resistance of the support cross-frames based on the sum of the horizontal components of the diagonal member resistance and the shear contributions due to bending of the top and bottom chords (Article 6.16.4.5.1d).
5. Calculate the scale factor  $\Omega$  for the ductile superstructure by dividing the lateral resistance obtained in Step 4 by the support base shear obtained in Step 1 (Eqn. 6.16.4.3-1). This will be used to scale the seismic forces in components that should remain elastic; e.g. the shear connectors (see Step 7).
6. Design the R/C deck based on the lateral resistance determined in Step 4 at the support under consideration (Article 6.16.4.2).
7. Design the shear connectors at the support locations. The forces obtained in Step 1 are multiplied by the scale factor calculated in Step 5 (Article 6.16.4.3).
8. Design the end connections with the design forces based on the diagonal member nominal resistance (Article 6.16.4.5.2). The nominal resistance is increased by 10% to ensure that inelasticity is concentrated only in the diagonal member.

### **Seismic Design of Diagonal Members**

The design of the diagonal members of the special support cross-frames will be discussed first since the design of other components depends on the resistance of this member. Detailed calculations are shown in Appendix 3-B under “Seismic Design of Diagonal Members”. Note that although the design procedure implemented is as shown above, the calculation shown in Appendix 3-B is not exactly arranged as

discussed here. The spreadsheet was formatted such that the arrangement of calculations is similar to that in Appendix 3-A (see also Section 3.2.4).

From Step 2, the design axial force of the diagonal member is

$$F = \frac{(Q_E)_{diagonal}}{R} = \frac{264.84}{3} = 88.3kips.$$

The selected section, L4x4x<sup>1</sup>/<sub>2</sub>, needs to satisfy the width-to-thickness (*b/t*) ratio limit specified in Article 6.16.4.5.1a.

$$\frac{b}{t} = 8.00 \leq 0.3 \sqrt{\frac{E}{F_y}} = 8.51$$

In addition, the slenderness ratio *KL/r* needs to satisfy the limit specified in Article 6.16.4.5.1b.

$$\frac{KL}{r_z} = 86.76 \leq 4.0 \sqrt{\frac{E}{F_y}} = 113.53$$

where *L* = 79.20 in, which is half of the diagonal length measured between the working points.

The nominal axial resistances in compression and tension are then determined as specified in Article 6.16.4.5.1c. The expected yield strength *R<sub>y</sub>F<sub>y</sub>* is used in these calculations.

$$\text{Compressive Resistance: } \phi P_n = 112.25kips > 88.3kips$$

$$\text{Tensile Resistance: } \phi R_y P_{ny} = 202.50kips > 88.3kips$$

The lateral resistance of the support cross-frames is then calculated from the sum of the horizontal components of the diagonal member resistances and the shear contributions due to bending of the chord members (Article 6.16.4.5.1d). The horizontal component of the tension diagonal is

$$R_y P_{ny} \cos \theta = 184.09kips$$

where *R<sub>y</sub>* = 1.5 for A36 steel and *P<sub>ny</sub>* is the nominal tensile resistance of the member calculated as specified in Article 6.8.2. The horizontal component of the nominal post-buckling resistance of the compression diagonal is

$$0.3 P_n \cos \theta = 30.61kips$$

The contribution of the top chord (2L6x6x<sup>7/8</sup>) to the lateral resistance is calculated as specified in Article 6.16.4.5.1d.

$$\frac{2R_y M_p}{h_1} = 39.99 \text{kips}$$

where  $M_p$  is the plastic moment of the member and  $h_1$  is the distance from the centerline of the bearing to the centerline of the top chord. The contribution of the bottom chord (2L2x2x<sup>1/4</sup>) to the lateral resistance is

$$\frac{2R_y M_p}{h_2} = 11.88 \text{kips}$$

where  $M_p$  is the plastic moment of the member and  $h_2$  is the distance from the centerline of the bearing to the centerline of the bottom chord. Therefore, the cross-frame capacity per bay is

$$V_{lat} / \text{bay} = 184.09 + 30.61 + 39.99 + 11.88 = 266.57 \text{kips} / \text{bay}.$$

Since there are the 4 bays, the total lateral resistance at Support 1 is

$$V_{lat} = 4(266.57) = 1,066 \text{kips}.$$

The scale factor for the ductile superstructure at Support 1 is then calculated as (Eqn. 6.16.4.3-1)

$$\Omega = \frac{V_{lat}}{V} = \frac{1,066}{997} = 1.07$$

where  $V$  is the base shear at Support 1 from the response spectrum analysis. This factor is used to scale the seismic forces in components that should remain elastic like the shear connectors.

Superstructure drift (calculated as the ratio of the relative displacement between the flanges to the girder depth) is to be less than the limit specified in Table 6.16.4.5-1. It should be noted that the lateral displacement  $\Delta$  obtained from response spectrum analysis must be multiplied by the scale factor  $\Omega$  calculated above.

$$\Delta_{inelastic\_Support\_1} = \Delta_{Support\_1} \Omega = 0.48(1.07) = 0.51 \text{in}$$

Therefore, the ductile superstructure drift is 0.55%, which is less than the maximum drift limit of 4%.

### **Seismic Design of Top Chord**

Design of the top chord members follows after the diagonal members are designed. Detailed calculations are shown in Appendix 3-B under “Seismic Design of Top Chord”. The design axial force is the larger of

$$(Q_E)_{top\_chord} / R = 74.46kips$$

$$R_y P_{ny} \cos \theta = 184.1kips$$

where  $R_y P_{ny}$  is the nominal tensile resistance of diagonal member and  $\theta$  is the angle of inclination of the diagonal member with respect to the horizontal.

The width-to-thickness ratio is checked against Eqn. 6.16.4.5.1a-1. The slenderness ratios for in-plane and out-of-plane buckling are calculated as before (see Section 3.2.4), but are checked against Eqn. 6.16.4.5.1b-1. The compressive and tensile resistances are determined as specified in Articles 6.8 and 6.9, respectively, where  $\phi$  is taken equal to 1.0.

$$\text{Compressive Resistance: } \phi P_n = 629kips > 184.1kips$$

$$\text{Tensile Resistance: } \phi P_{ny} = 702kips > 184.1kips$$

The calculation of the expected plastic moment  $R_y M_p$  is also shown. Note that this was used in the calculation of the support lateral resistance as discussed in “Seismic Design of Diagonal Members”.

The axial force in the bottom chord is very small so only the local buckling check and  $R_y M_p$  calculation are shown.

### **Seismic Design of R/C Deck**

Detailed calculations are shown in Appendix 3-B under “Seismic Design of R/C Deck”.

The displacements used in the deck classification are the displacements obtained from the response spectrum analysis multiplied by the scale factor  $\Omega$ . The deck was classified as a rigid diaphragm as shown.

The total deck seismic shear force is calculated as follows (Eqn. 6.16.4.2-3)

$$F_{px} = \frac{W_{px}}{W} F_{lat} = \frac{1,261}{1,430} (1,950) = 1,719kips$$

The seismic shear at Support 1 is then calculated by ratio-and-portion (see Section 3.2.4).

$$F_{px1} = \frac{V_{y1}}{\Sigma V} F_{px} = \frac{1,066}{1,950} (1,719) = 940 \text{ kips}$$

The deck transverse shear limits of Eqn. 6.16.4.2-2 do not apply for a ductile superstructure. The design of the R/C deck for lateral shear then follows the same procedure as that discussed in Section 3.2.4.

### **Seismic Design of Shear Connectors**

The shear connector forces obtained from the response spectrum analysis were multiplied by the scale factor  $\Omega = 1.07$ . The design procedure is then the same as that discussed in Section 3.2.4. Detailed calculations are shown in Appendix 3-B under “Seismic Design of Shear Connectors”.

### **Connection Design**

Detailed calculations are shown in Appendix 3-B under “Connection Design”. The required resistance of the end connections is based on the diagonal member resistance with 10% increase to ensure that inelasticity is concentrated in the diagonal member only (Article 6.16.4.5.2).

### **End and Middle Connection of Diagonal Member**

The required axial resistance of the diagonal member end connection is calculated as

$$1.1R_y P_{ny} = 222.8 \text{ kips.}$$

The weld resistance per length is

$$R_r = \phi 0.6 F_{EXX} 0.707s = 16.3 \text{ kip / in}$$

Therefore, the required weld length is

$$L_w = 222.8 / 16.3 = 13.6 \text{ in}$$

The provided weld length per leg is 8.0 in for a total weld length of 16.0 in.

According to Article 6.16.4.5.2, the end connection should be also capable of developing the flexural resistance of the member in addition to axial resistance. The moment at the end connection is calculated as follows

$$M = 1.1R_y F_y Z = 116.4 \text{ kip - in}$$

Therefore, the total weld shear flow coming from axial and flexural resistance of the diagonal member is

$$v = \frac{My}{I_p} + \frac{1.1R_y P_{ny}}{L_w} = 14.7 \text{ kip/in}$$

which is smaller than the weld resistance per length of  $R_r = 16.3 \text{ kip/in}$  calculated above.  $I_p$  in the above equation is the polar moment of inertia of the welds;  $y$  is the weld distance from its center of configuration; and  $L_w$  is the provided total length of weld.

The diagonal members shall be connected where the members cross by welds (Article 6.16.4.5.1). The required resistance of this connection is

$$0.25R_y P_{ny} = 0.25 * 202.50 = 50.6 \text{ kips}$$

The required total weld length is  $3.1 \text{ in}$  and the provided total weld length is  $3.5 \text{ in}$  ( $1.75 \text{ in}$  per leg) as shown.

#### End Connection of Top Chord

The required resistance of the top chord end connection is

$$1.1R_y P_{ny} \cos \theta = 202.5 \text{ kips}$$

where  $P_{ny}$  is the nominal tensile resistance of the diagonal member. The required weld length per leg is  $4.87 \text{ in}$  and the provided weld length per leg is  $5.00 \text{ in}$  for a total weld length of  $20.00 \text{ in}$ .

#### Gusset Plate and Gusset Plate to Stiffener Connection

The gusset plate design shear is calculated from the vertical component of the diagonal member tensile resistance increased by 10%.

$$V = 1.1R_y P_{ny} \sin \theta = 101.81 \text{ kips}$$

where  $\theta$  is the angle of inclination of the diagonal member. The design moment ( $M = 442.25 \text{ kip-in}$ ) is equal to the shear calculated above multiplied by the horizontal distance from the working point of the connection to the centroid of the bolt group.

The bolts connecting the gusset plate to the bearing stiffener are designed based on the combined shear and moment calculated above. The bolt resistance is determined from either the bolt shear resistance

$$\phi R_n = \phi(0.48A_b)F_u$$

or the plate bearing resistance

$$\phi R_n = \phi(2.4d_b t_p)F_u$$

with resistance factors  $\phi$  taken equal to 0.8.

The gusset plate resistance at gross and net sections is then evaluated against the combined shear and moment using the von Mises criterion

$$F_y = \sqrt{f_b^2 + 3f_v^2}$$

$$f_v = V / A$$

$$f_b = M / Z$$

At the gross section, the plastic section modulus is given by

$$Z_g = \frac{td^2}{4}$$

and at the net section it is given by

$$Z_n = Z_g \left( 1 - \frac{d_h}{s} \right)$$

where  $A$  = area at gross or net section,  $t$  is the gusset plate thickness,  $d$  is the height of gusset plate, and  $d_h$  is the bolt hole diameter ( $d_b + 1/16$  in).

### 3.3 Two-Span Bridge

The two-span bridge is designed with ductile superstructure only. Detailed calculations are shown in Appendix 3-C.

#### 3.3.1 Description

This design example represents a straight two-span composite steel I-girder bridge with span lengths equal to 90 ft and total out-to-out width of 37 ft. The superstructure is composed of a 4,000 psi concrete deck and four identical steel girders spaced 10 ft on centers. The deck thickness is 8 in with a haunch

thickness equal to 2 in throughout the whole length. The girders are composed of 1 in x 16 in top flange plate, 1½ in x 16 in bottom flange plate, and ½ in x 36 in web plate.

The cross-frames are arranged in an X-type configuration at supports and intermediate locations. Support cross-frames are composed of 2L6x6x7/8 top chords, L4x4x1/2 diagonals and 2L2x2x1/4 bottom chords. Intermediate cross-frames are located at 37 ft, 74ft, 106 ft, and 143 ft measured from Abutment 1 and all members are L2x2x1/4. The column is 4 ft in diameter and with a clear height of 30 ft measured from the top of the footing to the bottom of the cap beam.

### 3.3.2 Analytical Model

The analytical model (Figure 3-2) was developed using the computer program SAP2000. The deck was modeled as shell elements while the girders and cross-frames were modeled as frame elements. Shear connectors connecting the deck, cross-frame top chords and/or girder top flange were represented by rigid link elements. At the supports, the shear connectors are located only on the cross-frame top chords. Between the support locations, the shear connectors are located only at girder top flanges.

The ends of the bridge were restrained against translation in the transverse direction but free in the longitudinal direction. At the pier, pin connections were assumed between the bottom flange of the girders and the top of the cap beam. Only the tensile diagonal members of the support cross-frames are included in the analytical model. This was done to get a realistic stiffness at the supports after the diagonal member in compression was assumed to have buckled.

### 3.3.3 Seismic Analysis

The dynamic properties (modal periods and modal mass participation ratios) are tabulated in Appendix 3-C. The 1<sup>st</sup> mode (T = 2.418 sec) is the dominant translational mode in the longitudinal direction. The 6<sup>th</sup> mode (T = 0.237 sec) is the dominant translational mode in the transverse direction.

Seismic forces and displacements were obtained through multimode response spectrum analysis. Complete Quadratic Combination (CQC) was used to combine the modal responses. The seismic parameters are:

$$PGA = 0.91g$$

$$S_s = 2.157g$$

$$S_1 = 0.774g$$

It was assumed that the bridge was located on Site Class D soil. The design spectrum is shown in Appendix 3-C. The bridge was assumed to be under the Importance Category “Other”.

The base shears from modal response spectrum analysis at Supports 1, 2, and 3 are 906 kips, 307 kips and 906 kips, respectively. Support 1 is at Abutment 1, Support 2 is at pier, and Support 3 is at Abutment 3.

### **3.3.4 Seismic Design of a Two-Span Bridge with Ductile Superstructure**

The 2007 AASHTO LRFD Specifications, the proposed seismic provisions, and the AISC Specifications (2005) were used in the design of components. Appendix 3-C shows the output of the spreadsheet developed for the design calculations. The first part shows the seismic parameters including the design response spectrum. The second part shows the result of the modal analysis which includes the modal periods and base shears. The third part covers the seismic design of the reinforced concrete (R/C) deck, shear connectors, cross-frame members and connections.

Capacity design methodology is employed where the components other than the diagonal members are designed based on the resistance of the diagonal member. The diagonal members act as a “fuse” by controlled buckling and yielding which in turn dissipates the seismic input energy. The chord members of the support cross-frames, as well as the connections, are specially designed and detailed to remain elastic and limit the inelasticity to the diagonal members only.

The following is the step-by-step design procedure:

1. Perform a modal response spectrum analysis to obtain the elastic base shear and component forces ( $Q_E$ ).
2. Design the diagonal member by dividing the force obtained in Step 1 by the response modification factor,  $R$ , specified in Table 6.16.4.5-1. Nominal compressive and tensile resistances of the diagonal member are calculated based on the expected yield strength  $R_y F_y$  as specified in Article 6.16.4.5.1c.
3. Design the top chord members with the design force equal to the larger of either  $(Q_E)_{top\ chord} / R$  or the horizontal component of the nominal tensile resistance of the diagonal member taken as  $R_y P_{ny} \cos \theta$  (Article 6.16.4.5.1). The bottom chord forces are usually small due to the assumption of pinned supports. The nominal tensile and compressive resistances of the chord members are determined as specified in Articles 6.8 and 6.9, respectively, since they are to remain elastic.

4. Calculate the lateral resistance of the support cross-frames based on the sum of the horizontal components of the diagonal member resistance and the shear contributions due to bending of the top and bottom chords (Article 6.16.4.5.1d).
5. Calculate the scale factor  $\Omega$  for ductile superstructure by dividing the lateral resistance obtained in Step 4 by the support base shear obtained in Step 1 (Eqn. 6.16.4.3-1). This will be used to scale the seismic forces in components that should remain elastic; e.g. the shear connectors (see Step 7).
6. Design the R/C deck based on the lateral resistance determined in Step 4 at the support under consideration (Article 6.16.4.2).
7. Design the shear connectors at the support locations. The forces obtained in Step 1 are multiplied by the scale factor calculated in Step 5 (Article 6.16.4.3).
8. Design the end connections with the design forces based on the diagonal member nominal resistance (Article 6.16.4.5.2). The nominal resistance is increased by 10% to ensure that inelasticity is concentrated only in the diagonal member.

### **Seismic Design of Diagonal Members**

The design of the diagonal members of the special support cross-frames will be discussed first since the design of other components depends on the resistance of this member. Detailed calculations are shown in Appendix 3-C under “Seismic Design of Diagonal Members”. Note that although the design procedure implemented is as shown above, the calculation shown in Appendix 3-C is not exactly arranged as discussed here. The spreadsheet was formatted such that the arrangement of calculations is similar to that in Appendix 3-A (see also Section 3.2.4).

From Step 2, the design axial force of the diagonal member is

$$F = \frac{(Q_E)_{diagonal}}{R} = \frac{305.98}{3} = 102 \text{ kips.}$$

The selected section, L4x4x<sup>1</sup>/<sub>2</sub>, needs to satisfy the width-to-thickness ( $b/t$ ) ratio limit specified in Article 6.16.4.5.1a.

$$\frac{b}{t} = 8.00 \leq 0.3 \sqrt{\frac{E}{F_y}} = 8.51$$

In addition, the slenderness ratio  $KL/r$  needs to satisfy the limit specified in Article 6.16.4.5.1b.

$$\frac{KL}{r_z} = 67.36 \leq 4.0 \sqrt{\frac{E}{F_y}} = 113.53$$

where  $L = 61.50$  in, which is half of the diagonal length measured between working points.

The nominal axial resistances in compression and tension are then determined as specified in Article 6.16.4.5.1c. The expected yield strength  $R_y F_y$  is used in these calculations.

$$\text{Compressive Resistance: } \phi P_n = 141.88 \text{ kips} > 102 \text{ kips}$$

$$\text{Tensile Resistance: } \phi R_y P_{ny} = 202.50 \text{ kips} > 102 \text{ kips}$$

The lateral resistance of the support cross-frames is then calculated from the sum of the horizontal components of the diagonal member resistances and the shear contributions due to bending of the chord members (Article 6.16.4.5.1d). The horizontal component of the tension diagonal is

$$R_y P_{ny} \cos \theta = 197.56 \text{ kips}$$

where  $R_y = 1.5$  for A36 steel and  $P_{ny}$  is the nominal tensile resistance of the member calculated as specified in Article 6.8.2. The horizontal component of the nominal post-buckling resistance of the compression diagonal is

$$0.3 P_n \cos \theta = 41.53 \text{ kips}$$

The contribution of the top chord (2L6x6x<sup>7/8</sup>) to the lateral resistance is calculated as specified in Article 6.16.4.5.1d.

$$\frac{2R_y M_p}{h_1} = 89.67 \text{ kips}$$

where  $M_p$  is the plastic moment of the member and  $h_1$  is the distance from the centerline of the bearing to the centerline of the top chord. The contribution of the bottom chord (2L2x2x<sup>1/4</sup>) to the lateral resistance is

$$\frac{2R_y M_p}{h_2} = 15.84 \text{ kips}$$

where  $M_p$  is the plastic moment of the member and  $h_2$  is the distance from the centerline of the bearing to the centerline of the bottom chord. Therefore, the cross-frame capacity per bay is

$$V_{lat} / \text{bay} = 197.56 + 41.53 + 89.67 + 15.84 = 344.6 \text{ kips} / \text{bay}.$$

Since there are the 4 bays, the total lateral resistance at Support 1 is

$$V_{lat} = 3(344.6) = 1,034 \text{ kips.}$$

The scale factor for ductile superstructure at Support 1 is then calculated as (Eqn. 6.16.4.3-1)

$$\Omega = \frac{V_{lat}}{V} = \frac{1,034}{906} = 1.14$$

where  $V$  is the base shear at Support 1 from the modal response spectrum analysis. This factor is used to scale the seismic forces in components that should remain elastic like the shear connectors.

Superstructure drift (calculated as the ratio of the relative displacement between the flanges to the girder depth) is to be less than the limit specified in Table 6.16.4.5-1. It should be noted that the lateral displacement  $\Delta$  obtained from response spectrum analysis must be multiplied by the scale factor  $\Omega$  calculated above.

$$\Delta_{inelastic\_Support\_1} = \Delta_{Support\_1} \Omega = 0.38(1.14) = 0.43 \text{ in}$$

Therefore, the ductile superstructure drift is 0.89% which is less than the maximum drift limit of 4%.

### **Seismic Design of Top Chord**

Design of the top chord members follows after the diagonal members are designed. Detailed calculations are shown in Appendix 3-C under “Seismic Design of Top Chord”. The design axial force is the larger of

$$(Q_E)_{top\_chord} / R = 93.38 \text{ kips}$$

$$R_y P_{ny} \cos \theta = 197.6 \text{ kips}$$

where  $R_y P_{ny}$  is the nominal tensile resistance of diagonal member and  $\theta$  is the angle of inclination of the diagonal member with respect to the horizontal.

The width-to-thickness ratio is checked against Eqn. 6.16.4.5.1a-1. The slenderness ratios for in-plane and out-of-plane buckling are calculated as before (see Section 3.2.4) but are checked against Eqn. 6.16.4.5.1b-1. The compressive and tensile resistances are determined as specified in Articles 6.8 and 6.9, respectively, where  $\phi$  is taken equal to 1.0.

$$\text{Compressive Resistance: } \phi P_n = 650.54 \text{ kips} > 197.6 \text{ kips}$$

$$\text{Tensile Resistance: } \phi P_{ny} = 702 \text{ kips} > 197.6 \text{ kips}$$

The calculation of the expected plastic moment  $R_y M_p$  is also shown. Note that this was used in the calculation of the support lateral resistance as discussed in “Seismic Design of Diagonal Members”.

The axial force in the bottom chord is very small so only the local buckling check and  $R_y M_p$  calculation are shown.

### **Seismic Design of R/C Deck**

Detailed calculations are shown in Appendix 3-C under “Seismic Design of R/C Deck”.

The displacements used in deck classification are the displacements obtained from the modal response spectrum multiplied by the scale factor  $\Omega$ . The deck was classified as a rigid diaphragm as shown.

The total deck seismic shear force is calculated as follows (Eqn. 6.16.4.2-3)

$$F_{px} = \frac{W_{px}}{W} F_{lat} = \frac{737}{808} (2,418) = 2,205 \text{ kips}$$

The seismic shear at Support 1 is then calculated by ratio-and-proportion (see Section 3.2.4).

$$F_{px1} = \frac{V_{y1}}{\Sigma V} F_{px} = \frac{1,034}{2,418} (2,205) = 943 \text{ kips}$$

The deck transverse shear limits of Eqn. 6.16.4.2-2 do not apply for ductile superstructure. The design of the R/C deck for lateral shear then follows the same procedure as that discussed in Section 3.2.4.

### **Seismic Design of Shear Connectors**

The shear connector forces obtained from the response spectrum analysis were multiplied by the scale factor  $\Omega = 1.14$ . The design procedure is then the same as that discussed in Section 3.2.4. Detailed calculations are shown in Appendix 3-C under “Seismic Design of Shear Connectors”.

### **Connection Design**

Detailed calculations are shown in Appendix 3-C under “Connection Design”. The required resistance of the end connections is based on the diagonal member resistance with 10% increase to ensure that inelasticity is concentrated in the diagonal member only (Article 6.16.4.5.2).

### End and Middle Connection of Diagonal Member

The required axial resistance of the diagonal member end connection is calculated as

$$1.1R_y P_{ny} = 222.8 \text{ kips.}$$

The weld resistance per length is

$$R_r = \phi 0.6 F_{EXX} 0.707 s = 16.3 \text{ kip/in}$$

Therefore, the required weld length is

$$L_w = 222.8 / 16.3 = 13.6 \text{ in}$$

The provided weld length per leg is 8.0 in for a total weld length of 16.0 in.

According to Article 6.16.4.5.2, the end connection should be also capable of developing the flexural resistance of the member in addition to axial resistance. The moment at the end connection is calculated as follows

$$M = 1.1R_y F_y Z = 116.4 \text{ kip-in}$$

Therefore, the total weld shear flow coming from axial and flexural resistance of the diagonal member is

$$v = \frac{My}{I_p} + \frac{1.1R_y P_{ny}}{L_w} = 14.7 \text{ kip/in}$$

which is smaller than the weld resistance per length of  $R_r = 16.3 \text{ kip/in}$  calculated above.  $I_p$  in the above equation is the polar moment of inertia of the welds;  $y$  is the weld distance from its center of configuration; and  $L_w$  is the provided total length of weld.

The diagonal members shall be connected where the members cross by welds (Article 6.16.4.5.1). The required resistance of this connection is

$$0.25R_y P_{ny} = 0.25 * 202.50 = 50.6 \text{ kips}$$

The required total weld length is 3.1 in and the provided total weld length is 3.5 in (1.75 in per leg) as shown.

### End Connection of Top Chord

The required resistance of the top chord end connection is

$$1.1R_y P_{ny} \cos \theta = 217.3 \text{ kips}$$

where  $P_{ny}$  is the nominal tensile resistance of the diagonal member. The required weld length per leg is 5.23 in and the provided weld length per leg is 5.5 in for a total weld length of 22 in.

### Gusset Plate and Gusset Plate to Stiffener Connection

The gusset plate design shear is calculated from the vertical component of the diagonal member tensile resistance increased by 10%.

$$V = 1.1R_y P_{ny} \sin \theta = 57.39 \text{ kips}$$

where  $\theta$  is the angle of inclination of the diagonal member. The design moment ( $M = 222.40$  kip-in) is equal to the shear calculated above multiplied by the horizontal distance from the working point of the connection to the centroid of the bolt group.

The bolts connecting the gusset plate to the bearing stiffener are designed based on the combined shear and moment calculated above. The bolt resistance is determined from either the bolt shear resistance

$$\phi R_n = \phi(0.48 A_b) F_u$$

or the plate bearing resistance

$$\phi R_n = \phi(2.4 d_b t_p) F_u$$

with resistance factors  $\phi$  taken equal to 0.8.

The gusset plate resistance at gross and net sections is then evaluated against the combined shear and moment using the von Mises criterion

$$F_y = \sqrt{f_b^2 + 3f_v^2}$$

where  $f_v = V / A$        $f_b = M / Z$

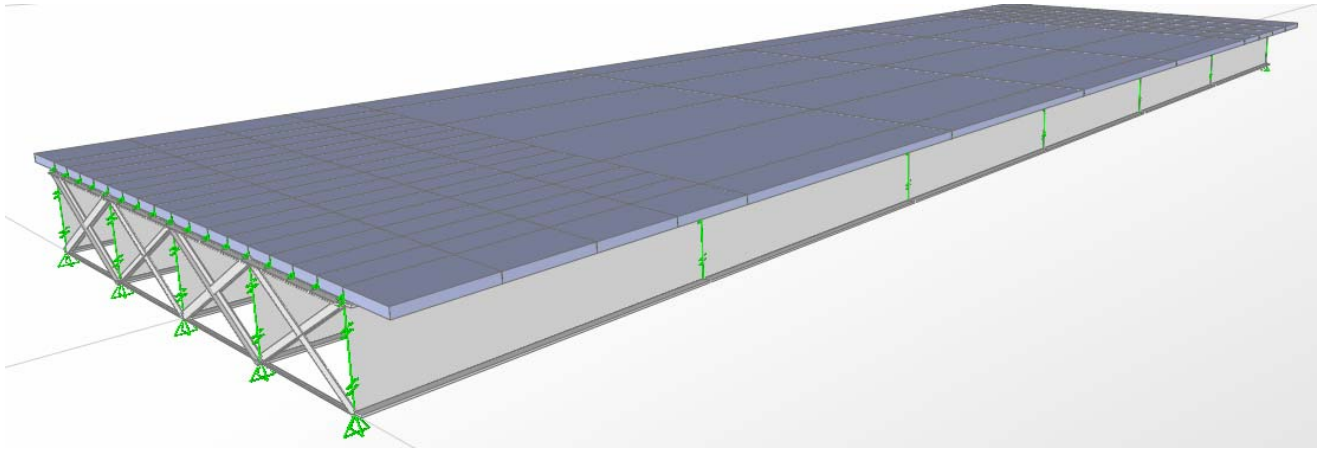
At the gross section, the plastic section modulus is given by

$$Z_g = \frac{td^2}{4}$$

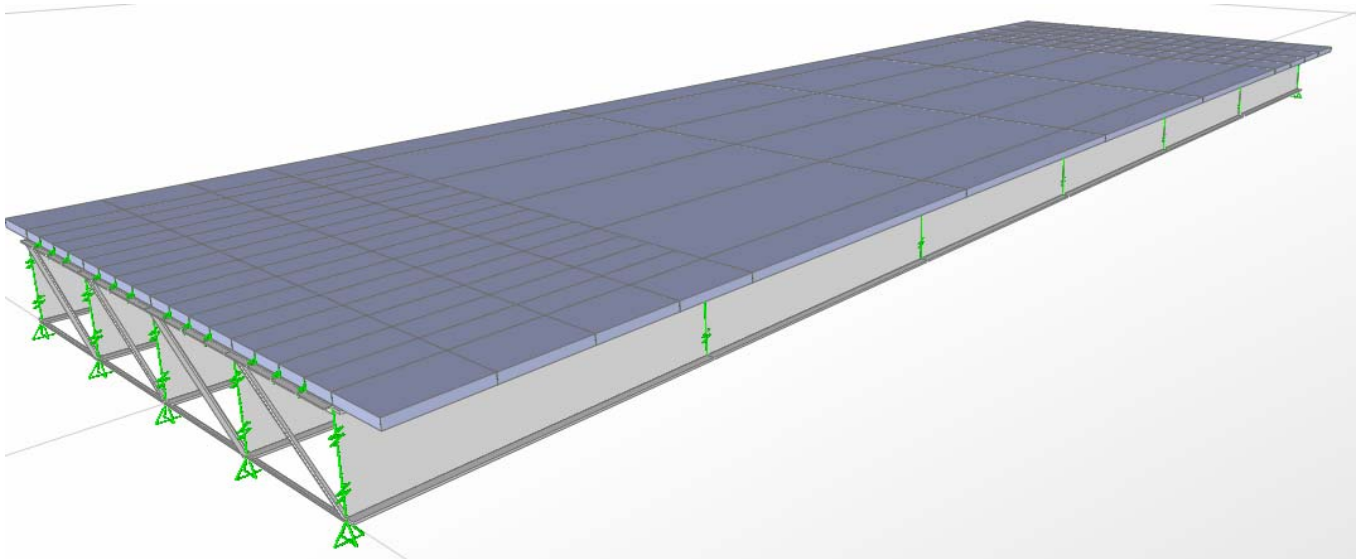
and at the net section it is given by

$$Z_n = Z_g \left( 1 - \frac{d_h}{s} \right)$$

where  $A$  = area at gross or net section,  $t$  is the gusset plate thickness,  $d$  is the height of gusset plate, and  $d_h$  is the bolt hole diameter ( $d_b + 1/16$  in).



(a) Single-span bridge with elastic superstructure



(b) Single-span bridge with inelastic superstructure

Figure 3-1 SAP2000 models of single-span bridges

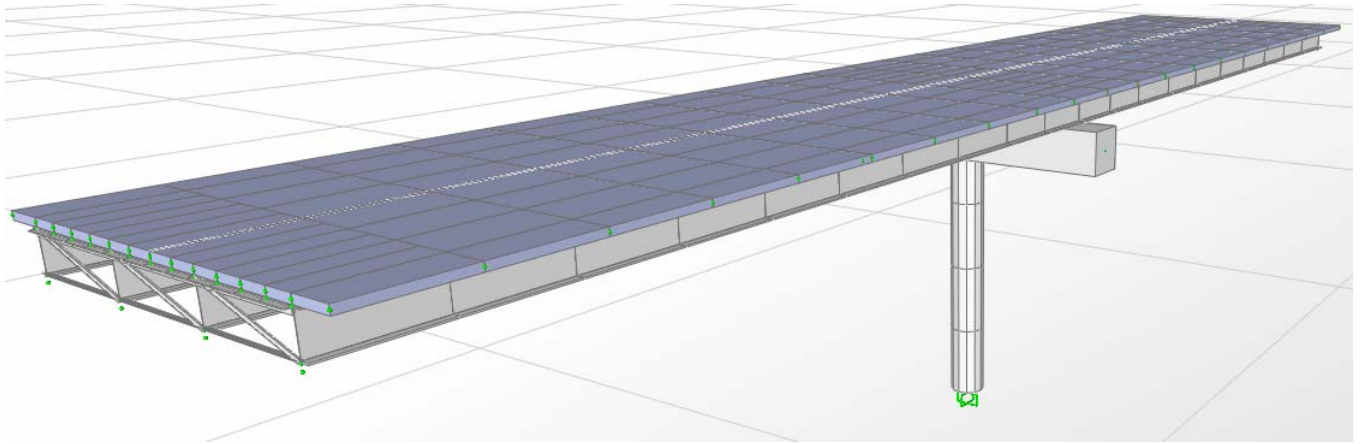


Figure 3-2 SAP2000 model of two-span bridge

## **Appendix 3-A**

### **Seismic Design of Single Span Bridge with Elastic Superstructure**

## Seismic Analysis and Design of Steel Plate Girder Bridges

AASHTO 2006

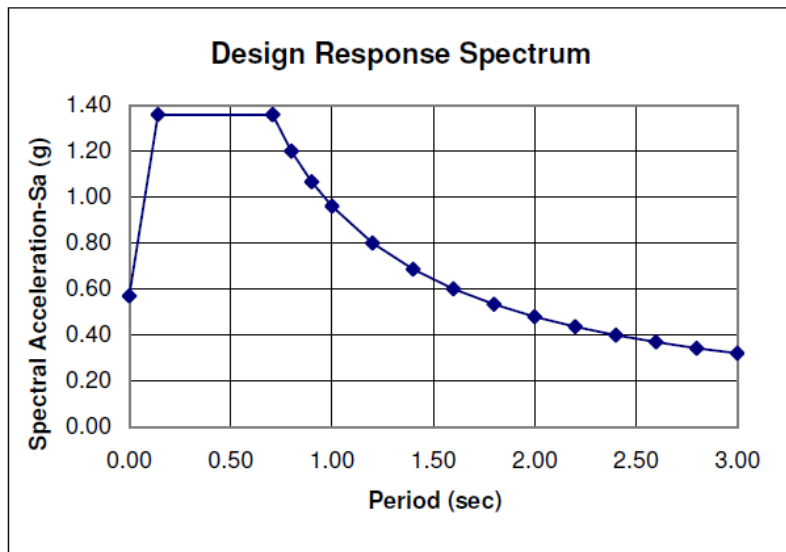
### Seismic Parameters

Latitude and Longitude =            37.79     -122.4  
 PGA =                                    0.572    g  
 $S_s$  =                                    1.36     g  
 $S_1$  =                                    0.641    g  
 Site Class =                            D  
 $F_{pga}$  =                                1        AASHTO Table 3.10.3.2-1  
 $F_a$  =                                    1        AASHTO Table 3.10.3.2-2  
 $F_v$  =                                    1.5      AASHTO Table 3.10.3.2-3

### Response Spectrum Curve

$F_{pga}$  PGA =                            0.572    g  
 $S_{DS}$  =                                    1.360    g  
 $S_{D1}$  =                                    0.962    g  
 $T_s$  =                                    0.707    sec  
 $T_o$  =                                    0.141    sec

T	Sa
0.00	0.57
0.14	1.36
0.71	1.36
0.71	1.36
0.80	1.20
0.90	1.07
1.00	0.96
1.20	0.80
1.40	0.69
1.60	0.60
1.80	0.53
2.00	0.48
2.20	0.44
2.40	0.40
2.60	0.37
2.80	0.34
3.00	0.32



### Seismic Weight Calculations

*Deck Dimensions:*

Deck Width =                            58        ft  
 Deck Length =                           165       ft  
 Deck Thickness =                        9.125    inch

*Steel Plate Girders:*

No. of Girder = 5  
 Top Flange Width = 18 in  
 Top Flange Thickness = 2 in  
 Web Depth = 78 in  
 Web Thickness = 0.875 in  
 Bottom Flange Width = 18 in  
 Bottom Flange Thickness = 2 in

Weight of Deck = 1092 kip  
 Weight of Girders = 394 kip  
 Seismic Weight = 1485 kip

**Modal Analysis**

SAP2000 File: [Span\\_1a\\_V12 \(12/26/2009\)](#)

TABLE: Modal Participating Mass Ratios							
Mode	Period	UX	UY	UZ	RX	RY	RZ
No	Sec	Unitless	Unitless	Unitless	Unitless	Unitless	Unitless
1	0.549	0.021	0.000	0.783	0.000	0.592	0.000
2	0.416	0.000	0.036	0.000	0.550	0.000	0.030
3	0.193	0.000	0.000	0.000	0.000	0.000	0.000
4	0.174	0.042	0.000	0.001	0.000	0.176	0.000
5	0.153	0.000	0.089	0.000	0.013	0.000	0.051
6	0.142	0.001	0.000	0.104	0.000	0.084	0.000
7	0.133	0.010	0.000	0.000	0.000	0.011	0.000
8	0.132	0.000	0.740	0.000	0.252	0.000	0.514
9	0.130	0.000	0.009	0.000	0.067	0.000	0.007
10	0.120	0.000	0.000	0.000	0.000	0.000	0.000
11	0.115	0.000	0.031	0.000	0.017	0.000	0.031
12	0.111	0.015	0.000	0.002	0.000	0.003	0.000

**Summary of Modal Response Spectrum Analysis**

Multimode Response Spectrum Analysis:

Base Shear at Support 1 = 842 kip  
 Lateral Displacement = 0.100 inch  
 Mid Deck Lateral Displacement = 0.251 inch  
 Base Shear at Support 2 = 680 kip  
 Lateral Displacement = 0.081 inch  
 Total Base Shear = 1,522 kip

### Seismic Design of Steel Plate Girder Bridge End Region

#### Deck Data

Concrete $f'_c$ =	4	ksi			
Deck Depth $t_s$ =	9.125	in			
Bridge Width $D$ =	58	ft			
Bridge Depth $d$ =	7.80	ft			
Wt of Deck =	6.62	k/ft	$W_{Deck} =$	1092	kip

#### Shear Connectors Data

Diameter $d$ =	0.88	in			
head dim =	0.38				
$F_u$ =	60	ksi			
Length =	5.06	in			
Provide $L$ =	5.375	in			
$L/d$ =	6.14	OK			

#### Bridge Geometrical Dimensions

Girder Spacing =	12	ft			
Span Length =	165	ft			
Haunch thickness =	2.5	in			
Top Flange $t$ =	2	in			
Top Flange $b$ =	18	in			
Web $t$ =	0.63	in			
Web $D$ =	78	in			
Bottom Flange $t$ =	2	in			
Bottom Flange $b$ =	18	in			
Bearing Stiffener $t$ =	1	in			
No. of Girders =	5				
Wt of Girders =	2.05	k/ft	$W_{Girders} =$	339	kip
Seismic Wt =	1430	kip			
$D/S$ =	0.54	Girder Depth / Spacing ratio			

### Seismic Design of R/C Deck

#### Seismic Base Shear at Supports

At Supp 1	$V_{y1} =$	842	kip
At Supp 2	$V_{y2} =$	680	kip
	$\Sigma V =$	1522	kip

#### Lateral Displacements

At Support 1, $\Delta_1 =$	0.100	in
At Support 2, $\Delta_2 =$	0.081	in
At mid Span, $\Delta_3 =$	0.251	in

$L/D = 2.84 = \text{span length} / \text{bridge width}$

$\Delta_{av} = 0.090 \text{ in} \quad 2\Delta_{av} = 0.180 \text{ in}$

$\Delta_{3net} = \Delta_3 - \Delta_{av} = 0.161 \text{ in}$

**Rigid Diaphragm, no special design for seismic.**

$W_{px} =$	1261	kips	$W =$	1,430	kips
$F = \Sigma V =$	1522	kips	$F_{px} =$	1342	kips
$F_{px1} =$	742	kips			

Limiting  $F_{px}$ :  $0.2S_{DS}W_{px} = 343$  kips  
 $0.4S_{DS}W_{px} = 686$  kips

Control  $F_{px1} = 686$  kips

**Shear Demand at Support 1**

Shear Demand = 11.83 k/ft

**Concrete Contribution:**

$\phi V_c = 0.75 * t_s * 12 * 2 * \text{SQRT}(f'_c)$  k/ft

$\phi V_c = 10.39$  k/ft

Reqd.  $A_s = 0.032$  in<sup>2</sup>/ft

Spacing of # 5 = 116.4 in

Provided s = 18 in

$\phi V_s = 9.3$  k/ft

$V_u = 19.69$  k/ft

**D/C = 0.60 OK!**

**Zone of Reinforcement**

Loc. Zero Shear = 86.14 ft From Support 1

Length of Reinf.  $L_1 = 10.5$  ft

Loc. (ft)	$V_{Demand}$	$V_{Demand}$	$V_{Resistance}$	$V_{Resistance}$
0.00	11.83	-11.83	19.69	-19.69
10.48	10.39	-10.39	19.69	-19.69
10.48	10.39	-10.39	10.39	-10.39
86.14	0.00	0.00		
161.81	-10.39	10.39	10.39	-10.39
161.81	-10.39	10.39	19.69	-19.69
165.00	-10.83	10.83	19.69	-19.69

**Shear Demand at Support 2**

Shear Demand = 10.83 k/ft

Reqd.  $A_s = 0.010$  in<sup>2</sup>/ft

Spacing of # 5 = 382.2 in

Provided s = 18 in

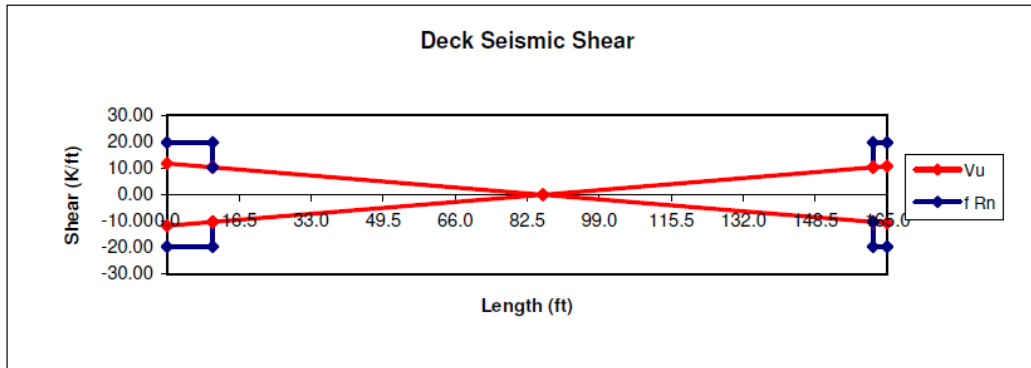
$\phi V_s = 9.30$  k/ft

$V_u = 19.69$  k/ft

**D/C = 0.55 OK!**

Loc. of Zero Shear = 78.86 ft From Support 2

Length of Reinf.  $L_2 = 3.19$  ft



**Seismic Design of Shear Connectors**

$A_{sc} = 0.60$  in<sup>2</sup>

$h_{eff} = 5.00$  in

**Shear Resistance**

$$A_{sc}F_u = 36.08 \text{ kip} \quad \text{Fracture of Connector}$$

$$E_c = 1820(f'_c)^{1/2} = 3640.00 \text{ ksi}$$

$$Q_n = 0.5A_{sc}(f'_cE_c)^{1/2} = 36.28 \text{ kip} \quad \text{Crushing of Concrete}$$

$$Q_n = \min(Q_n, A_{sc}F_u) = 36.08 \text{ kip}$$

$$Q_r = 0.85Q_n = 30.67 \text{ kips} \quad \text{Available Shear Resistance}$$

**Tensile Resistance Calculations**

For 1 Stud only

$$N_b = 0.76f'_c{}^{1/2}h_{eff}{}^{1.5} = 16.99 \text{ kip}$$

$$N_n = \min(N_b, A_{sc}F_u) = 16.99 \text{ kip}$$

$$N_r = 0.75 N_n = 12.75 \text{ kip}$$

$$A_{NCO} = 9 h_{eff}{}^2 = 225.00 \text{ in}^2$$

For a group of 2 Studs (1 row of 2 studs/row)

$$\text{Trans. Spacing, } S = 7.00 \text{ in}$$

$$A_{NC} = 3h_{eff}(3h_{eff}+S) = 330.00 \text{ in}^2$$

$$N_n = A_{NC}/A_{NCO} N_b = 24.92 \text{ kip}$$

$$\text{Control } N_n = \min(N_n, 2A_{sc}F_u) = 24.92 \text{ kip}$$

$$N_r = 0.75N_n = 18.69 \text{ kip}$$

For a group of 4 studs (2 rows of 2 studs/row)

$$\text{Long Spacing, } L = 4.00 \text{ in}$$

$$A_{NC} = (3h_{eff}+L)(3h_{eff}+S) = 418.00 \text{ in}^2$$

$$N_n = A_{NC}/A_{NCO} N_b = 31.57 \text{ kip}$$

$$\text{Control } N_n = \min(N_n, 4A_{sc}F_u) = 31.57 \text{ kip}$$

$$N_r = 0.75N_n = 23.68 \text{ kip}$$

For a group of 6 studs (3 rows of 2 studs/row)

$$A_{NC} = (3h_{eff}+2L)(3h_{eff}+S) = 506.00 \text{ in}^2$$

$$N_n = A_{NC}/A_{NCO} N_b = 38.22 \text{ kip}$$

$$\text{Control } N_n = \min(N_n, 6A_{sc}F_u) = 38.22 \text{ kip}$$

$$N_r = 0.75N_n = 28.66 \text{ kip}$$

For a group of 8 studs (4 rows of 2 studs/row)

$$A_{NC} = (3h_{eff}+3L)(3h_{eff}+S) = 594.00 \text{ in}^2$$

$$N_n = A_{NC}/A_{NCO} N_b = 44.86 \text{ kip}$$

$$\text{Control } N_n = \min(N_n, 8A_{sc}F_u) = 44.86 \text{ kip}$$

$$N_r = 0.75N_n = 33.65 \text{ kip}$$

Summary:

No.	Nr (kips)	Qr (kips)
1	12.75	30.67
2	18.69	61.33
4	23.68	122.67
6	28.66	184.00
8	33.65	245.34

**Connection Between Deck and Top Chord**

Location	N (kip)	Q <sub>L</sub> (kip)	Q <sub>T</sub> (kip)	Q <sub>u</sub>
Girder 1	15.00	118.19	33.20	122.77
A	2.60	0.38	48.01	48.01
B	1.29	0.03	40.80	40.80
C	2.50	0.23	44.25	44.25
Girder 2	4.57	56.71	66.30	87.24
D	2.50	0.23	44.25	44.25
E	0.59	0.01	44.32	44.32
F	2.45	0.25	49.02	49.02
Girder 3	0.01	0.02	72.18	72.18
G	2.45	0.25	49.02	49.02
H	0.59	0.01	44.32	44.32
I	2.96	0.29	52.47	52.47
Girder 4	4.58	56.72	66.30	87.25
J	2.50	0.23	44.25	44.25
K	1.29	0.03	40.80	40.80
L	2.60	0.38	48.01	48.02
Girder 5	15.09	118.20	33.20	122.78
		Σ	821	

**Shear Connector Interaction Equation**

$$(N_u/N_r)^{5/3} + (Q_u/Q_r)^{5/3} \leq 1$$

Location	Stud No.	$N_u$ kip	$Q_u$ kip	$N_r$ kip	$Q_r$ kip	D/C
Girder 1	6	15.00	122.77	28.66	184.00	0.85
A	2	2.60	48.01	18.69	61.33	0.70
B	2	1.29	40.80	18.69	61.33	0.52
C	2	2.50	44.25	18.69	61.33	0.62
Girder 2	4	4.57	87.24	23.68	122.67	0.63
D	2	2.50	44.25	18.69	61.33	0.62
E	2	0.59	44.32	18.69	61.33	0.58
F	2	2.45	49.02	18.69	61.33	0.72
Girder 3	4	0.01	72.18	23.68	122.67	0.41
G	2	2.45	49.02	18.69	61.33	0.72
H	2	0.59	44.32	18.69	61.33	0.58
I	2	2.96	52.47	18.69	61.33	0.82
Girder 4	4	4.58	87.25	23.68	122.67	0.63
J	2	2.50	44.25	18.69	61.33	0.62
K	2	1.29	40.80	18.69	61.33	0.52
L	2	2.60	48.02	18.69	61.33	0.70
Girder 5	6	15.09	122.78	28.66	184.00	0.85
$\Sigma$ Conn.	48					

**Seismic Design of Top Chord**

$Q_E / R = 69.52$  kip       $R = 1.00$

Control Force = 69.5 kip

**Material**       $F_y = 36$  ksi       $E = 29000$  ksi  
 $F_u = 58$  ksi

Length = 12 ft      Member Stitches @ 48 in

**Section**      2 L6X6X7/8      From Strength I Analysis and Design

**Section Properties of: L6X6X7/8**

$A = 9.75$  in<sup>2</sup>       $r_x = 1.81$  in       $I_y = 31.9$  in<sup>4</sup>  
 $x = 1.81$  in       $r_y = 1.81$  in       $t_{Gplate} = 1$  in

**Section Properties of: 2 L6X6X7/8**

$A = 19.5$  in<sup>2</sup>       $r_x = 1.81$  in       $r_{yy} = 2.93$  in

**Local Buckling:**

$b = 6$  in       $t = 0.875$  in       $b/t = 6.86$   
 $b/t \leq 0.45(E/F_y)^{1/2} = 12.77$       **Compact Section**

**Slenderness Ratio:**

In plane Buckling:       $L = 48$  in      buckling length for in-plane buckling  
 $(KL)_x = 40.8$  in  
 $(KL/r)_x = 22.54$

Out-of-plane Buckling:  $(KL)_y = 122.4$  in  
 $(a/r_{ib}) = 26.52$   
 $\alpha = 1.28$   
 $(KL/r)_y = 41.72$

Relative Shear Deformations  
 $h = 4.62$  in  
 $\alpha^2/(1+\alpha^2) = 0.62$   
 $(KL/r)_{ym} = 45.80$

Control  $KL/r = 45.80$

**Axial Capacity:**

Compression:  $\lambda = 0.26$   
 $P_{n1} = 629$  kip  
 $\phi P_n = 629$  kip

$P_{n2} = 2341$  kip

Tension:  $\phi P_{ny} = 702$  kip

D/C: Comp. = 0.11 OK  
Tens. = 0.10 OK

**Seismic Design of Diagonal Member**

$Q_E / R = 118.54$  kip  
 $R = 1.00$

Material  $F_y = 36$  ksi  
 $R_y = 1.5$   
 $E = 29000$  ksi

**Geometrical Dimensions of Working Points**

Gusset Plate Dimensions:  $w = 15$  in  
 $t = 1$  in  
 $h = 16.00$  in

Vertical Dimensions = 74 in  
Horizontal Dimensions = 144 in  
Length L = 13.49 ft

**Section 1 L8x4x3/4**

$A = 8.44$  in<sup>2</sup>  
 $r_x = 2.55$  in  
 $Z_x = 10.9$  in<sup>3</sup>

**Local Buckling:**

$b = 8$  in  
 $t = 0.75$  in  
 $b/t = 10.67$   
 $b/t \leq 0.45\text{SQRT}(E/F_y) = 12.77$  Compact Section

**Slenderness ratio:**

Buckling Length = 161.90 in  
For Equal-Leg Angles and Unequal-Leg Angles Connected through the Longer Leg  
 $(L/r)_x = 53.97$   
Effective Slenderness Ratio  
 $(KL/r)_{\text{eff}} = 112$   
governing  $(KL/r)_{\text{eff}} = 112$   
99

**Axial Capacity:**

Compression:  $\lambda = 1.59$   
 $P_{n1} = 157$  kip  
 $\phi P_n = 157$  kip

$P_{n1} = 168$  kip

Tension:  $\phi P_{ny} = 304$  kips

D/C: Comp. = 0.76 OK  
Tens. = 0.39 OK

### Connection Design

#### Diagonal Member

$Q_E = 118.54$  kip       $R = 0.8$

Section: L8x4x3/4       $b = 8$  in       $t = 0.75$  in

#### End Connection

Axial Force =  $Q_E / R = 148.2$  kip  
Max Weld Size = 0.6875 in  
Use: weld Size  $s = 0.688$  in  
 $R_r = \phi 0.6F_{EXX} 0.707s = 16.3$  k/in      weld resistance per length  
Total Weld Length = 9.07 in      reqd total weld length  
Per Leg = 4.54 in      reqd weld length per leg  
Weld Length/leg = 5.00 in      provided weld per leg

#### Top Chord Member

$Q_E = 69.516$  kip       $R = 0.8$

Section: 2 L6X6X7/8       $b = 6$  in       $t = 0.875$  in

#### End Connection

Axial Force =  $Q_E / R = 86.9$  kip  
Max Weld Size = 0.8125 in  
Use: weld Size  $s = 0.6875$  in  
 $R_r = \phi 0.6F_{EXX} 0.707s = 16.33$  k/in  
Total Weld Length = 5.32 in  
Per Leg = 1.33 in  
Weld Length/leg = 2.00 in

#### Gusset Plate Connection-Top Chord and Diagonal Member

Bearing Stiffener Width = 8.69 in  
Bearing Stiffener Thickness = 1 in  
Gusset Plate Thickness = 1 in

#### Diagonal Member Inclination:

Web depth = 78 in  
Top Chord = 6 in  
Bot Chord = 2 in  
Girder S = 144 in

#### Working Point (WP) Dimensions

Vertical Dim.:  $v = 74$  in  
Horizontal Dim.:  $h = 144$  in  
 $\sin \theta = 0.46$   
 $\cos \theta = 0.89$

Diagonal L from edge of Gusset to WP = 16.27 in

*Gusset Plate Dimensions:*

$t = 1$  in  
 $h = 15.93$  in  
 $h = 12$  in  
 Control  $h = 15.93$  in  
 $w = 14.47$  in  
 $h = 15.93$

Use:  $h = 16.00$  in  
Use:  $w = 15.00$  in

Steel Type = **A36** (A36 or A572)  
 $F_y = 36$  ksi  
 $F_u = 58$  ksi

*Gusset Plate Force Analysis:*

$V = 67.73$  kip vertical comp. of diagonal  $Q_E/R$   
 $M = 294.19$  k-in mom. @ c.g. of gusset =  $V \cdot x$

*A325-X Bolts Properties:*

$d = 0.875$  in  $A_b = 0.60$  in<sup>2</sup>  
 $F_u = 120$  ksi

Shear:  $\phi 0.48 A_b F_u = 27.71$  kip  
 Bearing:  $\phi 2.4 d_b t_p F_u = 97.44$  kip  
 Control:  $\phi F_v = 27.71$  kip

Use: No. of Bolts/line = 4  
 No of Lines = 2

**Bolts Analysis**

$I_p$  values for 2 lines of bolts,  $g = 3"$  and  $s = 3"$

3bolts/line **49.5** 4bolts/line **103.5** 5bolts/line **1180**

Control  $I_p = 103.50$   
 $y = 4.50$  in vert. dist of most stressed bolt from bolt c.g.

from V:  $F_{y1} = 8.47$  kip =  $V / \text{no. of bolts}$   
 from M:  $F_{y2} = 4.26$  kip =  $M \cdot (g/2) / I_p$  where  $g$  is the bolt hor. spacing  
 $F_x = 12.79$  kip =  $My / I_p$   
 $F_R = 18.05$  kip =  $[(F_x^2) + (F_{y1} + F_{y2})^2]^{1/2}$   
**D/C = 0.65 OK!**

**Gusset Plate Analysis**

$h = 16.00$  in  
 $t = 1$  in  
 $V = 67.73$  kip  
 $M = 294.19$  k-in

*At Gross Area:*

$A_g = 16.00$  in<sup>2</sup>  
 $Z_g = td^2/4 = 64.00$  in<sup>3</sup>  
 $f_v = V/A_g = 4.23$  ksi  
 $F_{cr} = (F_y^2 - 3f_v^2)^{1/2} = 35.25$  ksi  
 $\phi M_n = 2142.93$  k-in

*At Net Area*

$A_n =$	12.00	in <sup>2</sup>
$Z_n =$	44.00	in <sup>3</sup>
$f_v =$	5.64	ksi
$F_{cr} = (F_u^2 - 3f_v^2)^{1/2} =$	57.95	ksi
$\phi M_n =$	2039.89	k-in

Control

$\phi M_n =$	2039.89	k-in
D/C =	0.14	OK!

## **Appendix 3-B**

### **Seismic Design of Single-Span Bridge with Inelastic Superstructure**

## Seismic Analysis and Design of Steel Plate Girder Bridges

AASHTO 2007

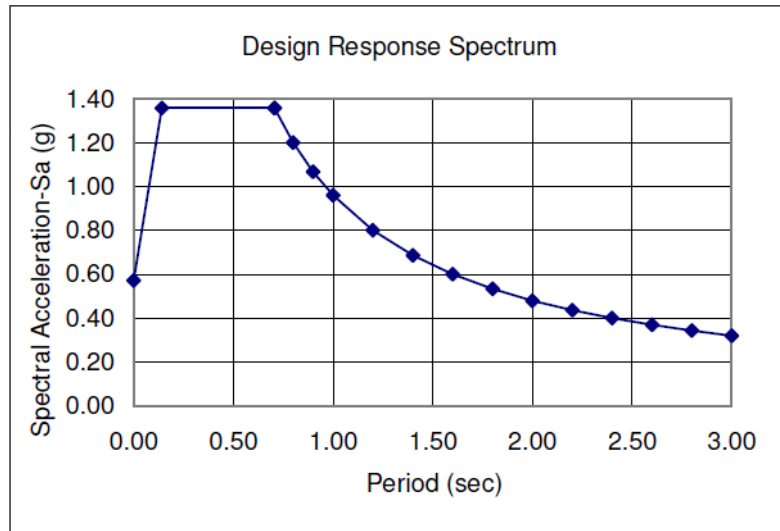
### Seismic Parameters

Latitude and Longitude =	37.79	-122.4
PGA =	0.572	g
$S_s$ =	1.36	g
$S_1$ =	0.641	g
Site Class =	D	
$F_{pga}$ =	1	AASHTO Table 3.10.3.2-1
$F_a$ =	1	AASHTO Table 3.10.3.2-2
$F_v$ =	1.5	AASHTO Table 3.10.3.2-3

### Response Spectrum Curve

$F_{pga}$ PGA =	0.572	g
$S_{DS}$ =	1.360	g
$S_{D1}$ =	0.962	g
$T_s$ =	0.707	sec
$T_o$ =	0.141	sec

T	Sa
0.00	0.57
0.14	1.36
0.71	1.36
0.71	1.36
0.80	1.20
0.90	1.07
1.00	0.96
1.20	0.80
1.40	0.69
1.60	0.60
1.80	0.53
2.00	0.48
2.20	0.44
2.40	0.40
2.60	0.37
2.80	0.34
3.00	0.32



### Seismic Weight

*Deck Dimensions:*

Deck Width =	58	ft
Deck Length =	165	ft
Deck Thickness =	9.125	inch

*Steel Plate Girders:*

No. of Girder = 5  
 Top Flange Width = 18 inch  
 Top Flange Thickness = 2 inch  
 Web Depth = 78 inch  
 Web Thickness = 0.625 inch  
 Bottom Flange Width = 18 inch  
 Bottom Flange Thick = 2 inch

Weight of Deck = 1092 kip  
 Weight of Girders = 339 kip  
 Seismic Weight = 1431 kip

**Modal Analysis**

SAP 2000 File: [Span\\_1c](#)

TABLE: Modal Participating Mass Ratios							
Mode	Period	UX	UY	UZ	RX	RY	RZ
No	Sec	Unitless	Unitless	Unitless	Unitless	Unitless	Unitless
1	0.561	0.020	0.000	0.788	0.000	0.597	0.000
2	0.436	0.000	0.041	0.000	0.548	0.000	0.043
3	0.211	0.000	0.001	0.001	0.000	0.003	0.000
4	0.209	0.000	0.000	0.000	0.000	0.029	0.000
5	0.207	0.000	0.917	0.000	0.256	0.000	0.615
6	0.196	0.000	0.000	0.046	0.000	0.034	0.000
7	0.183	0.033	0.000	0.000	0.000	0.157	0.000
8	0.179	0.000	0.006	0.000	0.005	0.000	0.004
9	0.172	0.000	0.000	0.000	0.069	0.000	0.000
10	0.168	0.002	0.000	0.000	0.000	0.006	0.000
11	0.155	0.000	0.005	0.000	0.007	0.000	0.001
12	0.150	0.003	0.000	0.058	0.000	0.048	0.000

**Summary of Modal Response Spectrum Analysis**

Model w/ Tensile End Cross Frames Only

Base Shear at Support 1 = 997 kip  
 Lateral Displacement @ Support1 = 0.48 in  
 Mid Deck Lateral Displacement = 0.60 in  
 Base Shear at Support 2 = 826 kip  
 Lateral Displacement @ Support 2 = 0.40 in  
 Total Base Shear = 1,823 kip

Based on Design

Base Shear at Support 1 = 1,066 kip  
 Base Shear at Support 2 = 883 kip  
 Total Base Shear = 1,950 kip  
 Lateral Displacement @ Sup 1 = 0.51 in  
 Lateral Displacement @ Sup 2 = 0.43 in  
 Lateral Displacement @ Mid = 0.64 in

### Seismic Design of Steel Plate Girder Bridge End Region

#### Deck Data

Concrete $f'_c$ =	4	ksi		
Deck Depth $t_s$ =	9.125	in		
Bridge Width $D$ =	58	ft		
Bridge Depth $d$ =	7.80	ft		
Wt of Deck =	6.62	k/ft	$W_{Deck} =$	1092 kip

#### Shear Connectors Data

Diameter $d$ =	1.250	in
head dim =	0.375	in
$F_u$ =	60	ksi
Length =	5.06	in
Provide $L$ =	6.5	in
$L/d$ =	5.20	OK

#### Bridge Geometrical Dimensions

Girder Spacing =	12	ft		
Span Length =	165	ft		
Haunch thickness =	2.5	in		
Top Flange $t$ =	2	in		
Top Flange $b$ =	18	in		
Web $t$ =	0.63	in		
Web $D$ =	78	in		
Bottom Flange $t$ =	2	in		
Bottom Flange $b$ =	18	in		
Bearing Stiffener $t$ =	1	in		
No. of Girders =	5			
Wt of Girders =	2.05	k/ft	$W_{Girders} =$	339 kip
Seismic Wt =	1430	kip		
$D/S$ =	0.54	Girder Depth / Spacing ratio		

### Seismic Design of R/C Deck

#### Seismic Base Shear at Support

At Supp 1	$V_{y1} =$	1,066	kip
At Supp 2	$V_{y2} =$	883	kip
	$\Sigma V$	1950	kip

#### Lateral Displacements

At Support 1, $\Delta_1 =$	0.51	in
At Support 2, $\Delta_2 =$	0.43	in
At mid Span, $\Delta_3 =$	0.64	in

$$L/D = 2.84 = \text{span length} / \text{bridge width}$$

$$\Delta_{av} = 0.470 \text{ in} \quad 2\Delta_{av} = 0.941 \text{ in}$$

$$\Delta_{3net} = \Delta_3 - \Delta_{av} = 0.171 \text{ in}$$

**Rigid Diaphragm, no special design for seismic**

$W_{px} = 1261$  kip  
 $F_{lat} = \Sigma V = 1950$  kips  
 $F_{px1} = 940$  kip

$W = 1,430$  kip  
 $F_{px} = 1719$  kip

Control  $F_{px1} = 940$  kip

**Shear Demand at Support 1**

Shear Demand = 16.21 k/ft

**Concrete Contribution:**

$\phi V_c = 0.75 * t_s * 12 * 2 * \text{SQRT}(f'_c)$  k/ft  
 $\phi V_c = 10.39$  k/ft  
 Req'd.  $A_s = 0.129$  in<sup>2</sup>/ft  
 Spacing of # 5 = 28.8 in  
 Provided s = 12 in  
 $\phi V_s = 13.95$  k/ft  
 $V_u = 24.34$  k/ft  
**D/C = 0.67 OK!**

Location	$V_{Demand}$	$V_{Demand}$	$V_{Resistance}$	$V_{Resistance}$
0.00	16.21	-16.21	24.34	-24.34
30.54	10.39	-10.39	24.34	-24.34
30.54	10.39	-10.39	10.39	-10.39
85.07	0.00	0.00		
139.59	-10.39	10.39	10.39	-10.39
139.59	-10.39	10.39	24.34	-24.34
165.00	-15.23	15.23	24.34	-24.34

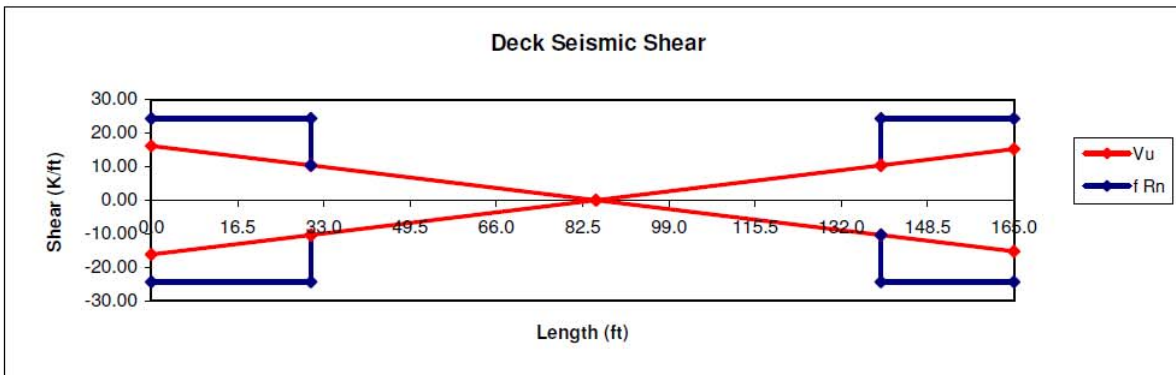
**Zone of Reinforcement**

Loc. Zero Shear = 85.07 ft From Support 1  
 Length of Reinf.  $L_1 = 30.5$  ft

**Shear Demand at Support 2**

Shear Demand = 15.23 k/ft  
 Req'd.  $A_s = 0.108$  in<sup>2</sup>/ft  
 Spacing of # 5 = 34.6 in  
 Provided s = 12 in  
 $\phi V_s = 13.95$  k/ft  
 $V_u = 24.34$  k/ft  
**D/C = 0.63 OK!**

Loc. of Zero Shear = 79.93 From Support 2  
 Length of Reinf.  $L_2 = 25.41$  ft



**Seismic Design of Shear Connectors**

$A_{sc} = 1.23$  in<sup>2</sup>  
 $h_{eff} = 6.13$  in

**Shear Resistance**

$$A_{sc}F_u = 73.63 \text{ kip}$$

$$E_c = 1820(f'_c)^{1/2} = 3640.00 \text{ ksi}$$

$$Q_n = 0.5A_{sc}(f'_cE_c)^{1/2} = 74.04 \text{ kip}$$

$$Q_n = \min(Q_n, A_{sc}F_u) = 73.63 \text{ kip}$$

$$Q_r = 0.85Q_n = 62.59 \text{ kips}$$

Fracture of Connector

Crushing of Concrete

Available Shear Resistance

**Tensile Resistance**

*For 1 Stud only*

$$N_b = 0.76f'_c{}^{1/2}h_{eff}{}^{1.5} = 23.04 \text{ kip}$$

$$N_n = \min(N_b, A_{sc}F_u) = 23.04 \text{ kip}$$

$$N_r = 0.75 N_n = 17.28 \text{ kip}$$

$$A_{NCO} = 9 h_{eff}{}^2 = 337.64 \text{ in}^2$$

*For a group of 2 Studs (1 row of 2 studs/row)*

$$\text{Trans. Spacing, } S = 7.00 \text{ in}$$

$$A_{NC} = 3h_{eff}(3h_{eff}+S) = 466.27 \text{ in}^2$$

$$N_n = A_{NC}/A_{NCO} N_b = 31.82 \text{ kip}$$

$$\text{Control } N_n = \min(N_n, 2A_{sc}F_u) = 31.82 \text{ kip}$$

$$N_r = 0.75N_n = 23.86 \text{ kip}$$

*For a group of 4 studs (2 rows of 2 studs/row)*

$$\text{Long Spacing, } L = 4.00 \text{ in}$$

$$A_{NC} = (3h_{eff}+L)(3h_{eff}+S) = 567.77 \text{ in}^2$$

$$N_n = A_{NC}/A_{NCO} N_b = 38.75 \text{ kip}$$

$$\text{Control } N_n = \min(N_n, 4A_{sc}F_u) = 38.75 \text{ kip}$$

$$N_r = 0.75N_n = 29.06 \text{ kip}$$

*For a group of 6 studs (3 rows of 2 studs/row)*

$$A_{NC} = (3h_{eff}+2L)(3h_{eff}+S) = 669.27 \text{ in}^2$$

$$N_n = A_{NC}/A_{NCO} N_b = 45.67 \text{ kip}$$

$$\text{Control } N_n = \min(N_n, 6A_{sc}F_u) = 45.67 \text{ kip}$$

$$N_r = 0.75N_n = 34.25 \text{ kip}$$

*For a group of 8 studs (4 rows of 2 studs/row)*

$$A_{NC} = (3h_{eff}+3L)(3h_{eff}+S) = 770.77 \text{ in}^2$$

$$N_n = A_{NC}/A_{NCO} N_b = 52.60 \text{ kip}$$

$$\text{Control } N_n = \min(N_n, 8A_{sc}F_u) = 52.60 \text{ kip}$$

$$N_r = 0.75N_n = 39.45 \text{ kip}$$

*Summary:*

No.	Nr (kips)	Qr (kips)
1	17.28	62.59
2	23.86	125.17
4	29.06	250.35
6	34.25	375.52
8	39.45	500.69

**Connection Between Deck and Top Chord**

$$\Omega = \text{Scale Factor Based on Diagonal Member Design} = 1.07$$

Location	N (kip)	Q <sub>L</sub> (kip)	Q <sub>T</sub> (kip)
<b>Girder 1</b>			
A	9.68	1.82	28.52
B	3.29	0.08	53.65
C	21.54	0.46	71.56
<b>Girder 2</b>			
D	23.01	1.25	88.05
E	0.77	0.04	64.31
F	20.95	0.68	89.66
<b>Girder 3</b>			
G	21.15	0.74	93.27
H	0.37	0.03	70.25
I	20.36	1.21	93.40
<b>Girder 4</b>			
J	21.54	0.50	108.48
K	8.20	0.08	101.49
L	8.54	2.00	109.16

$\Omega N_u$	$\Omega Q_L$	$\Omega Q_T$	$\Omega Q_u$
10.35	1.95	30.49	30.55
3.51	0.08	57.36	57.36
23.03	0.49	76.51	76.51
0.00	0.00	0.00	
24.61	1.34	94.15	94.16
0.83	0.04	68.76	68.76
22.40	0.72	95.87	95.87
0.00	0.00	0.00	
22.62	0.79	99.73	99.73
0.40	0.03	75.11	75.11
21.77	1.29	99.86	99.87
0.00	0.00	0.00	
23.03	0.53	115.99	115.99
8.77	0.09	108.51	108.51
9.13	2.14	116.71	116.73

**Shear Connector Interaction Equation**

$$(N_u/N_r)^{5/3} + (Q_u/Q_r)^{5/3} \leq 1$$

Location	Stud No.	$\Omega N_u$ kip	$\Omega Q_u$ kip	$N_r$ kip	$Q_r$ kip	D/C ratio
<b>Girder 1</b>						
A	4	10.35	30.55	29.06	250.35	0.21
B	4	3.51	57.36	29.06	250.35	0.12
C	4	23.03	76.51	29.06	250.35	0.82
<b>Girder 2</b>						
D	4	24.61	94.16	29.06	250.35	0.95
E	4	0.83	68.76	29.06	250.35	0.12
F	4	22.40	95.87	29.06	250.35	0.85
<b>Girder 3</b>						
G	4	22.62	99.73	29.06	250.35	0.87
H	4	0.40	75.11	29.06	250.35	0.14
I	4	21.77	99.87	29.06	250.35	0.83
<b>Girder 4</b>						
J	4	23.03	115.99	29.06	250.35	0.96
K	4	8.77	108.51	29.06	250.35	0.38
L	4	9.13	116.73	29.06	250.35	0.43
$\Sigma$ Conn.	48	Total number of shear connectors on all top chords				

**Seismic Design of Top Chord**

$Q_e/R = 74.46$  kip      Based on Diagonal Member  $R_y P_{ny} \cos \theta = 184.1$  kip  
 Control Force = 184.1 kip

**Material**       $F_y = 36$  ksi       $E = 29000$  ksi  
 $F_u = 58$  ksi  
 $R_y = 1.5$

Length = 12 ft      Member Stitches @ 48 in

**Section**      2 L6X6X7/8      From Strength I Analysis and Design

Section Properties of: L6X6X7/8

$A = 9.75$  in<sup>2</sup>       $r_x = 1.81$  in       $I_y = 31.9$  in<sup>4</sup>  
 $x = 1.81$  in       $r_y = 1.81$  in       $t_{Gplate} = 1$  in

Section Properties of: 2 L6X6X7/8

$A = 19.5$  in<sup>2</sup>       $r_x = 1.81$  in       $r_{yy} = 2.93$  in

**Local Buckling:**

$b = 6$  in       $t = 0.875$  in       $b/t = 6.86$   
 $b/t \leq 0.3(E/F_y)^{1/2} = 8.51$       **Seismically Compact Section**

**Slenderness Ratio:**

In plane Buckling:       $L = 48$  in      buckling length for in-plane buckling  
 $(KL)_x = 40.8$  in  
 $(KL/r)_x = 22.54$

Out-of-plane Buckling:  $(KL)_y = 122.4$  in      Relative Shear Deformations  
 $(a/r_b) = 26.52$        $h = 4.62$  in  
 $\alpha = 1.28$        $\alpha^2/(1+\alpha^2) = 0.62$   
 $(KL/r)_y = 41.72$        $(KL/r)_{ym} = 45.80$

Control  $KL/r = 45.80$   
 $KL/r \leq 4*(E/F_y)^{1/2} = 113.53$       **Seismic Slenderness Ratio Ok**

**Axial Capacity:**

Compression:  $\lambda = 0.26$   
 $P_{n1} = 629.10$  kip       $P_{n2} = 2341.29$  kip  
 $\phi P_n = 629.10$  kip       $\phi = 1.0$

Tension:  $\phi P_{ny} = 702.00$  kip       $\phi = 1.0$

D/C: Comp. = **0.29 OK**  
Tens. = **0.26 OK**

**Flexural Resistance:**  $Z_x = 27.4$  in<sup>3</sup>  
 $M_p = 986.40$  k-in  
 $R_y M_p = M_{pe} = 1479.6$  k-in

**Seismic Design of Bottom Chord**

$Q_E/R = 0$  kip

**Material**       $F_y = 36.00$  ksi       $E = 29000$  ksi  
 $F_u = 58.00$  ksi       $R_y = 1.5$

**Section**      **2 L2x2x1/4**

**Local Buckling**  
 $b/t = 8.00$        $b/t \leq 0.3(E/F_y)^{1/2} = 8.51$       **Seismically Compact Section**

**Flexural Resistance:**  $Z_x = 0.88$  in<sup>3</sup>  
 $M_p = 31.68$  k-in  
 $R_y M_p = M_{pe} = 47.52$  k-in

**Seismic Design of Diagonal Member**

$Q_E = 264.84$  kip       $R = 3$        $Q_E/R = 88.3$  kip

**Material**       $F_y = 36$  ksi       $E = 29000$  ksi  
 $R_y = 1.5$

**Geometrical Dimensions of Working Points**

Gusset Plate Dimensions:  $w = 16.5$  in       $h = 12$  in  
 $t = 1.00$  in

Vertical Dimension = **66** in  
Horizontal Dimension = **144** in  
Length L = **13.20** ft

**Section** 1 L4x4x1/2  
 $A = 3.75 \text{ in}^2$   $r_z = 0.776 \text{ in}$   $Z_x = 1.96 \text{ in}^3$

**Local Buckling**  
 $b = 4 \text{ in}$   $t = 0.5 \text{ in}$   $b/t = 8.00$   
 $b/t \leq 0.3(E/F_y)^{1/2} = 8.51$  **Seismically Compact Section**

**Slenderness Ratio**  
 Buckling Length = 79.20 in Biased Buckling Over 1/2 Length  
 $(KL/r)_z = 86.76$   $K = 0.85$   
 $KL/r \leq 4*(E/F_y)^{1/2} = 113.53$  **Seismic Slenderness Ratio, Ok**

**Axial Capacity:**

**Compression:**  $\lambda = 1.42$  Note: use  $F_{ye} = R_y F_y$   
 $P_{n1} = 112.25 \text{ kip}$   $P_{n2} = 125.49 \text{ kip}$   
 $\phi P_n = 112.25 \text{ kip}$   $\phi = 1.0$

**Tension:**  $\phi R_y P_{ny} = 202.50 \text{ kips}$   $\phi = 1.0$

**Control Axial Capacity = 112.25 kips**  
**Seismic Demand  $Q_E = 88.28 \text{ kips}$**   
**Axial D/C Ratio = 0.79 OK**

**Lateral Capacity of Inelastic Superstructure**  
from inelastic response of diagonal members

Horizontal Comp  $F_x = 184.09 \text{ kip}$  Based on hor. comp. of  $R_y P_{ny}$   
 Horizontal Comp  $F_x = 30.61 \text{ kip}$  Based on hor. comp. of  $0.3P_n$   
 No. of Diagonals = 8  
 $\Sigma V = 859 \text{ kip}$  total lateral shear from diagonal members

contribution of chord members to lateral shear

**Top Chord:**

Distance from bearing to CL of Top Chord,  $h_1 = 74 \text{ in}$   
 Shear Contribution  $2R_y M_p / h_1 = 39.99 \text{ kip}$

**Bottom Chord:**

Distance from bearing to CL of Bot Chord,  $h_2 = 8 \text{ in}$   
 Shear Contribution  $2R_y M_p / h_2 = 11.88 \text{ kip}$

**Shear Contribution / bay = 51.87 kip**

**No of Bays = 4**

**Total Shear Contribution = 207 kips** from top & bot chord members

**Total Lateral Capacity at Support = 1066 kips** from diagonals+chord members

**Elastic Shear from Model analysis = 997 kip**

**$\Omega = \text{Scale Factor for Inelastic Superstructure} = 1.07$**

**Drift Check**

Lateral Displacement  $\Delta = 0.51 \text{ in}$  inelastic lateral displacement  
 Drift (%) =  $\Delta / h_{\text{girder}} = 0.55 \%$  **< 4%, OK!**

## Connection Design

### Diagonal Member

Section: **L4x4x1/2**                      **b = 4**    in                      **t = 0.5**    in

#### End Connection

Axial Force =	<b>222.8</b>	kip	based on $1.1R_y P_{ny}$ of diagonal member
Weld Size s =	<b>0.438</b>	in	assuming max. weld size
$R_r = \phi 0.6F_{EXX} 0.707s =$	<b>16.3</b>	k/in	weld resistance per length
Total Weld Length =	<b>13.6</b>	in	reqd total weld length
Per Leg =	<b>6.8</b>	in	reqd weld length per leg
Use: Weld Length/leg =	<b>8.00</b>	in	provided weld per leg
End Moment = $1.1R_y F_y Z_x =$	<b>116.4</b>	k-in	$1.1xM_p$ of diagonal member
Weld Ip =	<b>149.3</b>	in <sup>3</sup>	= $I_x + I_y$ of weld
Weld Shear flow, v =	<b>15.5</b>	k/in	from axial force & end moment
D/C = $v / R_r =$	<b>0.95</b>	<b>OK!</b>	

#### Middle Connection

0.25* $R_y P_{ny} =$	<b>50.6</b>	kip	
Weld Size s =	<b>0.438</b>	in	
Total Weld Length =	<b>3.1</b>	in	reqd weld length
Use: Weld Length =	<b>3.5</b>	in	provided weld length

### Top Chord

Section: **2 L6X6X7/8**                      **b = 6**    in                      **t = 0.875**    in

#### End Connection

Axial Force =	<b>202.5</b>	kip	based on $1.1R_y P_{ny} \cos \theta$ of diagonal member
Max Weld Size =	<b>0.8125</b>	in	
Weld Size s =	<b>0.4375</b>	in	
$\phi 0.6F_{EXX} 0.707 s =$	<b>10.39</b>	k/in	weld resistance per length
Total Weld Length =	<b>19.48</b>	in	reqd total weld length
Per Leg =	<b>4.87</b>	in	reqd weld length per leg
Weld Length/leg =	<b>5.00</b>	in	provided weld per leg

### Gusset Plate Connection-Top Chord and Diagonal Member

Bearing Stiffener Width =	<b>8.69</b>	in	
Bearing Stiffener Thickness =	<b>1</b>	in	
Gusset Plate Thickness =	<b>1</b>	in	

#### Diagonal Member Inclination

Web depth =	<b>78</b>	in	
Top Chord =	<b>6</b>	in	
Bot Chord =	<b>2</b>	in	
Girder S =	<b>144</b>	in	

#### Working Point (WP) Dimensions

Vertical Dim.: v =	<b>74</b>		
Horizontal Dim.: h =	<b>144</b>		
sin $\theta =$	<b>0.46</b>		
cos $\theta =$	<b>0.89</b>		

Diagonal L from edge of Gusset to WP = **19.27**    in

Gusset Plate Dimensions:

t = 1 in  
h = 8.81 in  
w = 17.14 in  
Use: h = 12 in  
Use: w = 16.5 in

Steel Type = A36 (A36 or A572)  
F<sub>y</sub> = 36 ksi  
F<sub>u</sub> = 58 ksi

Gusset Plate Force Analysis:

V = 101.81 kip vertical comp. of diagonal member = 1.1R<sub>y</sub>P<sub>ny</sub>sinθ  
M = 442.25 k-in mom. @ c.g. of gusset = V\*x

A325-X Bolts Properties:

d = 1.000 in A<sub>b</sub> = 0.79 in<sup>2</sup>  
F<sub>u</sub> = 120 ksi

Shear: φ 0.48 A<sub>b</sub> F<sub>u</sub> = 36.19 kip  
Bearing: φ 2.4d t F<sub>u</sub> = 111.36 kip  
Control: φ F<sub>v</sub> = 36.19 kip

Use: No. of Bolts/line = 4  
No of Lines = 2

**Bolts Analysis**

l<sub>p</sub> values for 2 lines of bolts, g = 3" and s = 3"

3bolts/line 49.5 4bolts/line 103.5 5bolts/line 1180  
l<sub>p</sub> = 103.5

l<sub>p</sub> values for 1 line of bolts s = 3"

3bolts/line 18 4bolts/line 45 5bolts/line 58.5  
l<sub>p</sub> = 45

Control l<sub>p</sub> = 103.50  
y = 4.50

vert. dist of most stressed bolt from bolt c.g.

from V: F<sub>y1</sub> = 12.73 kip = V / no. of bolts  
from M: F<sub>y2</sub> = 6.41 kip = M\*(g/2) / l<sub>p</sub> where g is the bolt hor. spacing  
F<sub>x</sub> = 19.23 kip = My/l<sub>p</sub>  
F<sub>R</sub> = 27.13 kip = [(F<sub>x</sub><sup>2</sup>) + (F<sub>y1</sub> + F<sub>y2</sub>)<sup>2</sup>]<sup>1/2</sup>  
D/C = 0.75 OK

**Gusset Plate Analysis**

h = 12 in  
t = 1 in  
V = 101.81 kip  
M = 442.25 k-inch

At Gross Area:

$$A_g = 12.00 \text{ in}^2$$

$$Z_g = td^2/4 = 36.00 \text{ in}^3$$

$$f_v = V/A_g = 8.48 \text{ ksi}$$

$$F_{cr} = (F_y^2 - 3f_v^2)^{1/2} = 32.86 \text{ ksi}$$

$$\phi M_n = 1123.95 \text{ k-in}$$

At Net Area

$$A_n = 7.50 \text{ in}^2$$

$$Z_n = 23.25 \text{ in}^3$$

$$f_v = 13.57 \text{ ksi}$$

$$F_{cr} = (F_u^2 - 3f_v^2)^{1/2} = 57.88 \text{ ksi}$$

$$\phi M_n = 1076.62 \text{ k-in}$$

Control

$$\phi M_n = 1076.62 \text{ k-in}$$

$$D/C = 0.41 \text{ OK}$$

## **Appendix 3-C**

### **Seismic Design of Two-Span Bridge with Inelastic Superstructure**

## Seismic Analysis and Design of Steel Plate Girder Bridges

AASHTO 2006

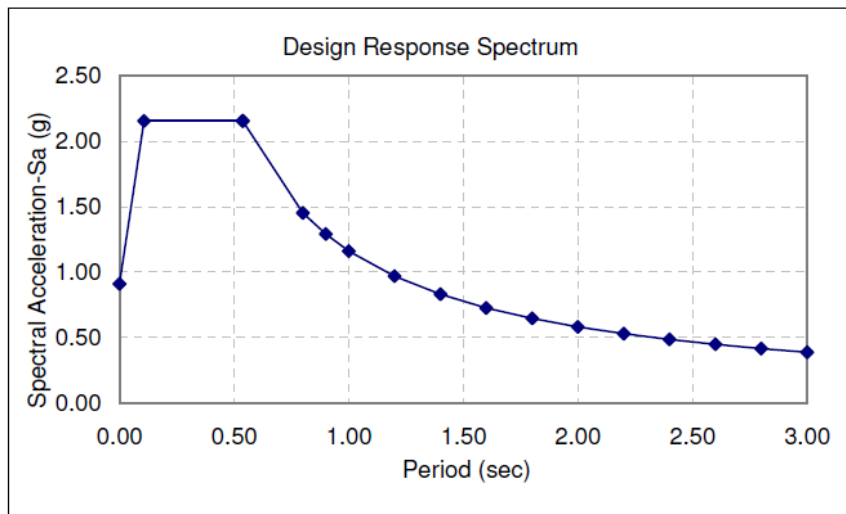
### Seismic Parameters

Latitude and Longitude =	34.1099	-117.721
PGA =	0.91	g
$S_s$ =	2.157	g
$S_1$ =	0.774	g
Site Class =	D	
$F_{pga}$ =	1	AASHTO Table 3.10.3.2-1
$F_a$ =	1	AASHTO Table 3.10.3.2-2
$F_v$ =	1.5	AASHTO Table 3.10.3.2-3

### Response Spectrum Curve

$F_{pga}$ PGA =	0.910	g
$S_{DS}$ =	2.157	g
$S_{D1}$ =	1.161	g
$T_s$ =	0.538	sec
$T_o$ =	0.108	sec

T	Sa
0.00	0.91
0.11	2.16
0.54	2.16
0.54	2.16
0.80	1.45
0.90	1.29
1.00	1.16
1.20	0.97
1.40	0.83
1.60	0.73
1.80	0.65
2.00	0.58
2.20	0.53
2.40	0.48
2.60	0.45
2.80	0.41
3.00	0.39



### Seismic Weight

#### Deck Dimensions:

Deck Width =	37	ft
Deck Length =	180	ft
Deck Thickness =	8	inch

#### Steel Plate Girders:

No. of Girder =	4	
Top Flange Width =	18	inch
Top Flange Thickness =	1	inch
Web Depth =	36	inch
Web Thickness =	0.5	inch
Bottom Flange Width =	16	inch
Bottom Flange Thick =	1.5	inch

Weight of Deck = 666 kip  
 Weight of Girders = 147 kip  
 Seismic Weight = 813 kip

**Modal Analysis**

SAP2000File: Example 2\_CA\_TensionOnly

TABLE: Modal Participating Mass Ratios							
Mode	Period	UX	UY	UZ	RX	RY	RZ
No	Sec	Unitless	Unitless	Unitless	Unitless	Unitless	Unitless
1	2.418	0.973	0.000	0.000	0.000	0.000	0.000
2	0.371	0.000	0.009	0.000	0.802	0.000	0.007
3	0.343	0.000	0.000	0.000	0.000	0.128	0.000
4	0.308	0.000	0.000	0.000	0.000	0.000	0.001
5	0.238	0.000	0.002	0.654	0.000	0.512	0.002
6	0.237	0.000	0.885	0.002	0.006	0.001	0.689
7	0.163	0.000	0.001	0.000	0.005	0.000	0.001
8	0.129	0.000	0.000	0.000	0.000	0.000	0.000
9	0.122	0.000	0.000	0.001	0.000	0.001	0.000
10	0.098	0.001	0.000	0.000	0.000	0.027	0.000
11	0.092	0.000	0.000	0.000	0.000	0.000	0.010
12	0.091	0.000	0.000	0.053	0.000	0.041	0.000

**Summary of Modal Response Spectrum Analysis**

Model with Tension Cross Frames Only

Base Shear at Support 1 = 906 kip  
 Lateral Displacement @ Support 1 = 0.38 in  
 Mid Deck Lateral Displacement = 1.09 in between Supports 1 & 2

Base Shear at Support 2 = 307 kip  
 Lateral Displacement @ Support 2 = 1.42 in

Base Shear at Support 3 = 906 kip  
 Lateral Displacement @ Support 3 = 0.38 in  
 Mid Deck Lateral Displacement = 1.09 in between Supports 2 & 3

Total Base Shear = 2,119 kip

Based on Design

Base shear at Support 1 = 1,034 kip  
 Base Shear at Support 2 = 350 kip  
 Base Shear at Support 3 = 1034 kip  
 Total Base Shear = 2,418 kip  
 Lateral Displacement @ Sup 1 = 0.43 in  
 Lateral Displacement @ Sup 2 = 1.62 in  
 Lateral Displacement @ Sup 3 = 0.43 in

### Seismic Design of Steel Plate Girder Bridge End Region

#### Deck Data

Concrete $f'_c$ =	4	ksi			
Deck Depth $t_s$ =	8	in			
Bridge Width $D$ =	37	ft			
Bridge Depth $d$ =	4.04	ft			
Wt of Deck =	3.70	k/ft	$W_{Deck} =$	333	kip

#### Shear Connectors Data

Diameter $d$ =	1.250	in			
head dim =	0.375				
$F_u$ =	60	ksi			
Length =	5.00	in			
Provide $L$ =	5.5	in			
$L/d$ =	4.40	OK			

#### Bridge Geometrical Dimensions

Girder Spacing =	10	ft			
Span Length =	90	ft			
Haunch thickness =	2	in			
Top Flange $t$ =	1	in			
Top Flange $b$ =	16	in			
Web $t$ =	0.50	in			
Web $D$ =	36	in			
Bottom Flange $t$ =	1.5	in			
Bottom Flange $b$ =	16	in			
Bearing Stiffener $t$ =	1	in			
No. of Girders =	4		$W_{Girders} =$	71	kip/span
Wt of Girders =	0.79	k/ft			
Seismic $W_t$ =	808	kip			
$D/S$ =	0.30	Girder Depth / Spacing ratio			

### Seismic Design of R/C Deck

#### Seismic Base Shear at Support

At Supp 1	$V_y =$	1,034	kip	
At Supp 2	$V_y =$	350	kip	
At Supp 3	$V_y =$	1,034	kip	
	$\Sigma V =$	2418	kip	

#### Lateral Displacements

At Support 1, $\Delta_1 =$	0.43	in	
At Support 2, $\Delta_2 =$	1.62	in	
At Support 3, $\Delta_3 =$	0.43	in	
At mid Span, $\Delta_3 =$	1.09	in	

$L/D = 2.43$  = span length / bridge width

$\Delta_{av} = 1.03$  in       $2\Delta_{av} = 2.05$  in

$\Delta_{3net} = \Delta_3 - \Delta_{av} = 0.06$  in

#### Rigid Diaphragm, no special design for seismic

$W_{px} =$	737	kip	$W =$	808	kip
$F_{lat} = \Sigma V =$	2418	kips	$F_{px} =$	2205	kip
$F_{px1} =$	943	kip			

Control  $F_{px1} = 943$  kip

**Shear Demand at Support 1**

Shear Demand = 25.48 k/ft

**Concrete Contribution:**

$\phi V_c = 0.75 \cdot t_s \cdot 12 \cdot 2 \cdot \text{SQRT}(f'_c)$  k/ft  
 $\phi V_c = 9.11$  k/ft  
 Reqd.  $A_s = 0.364$  in<sup>2</sup>/ft  
 Spacing of # 5 = 10.2 in  
 Provided s = 9 in  
 $\phi V_s = 18.6$  k/ft  
 $V_u = 27.71$  k/ft  
**D/C = 0.92 OK!**

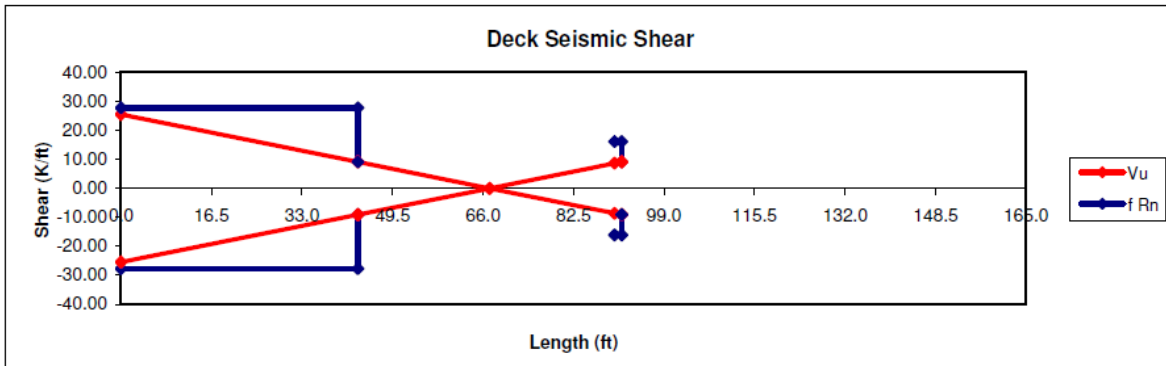
Location	$V_{\text{Demand}}$	$V_{\text{Demand}}$	$V_{\text{Resistance}}$	$V_{\text{Resistance}}$
0.00	25.48	-25.48	27.71	-27.70736
43.20	9.11	-9.11	27.71	-27.70736
43.20	9.11	-9.11	9.11	-9.10736
67.23	0.00	0.00		
91.26	-9.11	9.11	9.11	-9.10736
91.26	-9.11	9.11	16.08	-16.08236
90.00	-8.63	8.63	16.08	-16.08236

**Zone of Reinforcement**

Loc. Zero Shear = 67.23 ft From Support 1  
 Length of Reinf.  $L_1 = 43.2$  ft

**Shear Demand at Support 2**

Shear Demand = 8.63 k/ft  
 Reqd.  $A_s = -0.011$  in<sup>2</sup>/ft  
 Spacing of # 5 = -351.0 in \*negative means steel reinf not reqd  
 Provided s = 24 in  
 $\phi V_s = 6.98$  k/ft  
 $V_u = 16.08$  k/ft  
**D/C = 0.54 OK!**  
 Loc. of Zero Shear = 22.77 ft From Support 2  
 Length of Reinf.  $L_2 = -1.26$  ft



**Seismic Design of Shear Connectors**

$A_{sc} = 1.23$  in<sup>2</sup>  
 $h_{off} = 5.13$  in

**Shear Resistance**

$A_{sc} F_u = 73.63$  kip Fracture of Connector  
 $E_c = 1820(f'_c)^{1/2} = 3640.00$  ksi  
 $Q_n = 0.5 A_{sc} (f'_c E_c)^{1/2} = 74.04$  kip Crushing of Concrete  
 $Q_n = \min(Q_n, A_{sc} F_u) = 73.63$  kip  
 $Q_r = 0.85 Q_n = 62.59$  kips Available Shear Resistance

**Tensile Resistance**

*For 1 Stud only*

$$N_b = 0.76f_c^{1/2} h_{eff}^{1.5} = 17.64 \text{ kip}$$

$$N_n = \min(N_b, A_{sc} F_u) = 17.64 \text{ kip}$$

$$N_r = 0.75 N_n = 13.23 \text{ kip}$$

$$A_{NCO} = 9 h_{eff}^2 = 236.39 \text{ in}^2$$

*For a group of 2 Studs (1 row of 2 studs/row)*

$$\text{Trans. Spacing, } S = 7.00 \text{ in}$$

$$A_{NC} = 3h_{eff}(3h_{eff}+S) = 344.02 \text{ in}^2$$

$$N_n = A_{NC}/A_{NCO} N_b = 25.66 \text{ kip}$$

$$\text{Control } N_n = \min(N_n, 2A_{sc} F_u) = 25.66 \text{ kip}$$

$$N_r = 0.75 N_n = 19.25 \text{ kip}$$

*For a group of 4 studs (2 rows of 2 studs/row)*

$$\text{Long Spacing, } L = 4.00 \text{ in}$$

$$A_{NC} = (3h_{eff}+L)(3h_{eff}+S) = 433.52 \text{ in}^2$$

$$N_n = A_{NC}/A_{NCO} N_b = 32.34 \text{ kip}$$

$$\text{Control } N_n = \min(N_n, 4A_{sc} F_u) = 32.34 \text{ kip}$$

$$N_r = 0.75 N_n = 24.26 \text{ kip}$$

*For a group of 6 studs (3 rows of 2 studs/row)*

$$A_{NC} = (3h_{eff}+2L)(3h_{eff}+S) = 523 \text{ in}^2$$

$$N_n = A_{NC}/A_{NCO} N_b = 39.02 \text{ kip}$$

$$\text{Control } N_n = \min(N_n, 6A_{sc} F_u) = 39.02 \text{ kip}$$

$$N_r = 0.75 N_n = 29.26 \text{ kip}$$

*For a group of 8 studs (4 rows of 2 studs/row)*

$$A_{NC} = (3h_{eff}+3L)(3h_{eff}+S) = 612.52 \text{ in}^2$$

$$N_n = A_{NC}/A_{NCO} N_b = 45.70 \text{ kip}$$

$$\text{Control } N_n = \min(N_n, 8A_{sc} F_u) = 45.70 \text{ kip}$$

$$N_r = 0.75 N_n = 34.27 \text{ kip}$$

*Summary:*

No.	Nr (kips)	Qr (kips)
1	13.23	62.59
2	19.25	125.17
4	24.26	250.35
6	29.26	375.52
8	34.27	500.69

**Connection Between Deck and Top Chord**

$$\Omega = \text{Scale Factor Based of Diagonal Member Design} = 1.14$$

Location	N (kip)	Q <sub>L</sub> (kip)	Q <sub>T</sub> (kip)	$\Omega N_u$	$\Omega Q_L$	$\Omega Q_T$	$\Omega Q_u$
<b>Girder 1</b>							
A	5.12	0.49	57.42	5.84	0.56	65.52	65.52
B	10.14	0.08	49.25	11.57	0.09	56.20	56.20
C	10.92	0.07	70.09	12.46	0.07	79.97	79.97
<b>Girder 2</b>							
D	8.53	0.20	112.69	9.73	0.22	128.59	128.59
E	2.29	0.02	96.26	2.61	0.02	109.83	109.83
F	13.30	0.07	108.16	15.18	0.08	123.42	123.42
<b>Girder 3</b>							
G	12.40	0.08	119.85	14.15	0.09	136.76	136.76
H	1.96	0.07	104.67	2.23	0.08	119.43	119.43
I	5.29	0.12	155.31	6.03	0.14	177.22	177.22
<b>Girder 4</b>							

**Shear Connector Interaction Equation**

$$(N_u/N_r)^{5/3} + (Q_u/Q_r)^{5/3} \leq 1$$

Location	Stud No.	$\Omega_2 N_u$ kip	$\Omega_2 Q_u$ kip	N <sub>r</sub> kip	Q <sub>r</sub> kip	D/C ratio
<b>Girder 1</b>						
A	4	5.84	65.52	24.26	250.35	0.20
B	4	11.57	56.20	24.26	250.35	0.37
C	4	12.46	79.97	24.26	250.35	0.48
<b>Girder 2</b>						
E	4	9.73	128.59	24.26	250.35	0.55
F	4	2.61	109.83	24.26	250.35	0.28
G	4	15.18	123.42	24.26	250.35	0.77
<b>Girder 3</b>						
G	4	14.15	136.76	24.26	250.35	0.77
H	4	2.23	119.43	24.26	250.35	0.31
I	4	6.03	177.22	24.26	250.35	0.66
<b>Girder 4</b>						

Σ Conn. **36**

**Seismic Design of Top Chord**

$Q_E / R = 93.38$  kip      Based on Diagonal Member  $R_y P_{ny} \cos \theta = 197.6$  kip  
 Control Force = 197.6 kip

**Material**       $F_y = 36$  ksi       $E = 29000$  ksi  
 $F_u = 58$  ksi  
 $R_y = 1.5$

Length = 10 ft      Member Stitches @ 40 in

**Section**      2 L6X6X7/8      From Strength I Analysis and Design

Section Properties of: L6X6X7/8

$A = 9.75$  in<sup>2</sup>       $r_x = 1.81$  in       $I_y = 31.9$  in<sup>4</sup>  
 $x = 1.81$  in       $r_y = 1.81$  in       $t_{Gplate} = 1$  in

Section Properties of: 2 L6X6X7/8

$A = 19.5$  in<sup>2</sup>       $r_x = 1.81$  in       $r_{yy} = 2.93$  in

**Local Buckling:**

$b = 6$  in       $t = 0.875$  in       $b/t = 6.86$   
 $b/t \leq 0.3(E/F_y)^{1/2} = 8.51$       **Seismically Compact Section**

**Slenderness Ratio:**

In plane Buckling:       $L = 40$  in      buckling length for in-plane buckling  
 $(KL)_x = 34$  in  
 $(KL/r)_x = 18.78$

Out-of-plane Buckling:       $(KL)_y = 102$  in      Relative Shear Deformations  
 $(a/r_{ib}) = 22.10$        $h = 4.62$  in  
 $\alpha = 1.28$        $\alpha^2/(1+\alpha^2) = 0.62$   
 $(KL/r)_y = 34.77$        $(KL/r)_{ym} = 38.17$

Control  $KL/r = 38.17$   
 $KL/r \leq 4*(E/F_y)^{1/2} = 113.53$       **Seismic Slenderness Ratio Ok**

**Axial Capacity:**

Compression:       $\lambda = 0.18$   
 $P_{n1} = 650.54$  kip       $P_{n2} = 3371.46$  kip  
 $P_n = 650.54$  kip       $\phi = 1.0$

Tension:       $P_{ny} = 702.00$  kip       $\phi = 1.0$

D/C:      Comp. = 0.30 OK  
 Tens. = 0.28 OK

**Flexural Resistance:**

$Z_x = 27.4$  in<sup>3</sup>  
 $M_p = 986.40$  k-in  
 $R_y M_p = M_{pe} = 1479.6$  k-in

**Seismic Design of Bottom Chord**

$Q_E / R = 0$  kip

**Material**       $F_y = 36.00$  ksi       $E = 29000$  ksi  
 $F_u = 58.00$  ksi       $R_y = 1.5$

Section 2 L2x2x1/4

**Local Buckling:**

$b/t = 8.00$        $b/t \leq 0.3(E/F_y)^{1/2} = 8.51$       **Seismically Compact Section**

**Flexural Resistance:**

$Z_x = 0.88$  in<sup>3</sup>  
 $M_p = 31.68$  k-in  
 $R_y M_p = M_{pe} = 47.52$  k-in

**Seismic Design of Diagonal Member**

$Q_E = 305.98$  kip       $R = 3$        $Q_E / R = 102.0$  kip

**Material**

$F_y = 36$  ksi       $E = 29000$  ksi  
 $R_y = 1.5$

**Geometrical Dimensions of Working Points**

Gusset Plate Dimensions:       $w = 18$  in       $h = 9$  in  
    $t = 1.00$  in  
  
Vertical Dimension = 27 in  
Horizontal Dimension = 120 in  
Length L = 10.25 ft

**Section**

1 L4x4x1/2  
 $A = 3.75$  in<sup>2</sup>       $r_z = 0.776$  in       $Z_x = 1.96$  in<sup>3</sup>

**Local Buckling:**

$b = 4$  in       $t = 0.5$  in       $b/t = 8.00$   
 $b/t \leq 0.3(E/F_y)^{1/2} = 8.51$       **Seismically Compact Section**

**Slenderness Ratio:**

Buckling Length = 61.50 in      Biased Buckling\_Over 1/2 Length  
 $(KL/r)_z = 67.36$        $K = 0.85$   
 $KL/r \leq 4*(E/F_y)^{1/2} = 113.53$       **Seismic Slenderness Ratio, Ok**

**Axial Capacity:**

Compression:       $\lambda = 0.86$       Note: use  $F_{ye} = R_y F_y$   
 $P_{n1} = 141.88$  kip       $P_{n2} = 208.14$  kip  
 $\phi P_n = 141.88$  kip       $\phi = 1.0$

Tension:       $\phi R_y P_{ny} = 202.50$  kips       $\phi = 1.0$

Control Axial Capacity = 141.88 kips

Seismic Demand  $Q_E = 101.99$  kips

Axial D/C Ratio = 0.72 **OK**

**Lateral Capacity of Inelastic Superstructure**

*from inelastic response of diagonal members*

Horizontal Comp  $F_x = 197.56$  kip

Horizontal Comp  $F_x = 41.53$  kip

No. of Diagonals = 6

$\Sigma V = 717$  kip

Based on hor. comp. of  $R_y P_{ny}$

Based on hor. comp. of  $0.3P_n$

total lateral shear from diagonal members

**contribution of chord members to lateral shear**

*Top Chord:*

Distance from bearing to CL of Top Chord,  $h_1 = 33$  inch

Shear Contribution  $2R_y M_p / h_1 = 89.67$  kip

*Bottom Chord:*

Distance from bearing to CL of Bot Chord, h2 =	6	inch	
Shear Contribution $2R_yP_{ny}/h2 =$	15.84	kip	
Shear Contribution / bay =	105.51	kip	
No of Bays =	3		
Total Shear Contribution =	317	kips	from top & bot chord members
<b>Total Lateral Shear at Supports =</b>	<b>1034</b>	<b>kips</b>	<b>from diagonals+chord members</b>
<b>Elastic Shear from Model Analysis =</b>	<b>906</b>	<b>kip</b>	
<b><math>\Omega =</math> Scale Factor Inelastic Superstructure =</b>	<b>1.14</b>		

**Drift Check:**

Lateral Displacement $\Delta =$	0.43	in	
Drift (%) = $\Delta / h_{girder} =$	0.89	%	< 4%, OK!

**Connection Design**

**Diagonal Member**

Section: L4x4x1/2      b = 4 in      t = 0.5 in

End Connection

Axial Force =	222.8	kip	based on $1.1R_yP_{ny}$ of diagonal member
Weld Size s =	0.438	in	assuming max. weld size
$R_r = \phi 0.6F_{EXX} 0.707s =$	16.3	k/in	weld resistance per length
Total Weld Length =	13.6	in	reqd total weld length
Per Leg =	6.8	in	reqd weld length per leg
Use: Weld Length/leg =	8.00	in	provided weld per leg
End Moment = $1.1R_yF_yZ_x =$	116.4	k-in	$1.1xM_p$ of diagonal member
Weld $I_p =$	149.3	in <sup>3</sup>	= $I_x + I_y$ of weld
Weld Shear flow, v =	15.5	k/in	from axial force & end moment
D/C = $v / R_r =$	0.95		OK!

Middle Connection

$0.25R_yP_{ny} =$	50.6	kip	
Weld Size s =	0.438		
Total Weld Length =	3.1	in	reqd weld length
Use: Weld Length =	3.5	in	provided weld length

**Top Chord**

Section: 2 L6X6X7/8      b = 6 in      t = 0.875 in

End Connection

Axial Force =	217.3	kip	based on $1.1R_yP_{ny}\cos\theta$ of diagonal member
Max Weld Size =	0.8125	in	
Weld Size s =	0.4375	in	
$R_r = \phi 0.6F_{EXX} 0.707s =$	10.39	k/in	weld resistance per length
Total Weld Length =	20.91	in	reqd total weld length
Per Leg =	5.23	in	reqd weld length per leg
Weld Length/leg =	5.5	in	provided weld per leg

**Gusset Plate Connection-Top Chord and Diagonal Member**

Bearing Stiffener Width =	7.75	in
Bearing Stiffener Thickness =	1	in
Gusset Plate Thickness =	1	in

Diagonal Member Inclination

Web depth =	36	in
Top Chord =	6	in
Bot Chord =	2	in
Girder S =	120	in

**Working Point (WP) Dimensions**

Vertical Dim.:	v =	32	in
Horizontal Dim.:	h =	120	in
	sin $\theta$ =	0.26	
	cos $\theta$ =	0.97	
Diagonal L from edge of Gusset to WP =		17.52	in

**Gusset Plate Dimensions:**

	t =	1	in
	h =	4.51	in
	w =	16.93	in
<u>Use:</u>	h =	9	in
<u>Use:</u>	w =	18	in

Steel Type =	A36	(A36 or A572)
F <sub>y</sub> =	36	ksi
F <sub>u</sub> =	58	ksi

**Gusset Plate Force Analysis:**

V =	57.39	kip	vertical comp. of diagonal member = 1.1R <sub>y</sub> P <sub>ny</sub> sin $\theta$
M =	222.40	k-in	mom. @ c.g. of gusset = V*x

**A325-X Bolts Properties:**

d =	0.875	in	A <sub>b</sub> =	0.60	in <sup>2</sup>
F <sub>u</sub> =	120	ksi			

Shear:	$\phi$ 0.48 A <sub>b</sub> F <sub>u</sub> =	27.71	kip
Bearing:	$\phi$ 2.4d t F <sub>u</sub> =	97.44	kip
Control:	$\phi$ F <sub>v</sub> =	27.71	kip

<u>Use:</u>	No. of Bolts/line =	3
	No of Lines =	2

**Bolts Analysis**

l<sub>p</sub> values for 2 lines of bolts, g = 3" and s = 3"

3bolts/line	49.5	4bolts/line	103.5	5bolts/line	1180
l <sub>p</sub> =	49.5				

l<sub>p</sub> values for 1 line of bolts s = 3"

3bolts/line	18	4bolts/line	45	5bolts/line	58.5
l <sub>p</sub> =	18				

Control	l <sub>p</sub> =	49.50
	y =	3.00

vert. dist of most stressed bolt from bolt c.g.

from V:	F <sub>y1</sub> =	9.57	kip	= V / no. of bolts
from M:	F <sub>y2</sub> =	6.74	kip	= M*(g/2) / l <sub>p</sub> where g is the bolt hor. spacing
	F <sub>x</sub> =	13.48	kip	= My/l <sub>p</sub>
	F <sub>R</sub> =	21.16	kip	= [(F <sub>x</sub> <sup>2</sup> ) + (F <sub>y1</sub> + F <sub>y2</sub> ) <sup>2</sup> ] <sup>1/2</sup>
	D/C =	0.76	OK!	

**Gusset Plate Analysis**

h =	9	in
t =	1	in
V =	57.39	kip
M =	222.40	k-inch

<i>At Gross Area:</i>	$A_g =$	9.00	in <sup>2</sup>
	$Z_g = td^2/4 =$	20.25	in <sup>3</sup>
	$f_v = V/A_g =$	6.38	ksi
	$F_{cr} = (F_y^2 - 3f_v^2)^{1/2} =$	34.26	ksi
	$\phi M_n =$	659.15	k-in
<i>At Net Area</i>	$A_n =$	6.00	in <sup>2</sup>
	$Z_n =$	13.92	in <sup>3</sup>
	$f_v =$	9.57	ksi
	$F_{cr} = (F_u^2 - 3f_v^2)^{1/2} =$	57.92	ksi
	$\phi M_n =$	645.06	k-in
Control	$\phi M_n =$	645.06	k-in
	<b>D/C =</b>	<b>0.34</b>	<b>OK!</b>

## LIST OF CCEER PUBLICATIONS

<b>Report No.</b>	<b>Publication</b>
CCEER-84-1	Saiidi, M., and R. Lawver, "User's Manual for LZAK-C64, A Computer Program to Implement the Q-Model on Commodore 64," Civil Engineering Department, Report No. CCEER-84-1, University of Nevada, Reno, January 1984.
CCEER-84-1 Reprint	Douglas, B., Norris, G., Saiidi, M., Dodd, L., Richardson, J. and Reid, W., "Simple Bridge Models for Earthquakes and Test Data," Civil Engineering Department, Report No. CCEER-84-1 Reprint, University of Nevada, Reno, January 1984.
CCEER-84-2	Douglas, B. and T. Iwasaki, "Proceedings of the First USA-Japan Bridge Engineering Workshop," held at the Public Works Research Institute, Tsukuba, Japan, Civil Engineering Department, Report No. CCEER-84-2, University of Nevada, Reno, April 1984.
CCEER-84-3	Saiidi, M., J. Hart, and B. Douglas, "Inelastic Static and Dynamic Analysis of Short R/C Bridges Subjected to Lateral Loads," Civil Engineering Department, Report No. CCEER-84-3, University of Nevada, Reno, July 1984.
CCEER-84-4	Douglas, B., "A Proposed Plan for a National Bridge Engineering Laboratory," Civil Engineering Department, Report No. CCEER-84-4, University of Nevada, Reno, December 1984.
CCEER-85-1	Norris, G. and P. Abdollahiaee, "Laterally Loaded Pile Response: Studies with the Strain Wedge Model," Civil Engineering Department, Report No. CCEER-85-1, University of Nevada, Reno, April 1985.
CCEER-86-1	Ghusn, G. and M. Saiidi, "A Simple Hysteretic Element for Biaxial Bending of R/C in NEABS-86," Civil Engineering Department, Report No. CCEER-86-1, University of Nevada, Reno, July 1986.

- CCEER-86-2 Saiidi, M., R. Lawver, and J. Hart, "User's Manual of ISADAB and SIBA, Computer Programs for Nonlinear Transverse Analysis of Highway Bridges Subjected to Static and Dynamic Lateral Loads," Civil Engineering Department, Report No. CCEER-86-2, University of Nevada, Reno, September 1986.
- CCEER-87-1 Siddharthan, R., "Dynamic Effective Stress Response of Surface and Embedded Footings in Sand," Civil engineering Department, Report No. CCEER-86-2, University of Nevada, Reno, June 1987.
- CCEER-87-2 Norris, G. and R. Sack, "Lateral and Rotational Stiffness of Pile Groups for Seismic Analysis of Highway Bridges," Civil Engineering Department, Report No. CCEER-87-2, University of Nevada, Reno, June 1987.
- CCEER-88-1 Orié, J. and M. Saiidi, "A Preliminary Study of One-Way Reinforced Concrete Pier Hinges Subjected to Shear and Flexure," Civil Engineering Department, Report No. CCEER-88-1, University of Nevada, Reno, January 1988.
- CCEER-88-2 Orié, D., M. Saiidi, and B. Douglas, "A Micro-CAD System for Seismic Design of Regular Highway Bridges," Civil Engineering Department, Report No. CCEER-88-2, University of Nevada, Reno, June 1988.
- CCEER-88-3 Orié, D. and M. Saiidi, "User's Manual for Micro-SARB, a Microcomputer Program for Seismic Analysis of Regular Highway Bridges," Civil Engineering Department, Report No. CCEER-88-3, University of Nevada, Reno, October 1988.
- CCEER-89-1 Douglas, B., M. Saiidi, R. Hayes, and G. Holcomb, "A Comprehensive Study of the Loads and Pressures Exerted on Wall Forms by the Placement of Concrete," Civil Engineering Department, Report No. CCEER-89-1, University of Nevada, Reno, February 1989.
- CCEER-89-2 Richardson, J. and B. Douglas, "Dynamic Response Analysis of the Dominion Road Bridge Test Data," Civil Engineering Department, Report No. CCEER-89-2, University of Nevada, Reno, March 1989.

- CCEER-89-2 Vrontinos, S., M. Saiidi, and B. Douglas, "A Simple Model to Predict the Ultimate Response of R/C Beams with Concrete Overlays," Civil Engineering Department, Report NO. CCEER-89-2, University of Nevada, Reno, June 1989.
- CCEER-89-3 Ebrahimpour, A. and P. Jagadish, "Statistical Modeling of Bridge Traffic Loads - A Case Study," Civil Engineering Department, Report No. CCEER-89-3, University of Nevada, Reno, December 1989.
- CCEER-89-4 Shields, J. and M. Saiidi, "Direct Field Measurement of Prestress Losses in Box Girder Bridges," Civil Engineering Department, Report No. CCEER-89-4, University of Nevada, Reno, December 1989.
- CCEER-90-1 Saiidi, M., E. Maragakis, G. Ghosn, Y. Jiang, and D. Schwartz, "Survey and Evaluation of Nevada's Transportation Infrastructure, Task 7.2 - Highway Bridges, Final Report," Civil Engineering Department, Report No. CCEER 90-1, University of Nevada, Reno, October 1990.
- CCEER-90-2 Abdel-Ghaffar, S., E. Maragakis, and M. Saiidi, "Analysis of the Response of Reinforced Concrete Structures During the Whittier Earthquake 1987," Civil Engineering Department, Report No. CCEER 90-2, University of Nevada, Reno, October 1990.
- CCEER-91-1 Saiidi, M., E. Hwang, E. Maragakis, and B. Douglas, "Dynamic Testing and the Analysis of the Flamingo Road Interchange," Civil Engineering Department, Report No. CCEER-91-1, University of Nevada, Reno, February 1991.
- CCEER-91-2 Norris, G., R. Siddharthan, Z. Zafir, S. Abdel-Ghaffar, and P. Gowda, "Soil-Foundation-Structure Behavior at the Oakland Outer Harbor Wharf," Civil Engineering Department, Report No. CCEER-91-2, University of Nevada, Reno, July 1991.
- CCEER-91-3 Norris, G., "Seismic Lateral and Rotational Pile Foundation Stiffnesses at Cypress," Civil Engineering Department, Report No. CCEER-91-3, University of Nevada, Reno, August 1991.

- CCEER-91-4 O'Connor, D. and M. Saiidi, "A Study of Protective Overlays for Highway Bridge Decks in Nevada, with Emphasis on Polyester-Styrene Polymer Concrete," Civil Engineering Department, Report No. CCEER-91-4, University of Nevada, Reno, October 1991.
- CCEER-91-5 O'Connor, D.N. and M. Saiidi, "Laboratory Studies of Polyester-Styrene Polymer Concrete Engineering Properties," Civil Engineering Department, Report No. CCEER-91-5, University of Nevada, Reno, November 1991.
- CCEER-92-1 Straw, D.L. and M. Saiidi, "Scale Model Testing of One-Way Reinforced Concrete Pier Hinges Subject to Combined Axial Force, Shear and Flexure," edited by D.N. O'Connor, Civil Engineering Department, Report No. CCEER-92-1, University of Nevada, Reno, March 1992.
- CCEER-92-2 Wehbe, N., M. Saiidi, and F. Gordaninejad, "Basic Behavior of Composite Sections Made of Concrete Slabs and Graphite Epoxy Beams," Civil Engineering Department, Report No. CCEER-92-2, University of Nevada, Reno, August 1992.
- CCEER-92-3 Saiidi, M. and E. Hutchens, "A Study of Prestress Changes in A Post-Tensioned Bridge During the First 30 Months," Civil Engineering Department, Report No. CCEER-92-3, University of Nevada, Reno, April 1992.
- CCEER-92-4 Saiidi, M., B. Douglas, S. Feng, E. Hwang, and E. Maragakis, "Effects of Axial Force on Frequency of Prestressed Concrete Bridges," Civil Engineering Department, Report No. CCEER-92-4, University of Nevada, Reno, August 1992.
- CCEER-92-5 Siddharthan, R., and Z. Zafir, "Response of Layered Deposits to Traveling Surface Pressure Waves," Civil Engineering Department, Report No. CCEER-92-5, University of Nevada, Reno, September 1992.
- CCEER-92-6 Norris, G., and Z. Zafir, "Liquefaction and Residual Strength of Loose Sands from Drained Triaxial Tests," Civil Engineering Department, Report No. CCEER-92-6, University of Nevada, Reno, September 1992.
- CCEER-92-6-A Norris, G., Siddharthan, R., Zafir, Z. and Madhu, R. "Liquefaction and Residual Strength of Sands from Drained Triaxial Tests," Civil Engineering Department, Report No.

CCEER-92-6-A, University of Nevada, Reno, September 1992.

- CCEER-92-7 Douglas, B., "Some Thoughts Regarding the Improvement of the University of Nevada, Reno's National Academic Standing," Civil Engineering Department, Report No. CCEER-92-7, University of Nevada, Reno, September 1992.
- CCEER-92-8 Saiidi, M., E. Maragakis, and S. Feng, "An Evaluation of the Current Caltrans Seismic Restrainer Design Method," Civil Engineering Department, Report No. CCEER-92-8, University of Nevada, Reno, October 1992.
- CCEER-92-9 O'Connor, D., M. Saiidi, and E. Maragakis, "Effect of Hinge Restrainers on the Response of the Madrone Drive Undercrossing During the Loma Prieta Earthquake," Civil Engineering Department, Report No. CCEER-92-9, University of Nevada, Reno, February 1993.
- CCEER-92-10 O'Connor, D., and M. Saiidi, "Laboratory Studies of Polyester Concrete: Compressive Strength at Elevated Temperatures and Following Temperature Cycling, Bond Strength to Portland Cement Concrete, and Modulus of Elasticity," Civil Engineering Department, Report No. CCEER-92-10, University of Nevada, Reno, February 1993.
- CCEER-92-11 Wehbe, N., M. Saiidi, and D. O'Connor, "Economic Impact of Passage of Spent Fuel Traffic on Two Bridges in Northeast Nevada," Civil Engineering Department, Report No. CCEER-92-11, University of Nevada, Reno, December 1992.
- CCEER-93-1 Jiang, Y., and M. Saiidi, "Behavior, Design, and Retrofit of Reinforced Concrete One-way Bridge Column Hinges," edited by D. O'Connor, Civil Engineering Department, Report No. CCEER-93-1, University of Nevada, Reno, March 1993.
- CCEER-93-2 Abdel-Ghaffar, S., E. Maragakis, and M. Saiidi, "Evaluation of the Response of the Aptos Creek Bridge During the 1989 Loma Prieta Earthquake," Civil Engineering Department, Report No. CCEER-93-2, University of Nevada, Reno, June 1993.
- CCEER-93-3 Sanders, D.H., B.M. Douglas, and T.L. Martin, "Seismic Retrofit Prioritization of Nevada

Bridges," Civil Engineering Department, Report No. CCEER-93-3, University of Nevada, Reno, July 1993.

- CCEER-93-4 Abdel-Ghaffar, S., E. Maragakis, and M. Saiidi, "Performance of Hinge Restrainers in the Huntington Avenue Overhead During the 1989 Loma Prieta Earthquake," Civil Engineering Department, Report No. CCEER-93-4, University of Nevada, Reno, June 1993 (in final preparation).
- CCEER-93-5 Maragakis, E., M. Saiidi, S. Feng, and L. Flournoy, "Effects of Hinge Restrainers on the Response of the San Gregorio Bridge during the Loma Prieta Earthquake," (in final preparation) Civil Engineering Department, Report No. CCEER-93-5, University of Nevada, Reno.
- CCEER-93-6 Saiidi, M., E. Maragakis, S. Abdel-Ghaffar, S. Feng, and D. O'Connor, "Response of Bridge Hinge Restrainers during Earthquakes -Field Performance, Analysis, and Design," Civil Engineering Department, Report No. CCEER-93-6, University of Nevada, Reno, May 1993.
- CCEER-93-7 Wehbe, N., Saiidi, M., Maragakis, E., and Sanders, D., "Adequacy of Three Highway Structures in Southern Nevada for Spent Fuel Transportation, Civil Engineering Department, Report No. CCEER-93-7, University of Nevada, Reno, August 1993.
- CCEER-93-8 Roybal, J., Sanders, D.H., and Maragakis, E., "Vulnerability Assessment of Masonry in the Reno-Carson City Urban Corridor," Civil Engineering Department, Report No. CCEER-93-8, University of Nevada, Reno, May 1993.
- CCEER-93-9 Zafir, Z. and Siddharthan, R., "MOVLOAD: A Program to Determine the Behavior of Nonlinear Horizontally Layered Medium Under Moving Load," Civil Engineering Department, Report No. CCEER-93-9, University of Nevada, Reno, August 1993.
- CCEER-93-10 O'Connor, D.N., Saiidi, M., and Maragakis, E.A., "A Study of Bridge Column Seismic Damage Susceptibility at the Interstate 80/U.S. 395 Interchange in Reno, Nevada," Civil Engineering Department, Report No. CCEER-93-10, University of Nevada, Reno, October 1993.

- CCEER-94-1 Maragakis, E., B. Douglas, and E. Abdelwahed, "Preliminary Dynamic Analysis of a Railroad Bridge," Report CCEER-94-1, January 1994.
- CCEER-94-2 Douglas, B.M., Maragakis, E.A., and Feng, S., "Stiffness Evaluation of Pile Foundation of Cazenovia Creek Overpass," Civil Engineering Department, Report No. CCEER-94-2, University of Nevada, Reno, March 1994.
- CCEER-94-3 Douglas, B.M., Maragakis, E.A., and Feng, S., "Summary of Pretest Analysis of Cazenovia Creek Bridge," Civil Engineering Department, Report No. CCEER-94-3, University of Nevada, Reno, April 1994.
- CCEER-94-4 Norris, G.M., Madhu, R., Valceschini, R., and Ashour, M., "Liquefaction and Residual Strength of Loose Sands from Drained Triaxial Tests," Report 2, Vol. 1&2, Civil Engineering Department, Report No. CCEER-94-4, University of Nevada, Reno, August 1994.
- CCEER-94-5 Saiidi, M., Hutchens, E., and Gardella, D., "Prestress Losses in a Post-Tensioned R/C Box Girder Bridge in Southern Nevada," Civil Engineering Department, CCEER-94-5, University of Nevada, Reno, August 1994.
- CCEER-95-1 Siddharthan, R., El-Gamal, M., and Maragakis, E.A., "Nonlinear Bridge Abutment , Verification, and Design Curves," Civil Engineering Department, CCEER-95-1, University of Nevada, Reno, January 1995.
- CCEER-95-2 Ashour, M. and Norris, G., "Liquefaction and Undrained Response Evaluation of Sands from Drained Formulation," Civil Engineering Department, Report No. CCEER-95-2, University of Nevada, Reno, February 1995.
- CCEER-95-3 Wehbe, N., Saiidi, M., Sanders, D. and Douglas, B., "Ductility of Rectangular Reinforced Concrete Bridge Columns with Moderate Confinement," Civil Engineering Department, Report No. CCEER-95-3, University of Nevada, Reno, July 1995.
- CCEER-95-4 Martin, T., Saiidi, M. and Sanders, D., "Seismic Retrofit of Column-Pier Cap Connections in Bridges in Northern Nevada," Civil Engineering Department, Report No. CCEER-95-4, University of Nevada, Reno, August 1995.

- CCEER-95-5 Darwish, I., Saiidi, M. and Sanders, D., "Experimental Study of Seismic Susceptibility Column-Footing Connections in Bridges in Northern Nevada," Civil Engineering Department, Report No. CCEER-95-5, University of Nevada, Reno, September 1995.
- CCEER-95-6 Griffin, G., Saiidi, M. and Maragakis, E., "Nonlinear Seismic Response of Isolated Bridges and Effects of Pier Ductility Demand," Civil Engineering Department, Report No. CCEER-95-6, University of Nevada, Reno, November 1995.
- CCEER-95-7 Acharya, S., Saiidi, M. and Sanders, D., "Seismic Retrofit of Bridge Footings and Column-Footing Connections," Civil Engineering Department, Report No. CCEER-95-7, University of Nevada, Reno, November 1995.
- CCEER-95-8 Maragakis, E., Douglas, B., and Sandirasegaram, U., "Full-Scale Field Resonance Tests of a Railway Bridge," A Report to the Association of American Railroads, Civil Engineering Department, Report No. CCEER-95-8, University of Nevada, Reno, December 1995.
- CCEER-95-9 Douglas, B., Maragakis, E. and Feng, S., "System Identification Studies on Cazenovia Creek Overpass," Report for the National Center for Earthquake Engineering Research, Civil Engineering Department, Report No. CCEER-95-9, University of Nevada, Reno, October 1995.
- CCEER-96-1 El-Gamal, M.E. and Siddharthan, R.V., "Programs to Computer Translational Stiffness of Seat-Type Bridge Abutment," Civil Engineering Department, Report No. CCEER-96-1, University of Nevada, Reno, March 1996.
- CCEER-96-2 Labia, Y., Saiidi, M. and Douglas, B., "Evaluation and Repair of Full-Scale Prestressed Concrete Box Girders," A Report to the National Science Foundation, Research Grant CMS-9201908, Civil Engineering Department, Report No. CCEER-96-2, University of Nevada, Reno, May 1996.
- CCEER-96-3 Darwish, I., Saiidi, M. and Sanders, D., "Seismic Retrofit of R/C Oblong Tapered Bridge Columns with Inadequate Bar Anchorage in Columns and Footings," A Report to the

Nevada Department of Transportation, Civil Engineering Department, Report No. CCEER-96-3, University of Nevada, Reno, May 1996.

CCEER-96-4 Ashour, M., Pilling, R., Norris, G. and Perez, H., "The Prediction of Lateral Load Behavior of Single Piles and Pile Groups Using the Strain Wedge Model," A Report to the California Department of Transportation, Civil Engineering Department, Report No. CCEER-96-4, University of Nevada, Reno, June 1996.

CCEER-97-1-A Rimal, P. and Itani, A. "Sensitivity Analysis of Fatigue Evaluations of Steel Bridges", Center for Earthquake Research, Department of Civil Engineering, University of Nevada, Reno, Nevada Report No. CCEER-97-1-A, September, 1997.

CCEER-97-1-B Maragakis, E., Douglas, B., and Sandirasegaram, U. "Full-Scale Field Resonance Tests of a Railway Bridge," A Report to the Association of American Railroads, Civil Engineering Department, University of Nevada, Reno, May, 1996.

CCEER-97-2 Wehbe, N., Saiidi, M., and D. Sanders, "Effect of Confinement and Flares on the Seismic Performance of Reinforced Concrete Bridge Columns," Civil Engineering Department, Report No. CCEER-97-2, University of Nevada, Reno, September 1997.

CCEER-97-3 Darwish, I., M. Saiidi, G. Norris, and E. Maragakis, "Determination of In-Situ Footing Stiffness Using Full-Scale Dynamic Field Testing," A Report to the Nevada Department of Transportation, Structural Design Division, Carson City, Nevada, Report No. CCEER-97-3, University of Nevada, Reno, October 1997.

CCEER-97-4-A Itani, A. "Cyclic Behavior of Richmond-San Rafael Tower Links," Center for Civil Engineering Earthquake Research, Department of Civil Engineering, University of Nevada, Reno, Nevada, Report No. CCEER-97-4, August 1997.

- CCEER-97-4-B Wehbe, N., and M. Saiidi, "User's manual for RCMC v. 1.2 : A Computer Program for Moment-Curvature Analysis of Confined and Unconfined Reinforced Concrete Sections," Center for Civil Engineering Earthquake Research, Department of Civil Engineering, University of Nevada, Reno, Nevada, Report No. CCEER-97-4, November, 1997.
- CCEER-97-5 Isakovic, T., M. Saiidi, and A. Itani, "Influence of new Bridge Configurations on Seismic Performance," Department of Civil Engineering, University of Nevada, Reno, Report No. CCEER-97-5, September, 1997.
- CCEER-98-1 Itani, A., Vesco, T. and Dietrich, A., "Cyclic Behavior of "as Built" Laced Members With End Gusset Plates on the San Francisco Bay Bridge" Center for Civil Engineering Earthquake Research, Department of Civil Engineering, University of Nevada, Reno, Nevada Report No. CCEER-98-1, March, 1998.
- CCEER-98-2 G. Norris and M. Ashour, "Liquefaction and Undrained Response Evaluation of Sands from Drained Formulation." Center for Civil Engineering Earthquake Research, Department of Civil Engineering, University of Nevada, Reno, Nevada, Report No. CCEER-98-2, May, 1998.
- CCEER-98-3 Qingbin, Chen, B. M. Douglas, E. Maragakis, and I. G. Buckle, "Extraction of Nonlinear Hysteretic Properties of Seismically Isolated Bridges from Quick-Release Field Tests", Center for Civil Engineering Earthquake Research, Department of Civil Engineering, University of Nevada, Reno, Nevada, Report No. CCEER-98-3, June, 1998.
- CCEER-98-4 Maragakis, E., B. M. Douglas, and C. Qingbin, "Full-Scale Field Capacity Tests of a Railway Bridge", Center for Civil Engineering Earthquake Research, Department of Civil Engineering, University of Nevada, Reno, Nevada, Report No. CCEER-98-4, June, 1998.
- CCEER-98-5 Itani, A., Douglas, B., and Woodgate, J., "Cyclic Behavior of Richmond-San Rafael Retrofitted Tower Leg". Center for Civil Engineering Earthquake Research, Department

of Civil Engineering, University of Nevada, Reno. Report No. CCEER-98-5, June 1998

- CCEER-98-6 Moore, R., Saiidi, M., and Itani, A., "Seismic Behavior of New Bridges with Skew and Curvature". Center for Civil Engineering Earthquake Research, Department of Civil Engineering, University of Nevada, Reno. Report No. CCEER-98-6, October, 1998.
- CCEER-98-7 Itani, A and Dietrich, A, "Cyclic Behavior of Double Gusset Plate Connections", Center for Civil Engineering Earthquake Research, Department of Civil Engineering, University of Nevada, Reno, Nevada, Report No. CCEER-98-5, December, 1998.
- CCEER-99-1 Caywood, C., M. Saiidi, and D. Sanders, "Seismic Retrofit of Flared Bridge Columns with Steel Jackets," Civil Engineering Department, University of Nevada, Reno, Report No. CCEER-99-1, February 1999.
- CCEER-99-2 Mangoba, N., M. Mayberry, and M. Saiidi, "Prestress Loss in Four Box Girder Bridges in Northern Nevada," Civil Engineering Department, University of Nevada, Reno, Report No. CCEER-99-2, March 1999.
- CCEER-99-3 Abo-Shadi, N., M. Saiidi, and D. Sanders, "Seismic Response of Bridge Pier Walls in the Weak Direction", Civil Engineering Department, University of Nevada, Reno, Report No. CCEER-99-3, April 1999.
- CCEER-99-4 Buzick, A., and M. Saiidi, "Shear Strength and Shear Fatigue Behavior of Full-Scale Prestressed Concrete Box Girders", Civil Engineering Department, University of Nevada, Reno, Report No. CCEER-99-4, April 1999.
- CCEER-99-5 Randall, M., M. Saiidi, E. Maragakis and T. Isakovic, "Restrainer Design Procedures For Multi-Span Simply-Supported Bridges", Civil Engineering Department, University of Nevada, Reno, Report No. CCEER-99-5, April 1999.
- CCEER-99-6 Wehbe, N. and M. Saiidi, "User's Manual for RCMC v. 1.2, A Computer Program for Moment-Curvature Analysis of Confined and Unconfined Reinforced Concrete Sections", Civil Engineering Department, University of Nevada, Reno, Report No.

CCEER-99-6, May 1999.

- CCEER-99-7 Burda, J. and A. Itani, "Studies of Seismic Behavior of Steel Base Plates," Civil Engineering Department, University of Nevada, Reno, Report No. CCEER-99-7, May 1999.
- CCEER-99-8 Ashour, M. and G. Norris, "Refinement of the Strain Wedge Model Program," Civil Engineering Department, University of Nevada, Reno, Report No. CCEER-99-8, March 1999.
- CCEER-99-9 Dietrich, A., and A. Itani, "Cyclic Behavior of Laced and Perforated Steel Members on the San Francisco-Oakland Bay Bridge," Civil Engineering Department, University, Reno, Report No. CCEER-99-9, December 1999.
- CCEER 99-10 Itani, A., A. Dietrich, "Cyclic Behavior of Built Up Steel Members and their Connections," Civil Engineering Department, University of Nevada, Reno, Report No. CCEER-99-10, December 1999.
- CCEER 99-10-A Itani, A., E. Maragakis and P. He, "Fatigue Behavior of Riveted Open Deck Railroad Bridge Girders," Civil Engineering Department, University of Nevada, Reno, Report No. CCEER-99-10-A, August 1999.
- CCEER 99-11 Itani, A., J. Woodgate, "Axial and Rotational Ductility of Built Up Structural Steel Members," Civil Engineering Department, University of Nevada, Reno, Report No. CCEER-99-11, December 1999.
- CCEER-99-12 Sgambelluri, M., Sanders, D.H., and Saiidi, M.S., "Behavior of One-Way Reinforced Concrete Bridge Column Hinges in the Weak Direction,"  
Department of Civil Engineering, University of Nevada, Reno, Report No. CCEER-99-12, December 1999.
- CCEER-99-13 Laplace, P., Sanders, D.H., Douglas, B., and Saiidi, M., "Shake Table Testing of Flexure

Dominated Reinforced Concrete Bridge Columns”, Department of Civil Engineering, University of Nevada, Reno, Report No. CCEER-99-13, December 1999.

- CCEER-99-14 Ahmad M. Itani, Jose A. Zepeda, and Elizabeth A. Ware "Cyclic Behavior of Steel Moment Frame Connections for the Moscone Center Expansion," Department of Civil Engineering, University of Nevada, Reno, Report No. CCEER-99-14, December 1999.
- CCEER 00-1 Ashour, M., and Norris, G. "Undrained Lateral Pile and Pile Group Response in Saturated Sand", Civil Engineering Department, University of Nevada, Reno, Report No. CCEER-00-1, May 1999. January 2000.
- CCEER 00-2 Saiidi, M. and Wehbe, N., "A Comparison of Confinement Requirements in Different Codes for Rectangular, Circular, and Double-Spiral RC Bridge Columns," Civil Engineering Department, University of Nevada, Reno, Report No. CCEER-00-2, January 2000.
- CCEER 00-3 McElhaney, B., M. Saiidi, and D. Sanders, "Shake Table Testing of Flared Bridge Columns With Steel Jacket Retrofit," Civil Engineering Department, University of Nevada, Reno, Report No. CCEER-00-3, January 2000.
- CCEER 00-4 Martinovic, F., M. Saiidi, D. Sanders, and F. Gordaninejad, "Dynamic Testing of Non-Prismatic Reinforced Concrete Bridge Columns Retrofitted with FRP Jackets," Civil Engineering Department, University of Nevada, Reno, Report No. CCEER-00-4, January 2000.
- CCEER 00-5 Itani, A., and M. Saiidi, "Seismic Evaluation of Steel Joints for UCLA Center for Health Science Westwood Replacement Hospital," Civil Engineering Department, University of Nevada, Reno, Report No. CCEER-00-5, February 2000.
- CCEER 00-6 Will, J. and D. Sanders, "High Performance Concrete Using Nevada Aggregates," Civil Engineering Department, University of Nevada, Reno, Report No. CCEER-00-6, May 2000.

- CCEER 00-7 French, C., and M. Saiidi, "A Comparison of Static and Dynamic Performance of Models of Flared Bridge Columns," Civil Engineering Department, University of Nevada, Reno, Report No. CCEER-00-7, October 2000.
- CCEER 00-8 Itani, A., H. Sedarat, "Seismic Analysis of the AISI LRFD Design Example of Steel Highway Bridges," Civil Engineering Department, University of Nevada, Reno, Report No. CCEER 00-08, November 2000.
- CCEER 00-9 Moore, J., D. Sanders, and M. Saiidi, "Shake Table Testing of 1960's Two Column Bent with Hinges Bases," Civil Engineering Department, University of Nevada, Reno, Report No. CCEER 00-09, December 2000.
- CCEER 00-10 Asthana, M., D. Sanders, and M. Saiidi, "One-Way Reinforced Concrete Bridge Column Hinges in the Weak Direction," Civil Engineering Department, University of Nevada, Reno, Report No. CCEER 00-10, April 2001.
- CCEER 01-1 Ah Sha, H., D. Sanders, M. Saiidi, "Early Age Shrinkage and Cracking of Nevada Concrete Bridge Decks," Civil Engineering Department, University of Nevada, Reno, Report No. CCEER 01-01, May 2001.
- CCEER 01-2 Ashour, M. and G. Norris, "Pile Group program for Full Material Modeling an Progressive Failure." Civil Engineering Department, University of Nevada, Reno, Report No. CCEER 01-02, July 2001.
- CCEER 01-3 Itani, A., C. Lanaud, and P. Dusicka, "Non-Linear Finite Element Analysis of Built-Up Shear Links." Civil Engineering Department, University of Nevada, Reno, Report No. CCEER 01-03, July 2001.

- CCEER 01-4 Saiidi, M., J. Mortensen, and F. Martinovic, "Analysis and Retrofit of Fixed Flared Columns with Glass Fiber-Reinforced Plastic Jacketing," Civil Engineering Department, University of Nevada, Reno, Report No. CCEER 01-4, August 2001
- CCEER 01-5 Saiidi, M., A. Itani, I. Buckle, and Z. Cheng," Performance of A Full-Scale Two-Story Wood Frame Structure Supported on Ever-Level Isolators," Civil Engineering Department, University of Nevada, Reno, Report No. CCEER 01-5, October 2001
- CCEER 01-6 Laplace, P., D. Sanders, and M. Saiidi, "Experimental Study and Analysis of Retrofitted Flexure and Shear Dominated Circular Reinforced Concrete Bridge Columns Subjected to Shake Table Excitation," Civil Engineering Department, University of Nevada, Reno, Report No. CCEER 01-6, June 2001.
- CCEER 01-7 Reppi, F., and D. Sanders, "Removal and Replacement of Cast-in-Place, Post-tensioned, Box Girder Bridge," Civil Engineering Department, University of Nevada, Reno, Report No. CCEER 01-7, December 2001.
- CCEER 02-1 Pulido, C., M. Saiidi, D. Sanders, and A. Itani, "Seismic Performance and Retrofitting of Reinforced Concrete Bridge Bents," Civil Engineering Department, University of Nevada, Reno, Report No. CCEER 02-1, January 2002.
- CCEER 02-2 Yang, Q., M. Saiidi, H. Wang, and A. Itani, "Influence of Ground Motion Incoherency on Earthquake Response of Multi-Support Structures," Civil Engineering Department, University of Nevada, Reno, Report No. CCEER 02-2, May 2002.
- CCEER 02-3 M. Saiidi, B. Gopalakrishnan, E. Reinhardt, and R. Siddharthan, A Preliminary Study of Shake Table Response of A Two-Column Bridge Bent on Flexible Footings Civil Engineering Department, University of Nevada, Reno, Report No. CCEER 02-03, June 2002.

- CCEER 02-4 Not Published
- CCEER 02-5 Banghart, A., Sanders, D., Saiidi, M., "Evaluation of Concrete Mixes for Filling the Steel Arches in the Galena Creek Bridge," Civil Engineering Department, University of Nevada, Reno, Report No. CCEER 02-05, June 2002.
- CCEER 02-6 Dusicka, P., Itani, A., Buckle, I. G., "Cyclic Behavior of Shear Links and Tower Shaft Assembly of San Francisco – Oakland Bay Bridge Tower" Civil Engineering Department, University of Nevada, Reno, Report No. CCEER 02-06, July 2002.
- CCEER 02-7 Mortensen, J., and M. Saiidi, "A Performance-Based Design Method for Confinement in Circular Columns," Civil Engineering Department, University of Nevada, Reno, Report No. CCEER 02-07, November 2002.
- CCEER 03-1 Wehbe, N., and M. Saiidi, "User's manual for SPMC v. 1.0 : A Computer Program for Moment-Curvature Analysis of Reinforced Concrete Sections with Interlocking Spirals," Center for Civil Engineering Earthquake Research, Department of Civil Engineering, University of Nevada, Reno, Nevada, Report No. CCEER-03-1, May, 2003.
- CCEER 03-2 Wehbe, N., and M. Saiidi, "User's manual for RCMC v. 2.0 : A Computer Program for Moment-Curvature Analysis of Confined and Unconfined Reinforced Concrete Sections," Center for Civil Engineering Earthquake Research, Department of Civil Engineering, University of Nevada, Reno, Nevada, Report No. CCEER-03-2, June, 2003.
- CCEER 03-3 Nada, H., D. Sanders, and M. Saiidi, "Seismic Performance of RC Bridge Frames with Architectural-Flared Columns," Civil Engineering Department, University of Nevada, Reno, Report No. CCEER 03-3, January 2003.

- CCEER 03-4 Reinhardt, E., M. Saiidi, and R. Siddharthan, "Seismic Performance of a CFRP/Concrete Bridge Bent on Flexible Footings." Civil Engineering Department, University of Nevada, Reno. Report No. CCEER 03-4, August 2003.
- CCEER 03-5 Johnson, N., M. Saiidi, A. Itani, and S. Ladhany, "Seismic Retrofit of Octagonal Columns with Pedestal and One-Way Hinge at the Base," Center for Civil Engineering Earthquake Research, Department of Civil Engineering, University of Nevada, Reno, Nevada, and Report No. CCEER-03-5, August 2003.
- CCEER 03-6 Mortensen, C., M. Saiidi, and S. Ladhany, "Creep and Shrinkage Losses in Highly Variable Climates," Center for Civil Engineering Earthquake Research, Department of Civil Engineering, University of Nevada, Reno, Nevada, Report No. CCEER-03-6, September 2003.
- CCEER 03-7 Ayoub, C., M. Saiidi, and A. Itani, "A Study of Shape-Memory-Alloy-Reinforced Beams and Cubes," Center for Civil Engineering Earthquake Research, Department of Civil Engineering, University of Nevada, Reno, Nevada, Report No. CCEER-03-7, October 2003.
- CCEER 03-8 Chandane, S., D. Sanders, and M. Saiidi, "Static and Dynamic Performance of RC Bridge Bents with Architectural-Flared Columns," Center for Civil Engineering Earthquake Research, Department of Civil Engineering, University of Nevada, Reno, Nevada, Report No. CCEER-03-8, November 2003.
- CCEER 04-1 Olaegbe, C., and Saiidi, M., "Effect of Loading History on Shake Table Performance of A Two-Column Bent with Infill Wall," Center for Civil Engineering Earthquake Research, Department of Civil Engineering, University of Nevada, Reno, Nevada, Report No. CCEER-04-1, January 2004.
- CCEER 04-2 Johnson, R., Maragakis, E., Saiidi, M., and DesRoches, R., "Experimental Evaluation of Seismic Performance of SMA Bridge Restrainers," Center for Civil Engineering Earthquake Research, Department of Civil Engineering, University of Nevada, Reno, Nevada, Report No. CCEER-04-2, February 2004.

- CCEER 04-3 Moustafa, K., Sanders, D., and Saiidi, M., "Impact of Aspect Ratio on Two-Column Bent Seismic Performance," Center for Civil Engineering Earthquake Research, Department of Civil Engineering, University of Nevada, Reno, Nevada, Report No. CCEER-04-3, February 2004.
- CCEER 04-4 Maragakis, E., Saiidi, M., Sanchez-Camargo, F., and Elfass, S., "Seismic Performance of Bridge Restrainers At In-Span Hinges," Center for Civil Engineering Earthquake Research, Department of Civil Engineering, University of Nevada, Reno, Nevada, Report No. CCEER-04-4, March 2004.
- CCEER 04-5 Ashour, M., Norris, G. and Elfass, S., "Analysis of Laterally Loaded Long or Intermediate Drilled Shafts of Small or Large Diameter in Layered Soil," Center for Civil Engineering Earthquake Research, Department of Civil Engineering, University of Nevada, Reno, Nevada, Report No. CCEER-04-5, June 2004.
- CCEER 04-6 Correal, J., Saiidi, M. and Sanders, D., "Seismic Performance of RC Bridge Columns Reinforced with Two Interlocking Spirals," Center for Civil Engineering Earthquake Research, Department of Civil Engineering, University of Nevada, Reno, Nevada, Report No. CCEER-04-6, August 2004.
- CCEER 04-7 Dusicka, P., Itani, A. and Buckle, I., "Cyclic Response and Low Cycle Fatigue Characteristics of Plate Steels," Center for Civil Engineering Earthquake Research, Department of Civil Engineering, University of Nevada, Reno, Nevada, Report No. CCEER-04-7, November 2004.
- CCEER 04-8 Dusicka, P., Itani, A. and Buckle, I., "Built-up Shear Links as Energy Dissipaters for Seismic Protection of Bridges," Center for Civil Engineering Earthquake Research, Department of Civil Engineering, University of Nevada, Reno, Nevada, Report No. CCEER-04-8, November 2004.
- CCEER 04-9 Sureshkumar, K., Saiidi, S., Itani, A. and Ladkany, S., "Seismic Retrofit of Two-Column Bents with Diamond Shape Columns," Center for Civil Engineering Earthquake Research, Department of Civil Engineering, University of Nevada, Reno, Nevada, Report No. CCEER-04-9, November 2004.

- CCEER 05-1 Wang, H. and Saiidi, S., "A Study of RC Columns with Shape Memory Alloy and Engineered Cementitious Composites," Center for Civil Engineering Earthquake Research, Department of Civil Engineering, University of Nevada, Reno, Nevada, Report No. CCEER-05-1, January 2005.
- CCEER 05-2 Johnson, R., Saiidi, S. and Maragakis, E., "A Study of Fiber Reinforced Plastics for Seismic Bridge Restrainers," Center for Civil Engineering Earthquake Research, Department of Civil Engineering, University of Nevada, Reno, Nevada, Report No. CCEER-05-2, January 2005.
- CCEER 05-3 Carden, L.P., Itani, A.M., Buckle, I.G., "Seismic Load Path in Steel Girder Bridge Superstructures," Center for Civil Engineering Earthquake Research, Department of Civil Engineering, University of Nevada, Reno, Nevada, Report No. CCEER-05-3, January 2005.
- CCEER 05-4 Carden, L.P., Itani, A.M., Buckle, I.G., "Seismic Performance of Steel Girder Bridge Superstructures with Ductile End Cross Frames and Seismic Isolation," Center for Civil Engineering Earthquake Research, Department of Civil Engineering, University of Nevada, Reno, Nevada, Report No. CCEER-05-4, January 2005.
- CCEER 05-5 Goodwin, E., Maragakis, M., Itani, A. and Luo, S., "Experimental Evaluation of the Seismic Performance of Hospital Piping Subassemblies," Center for Civil Engineering Earthquake Research, Department of Civil Engineering, University of Nevada, Reno, Nevada, Report No. CCEER-05-5, February 2005.
- CCEER 05-6 Zadeh M. S., Saiidi, S, Itani, A. and Ladkany, S., "Seismic Vulnerability Evaluation and Retrofit Design of Las Vegas Downtown Viaduct," Center for Civil Engineering Earthquake Research, Department of Civil Engineering, University of Nevada, Reno, Nevada, Report No. CCEER-05-6, February 2005.
- CCEER 05-7 Phan, V., Saiidi, S. and Anderson, J., "Near Fault (Near Field) Ground Motion Effects on Reinforced Concrete Bridge Columns" Center for Civil Engineering Earthquake Research, Department of Civil Engineering, University of Nevada, Reno, Nevada, Report No. CCEER-05-7, August 2005.

- CCEER 05-8 Carden, L., Itani, A. and Laplace, P., "Performance of Steel Props at the UNR Fire Science Academy subjected to Repeated Fire" Center for Civil Engineering Earthquake Research, Department of Civil Engineering, University of Nevada, Reno, Nevada, Report No. CCEER-05-8, August 2005.
- CCEER 05-9 Yamashita, R. and Sanders, D., "Shake Table Testing and an Analytical Study of Unbonded Prestressed Hollow Concrete Column Constructed with Precast Segments" Center for Civil Engineering Earthquake Research, Department of Civil Engineering, University of Nevada, Reno, Nevada, Report No. CCEER-05-9, August 2005.
- CCEER 05-10 Not Published
- CCEER 05-11 Carden, L., Itani, A., and Peckan, G., "Recommendations for the Design of Beams and Posts in Bridge Falsework," Center for Civil Engineering Earthquake Research, Department of Civil Engineering, University of Nevada, Reno, Nevada, Report No. CCEER-05-11, October 2005.
- CCEER 06-01 Cheng, Z., Saiidi, M., and Sanders, D., "Development of a Seismic Design Method for Reinforced Concrete Two-Way Bridge Column Hinges," Center for Civil Engineering Earthquake Research, Department of Civil Engineering, University of Nevada, Reno, Nevada, Report No. CCEER-06-01, February 2006.
- CCEER 06-02 Johnson, N., Saiidi, M., and Sanders, D., "Large-Scale Experimental and Analytical Studies of a Two-Span Reinforced Concrete Bridge System," Center for Civil Engineering Earthquake Research, Department of Civil Engineering, University of Nevada, Reno, Nevada, Report No. CCEER-06-02, March 2006.
- CCEER 06-03 Saiidi, M., Ghasemi, H. and Tiras, A., "Seismic Design and Retrofit of Highway Bridges," Proceedings, Second US-Turkey Workshop, Center for Civil Engineering Earthquake Research, Department of Civil Engineering, University of Nevada, Reno, Nevada, Report No. CCEER-06-03, May 2006.

- CCEER 07-01 O'Brien, M., Saiidi, M. and Sadrossadat-Zadeh, M., "A Study of Concrete Bridge Columns Using Innovative Materials Subjected to Cyclic Loading," Center for Civil Engineering Earthquake Research, Department of Civil Engineering, University of Nevada, Reno, Nevada, Report No. CCEER-07-01, January 2007.
- CCEER 07-02 Sadrossadat-Zadeh, M. and Saiidi, M., "Effect of Strain rate on Stress-Strain Properties and Yield Propagation in Steel Reinforcing Bars," Center for Civil Engineering Earthquake Research, Department of Civil Engineering, University of Nevada, Reno, Nevada, Report No. CCEER-07-02, January 2007.
- CCEER 07-03 Sadrossadat-Zadeh, M. and Saiidi, M., " Analytical Study of NEESR-SG 4-Span Bridge Model Using OpenSees," Center for Civil Engineering Earthquake Research, Department of Civil Engineering, University of Nevada, Reno, Nevada, Report No. CCEER-07-03, January 2007.
- CCEER 07-04 Nelson, R., Saiidi, M. and Zadeh, S., "Experimental Evaluation of Performance of Conventional Bridge Systems," Center for Civil Engineering Earthquake Research, Department of Civil Engineering, University of Nevada, Reno, Nevada, Report No. CCEER-07-04, October 2007.
- CCEER 07-05 Bahen, N. and Sanders, D., "Strut-and-Tie Modeling for Disturbed Regions in Structural Concrete Members with Emphasis on Deep Beams," Center for Civil Engineering Earthquake Research, Department of Civil Engineering, University of Nevada, Reno, Nevada, Report No. CCEER-07-05, December 2007.
- CCEER 07-06 Choi, H., Saiidi, M. and Somerville, P., "Effects of Near-Fault Ground Motion and Fault-Rupture on the Seismic Response of Reinforced Concrete Bridges," Center for Civil Engineering Earthquake Research, Department of Civil Engineering, University of Nevada, Reno, Nevada, Report No. CCEER-07-06, December 2007.
- CCEER 07-07 Ashour M. and Norris, G., "Report and User Manual on Strain Wedge Model Computer Program for Files and Large Diameter Shafts with LRFD Procedure," Center for Civil Engineering Earthquake Research, Department of Civil Engineering, University of Nevada, Reno, Nevada, Report No. CCEER-07-07, October 2007.

- CCEER 08-01 Doyle, K. and Saiidi, M., "Seismic Response of Telescopic Pipe Pin Connections," Center for Civil Engineering Earthquake Research, Department of Civil Engineering, University of Nevada, Reno, Nevada, Report No. CCEER-08-01, February 2008.
- CCEER 08-02 Taylor, M. and Sanders, D., "Seismic Time History Analysis and Instrumentation of the Galena Creek Bridge," Center for Civil Engineering Earthquake Research, Department of Civil Engineering, University of Nevada, Reno, Nevada, Report No. CCEER-08-02, April 2008.
- CCEER 08-03 Abdel-Mohti, A. and Pekcan, G., "Seismic Response Assessment and Recommendations for the Design of Skewed Post-Tensioned Concrete Box-Girder Highway Bridges," Center for Civil Engineering Earthquake Research, Department of Civil and Environmental Engineering, University of Nevada, Reno, Nevada, Report No. CCEER-08-03, September 2008.
- CCEER 08-04 Saiidi, M., Ghasemi, H. and Hook, J., "Long Term Bridge Performance Monitoring, Assessment & Management," Proceedings, FHWA/NSF Workshop on Future Directions," Center for Civil Engineering Earthquake Research, Department of Civil and Environmental Engineering, University of Nevada, Reno, Nevada, Report No. CCEER-08-04, September 2008.
- CCEER 09-01 Brown, A., and Saiidi, M., "Investigation of Near-Fault Ground Motion Effects on Substandard Bridge Columns and Bents," Center for Civil Engineering Earthquake Research, Department of Civil and Environmental Engineering, University of Nevada, Reno, Nevada, Report No. CCEER-09-01, July 2009.
- CCEER 09-02 Linke, C., Pekcan, G., and Itani, A., "Detailing of Seismically Resilient Special Truss Moment Frames," Center for Civil Engineering Earthquake Research, Department of Civil and Environmental Engineering, University of Nevada, Reno, Nevada, Report No. CCEER-09-02, August 2009.
- CCEER 09-03 Hills, D., and Saiidi, M., "Design, Construction, and Nonlinear Dynamic Analysis of Three Bridge Bents Used in a Bridge System Test," Center for Civil Engineering

Earthquake Research, Department of Civil and Environmental Engineering, University of Nevada, Reno, Nevada, Report No. CCEER-09-03, August 2009.

- CCEER 09-04 Bahrami, H., Itani, A., and Buckle, I., “Guidelines for the Seismic Design of Ductile End Cross Frames in Steel Girder Bridge Superstructures,” Center for Civil Engineering Earthquake Research, Department of Civil and Environmental Engineering, University of Nevada, Reno, Nevada, Report No. CCEER-09-04, September 2009.
- CCEER 10-01 Zaghi, A. E., and Saiidi, M., “Seismic Design of Pipe-Pin Connections in Concrete Bridges,” Center for Civil Engineering Earthquake Research, Department of Civil and Environmental Engineering, University of Nevada, Reno, Nevada, Report No. CCEER-10-01, January 2010.
- CCEER 10-02 Pooranampillai, S., Elfass, S., and Norris, G., “Laboratory Study to Assess Load Capacity Increase of Drilled Shafts through Post Grouting,” Center for Civil Engineering Earthquake Research, Department of Civil and Environmental Engineering, University of Nevada, Reno, Nevada, Report No. CCEER-10-02, January 2010.
- CCEER 10-03 Itani, A., Grubb, M., and Monzon, E., “Proposed Seismic Provisions and Commentary for Steel Plate Girder Superstructures,” Center for Civil Engineering Earthquake Research, Department of Civil and Environmental Engineering, University of Nevada, Reno, Nevada, Report No. CCEER-10-03, June 2010.